



UNIVERSITÀ
POLITECNICA
DELLE MARCHE

SCUOLA DI DOTTORATO DI RICERCA IN SCIENZE DELL'INGEGNERIA
CORSO DI DOTTORATO IN INGEGNERIA INDUSTRIALE

Energy storage in multi-energy carrier communities: Li-ion batteries and hydrogen multi-physical details for integration into the planning stage

Ph.D. Dissertation of:
Lingkang Jin

Supervisor:

Prof. Gabriele Comodi

Ph.D. Course Coordinator:

Prof. Giovanni Di Nicola



UNIVERSITÀ
POLITECNICA
DELLE MARCHE

SCUOLA DI DOTTORATO DI RICERCA IN SCIENZE DELL'INGEGNERIA
CORSO DI DOTTORATO IN INGEGNERIA INDUSTRIALE

Energy storage in multi-energy carrier communities: Li-ion batteries and hydrogen multi-physical details for integration into the planning stage

Ph.D. Dissertation of:
Lingkang Jin

Supervisor:
Prof. Gabriele Comodi

Ph.D. Course Coordinator:
Prof. Giovanni Di Nicola

UNIVERSITÀ POLITECNICA DELLE MARCHE
SCUOLA DI DOTTORATO DI RICERCA IN SCIENZE DELL'INGEGNERIA
CORSO DI DOTTORATO IN INGEGNERIA INDUSTRIALE
Via Brecce Bianche – 60131 Ancona (AN), Italy

*To all wonderful people met
in this journey*

Acknowledgments

Your smile is your logo, your personality is your business card, how you leave others feeling after having an experience with you becomes your trademark.

Jay Danzie

These PhD years have not been easy, yet they marked the most crucial period of my life, as they granted me both personal and research growth. Furthermore, quite a few movements have occurred during these years, shifting from the coastal city of Ancona to the cold Nordic city of Copenhagen, and finally to the rainy city of Eindhoven. As I reach this milestone in my journey, I want to express my gratitude to all those who have played a part.

First, I would like to thank Prof. Gabriele Comodi, supervisor and mentor. This journey has only been possible because of the opportunities he provided, and I am deeply appreciative of his unwavering support. He allowed me to explore the various facets of research, and for that, I am truly grateful.

I would also like to express my gratitude to Ing. Mosè Rossi, whose consistent support for all my research activities over the years has been invaluable. Without him, my PhD journey would have taken a very different path.

I extend my heartfelt gratitude to all my colleagues at the Technical University of Denmark whom I had the pleasure of meeting during my visiting period. Their kindness and support have been greatly appreciated. I would like to offer special thanks to Prof. Henrik Lund Frandsen for allowing me to join his research group. It was there that I had the opportunity to collaborate with researcher Rafael Nogueira Nakashima, whose knowledge and insights were invaluable in gaining experience in multi-physical modelling.

On the other hand, I want to express my deep appreciation to my wonderful colleagues at the Technical University of Eindhoven. They not only provided technical support but also brightened the rainy days in Eindhoven with their kind and friendly attitude. I would like to give special recognition to Prof. Christina Papadimitriou for her support, not only during the supervision period but also after my visiting period.

Embarking on the journey of a PhD is a challenging and often misunderstood path. I am grateful for the opportunity to share these experiences with my fellow PhD colleagues in the department, and I want to extend special thanks to two dear friends, Matteo and Giovanni, who have walked this PhD journey alongside me.

I am also thankful to all my "old friends", those I have known for many years, who have remained through numerous changes and re-locations. Their warmth has been a guiding light on the coldest of nights.

To my "new friends" met during this journey, I appreciate the adventures and discoveries that we've shared together. Many of these experiences would not have been possible without them.

My most profound gratitude, however, goes to my family. Despite not fully comprehending the importance of research, they have fully supported me throughout this arduous path.

In conclusion, I reserve my deepest recognition for myself. It is a testament to my own sacrifice, resilience, and determination that I have navigated this lengthy and challenging journey.

Ancona, January 2024

Lingkang Jin

Abstract

The energy transition process, towards a carbon-neutral society, is undergoing, yet, still at a gradual pace. To facilitate it, the implementation of sector coupling measures is required. While the primary type of sector coupling measure, i.e. end-users' electrification, is a straightforward option, supported by the rapid growth of renewable electricity production, however, it fails to meet the overall energy needs. To overcome such limitations, the second type of sector coupling measure, i.e. cross-vector integration, for example, adopting hydrogen integration, which enables the coupling of two different energy vectors (thermal and electrical energy), can assume a decisive role.

Furthermore, the energy end-users' role must be reconsidered in the energy paradigm. Indeed, while they played as passive actors previously, as they would consume energy based on habits without doubting the consequences, now they would be actively involved, by locally producing the energy, sharing it and even trading it for economic revenues. Such a concept is the foundation of the Local Energy Communities (LEC). By the European Commission's definition, LECs are legal entities that encompass the production, distribution, and utilisation of diverse energy carriers. They aim to maximise local energy benefits, which include community sharing, bolstering energy independence from the national grid, reducing the community's carbon footprint, and enhancing energy flexibility. Moreover, energy storage systems are central to the adoption of LECs. Enabling the decoupling of production and consumption, and unlocking cross-vector potential by the use of hydrogen or thermal energy vectors.

With the ever-growing interest in this, also scientific research is thriving, indeed energy systems modelling, which is the research topic to assess the impact of such measures, to provide key insights to policymakers, supporting them in making energy-related decisions, has been gaining progressively emphasis. Moreover, energy systems modelling has different sub-categories. Indeed, from a system-level perspective, where the focus is on the interconnection of different energy assets, each of them modelled as a single entity, through the optimisation of the planning and scheduling of LECs, i.e. management of the synergies among various energy vectors, delivering the requested energy demands, in the most efficient way.

Commonly, for LEC energy planning, a bottom-up approach is adopted, meaning the energy asset's details are first investigated, to be then connected with proper connections and limitations, finalising the whole energy community of interest. The dominant mathematical formulation used is Mixed Integer Linear Programming, with

time-dependent data at hourly resolution spanning a one-year planning horizon minimum. However, there is a lack of proper models, that are capable of accommodating dynamic variations in input parameters, such as energy costs, and investments. Additionally, correlations among different technology deployments, are not widely discussed.

From the technological perspective of energy system modelling, the single energy asset is studied in detail, with all its subcomponents. Nevertheless, many cross-vector technologies, like hydrogen-related energy conversion technologies, have not received comprehensive coverage in the energy system modelling literature, due to their technology readiness level. Likewise, the Li-ion battery, despite being a mature energy storage solution, its technology degradation is not sufficiently explored, especially in stationary applications within the LEC context, which affects the system level planning, causing a mismatch of financial assessment due to its premature replacement.

To address these limitations, from both system and technological perspectives, this thesis serves as a comprehensive exploration of energy storage integration within Local Energy Communities. Specifically addressing hydrogen and Li-ion battery technology. Moreover, this work has the aim to bridge both the technology and system perspectives of energy planning, indeed, single system details and limitations are first analysed, to be considered further at the system level. From the system perspective, this work addresses the necessity of having optimal alternatives during the energy planning stage. Indeed, the correlation between different technologies that is usually hindered, can be unveiled, thanks to these alternatives. Furthermore, the inclusion of dynamic variations of input parameters, along with different investment stages over the planning horizon, is explored.

As a demonstration of proposed methodologies, this thesis presents two distinct case studies, that effectively take into account both levels of detail (technological and system). The first reported case study concerns the optimal design of a green hydrogen production plant, which consists of an offshore wind turbine, and an alkaline electrolyser system with all its auxiliary components. The second case study instead, has the the objective of analysing long-term storage solutions for a fully electrical energy-independent LEC, through the comparison of hydrogen and Li-ion battery solutions, taking into account the challenges posed by battery degradation.

Contents

1. Introduction & scope of the thesis	9
1.1. Local Energy Community for energy transition	11
1.2. Energy storage technologies, and their potential	14
1.2.1. Mechanical Energy Storage Systems	15
1.2.2. Electrical and electrochemical Energy Storage Systems	18
1.2.3. Hydrogen Energy Storage	20
1.2.4. Energy Storage Systems comparison	20
1.2.5. Energy storage systems for local energy communities	21
1.3. Energy planning & system modelling: tools to boost energy community deployment	23
1.3.1. Energy planning: methodology	24
1.3.2. Energy planning: Assessment criteria	24
1.3.3. Energy planning: Multi-objective approach	25
1.3.4. Energy planning: Spatial & temporal resolution and coverage	26
1.3.5. Energy planning: Analytic approach	26
1.3.6. Energy Planning: Mathematical approach	27
1.3.7. Energy planning: Technical coverage	27
1.3.8. Energy system modelling applied to Local Energy Communities	28
1.4. Research question	31
1.5. Outline of the thesis	32
I. Technological approach: Hydrogen and Lithium-ion battery modelling	35
2. Hydrogen as energy storage	37
2.1. Hydrogen limitations and opportunities	38
2.2. Power-to-hydrogen: water electrolysis	39
2.3. Alkaline water electrolysis modelling	42
2.4. Alkaline electrolyser: modelling and temperature control effects	44
2.4.1. Semi-empirical model	45
2.4.2. Semi-empirical model validation and comparison	53
2.4.3. System level temperature control effects	57
2.4.4. Model limitations and opportunities	59
2.5. Innovative hydrogen storage: Metal hydrides	60
2.5.1. Metal hydrides working principle	63

Contents

2.5.2. Metal hydrides and ancillary systems	65
2.5.3. Metal hydride system modelling and testing	66
2.5.4. Evaluation of operational strategies	69
2.5.5. Study's potential and limitation	69
3. Battery Energy Storage Systems: Li-ion battery	73
3.1. Li-ion modelling: Equivalent Circuit Models' robustness	75
3.1.1. Sensitivity analysis	77
3.1.2. Selected models	80
3.1.3. Comparison metric	81
3.1.4. Comparison results	81
3.1.5. Study's remarks and limitations	83
3.2. Li-ion battery degradation modelling: State of health as Pareto frontier indicator	83
3.2.1. Pybamm framework and battery parameterization	84
3.2.2. State Of Health assessment	87
3.2.3. Results of the case study and limitation of the approach	88
II. System approach: energy planning	91
4. Energy systems planning	93
4.1. Energy planning: Optimal alternatives	94
4.1.1. Calliope framework and scenario analysis	95
4.1.2. Three phases analysis and the case study	96
4.1.3. Results and limitations of the approach	102
4.2. Energy planning: Dynamic medium-term energy planning	107
4.2.1. Methodology	109
4.2.2. Results of the case study	112
4.2.3. Methodology's potential and limitation	118
III. Energy storage details into systems approach: case studies	121
5. Bi-level interconnection case studies	123
5.1. Case study 1: Wind turbine design optimisation for hydrogen production	125
5.1.1. The HWT model	126
5.1.2. System evaluation	131
5.1.3. Results of the case study	133
5.1.4. Approach's potential and case study's results	135
5.2. Case study 2: Storage solutions comparison	137
5.2.1. Methodology adopted	138
5.2.2. Calliope set-up	144

5.2.3. Results of the case study	147
5.2.4. Case study's insights	150
6. Conclusions, recommendations and future developments	153
6.1. Conclusions	153
6.2. Recommendations	157
6.3. A glimpse of the future	159
Appendices	161
A. Hydrogen technologies	163
B. Li-ion battery	165
C. Energy Planning	175
D. Bi-level case studies	191
References	195
List of publications	217

List of Figures

1.1. European countries share from renewables in 2020-2021 ([2])	10
1.2. Illustrated diagrams about mechanical ESS, namely Pumped Hydro Energy Storage (PHES), Compressed Air Energy Storage (CAES), Gravity Energy Storage (GES), Liquid Air Energy Storage (LAES), Pumped Thermal Energy Storage (PTES) and Flywheel	15
1.3. Electrical and electrochemical ESS. while the supercapacitor is the only electrical energy storage, both Lithium-ion battery (LiB) and Redox Flow Battery (RFB) are electrochemical ones.	19
1.4. Chemical ESS/Power-to-hydrogen	20
1.5. Energy storage technologies comparison: power rating vs. operational time.	22
1.6. Energy storage technologies comparison: energy density and power density.	23
1.7. Illustration of different mathematical approaches: the intersection point represents the solution of the model.	28
1.8. Energy planning tool properties and categorization.	30
2.1. Chemical reactions of four types of available electrolyser technologies.	41
2.2. Classification of alkaline electrolysis models	44
2.3. Electrolysis polarisation curve, distinguished into its components. The bubble formation overpotential is not presented as it is for high current densities, where alkaline electrolysers commonly do not operate. . .	46
2.4. Thermal model differences: Lumped model vs ODE.	52
2.5. Parameters estimation procedure. Divided into three steps: 1) collection of experimental data at different temperatures, 2) parameter estimation, and 3) temperature and pressure influence validation. . .	54
2.6. Parameter estimation and validation with temperature variation. Where squared-dotted data are from the training dataset while the circle ones are from the test dataset.	55
(a). Sakas	55
(b). Ulleberg	55
(c). Sanchez	55
(d). Ulleberg	55

List of Figures

2.7. Alkaline 1D stack model flowchart. Starting with the single cell 0D model, extended to the 1D cell model, solving mass and thermal balance, and finally 1D stack model, based on the electrical configuration among cells.	57
2.8. 1D model at 1-2-10 °C temperature difference. Illustrating namely i) temperature, ii) hydrogen production, and iii) voltage efficiency along the cell. Where the outlet temperature is kept constant. Despite having a higher temperature difference and achieving a higher efficiency, the produced hydrogen flow is lower.	57
2.9. Different scales of electrolyser models' comparison, at different temperatures increase over the stack. Where error is the difference between the models' average current density, compared with the 1D model's average current density, in percentage.	58
2.10. Systems connections. Illustrating auxiliary systems to be coupled with electrolyser stack.	58
2.11. Influence of temperature difference (inlet to outlet) in system efficiency. Where the outlet temperature is set as 80°C.	60
2.12. Influence of temperature difference (inlet to outlet) in the levelised cost of hydrogen. Where the outlet temperature is set as 80°C.	61
(a). LCOH with minimum LCOE	61
(b). LCOH with maximum LCOE	61
2.13. Hydrogen storage pathways: Gas, liquid, solid.	62
2.14. Metal hydrides: different phases	63
2.15. P-X-T diagram and Van't Hoff plot	64
2.16. Metal hydride phases: i) solid solution phase, ii) metal-hydrogen solution phase, and iii) hydride phase.	65
2.17. Metal hydrides hydrogen storage system: pressurized hydrogen is injected into the tank where the metal powder is contained.	65
2.18. Systems' layout for both charging and discharging stages.	66
2.19. Examples of metal hydrides hydrogenation and de-hydrogenation kinetics.	70
(a). Absorption stage dynamics	70
(b). Desorption stage dynamics	70
2.20. Performance indicators for the evaluation of metal hydrides operational strategy.	71
(a). Performance indicators in the absorption phase. Various colours representing different set temperatures (blue, green, and red), shapes indicating setting pressures (●, +, and ■), and dotted lines denoting the time needed for charging.	71
(b). Performance indicators during desorption.	71
3.1. Battery models comparison	75

3.2. Relation between calendar and cycle ageing: as a result, the capacity drops and the resistance increases.	76
3.3. Simulated data for the temperature sensitivity analysis	78
3.4. Simulated data for the current sensitivity analysis	79
3.5. Simulated data for the temperature sensitivity analysis	80
3.6. Workflow of the initialization of Pybamm model.	86
3.7. Parameters selection and tuning process	87
3.8. Workflow of the parameters tuning for Pybamm model: 1) electrochemical parameterization, 2) thermal parameterization, and 3) ageing parameterization	88
3.9. Workflow of assessing the Pareto curve using SOH as indicator . . .	89
3.10. SOH as Pareto indicator. The differences among the different cases are extremely low due to the limited time frame of the study.	89
(a). Pareto	89
(b). Difference	89
4.1. First phase flowchart.	97
4.2. Second phase flowchart.	98
4.3. Third phase flowchart.	98
4.4. UNIVPM Campus map, recreated with Geopandas [144].	99
4.5. Multiple energy demands with hourly resolution.	100
(a). Electrical energy demand in the year 2019	100
(b). Thermal energy demand in the year 2019	100
(c). Cooling energy demand in the year 2019	100
4.6. Functional scheme of the energy carriers and technologies involved in all the scenarios	101
4.7. Energy share of the baseline scenario.	102
(a). Electrical energy	102
(b). Thermal energy	102
(c). Cooling energy	102
4.8. LCOE of the energy carriers in the baseline scenario	103
4.9. Energy matrix of the optimal scenario.	104
(a). Electrical energy	104
(b). Thermal energy	104
(c). Cooling energy	104
4.10. Technologies difference between the optimal and baseline scenario.	104
4.11. LCOE of the optimal scenario	105
4.12. Spearman correlation matrix of technologies from twenty optimal alternatives.	106

List of Figures

4.13. Outlook of the trends of investment costs: BESS and hydrogen technologies.	111
(a). Cost forecast of BESS equipment available in the 3 variants of 500-1500-2500 kW.	111
(b). Cost forecast of hydrogen technologies: electrolyser and fuel cell devices are considered in 3 available variants of size.	111
4.14. Flowchart of the iterative MILP-based two-step approach	111
4.15. BAU: levelised costs and investment stages	113
4.16. Sector coupling scenario: multi-stage investment decisions.	114
4.17. Hydrogen deployment scenario: multi-stage investment decisions	115
4.18. Scenarios comparison: LCOEs of different energy carriers.	115
4.19. Scenarios comparison with overall costs of the entire planning.	116
4.20. Operations' results. To illustrate energy balances during the scheduling.	117
4.21. Examples of load distribution among the same technologies. Data taken from the <i>Hydrogen deployment</i> scenario, year 1, week 2.	118
5.1. Approach adopted for connecting two levels of energy systems analysis.	124
5.2. The subsystems of HWT model: the wind climate, the wind turbine with an integrated battery, and the electrolysis system.	127
5.3. The power curve of the reference wind turbine	128
5.4. Flowsheet of the electrolysis system	130
5.5. Comparison of cell voltage model results with experimental data reported by [73].	131
5.6. Comparison of Faraday efficiency model results with experimental data reported by [73].	132
5.7. Impact of the electrolysis stack rating (upper) and battery capacity (lower) on AHP, curtailment and LCOH. The battery capacity and battery rating are assumed to be the same.	134
5.8. Left: LCOH as a function of rated power and rotor diameter for a hub height of 110m. The initial (RWT) and optimal (min LCOH) points are also indicated. Right: LCOE as a function of rated power and rotor diameter for a hub height of 90m.	135
5.9. Baseline scenario (on-grid operation of consumers).	139
5.10. BESS scenario (off-grid operation of consumers).	140
5.11. Hydrogen system scenario (off-grid operation of consumers).	140
5.12. Single National Price/PUN trend	141
5.13. Trend of the hourly power output of the small-scale hydropower plant in 2019	143
5.14. Daily electrical load of the LEC [185].	143
5.15. Production and load frequencies (sorted by power).	147
5.16. Baseline scenario results	148
5.17. Available electrical energy to end-users from the two ESS solutions	150

5.18. LCOS as a function of the storage period	150
B.1. Electrochemical parameterization	168
(a). Voltage drop inconsistency	168
(b). parameterized model	168
B.2. Thermal parameterization	170
B.3. Ageing parameterization	171
B.4. Pareto curve from HEMS	171

List of Tables

2.1. Key performance indicators for four electrolyser technologies [67, 68, 69, 70].	42
2.2. Semi-empirical model validation: Despite different operational conditions (temperatures and pressures), parameters for the different datasets are similar.	56
2.3. Hydrogen pressure standard for different applications	62
2.4. Intermetallic compounds families for metal hydrides [96].	65
2.5. MH numerical testing: Operation parameters' range and conditions.	67
3.1. Operating conditions of simulated data through the univariate analysis	78
3.2. Variation in operating conditions of simulated data for the multivariate analysis	79
3.3. Other parameters used in the testing process	80
3.4. Training & test sets	81
3.5. MAPE computed in the temperature sensitivity analysis	82
3.6. MAPE computed in the current sensitivity analysis.	82
3.7. MAPE computed for the multivariate sensitivity.	83
4.1. Scenarios analysis: LCOEs variation	116
5.1. Parameters of the reference wind climate	127
5.2. The main parameters of the reference wind turbine including the design parameters.	129
5.3. Parameters fitted for experimental data reported by [73].	131
5.4. Faraday efficiency parameters fitted for experimental data reported by [73].	131
5.5. Range of wind turbine design parameters	135
5.6. Main characteristics of the Kaplan turbine	142
5.7. BESS scenario results	148
5.8. Hydrogen scenario results	149
A.1. Modelling parameters for alkaline water electrolysis temperature control	163
A.2. MH Modelling parameters	164
B.1. LFP Li-ion battery specifications	172
B.2. HEMS results: battery	172
B.3. Battery design	172

List of Tables

B.4. Computational specs for the case study	173
B.5. Pybamm model tuned parameters	174
C.1. Baseline technologies	175
C.2. Supply costs	175
C.3. Energy conversion technologies costs	176
C.4. Storage technologies parameters	176
C.5. Scenario parameters employed in the case study.	186
C.6. Performance characteristics and cost coefficients of PV technology.	186
C.7. Sets, parameters and variables common to the two formulations, exclusive of M_y and M_w	187
C.8. Performance characteristics and cost coefficients of conversion technologies.	188
C.9. Dynamic costs of storage technology EES, PEM conversion technologies FC and EL for the 30-year planning horizon.	189
D.1. Modelling assumptions for the electrolysis system	192
D.2. Parameters of the LCOH modelling	192
D.3. Main characteristics of the ESSs	193
D.4. Cost parameters of the study	193

Nomenclature

Acronyms

AC	Absorption Chillers/ Alternate Current
AEM	Anion Exchange Membrane
AEP	Annual Energy Production
AHP	Annual Hydrogen Production
ALK	Alkaline electrolyser
BAU	Business As Usual
BESS	Battery Energy Storage System
BMS	Battery Management System
BOP	Balance Of Plant
CAES	Compressed Air Energy Storage
CC	Constant Current
CHP	Combined Heat and Power
COP	Coefficient Of Performance
CTES	Cold Thermal Energy Storage
CV	Constant Voltage
DC	Direct Current
DER	Distributed Energy Resources
DFN	Doyle-Fuller-Newman
DOD	Depth of Discharge
EC	Electrical Chiller
ECM	Equivalent Circuit Model
ES	Electrolyser System

Nomenclature

ESS	Energy Storage Systems
EZ	Electrolyser
FC	Fuel Cell
GB	Gas Boiler
GES	Gravity Energy Storage
HEMS	Home Energy Management System
HES	Hydrogen Energy Storage
HP	Heat Pump
HTES	Hot Thermal Energy Storage
HWT	Hydrogen Wind Turbine
KOH	Potassium Hydroxide
KPI	Key Performance Indicator
LAES	Liquid Air Energy Storage
LAM	Loss of Active Material
LCOE	Levelised Cost of Energy
LCOH	Levelised Cost of Hydrogen
LCOS	Levelised Cost Of Storage
LEC	Local Energy Community
LFP	Lithium iron phosphate
Li-NCA	Lithium Nickel Nickel Cobalt Aluminum oxide
Li-NMC	Lithium Nickel Maganese Cobalt oxide
LiB	Lithium-ion Battery
LMO	Lithium Manganese Oxide
MAE	Mean Average Error
MAPE	Mean Average Percentage Error
MES	Multi Energy Systems
MH	Metal Hydrides

MILP	Mixed Integer Linear Programming
NaOH	Sodium Hydroxide
O&M	Operation and Maintenance
ODE	Ordinary Differential Equation
OH	Hydroxide Ions
P-C-T	Pressure-Concentration-Temperature
PBM	Physic-based model
PDE	Partial Differential Equation
PEM	Proton Exchange Membrane
PHES	Pumped Hydro Energy Storage
PS2D	Pseudo Two Dimensional model
PTES	Pumped Thermal Energy Storage
PUN	Italian Single National Electrical Energy Price
PV	Photovoltaic
PyBaMM	Python Battery Mathematical Modelling
RED	Renewable Energy Directive
RES	Renewable Energy Systems
RUL	Remaining Useful Life
RWT	Reference Wind Turbine
SEI	Solid Electrolyte Interface
SH	Storage of Hydrogen
SOC	State Of Charge
SOEC	Solid Oxide Electrolyser
SOH	State of Health
SPM	Single Particle Model
SPMe	Single Particle Model with electrolyte
SPORES	Spatially explicit Practically Optimal Results

Nomenclature

TRL	Technology Readiness level
UNIVPM	Marche Polytechnic University
WT	Wind Turbine

Constants

F	Faraday constant, 96500 [C/mol]
LHV_{H_2}	Hydrogen Low Heating Value, 242 [kJ/mol]
R	Universal gas constant, 8.314 [J/mol K]

Subscripts

a	Absorption (MH)
act	Activation
an	Anodic
$batt$	Battery
BAU	Business As Usual
$bubble$	Bubble formation
ca	Cathodic
$cell$	Cell level
$cons$	Consumed
d	Diaphragm (electrolysis)/ Desorption (MH)
el	Electrolyte
ESS	Energy Storage System
f	Conditioning fluid
g	Wind turbine generator
gen	Generated
h	Hour
H_2	Hydrogen
H_2O	Water
HEX	Heat exchanger

<i>in</i>	Inlet
<i>mass</i>	Mass based
O_2	Oxygen
OH	Hydroxide ions
<i>ohm</i>	Ohmic
<i>out</i>	Outlet
<i>prod</i>	Produced
<i>pump</i>	Water pump
<i>ref</i>	Reference
<i>res</i>	Residual
<i>rev</i>	Reversible
<i>s</i>	Solid/metal (MH)
<i>stack</i>	Stack level
<i>th</i>	Thermo-neutral
<i>y</i>	Annualised

Variables

α	Charge transfer coefficient, [-]
δ	Reaction distance, [cm]
\dot{m}	Mass flow rate, [kg/s]
\dot{n}	Molar flow rate, [mol/s]
\dot{Q}	Thermal power, [W]
ϵ	Heat exchange efficiency, [-]
ϵ_j	Self-discharge ratio of BESS, [-]
η	Energy system efficiency, [-]
η_f	Faraday efficiency, [-]
Ω_r	Wind turbine rated rotational speed, [rpm]
ϕ_c	Curtailment ratio, [-]

Nomenclature

ρ	Density, [kg/m ³]
σ	Ionic conductivity, [S/cm]
A	Area, [cm ²]
C	Electrical Capacity, [Ah]; or Economical costs, [€]
C_0	Battery rated capacity, [Ah]
C_f	Capacity factor, [-]
C_p	Wind turbine power coefficient, [-]
c_{var}	Operational/variable costs, [€/kWh]
$CAPEX$	Capital Expenditure, [€]
C_p	Specific heat, [J/kg K] or [J/mol K]
D	Wind turbine diameter, [m]
d_r	Depreciation rate, [-]
E	Energy, [kWh] or [Wh]
E_a	Activation energy, [J/mol]
E_b	Battery rated energy, [kWh]
E_c	Curtailed energy, [kWh]
$f(v)$	Frequency of occurrences of the wind speed (v), [-]
f_1, f_2	Faraday efficiencies coefficients, [-],[A/m ²]
H	Enthalpy, [J/mol]
H_h	Wind turbine hub height, [m]
I	Current, [A]
i	Interest rate, [-]
j	Current density, [A/m ²] or [mA/cm ²]
k	Arrhenius scale factor, [mA/cm ²] or [A/m ²]
$LCOE$	Levelised Cost of Energy, [€/kWh]
$LCOH$	Levelised Cost of Hydrogen, [€/kg _{H₂}]
lt	Lifetime of the technology, [years]

Nomenclature

m	Mass (<i>with subscript</i>), [kg]
m	Molality (<i>no subscript</i>), [mol/kg]; Slack for alternatives, [-]
MW	Molecular Weight, [g/mol]
n	Mols of the species, [mol]
P	Pressure, [bar] or [Pa]
p	Power, [W]
P_g	Wind turbine rated power, [MW]
R	Electrical resistance, [ohm]
R_0	Battery internal resistance, [ohm]
S	Entropy, [J/mol K]; Design energy system size, [kW] or [kWh]
SP	Specific power, [W/m ²]
T	Temperature, [K] or [°C]
t	Time, [s]
V	Voltage, [V]
v	Wind speed, [m/s]
w	Electrolysis cell width, [cm]
wt	Weight concentration, [0-1]
X	Hydrogen mass concentration in MH, [%]
z_{ref}	Reference Height for wind profile, [m]

Chapter 1.

Introduction & scope of the thesis

Nothing in life is to be feared, it is only to be understood. Now is the time to understand more, so that we may fear less.

Maria Skłodowska-Curie

The environmental issue is undoubtedly one of the crucial problems of our era and to tackle it, the energy transition is undergoing, with the focus on limiting global warming to 1.5°C above pre-industrial levels, however, it is happening at a slow pace, as the report from Intergovernmental Panel on Climate Change [1] illustrated.

The European Union's energy demand is not yet entirely sustainable, as evidenced by data from the Eurostat repository [2]. In 2021, renewable generation accounted for 37.4% of the total energy demand (Fig. 1.1). However, it's important to note that this figure represents the aggregate data for all 27 countries within the Union. The energy landscape varies significantly from one country to another.

For instance, two Nordic countries, Norway and Iceland, have emerged as noteworthy exceptions. They managed to produce more renewable energy than their local demand. This achievement can be attributed to several factors, including their lower population density compared to other countries and their substantial renewable energy system (RES) capacities. Furthermore, the abundant wind resources in these regions have contributed significantly to their renewable energy production. On the contrary, some other countries are still lagging behind, in the sense of the penetration of the RES, where Malta has less than 10% of the share of the energy consumption from renewables.

Thus, it requires a compelling effort and investment in zero-carbon power technologies, energy intensity improvements, and the development of new technologies that can decarbonize the hard-to-abate industrial operation [3].

Indeed, To keep global warming to no more than 1.5°C, based on the statement of the United Nations, Climate action sector [4], emissions need to be reduced by 45 % by 2030 and reach net zero by 2050. Without a global, extensive, and near-term action, the 1.5-degree pathway is likely out of reach. With this regard, the European Union has taken decisive actions and set up different frameworks, to reach its established goals which are i) cut greenhouse gas emissions by at least 55% by

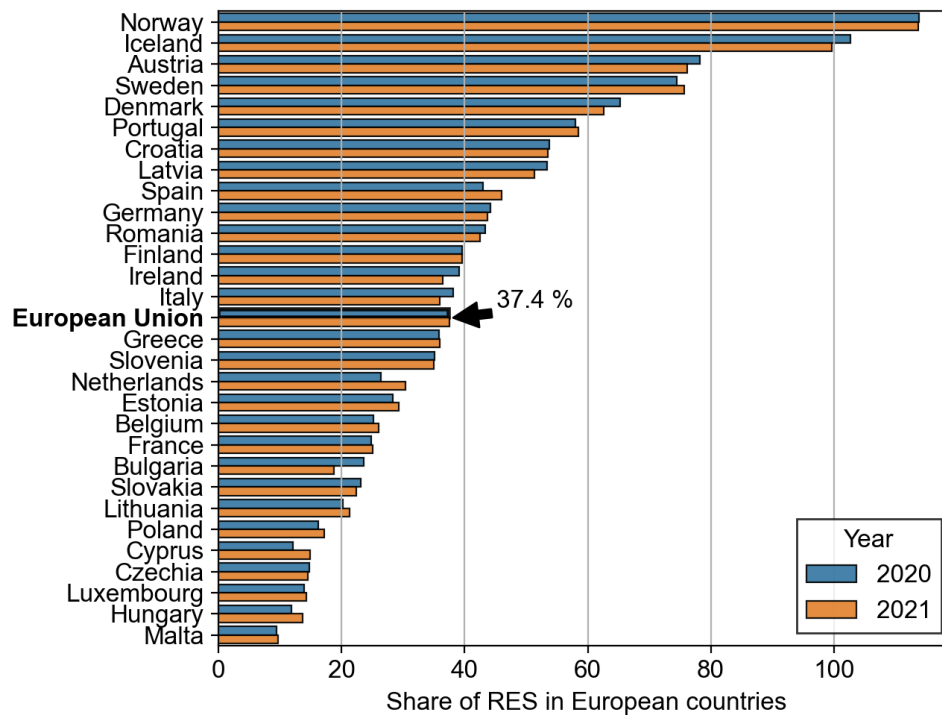


Figure 1.1.: European countries share from renewables in 2020-2021 ([2])

2030, under the so-called "Fit-for-55" framework [5], as a follow-up framework of European Green Deal [6], and ii) Making the EU climate-neutral by 2050. the latest European framework regarding energy is the REPowerEU [7], which was launched in May 2022, helping the EU to deliver:

1. Diversifying and finding alternative energy supplies.
2. Green transition and investment in renewable energy.
3. Energy saving and efficiency.

The REPowerEU plan also includes numerous mid to long-term measures to bring much of energy generation within the EU's borders through renewable sources, coupled with renewable import capacity to cover the remaining energy requirements. These measures include increasing the target in the "Renewable Energy Directive" (RED) to 45% by 2030, up from 40 % under the Fit for 55 Package, and targeting 320 Gigawatts (GW) of solar photovoltaic (PV) capacity installed by 2025 rising to 600 GW by 2030 [8]. Thus, different measures and research topics are undergoing, all to enhance and permit the success of pre-established goals.

Regarding the historical and current situation of RES capacities, Europe has been steadily increasing its wind energy generation capacity, with 489 TWh generated in 2022. In terms of new installations, Europe installed 19.1 GW of new wind farms in 2022, which was a record year for installations with an increase of 4% compared to the previous year. Looking ahead, Europe is expected to install 116 GW of new wind

1.1. Local Energy Community for energy transition

farms over the period from 2022-2026, with three-quarters of these new capacity additions being onshore wind. The EU-27 is expected to build on average 18 GW of new wind farms between 2022-26, but they need to build 32 GW a year to meet the EU's new 40% renewable energy target [9]. In terms of solar PV and wind capacity, the latest European Commission staff working document states that capacities of 592 GW of solar PV and 510 GW of wind are required by 2030 to achieve the 69% share of renewable electricity modelled by the Commission. However, the current expansion of solar PV and wind capacity is insufficient to reach the REPowerEU plan's renewable electricity objectives for 2030. In fact, the main-case forecast predicts that average annual net additions need to be 22% higher for solar PV and more than two times greater for wind to reach the installed capacity needed to generate 69% of electricity from renewables by 2030 [10]. Despite these challenges, the EU is expected to put more effort into making objectives real.

Besides the renewable production side, the European Commission has put considerable efforts into promoting the development of energy communities [11], which is defined as follows: "A Local Energy Community (LEC) is a legal entity that is involved in power production, distribution, and use, to provide environmental, economic, and social benefits to the local community. These communities can be physical, originating from local initiatives and occupying a small piece of territory, such as a neighbourhood, village, or campus, or virtual, with geographically dispersed energy resources", which has the objective to offer a means to re-structure energy systems by harnessing the energy and allowing citizens to participate actively in the energy transition and thereby enjoy greater benefits, switching citizens from the passive role, into an active player of the energy transition. Indeed, the end-users actions have always impact on the overall energy system, yet, only with the LEC concept, the end-user role will shift from the traditional passive subject into an active one, i.e. their actions would be affected by the energy system behavior, to reach a common energy beneficial goal.

This thesis has the objective of assessing energy storage integration, from both a systematical and technological perspectives. In particular, hydrogen and Lithium-ion battery technologies are deeply investigated in physical detail. Then the thesis presents the illustration of their impacts, through two different case studies, within the context of the Local Energy Community.

1.1. Local Energy Community for energy transition

The tools to achieve the energy transitions are well defined and can be divided into two approaches of sector coupling, that are i) high electrification of end-user loads, supported by an increasing capacity of RESs, and for the reason of easy installation, the RES technology such as photovoltaic and wind turbines are the ones gaining more interest, and since currently not all users can be electrified, due to

different technological reasons, it is required to adopt ii) cross-vector coupling, that allows coupling different energy vectors, such as power-to-hydrogen or power-to-heat, so that also users that are not electrified, because different technical issues, like hard-to-abate sectors, could reach the predefined energy transition goal.

While the first approach, the solution is straightforward, which consists of a change of end users' appliances, supported by the dedicated energy policies to increase the production of renewable, moreover, the application is economical and policy-driven, rather than technology-constrained, therefore has been left out from this work. For the second approach, however, because several technologies have not reached the complete technology readiness required, the synergies among multiple energy carriers, indeed their impact on the current energy systems, are not widely addressed. Both solutions can be properly integrated and tested in the context of LECs, where the end-users have an active role, moreover, since it is easier to apply, due to its main goal to be a smaller scale, indeed, by definition, LEC can be formed by a small aggregate of energy consumers, which makes it a viable solution to be easy implemented and replicated. For such context, proper energy management, through the use of a systematic approach with advanced energy planning tools, the synergic operation of the use of multi-energy carriers, with the integration of energy storage solutions and distributed energy sources, all to increase energy flexibility, reducing in the same time both economical and environmental impact of the community can be achieved.

In the deployment of sector coupling through LECs, the role of enabling technologies is of paramount importance. The LEC concept encompasses a community of proactive energy consumers who utilise optimisation techniques to maximize the advantages and minimise the expenses associated with generating and distributing energy from various sources (e.g., electricity, heating/cooling, etc.). Precisely, the efficient management of diverse energy carriers is pivotal in attaining optimal operational conditions for LECs, encompassing both energy and economic considerations.

So far, numerous energy conversion and storage technologies have been developed to handle more than two energy carriers concurrently [12]. Nazar-Heris et al. [13] investigated the inter-dependencies among various energy carriers within multi-carrier energy networks encompassing power, gas, heating, and water carriers. Their study encompassed a range of generation units, such as Combined Heat and Power (CHP) systems and gas-fired boilers, as well as storage facilities like pump storage, water desalination units, and heat and gas storage solutions. Storage units play a pivotal role in enhancing the overall system's flexibility, consequently driving down its operational costs [14]. Additionally, the adoption of multi-carrier energy networks has significant implications for the energy market, as underscored by Nasiri et al. [15]. Their study employed a bi-level approach to assess the impact of coupling renewables with energy storage on both local and regional markets. Notably, their analysis encompassed the minimisation of purchase costs (e.g., maximising energy storage utilisation and wind energy production) and selling costs (e.g., minimising

1.1. Local Energy Community for energy transition

the utilisation of generation units and natural gas producers). The results revealed a 7.01% reduction in daily operation costs at the local level and a 1.7% decrease at the regional level.

It's worth noting that most of the technologies involved in multi-energy carrier systems have already reached a Technology Readiness Level (TRL) of 9, signifying their maturity and availability in the market. Nevertheless, some technologies are still in development, particularly emerging energy carriers like hydrogen, which are destined to play a significant role in advancing the decarbonisation efforts across various energy-intensive sectors [16]. However, there are still technical and non-technical (e.g., regulatory) barriers/limitations that do not allow their proper implementation in LECs and need to be overcome quickly [16]. Technical limitations refer to those technologies involved in the definition of multi-energy carrier systems like generation, storage, and transportation. Technologies with different TRLs affect considerably the deployment of LECs, particularly the definition and the final efficiency of the overall system in which they are installed. Apart from this, the low flexibility of some technologies has also an important impact, and flexibility services are crucial in LECs for adjusting generation, storage, and consumption. Most of the consolidated technologies are already available in the market and operate mainly at rated conditions, while their efficiencies are lower when operating at part-load conditions due to the end-users demand variation. This issue can be overcome by using the same or complementary technologies, with different sizes together with energy storage ones, capable of operating efficiently while the end-users demand changes. In this case, proper control strategies allow to identify the most suitable technology to operate under certain load conditions and guarantee high grid stability, reliability, and main economic goals [17].

When it comes to modelling Multi Energy Systems (MES), as elaborated in the subsequent section (1.3), a multitude of commercially available tools are applicable for analysing and optimising their performance. These tools have distinct methodologies and techniques, yet, all towards tackling the inherent complexities of multi-carrier systems. Nonetheless, it's important to note that each tool has its own set of strengths, target applications, and unique functionalities. Consequently, selecting the most suitable tool for a particular study hinges on the specific requirements, objectives, as well as the spatial and temporal scope of the research.

The implementation of sector coupling technologies is facing a significant limitation related to their economic feasibility. Many of these technologies are currently not competitive in various applications and regions, restraining their widespread adoption. Given that the adoption of these solutions is still at its early stage, further technological and economic investigations must be carried out [18]. In addition to economic challenges, national and international regulations may pose restrictions on sector coupling according to [19]; for instance, in the case study of the German energy sector, renewable energies and storage solutions may encounter obstacles due to CO₂ emission restrictions. While cross-sector coupling measures that involve

different energy carriers are on the rise, electrification remains the dominant approach for integrating end-use sectors [20]. Consequently, technologies such as power-to-hydrogen and power-to-heat, which enable cross-sector coupling, are not yet widely adopted. Based on the findings presented in [21], the integration of power-to-hydrogen infrastructure with other sector-coupling measures becomes vital in achieving a zero-emission energy system in Germany. Hence, the primary technical constraint impeding the implementation of sector coupling technologies lies in the lack of economic and technical competitiveness of certain technologies.

While the electrification of end-user facilities has been extensively studied, cross-sector coupling technologies still require further development both from a technological and environmental perspective due to their relatively recent adoption.

Several reviews have been produced so far on multi-carrier energy systems addressing a wide range of aspects going from technologies to modelling, optimisation and management approaches. Most of them only focus on technical aspects such as [22]-[23], which deal with the typical configurations of MES and the conversion technologies composing them. Mohammadi-Ivatloo et al. [24] addressed the issue of the storage facilities within the MES, whereas [25] dealt with the different demand response services that can be offered by MESs. Mohammadi et al. [26] reviewed the energy management approaches used for the MESs, whereas [27, 28] also reviewed the modelling approaches related to MESs, with the latter focusing the attention also on their interaction with external markets and networks.

1.2. Energy storage technologies, and their potential

Energy Storage Systems (ESS) represent technologies that facilitate the decoupling of energy production and consumption, allowing for asynchronous behaviour between the two. This characteristic enables a multitude of energy services, with the primary goal of optimising energy usage and addressing the intermittent nature of Renewable Energy Sources. Consequently, ESS holds a critical role, as it accelerates the energy transition process while ensuring efficiency. Research on ESS has numerous directions, ranging from technological advancements to material science. For instance, there is ongoing exploration of less expensive or higher energy density catalysts to enhance the technical performance of ESS. Additionally, the effective integration and operation of ESS with other systems are crucial considerations in this field.

Thanks to ongoing research efforts in this field, a diverse design of energy storage technologies has emerged, each boosting distinct key performance metrics. These technologies can be categorized in various ways, as illustrated by the works of different researchers [29, 30, 31]. However, the most prevalent classification involves categorizing them based on the storage phenomena they employ to absorb and release energy. Presently, the most widely utilised ESS technologies fall into four

1.2. Energy storage technologies, and their potential

main categories, which are briefly outlined below:

- Mechanical Storage: These technologies store energy through mechanical means.
- Electrochemical Storage: Energy is stored through electrochemical reactions.
- Electrical Storage: Energy is stored in an electrical form.
- Chemical Storage: Energy is stored via chemicals such as alternative fuels such as hydrogen.

The following sections provide a concise overview of these technologies, aiming to provide a general understanding of the key attributes associated with each.

1.2.1. Mechanical Energy Storage Systems

Mechanical ESS are storage solutions based on converting electrical energy into kinetic energy, and some of them are realized using the variation of the internal energy of a working medium such as water, air, or rocks. The most used mechanical ESS and their working diagrams are reported in Fig. 1.2, underlining the process of charging and discharging energy in each of them.

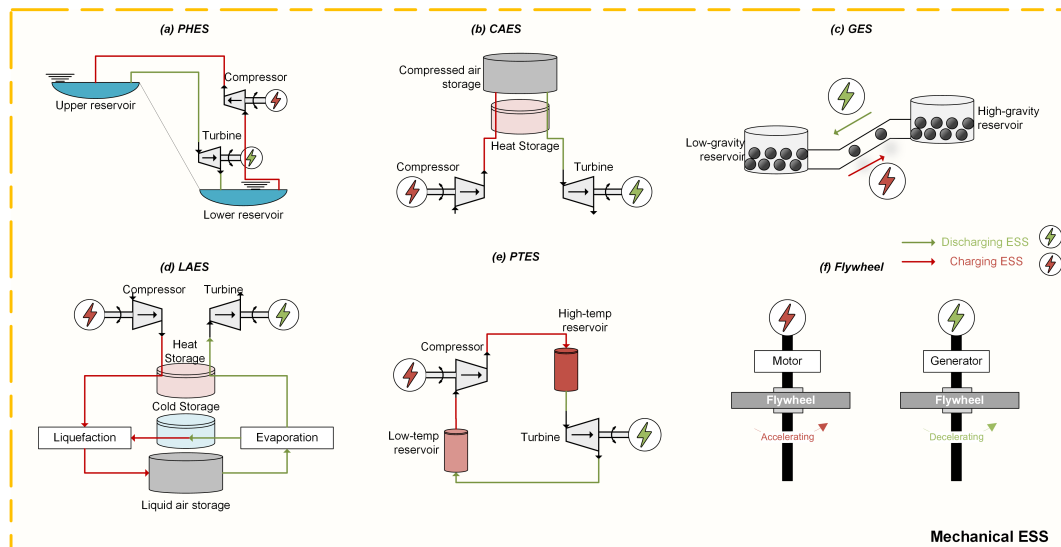


Figure 1.2.: Illustrated diagrams about mechanical ESS, namely Pumped Hydro Energy Storage (PHEs), Compressed Air Energy Storage (CAES), Gravity Energy Storage (GES), Liquid Air Energy Storage (LAES), Pumped Thermal Energy Storage (PTES) and Flywheel .

Pumped Hydro Energy Storages

Pumped Hydro stands as one of the most well-established energy storage technologies. It exploits the height difference of different reservoirs, using such differences

to convert energy between potential energy and electrical one in both ways, thanks to the use of a turbine and a compressor. This concept is illustrated in Fig. 1.2. It constitutes the overwhelming majority of global energy storage, capturing over 90% of the market share with an installed capacity exceeding 130 GW worldwide [30]. Being an exceptionally mature technology, much of its adoption occurred in Europe and the USA before 1990. More recently, China and India have been swiftly embracing PHES, as highlighted in the comprehensive review by Barbour et al. [32] on the current status and prospects of PHES. China's rapid growth in PHES is particularly notable, with the Fengning Pumped Storage Power Station boasting an impressive 3,600 MW capacity, making it the largest installed capacity globally as of 2021 [33]. Nevertheless, this record is destined to be exceeded, by an ambitious Australian project aiming to deploy a 5 GW PHES facility in Queensland [34]. The continued expansion of PHES highlights its enduring significance in the global energy storage landscape.

Having water as the working medium, the major limitation of this technology resides in its geographical limitations. Moreover, in recent years, the researchers' focus has switched to exploiting the smaller scale reservoirs, compared with the traditional ones, such approaches are so-called closed-loop, off-river-based PHES, which allows accomplishing a deeper penetration of the PHES, indeed they can be also installed in water supply systems, as demonstrated by the research carried out by Spedaletti et al. [35], using the Pumps-as-Turbine technology, which is a single machine that can work either as turbine or pump.

Compressed Air Energy Storage

CAES is a mechanical ESS that leverages the conversion of energy between the electrical and internal energy of compressed air. In its charging phase, electrical energy is employed to power air compressors, raising the air pressure to store it in designated reservoirs. During discharging, the high-pressure compressed air is released through turbines, thus converting the stored energy back into electricity. This process is depicted in Fig. 1.2. Furthermore, it can be categorized into three types based on the thermal treatment during the charging process: i) Diabatic CAES, ii) Adiabatic CAES, and iii) Isothermal CAES.

Among various demonstrators, two of the most renowned CAES plants are the Huntorf plant (321 MW) located in Germany and the McIntosh plant (108 MW) in the USA. Both of these plants have been operational for decades. Despite several large-scale CAES projects being announced during the 2010s, many of them faced challenges that prevented their completion or led to them being put on hold. These challenges included technical difficulties such as finding suitable storage reservoirs and managing high operating pressures, as discussed in [36]. In contrast, small-scale applications are not as cost-efficient as electrochemical competitors, partly due to the decreasing costs of lithium-ion batteries.

Gravity Energy Storage

GES employs a similar principle to PHES, involving the conversion of electrical energy into gravitational potential energy. However, GES replaces water with solid materials, offering a way to overcome the geographical constraints associated with traditional PHES setups. As illustrated in Fig. 1.2, during the charging phase, electrical energy is used to power electric motors that lift the mass from a low-gravity reservoir to a high-gravity one. Conversely, during the discharging phase, the gravitational potential energy of the mass is converted back into electricity through an electric generator.

GES provides a compelling solution for long-term energy storage, a prolonged lifecycle and low-generation capacity. It effectively covers the capacity range of 1-20 MW, offering storage times spanning from 7 days to 3 years, as highlighted in [37].

Liquid Air Energy Storage

LAES operates by utilising liquid air as its working fluid, employing a thermo-mechanical process. As depicted in Fig. 1.2, the system involves the liquefaction of atmospheric air from its gaseous state, storing it in cryogenic liquid form. When needed, the cryogenic liquid air is evaporated and heated before being expanded through turbines to generate electrical energy. The heat released during the liquefaction and the cold energy released during evaporation can be efficiently stored in specialized thermal energy storage systems, enhancing overall energy efficiency by their integration into the cycle.

LAES stands as a distinctive evolution of CAES, addressing the reservoir limitations while also increasing energy density owing to its liquid state [38]. These characteristics make LAES suitable for large-scale, long-duration energy storage without geographical constraints. Notably, the largest LAES facility, with a capacity of 50 MW_e/250 MWh, is situated in the UK and was announced in 2019 [39].

Thermal Energy Storage

The TESs are indispensable parts of the power system as they can recover the waste heat or thermal energy that is not possible to convert into another form of energy, to be used in heat demands like for the residential cases. Indeed they are widely deployed as support for concentrating solar panels, furthermore, they can be used also in CAES and LAES, to reduce overall energy consumption. However, these technologies do not couple different energy vectors, as only the thermal one is considered. To complete the Power-to-heat-to-Power cycle, as illustrated in Fig. 1.2 the Pumped Thermal Energy Storage adopts a conventional thermal engine cycle with a motor-compressor and expander-generator set to achieve the bidirectional energy conversion.

As a demonstrator of the technology, a team from Newcastle University developed a PTES plant in 2019, with 150kW/600kWh capacity with a round trip efficiency of

65% with the pressure ratio of 12 and stores the heat at 773 K [40].

Flywheels

A flywheel is a mechanical energy storage solution that transforms bidirectionally electrical energy into kinetic rotational energy through the acceleration or deceleration of a rotating mass known as the flywheel. In the charging phase, electric energy propels the electric motor to accelerate the flywheel, storing energy in kinetic form. Conversely, when required, the kinetic energy of the flywheel is harnessed by a generator, converting it back into electrical energy. Its performance mainly depends on the moment of inertia of the rotor and rotating speed. They are usually categorized as low-speed flywheel (<10'000 rpm) and high-speed flywheel (10'000-100'000 rpm). They are characterized to have high power density and extremely low energy density ESS solution, thus they are primarily used for short-duration applications such as power quality and stabilization in power grids.

Currently, the largest flywheel energy storage system installed accounts capacity of 300 kW, built in at Mt. Komekura in Yamanashi prefecture in 2015, used for balancing a 1MW solar plant [41].

1.2.2. Electrical and electrochemical Energy Storage Systems

As for electrical and electrochemical energy storage solutions, they store the electrical energy based on an electrical capacitive process or reversible electrical reactions to store electrical energy. Due to their storage process, these energy storages guarantee higher round-trip efficiency, compared to competitors, yet due to their raw material cost, the large-scale applications (>GW) of these solutions are still not widespread.

The ones mostly adopted are illustrated in the Fig. 1.3, illustrating their working principles, furthermore, in the subsequent paragraphs they are briefly described.

Lithium-ion batteries

Lithium-ion batteries (LiBs) have been the dominant ESS technology in the realm of portable electronics for decades. Their exceptional energy density and cycling performance, coupled with continuous cost reductions in raw materials, have solidified their position. However, beyond their conventional role in small-scale applications, LiBs have also experienced rapid adoption for grid-level energy storage. This trend addresses the challenge of managing the intermittent output of renewable energy sources.

As depicted in Fig. 1.3, a LiB comprises two electrodes: typically a lithium-oxide cathode and a graphite-based anode, separated by a nonaqueous lithium-ion-conducting electrolyte. During charging, an external electrical source prompts Li^+

1.2. Energy storage technologies, and their potential

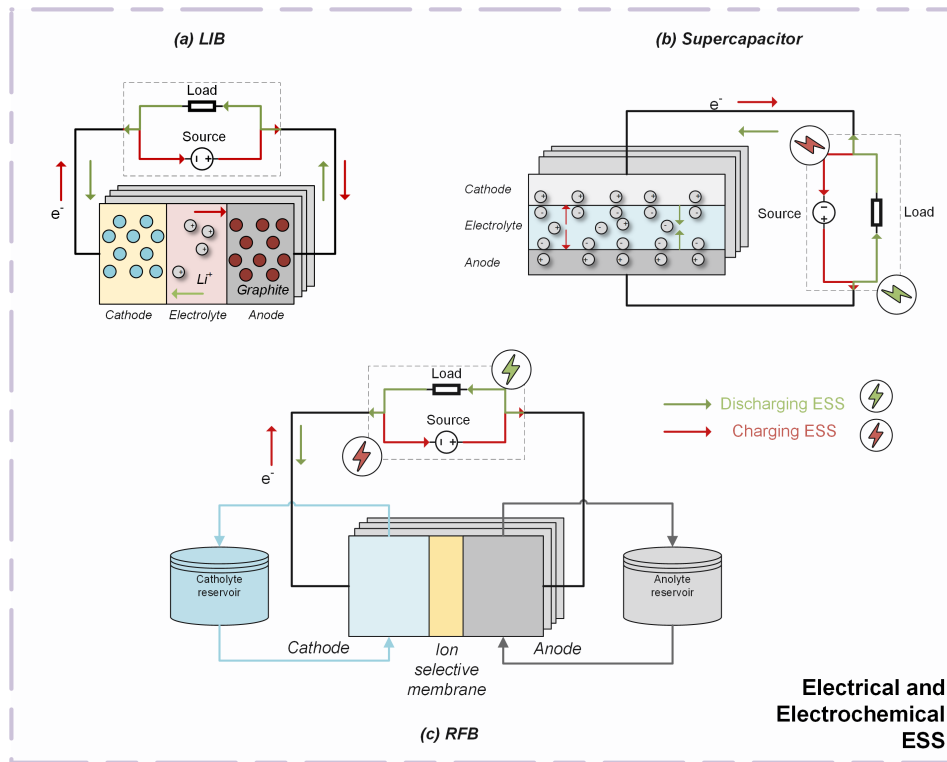


Figure 1.3.: Electrical and electrochemical ESS. while the supercapacitor is the only electrical energy storage, both Lithium-ion battery (LiB) and Redox Flow Battery (RFB) are electrochemical ones.

ions to migrate from the cathode, traversing the electrolyte layer, until they reach the graphite layers of the anode. Simultaneously, electrons flow externally. In contrast, during discharging, ions move from the anode to the cathode, while electrons follow the reverse path, inverting the process compared to charging.

LiBs are frequently classified according to the various cathode materials they employ, as the cathode plays a pivotal role in their performance. Common cathode materials encompass Lithium iron phosphate (LFP), Lithium manganese oxide (LMO), Lithium nickel cobalt oxide (Li-NCA), and Lithium nickel manganese cobalt oxide (Li-NMC). These distinct chemistries yield diverse performance indicators and trade-offs.

At present, the evolution and widespread use of LiBs are experiencing a remarkable surge, driven in part by the rapidly growing electric vehicle market. Furthermore, applying LiBs in stationary scenarios has gathered attention due to their adaptability, remarkable energy density, and fast response time. Indeed, LiBs are beginning to be integrated into Local Energy Communities as supporting tools. This technology has been extensively explored, evaluating its potential influence and significance within the broader energy community context.

1.2.3. Hydrogen Energy Storage

Over the past years, hydrogen has gained increasing attention, both from policymakers and researchers, thanks to its vast applicability as an energy carrier, indeed it can substitute the conventional fuel consumption sectors, using the so-called green hydrogen, which is the hydrogen produced using renewable energy through the water electrolysis process, cutting down the emissions.

Moreover, hydrogen can be effectively converted back into electric energy through fuel cells. These technologies draw hydrogen from the storage, and oxygen from the atmosphere, generating electric energy and water as a byproduct, as depicted in Fig. 1.4.

Hydrogen stands apart from other energy storage solutions due to its stand-alone components for each stage, namely production, storage, and consumption technologies. This characteristic results in a comparatively lower round-trip efficiency (approximately 40%) compared to its counterparts. However, it offers distinctive advantages, including cross-vector solutions, long-term storage, and energy and power decoupling.

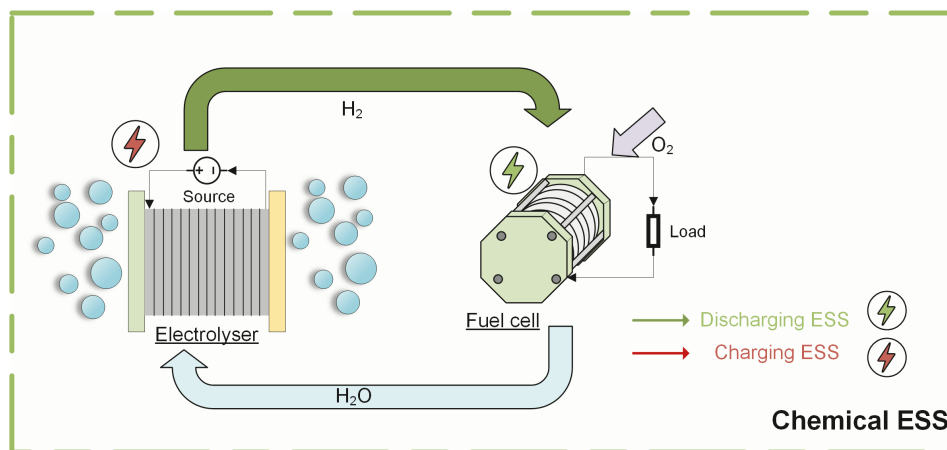


Figure 1.4.: Chemical ESS/Power-to-hydrogen

1.2.4. Energy Storage Systems comparison

Power and energy serve as crucial performance indicators for ESS technologies. Based on these indicators, the most suitable technology is selected for a specific application. Power refers to the peak power that can be injected or extracted from the system. For the majority of ESS, this power rating remains consistent during both the charging and discharging phases. On the other hand, energy capacity signifies how long the ESS can sustain operation, representing the accumulation of power over time. Fig. 1.5 provides an illustration of power ratings and operation times for different ESS technologies. In Fig. 1.6, the energy and power density among these ESS technologies are presented. These indicators offer insights into

1.2. Energy storage technologies, and their potential

the energy-to-power ratio for the same volume. A higher value in these indicators implies that less volume is required to store a certain amount of energy or power. By considering these key metrics, stakeholders can effectively match ESS technologies with specific applications, optimising their performance for various energy storage needs.

Generally speaking, mechanical ESS is adopted for large-scale and stationary applications, for their low energy and power densities, however, they possess an extended lifetime with slow response time, with flywheels being a notable exception. In contrast, electrical and electrochemical ESS provide higher energy and power densities, making them well-suited for dynamic operations such as transportation or electronic devices. Nonetheless, these technologies generally have a shorter lifespan compared to their mechanical counterparts. Estimating their lifetime is intricate, as it depends on various operational strategies such as temperature, depth of discharge, and C-rates. Hydrogen-based solutions offer an expansive power rating range and possess response times that complement electrochemical systems. Additionally, they provide energy and power densities comparable to Lithium-ion batteries.

1.2.5. Energy storage systems for local energy communities

To integrate ESSs, as a support measure and enhance the deployment of LECs, as discussed in Section 1.1, it is essential to identify the appropriate type, that meets specific criteria:

- **Suitable Power Range:** Given that LECs are typically designed for residential end-users, the selected ESS should fall within the power scale of 100-1000 kW to effectively cater to the aggregated power demand.
- **Modularity:** The ESS should be modular in design, allowing it to be deployed at a smaller scale if necessary. In extreme cases, it should even be deployable on a per-end-user basis, providing flexibility and scalability.
- **High Energy and Power Density:** An ESS with high energy and power density is preferable, as it maximises the use of available space within the LEC. This is particularly important considering the overarching goal of energy transition and increased penetration of renewable energies.
- **Stationary Application:** The chosen ESS should be optimised for stationary applications, aligning with the typical requirements of LECs for consistent and reliable energy supply.
- **Operational Time frame:** The ESS should be capable of operating efficiently within daily cycles, typically spanning a few hours. This aligns with the recurrent patterns of energy consumption and solar production within the LEC.

While there are several ESS that could potentially meet these requirements, two technologies have gathered significant research attention due to their capacity to fulfil the specified criteria. These technologies are Lithium-ion batteries and hydrogen energy storage. Lithium-ion batteries stand out as they fulfil all the outlined specifications, with a high round-trip efficiency. They not only offer the potential to enhance the electrification of end-users within the specified power range, but they also possess the necessary modularity, high energy, and power density, and are well-suited for stationary applications with an operational time frame matching the recurrent behaviour of energy consumption and solar PV production in LECs. On the other hand, hydrogen energy storage is an appealing solution for coupling different energy carriers, such as electric and heat energy, effectively substituting conventional natural gas-fed systems. This technology has demonstrated promise in enhancing the energy transition within LECs. Given the suitability and importance of both lithium-ion batteries and hydrogen energy storage, these two technologies have been selected as the focus of this thesis study.

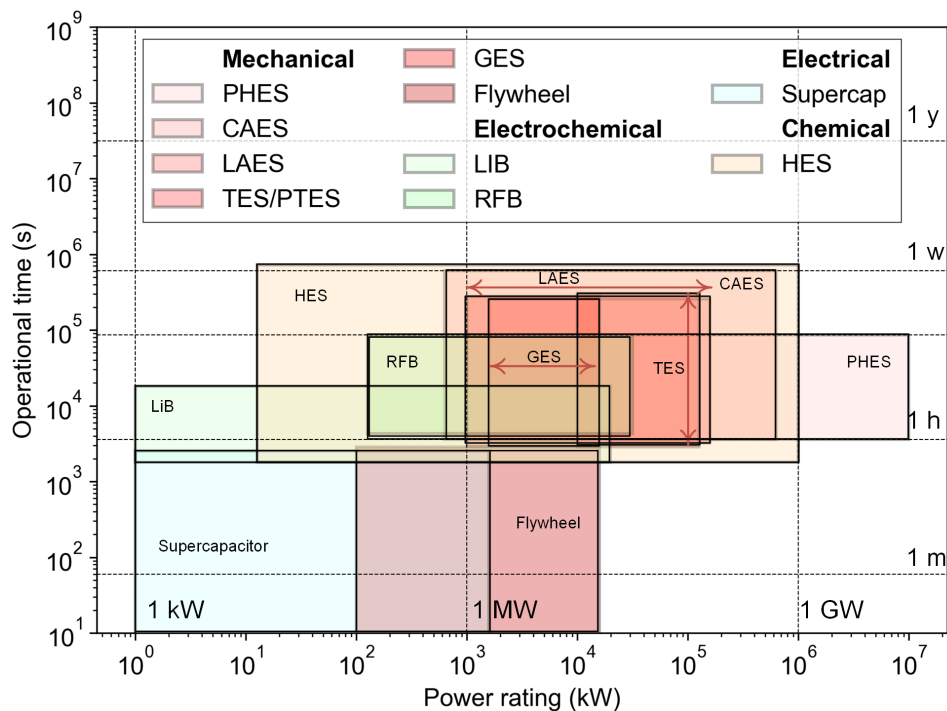


Figure 1.5.: Energy storage technologies comparison: power rating vs. operational time.

1.3. Energy planning & system modelling: tools to boost energy community deployment

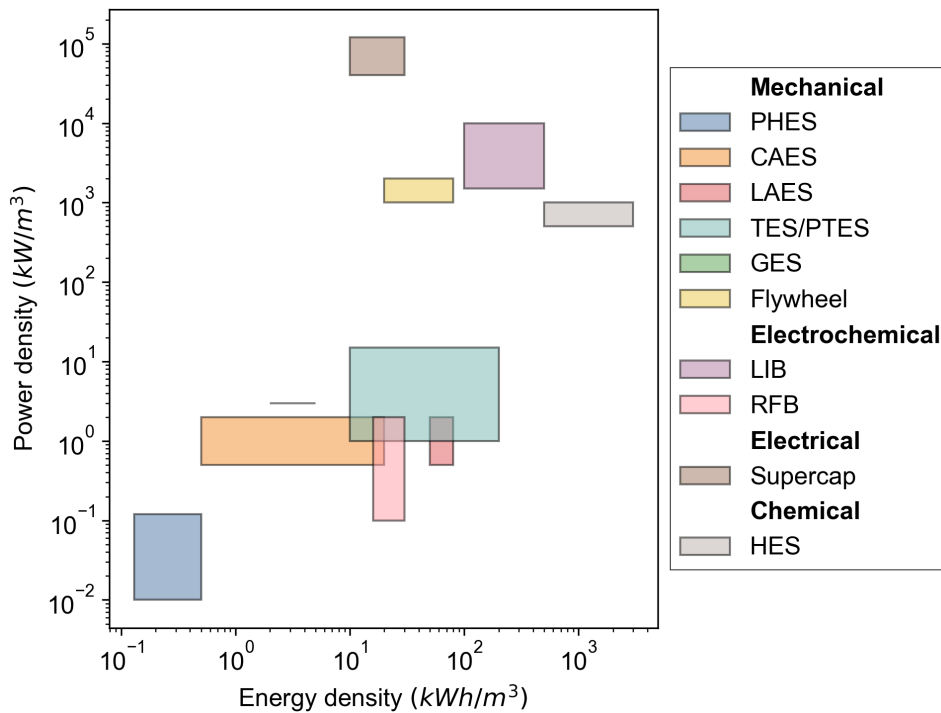


Figure 1.6.: Energy storage technologies comparison: energy density and power density.

1.3. Energy planning & system modelling: tools to boost energy community deployment

Models play a vital role in the strategic planning and day-to-day operation of energy systems. They provide the capability to forecast, assess, and enhance energy frameworks, an achievement that would be challenging without their aid. Notably, research in local-scale energy planning has captured substantial interest over the past years, with the goal of addressing local-scale energy policies oriented to environmental goals. When comes to LEC energy planning, the primary constraint of the research is to have a comprehensive overview of the interactions and synergies among different types of Distributed Energy Resources (DERs), energy vectors, and energy distribution networks. Furthermore, a vast amount of tools have been developed over the years. Moreover, Chang et al. [42] reviewed 54 of them, dedicated to energy transition planning.

The multitude of energy modelling tools available is derived from their inherent flexibility, allowing them to be tailored to specific application cases. In theory, an energy modelling tool can incorporate an array of characteristics without bounds. However, such customisation comes with a trade-off of escalating computational demands, a challenge that is yet to be fully addressed. Moreover, energy modelling tools can be generally categorised based on several criteria: i) the adopted methodology, ii) assessment criteria, iii) multi-objective approach, iv) spatial and

temporal resolution, v) geographical and temporal coverage, vi) analytic approach, vii) mathematical approach, and viii) technical coverage and multiple energy carriers integration. Despite these categorisations, energy modelling tools commonly provide the flexibility to adapt, customise, and switch among different criteria. Furthermore, the following paragraphs provide a brief description of these criteria, where in Fig. 1.3 the provided categorisation is summarised.

1.3.1. Energy planning: methodology

The methodology of the energy planning tools refers to the scope of the tool since it can be used for various purposes, generally, it can be used for:

- **Optimisation:** Is the prevailing application case for energy modelling [43]. In this approach, the model simulates all possible scenarios within an energy framework and evaluates them using an objective function. By minimising or maximising this function, the tool generates an optimised scenario [44]. Such scenarios provide the most suitable energy system mix based on the specified objective, and optimisation is commonly used for district-level energy system modelling.
- **Forecasting:** Serve for scenario analysis purposes. They facilitate the exploration of energy systems under specific conditions, enabling predictions of system behaviours such as future energy demands or costs [45].
- **Back-casting:** Are specialised for specific scenario analysis tools. Modellers begin with a predefined future state or a set of system parameters. The objective of back-casting models is to chart plausible pathways for the system to reach that desired state. These models are typically employed in national-scale energy planning, assisting energy policymakers in formulating suitable actions to achieve their envisioned goals [46].

These diverse methods can be integrated into a single energy planning tool. Depending on the modeller's focus and initial conditions, the appropriate methodology can be selected to suit the context and objectives of the analysis.

1.3.2. Energy planning: Assessment criteria

Assessment criteria function as performance indicators in models to determine the optimal solutions, particularly in the context of optimisation methodologies. While the specific objectives can vary based on the modeller's preferences, several widely used criteria include:

- **Financial:** This is among the most commonly employed criteria, aiming to identify the most cost-effective scenario. The assessment can be conducted using various metrics such as the Levelised Cost of Energy (LCOE) or by

1.3. Energy planning & system modelling: tools to boost energy community deployment

considering the total investment in technologies, encompassing both capital and operational expenses.

- **Environmental:** Focusing on reducing the carbon emissions of the energy framework, this criterion addresses the environmental impact of the considered scenarios.
- **Energy efficiency:** This criterion seeks to maximise the ratio of energy delivered to end-users to the consumed energy resources.
- **Grid independence:** To minimise the reliance on imported energy from the national grid, this criterion aims to encourage solutions that enable island operation.

While these criteria represent common objectives, the modeller's choice of criteria can align with the specific goals and context of the analysis.

1.3.3. Energy planning: Multi-objective approach

Given the variety of potential assessment criteria, some applications require the simultaneous evaluation of multiple objectives. This leads to multiple-objective optimisation, yielding the so-called Pareto curve, which comprises the optimal solutions for the various considered objectives. Each point on the Pareto curve represents an optimal solution, though different points correspond to varying indicators for distinct objectives. Ultimately, the selection of the best solution from the Pareto curve depends on the modeller's preferences and expertise.

Hence, the process of addressing the Pareto curve solutions is at the core of multi-objective modelling, and there are several approaches to accomplish this in the context of energy system modelling:

- **Weighted-Sum:** This involves converting a set of objectives into a single objective by assigning weights to each individual objective function. By adjusting these weights, different solutions along the Pareto curve can be obtained, allowing for trade-offs between the objectives [47].
- **Epsilon-Constraint:** Developed by Mavrotas in 2009 [48], this approach transforms the multi-objective problem into a sequence of single-objective sub-problems. It treats one objective as the main objective and the others as constraints. Each sub-problem incorporates a constraint that limits the value of the constrained objectives, with the trade-off governed by the parameter ϵ (epsilon).

Both of these methods provide means to navigate the complexity of multi-objective modelling and it is completely based on the modeller's preferences and the goals of the analysis which approach to adopt.

1.3.4. Energy planning: Spatial & temporal resolution and coverage

Spatial resolution is essential in scenarios involving interconnected technologies like district heating, district cooling, as well as distribution and transmission grids. Depending on the level of detail required, the spatial resolution allows for the mapping of energy demand at various scales, ranging from individual users and buildings to entire districts or even entire cities.

Temporal resolution is highly application-dependent. For technologies necessitating rapid dynamics, such as frequency regulation, a high-resolution time scale of milliseconds to seconds is imperative. On the other hand, power flow or generation control might require resolutions in the range of minutes to hours. For medium-term planning, like technology expansion plans and demand predictions, an hourly resolution is generally adequate. For broader energy policy analysis, scenario assessments, and production cost modelling, an annual resolution might suffice.

Spatial coverage means the geographical extent covered by the model. It can span from a local level (single consumer) to continental, intercontinental, or regional scales [49]. Energy modelling tools can operate on various time frames, ranging from a single day or year to multiple decades or the lifespan of technologies. For district-level modelling, a time frame of at least one year is often required to capture seasonal variations and annual patterns [46].

1.3.5. Energy planning: Analytic approach

Depending on the perspective and emphasis of the modelling, the analytical approach can be categorised as follows:

- **Bottom-up:** This method starts with subsystems, which are then interconnected to create an overarching system. It offers a detailed insight into technological aspects but may struggle to accurately estimate macro-economic factors. This approach is often used for identifying suitable technologies for specific applications and is sometimes referred to as techno-economic modelling [50].
- **Top-down:** Beginning with a broad view of the entire system, this approach breaks down into subsystems. It allows for the inclusion of the entire economy but may lack technological specifics. It frequently relies on historical data to forecast future system behaviours.
- **Hybrid:** Combining elements of both the bottom-up and top-down methods, the hybrid approach brings more complexity to the model. Despite its intricacies, more energy planning tools are adopting this approach [51].

For the modelling of local energy communities, which is a district-level challenge, high technical detail is essential. Consequently, district modelling tools typically opt for a bottom-up approach to ensure an accurate representation of the technological aspects involved.

1.3.6. Energy Planning: Mathematical approach

Various energy models employ diverse mathematical and computational approaches to achieve their objectives. In Fig. 1.7, the distinctions among traditional mathematical methods are depicted. Other methods can also be employed:

- **Linear Programming:** This approach describes the system's behaviour using linear mathematical functions, to be merged finally into an objective function. While it is one of the oldest and easiest methods, its application is limited due to the inherent non-linearity of real-world systems [52].
- **Dynamic Programming:** To handle non-linear relationships, dynamic programming divides the overarching problem into smaller sub-problems that can be solved using linear relations. Alternatively, piece-wise linearisation functions can be used.
- **Mixed Integer Linear Programming (MILP):** Combining elements from the previous approaches, MILP introduces integer values for specific decisions. This is beneficial for binary decisions like turning technologies on/off or specifying the number of certain technologies [49].
- **Stochastic Programming:** An extension of linear and dynamic programming, stochastic programming considers the statistical fluctuations of parameters and their uncertainties. This approach provides not only an estimated solution but also an understanding of potential solution variations [53].
- **Heuristic and Artificial Intelligence (AI) approaches:** Heuristic models use a trial-and-error approach to approximate solutions. While offering detailed problem analysis and flexibility in considering changing system properties, these methods require significant programming knowledge and parameter tuning. AI approaches like Fuzzy logic, agent-based programming, Particle Swarm Optimisation, genetic algorithms, and neural networks are gaining attention but are still relatively rare in energy modelling.

For district-level modelling, Mixed Integer Linear Programming is commonly utilised due to its balanced complexity and level of detail. Dynamic programming approaches are used less frequently. The use of AI techniques is still limited but is gaining traction, while stochastic programming is applied on an occasional basis.

1.3.7. Energy planning: Technical coverage

Originally, energy modelling tools were predominantly employed for power system analysis, focusing solely on electricity as the energy carrier and all associated electric energy systems [54]. However, to effectively utilise energy resources and meet evolving customer needs, these limitations need to be addressed. Consequently,

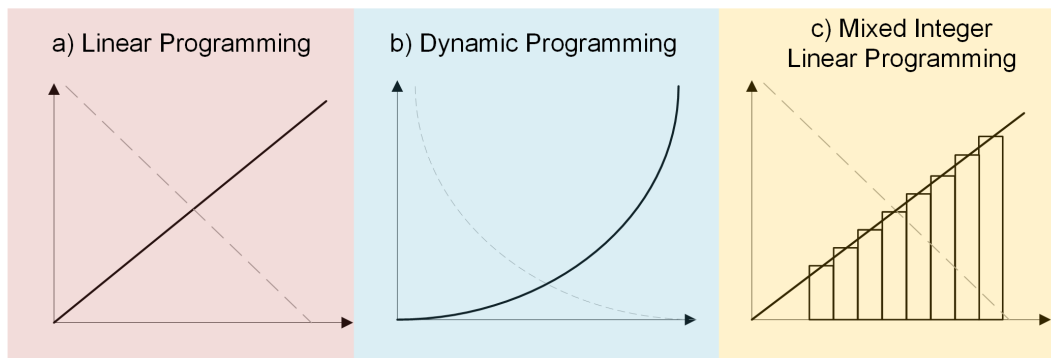


Figure 1.7.: Illustration of different mathematical approaches: the intersection point represents the solution of the model.

modern energy modelling tools are increasingly designed to accommodate multiple energy carriers. This expansion typically includes electricity, heat and cooling energy, water, and natural gas energy carriers. Moreover, in recent years, the integration of hydrogen as an energy vector for sector coupling has also gained prominence in these tools.

For the concept of the local energy community, the chosen tool must consider multiple energy carriers, as the cross-sector coupling approach forms one of its foundational pillars.

1.3.8. Energy system modelling applied to Local Energy Communities

As discussed in this section, the world of energy system modelling is expansive and highly customisable. Consequently, pinpointing the ideal tool for each specific application is a challenging endeavour. In the context of this thesis, which centres on district-level, multi-energy carrier local energy communities and includes assessments of energy storage integration and their ramifications, certain features become essential criteria for selecting an appropriate tool. These features encompass:

- **Methodology:** Primarily optimisation-oriented, aiming to determine the optimal energy mix, including extensive energy storage integration.
- **Assessment criteria:** Diverse, contingent upon the specific application's objectives. Given the local energy communities' role in decarbonisation, multi-objective (financial and environmental) modelling is essential.
- **Spatial resolution and coverage:** Ideally, a spatial resolution covering each building within the energy community would be the best case. However, obtaining the requisite energy demand data for such detailed spatial granularity is often challenging.
- **Time resolution and horizon:** Ranging from minutes to hours, covering at least a year to provide the granularity needed for identifying optimal technology

1.3. Energy planning & system modelling: tools to boost energy community deployment

configurations.

- **Analytic approach:** Bottom-up, focusing on technological details, which is a central theme of this thesis and vital for comprehensive impact assessments.
- **Mathematical approach:** Mixed Integer Linear Programming is preferable, striking the right balance between required detail and programming complexity.
- **Technical coverage:** Encompassing the potential expansion for multiple energy carriers, given the multi-energy carrier nature of local energy communities.

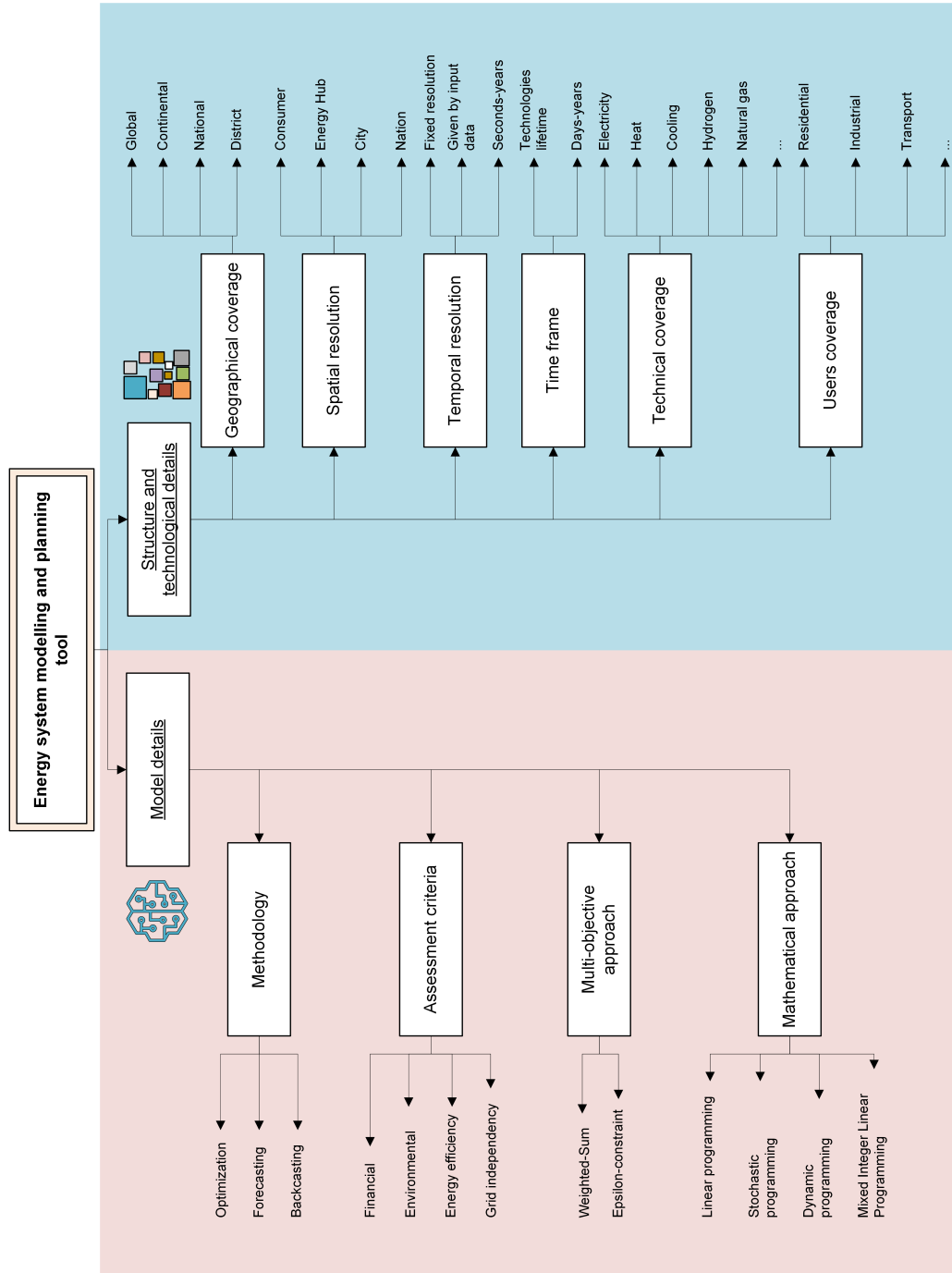


Figure 1.8.: Energy planning tool properties and categorization.

1.4. Research question

Having laid the foundational groundwork for this thesis by addressing the general background (subsection 1.1), continuing with the technological perspective (subsection 1.2), and providing an overview of the system level (subsection 1.3), the research question that this thesis wants to address is the following:

"Within the context of energy storage integration, how to bridge both technical and system perspectives of the energy system modelling, where the subsystem's critical properties are included at the system level, as well as systematic limitations?"

Moreover, it can be divided into the following more detailed research sub-questions:

1. ***How to capture the technological details of the Power-to-Hydrogen process?***

Since hydrogen production is not yet a mature technology, its production has still many technological uncertainties, such as dynamic operations, inefficiencies and most influenced operational parameters.

2. ***How to model the integration of Power-to-Hydrogen and all its related auxiliaries?***

Compared to the lithium-ion battery, which is a stand-alone technology, hydrogen production requires many more auxiliary technological components, such as heat exchangers, pumps, compressors etc. To effectively consider all these components their interconnection has to be effectively modelled.

3. ***How to deal with fluctuation in power supply for Power-to-Hydrogen?***

To produce green hydrogen, the intermittency of energy production from renewable energies must be considered. Furthermore, it has a significant impact on the operational state of the hydrogen production plant.

4. ***How to capture the degradation phenomena of Lithium-ion batteries?***

Compared to hydrogen, the Li-ion battery, thanks to its wide application over the last decades, is technologically mature. However, its efficient energy management, within the context of stationary application, where it is integrated with other energy systems, its degradation phenomena is not fully explored.

5. ***Which is the best solution for long-term storage?***

Although for short-term energy storage, the Li-ion battery is the absolute winner, thanks to its excellent round-trip efficiency, things can differ for long-term storage applications, especially due to the self-discharge phenomena of batteries.

6. How to effectively include these technologies into a system modelling and assess their impact?

Their integration into the LEC context, moreover their integration impacts, among them and also other technologies are investigated and discussed.

7. How to include the dynamic variation and investment stages of parameters in medium-term energy planning?

The common approach of energy planning is to consider a typical year and based on it, estimate future trends. However this approach is not suitable due to the ever-changing energy policy situation, moreover, different investment stages, i.e. change of the already existent technologies during the planning horizon, due to the change of parameters, such as cost reduction, have to be assessed.

All these compelling questions are rigorously examined and answered throughout this thesis, spotlighting the insights discovered and their profound implications for future advancements.

1.5. Outline of the thesis

The thesis is structured into three main parts. The initial two delve into the technological details of the ESSs under examination. Following this, the thesis transitions into the third part, which encompasses the system-level analysis. The subsequent part of the thesis encompasses two distinct case studies that establish an interconnection between the technology and system-level analyses, with the primary objective of exploring the integration of ESS. Finally, Chapter 6, encapsulates the Conclusions and Recommendations, offering a comprehensive overview of the the thesis.

Part I. Technological approach: Hydrogen and Lithium-ion battery modelling

In this part, the technical modelling of the ESS is discussed, namely power-to-hydrogen and lithium-ion battery degradation models are deeply investigated.

Part II. System approach: energy planning

Following a system approach, research gaps about searching for optimal alternatives, and multiple investment stages are examined in this part.

Part III. Energy storage details into systems approach: case studies

This part presents two distinct case studies, that effectively integrate technological aspects into a system-level approach.

Conclusions, Recommendations and future development

This chapter encapsulates the thesis's findings, offers recommendations regarding energy system analysis, and provides insights into prospects and developments.

Part I.

Technological approach: Hydrogen and Lithium-ion battery modelling

Chapter 2.

Hydrogen as energy storage

I believe that water will one day be employed as fuel, that hydrogen and oxygen which constitute it, used singly or together, will furnish an inexhaustible source of heat and light, of an intensity of which coal is not capable.

Jules Verne

As briefly explained in the Introduction section, hydrogen is one of the key players in tackling climate change. Since it is an energy carrier that can be adopted in several sectors, like hard-to-abate industries such as the chemical and petrochemical sectors, the steel-making industries, and the transportation sector to reduce their carbon footprint [55]; Indeed, policymakers put substantial effort, through a dedicated framework to incentive its adoption and research activities. Thus, almost over than half of EU countries have developed their national hydrogen development plan [56].

Moreover, hydrogen, despite of being a versatile energy carrier, its supply chain is far from being mature. Indeed, different perspectives, including its production, storage, and consumption are subject to be further explored before being fully commercially available.

With the focus on integrating hydrogen into the local energy communities, this chapter has the goal to illustrate the research activities developed, focusing primarily on the production and storage aspects, the reason for excluding the consumption side are twofolds:

1. The fuel cell technology, which is the conversion system that consumes hydrogen to produce the electricity and heat, is similar to electrolyser ones. Moreover, the electrochemistry process and physical equations are the same but with the process reversed.
2. Hydrogen's high adaptability allows it to be consumed from many potential end-users, makes it difficult to handle the technological overview of all applications of the potential users.

Therefore, hydrogen consumption has not been investigated in detail.

The chapter is structured as follows; first, the introduction about hydrogen limitations and applications in the local energy community context is discussed, to be followed by the technology detailed models, developed for alkaline water electrolysis and the metal hydrides storage¹. Of course, many technologies can be adopted, for both hydrogen production and storage, the selection of these specific ones is as result of the low-investment cost of alkaline water electrolysis, which allows its penetration faster, compared with other technologies, and metal hydrides storage, as the innovative solution of storage, since is stored in the solid matter.

2.1. Hydrogen limitations and opportunities

Hydrogen, as an energy carrier, is still subject to numerous limitations from various perspectives. From a regulatory standpoint, as of October 2023, no well-defined national or international standards have been established. These standards should address aspects like the adoption of green hydrogen production, standardisation of purity levels, certification of hydrogen sources (colour-coded hydrogen categories), and the provision of incentives. Additionally, safety concerns are associated with hydrogen due to its highly flammable nature and lack of odour, making leaks more difficult to detect. Furthermore, its flame is nearly invisible, adding another layer of complexity to its safe handling.

In this thesis, two specific technological aspects of hydrogen have been thoroughly examined. These include its low production efficiency and associated costs, as well as challenges related to its storage. Hydrogen has an exceptionally low density of 0.0899 kg/Nm³, which is approximately ten times lower than that of natural gas [59]. This low density translates to a higher volume requirement under the same conditions, in comparison to other gases. Despite possessing a commendable gravimetric heating value of 141.80 MJ/kg, its volumetric heating value is approximately 12.7 MJ/Nm³, which is almost four times lower than that of natural gas.

However, hydrogen presents numerous advantages, particularly from the perspective of energy communities, which are as follows:

- High energy density and stability for long-term storage: Hydrogen offers the advantage of high energy density and stability, making it an ideal solution for long-term energy storage in energy communities. This capability contributes to the potential achievement of energy independence for these communities [60]. Its suitability is particularly notable in the context of renewable energy sources with their inherent seasonality, addressing the differing electricity production and consumption patterns, especially during peak periods such as summer and winter.
- Residential gas reduction: Hydrogen, when mixed with natural gas, provides

¹Some of the work described in this chapter has been previously published in [57], [58]

2.2. Power-to-hydrogen: water electrolysis

a viable avenue for decarbonising residential gas consumption. Demonstrators and pilot projects have showcased the feasibility of incorporating 10%_{vol} hydrogen content into the existing infrastructure without requiring significant alterations [61, 62].

- Power-to-Heat coupling: Through the utilisation of high-temperature fuel cells, hydrogen enables simultaneous electricity and heat generation. This capability holds the potential to effectively meet both the electricity and heat demands within energy communities.
- Energy storage for enhanced flexibility: Hydrogen's can serves as an energy storage technology, which provides the necessary energy flexibility. Beyond a certain power threshold, energy communities can actively participate in the flexibility market, thereby gaining additional economic advantages.

Therefore, despite numerous bottlenecks, hydrogen's distinctive characteristics make it a versatile and promising option for energy communities seeking sustainable and efficient energy solutions.

2.2. Power-to-hydrogen: water electrolysis

Hydrogen can be produced in different ways, and based on the technology process used, it can be categorised using colour codes. Despite its various colours, the main colour codes of hydrogen are:

- Grey hydrogen: which is the hydrogen produced using the Steam Methane Reforming or auto thermal reforming process, which requires natural gas as feedstock. It is the most common and cheapest form of hydrogen production but is also the most carbon-intensive.
- Blue hydrogen: It is based on the grey hydrogen process, in addition to carbon capture technologies, yet has still a low-carbon form of hydrogen production.
- Green hydrogen: It is produced using renewable energy through water electrolysis, therefore, it is considered the most sustainable and environmentally friendly form of hydrogen production.

As the solution to the energy transition, the future perspective should be based on the adoption of the green hydrogen pathway, using water electrolyser technologies.

Indeed, a variety of electrochemical devices designed for hydrogen production through water electrolysis (electrolysers) are available, each at different levels of technological maturity, each with its own distinct advantages and disadvantages. As of the current state, there are four primary electrolyser technologies: alkaline electrolyser, Proton Exchange Membrane (PEM) electrolyser, solid oxide electrolyser (SOEC), and anion exchange membrane (AEM) electrolyser. Among these, only

the first two technologies are considered commercially available on a large scale, while the latter two are still in the demonstration phase and are not yet suitable for large-scale commercial projects (>MW) [63].

The alkaline electrolyser technology has been in use for over a century, making it the most mature electrolysis technology available. It boasts the longest proven lifetime among electrolysis technologies. This technology employs a liquid electrolyte, with the electrodes immersed in a solution containing either potassium hydroxide (KOH) or sodium hydroxide (NaOH). Additionally, a diaphragm is used to separate the two electrodes, allowing only hydroxide ions (OH⁻) to move from the cathode to the anode. This design facilitates the electrochemical reaction responsible for hydrogen production. Alkaline electrolysers offer numerous advantages for various applications, with their main strengths encompassing:

1. Low investment cost, This is attributed to their technology readiness and the use of cost-effective catalysts [64].
2. Extended lifetime, Alkaline electrolysers can operate for more than 20-25 years. In contrast, PEM electrolysers currently offer an operational life of approximately 10 years.

Thanks to these characteristics, alkaline technologies are highly appealing for large-scale hydrogen production applications. However, they also come with several technical limitations:

1. Low current density: The low current density (0.7-0.7 A/cm²) leads to lower efficiency, as current density is directly tied to hydrogen production through the Faraday equation [63].
2. Partial load safety threshold: Alkaline electrolysers have a lower safety threshold for partial load operation (15-20 %). Operating below this threshold increases the hydrogen content on the anode side, potentially reaching flammable levels. International standards set the safety threshold for hydrogen to oxygen side at 2%, rendering partial load operation below 15-20% unfeasible [65].
3. Low working temperature: The use of a liquid electrolyte imposes a limitation on the working temperature, generally not exceeding 80°C. Although higher temperatures reduce electrical losses, using thermal energy recirculation (possible only in SOECs), this restriction hinders the electrolyser's operating range [66].
4. Low working pressure: Alkaline electrolysers generally operate at low pressure to minimise internal losses. This contrasts with the higher pressure operation, which mitigates the compression of gaseous hydrogen at the electrolyser outlet. Currently, alkaline electrolysers can achieve a maximum pressure of 30 bars [67].

2.2. Power-to-hydrogen: water electrolysis

Other electrolyser technologies offer solutions to overcome these limitations but often require a higher investment in catalyst materials.

This thesis exclusively delves into the technological specifics of alkaline electrolysis, due to its strong potential for integration into energy communities in the near future, driven by its aforementioned strengths.

For the sake of clarity, other technology concepts are presented in Fig. 2.1, and a comparative table highlighting the main differences between these technologies is provided in Tbl. 2.1.

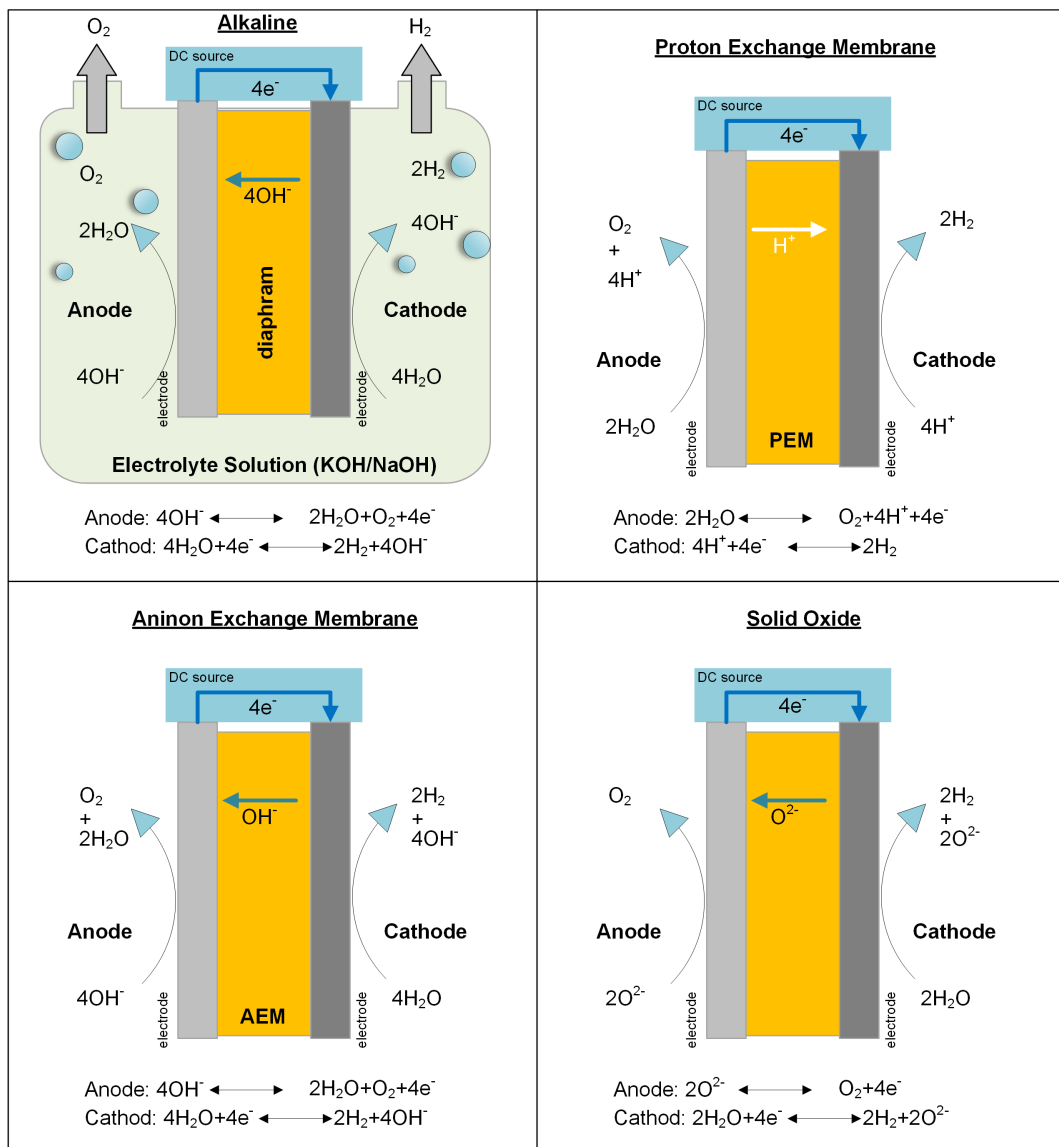


Figure 2.1.: Chemical reactions of four types of available electrolyser technologies.

Table 2.1.: Key performance indicators for four electrolyser technologies [67, 68, 69, 70].

	Alkaline	PEM	AEM	SOEC
Cell pressure [bars]	<30	<70	<35	<10
Cell temperature [°C]	60-80	50-80	60-80	800-1000
System efficiency [kWh/kg _{H₂}]	50-78	50-83	57-79	<45-55
Lifetime [khs]	60	50	<5	<20
Partial load range [%]	15/20-100	0-100	NA	0-100
Degradation range [μ V/h]	<3	<14	NA	NA
Investment cost [\$/kW _{el}]	500-1000	700-1400	NA	NA

2.3. Alkaline water electrolysis modelling

The alkaline water electrolysis reaction is achieved in an electrolysis cell, illustrated in Fig. 2.1. Moreover in order to achieve hydrogen production at a large scale, cells are assembled into a stack by the mean of bipolar plates, i.e. the cells are electrically connected in series. Understanding the dynamics of water electrolysis requires a combination of experimental investigation and modelling. Although the experimental approach provides higher accuracy, it comes with certain limitations:

1. High operational cost: Setting up and operating the experimental plant incurs significant expenses.
2. Lack of customisability: Not all relevant parameters can be effectively monitored in many cases.
3. Time-consuming: Experiment setup time can be considerable.

To circumvent these limitations, numerical modelling of alkaline electrolysis plays a pivotal role. While most models require a limited amount of experimental data for characterisation and validation, they effectively overcome the aforementioned constraints. Additionally, numerical models provide insights into hydrogen production, energy conversion efficiency, sizing, thermal energy management, and optimisation. However, the numerical modelling of alkaline water electrolysis is intricate, encompassing multiple physical phenomena:

1. Electrochemical: This forms the core of any electrolysis modelling effort, establishing the relationship between input electrical power and hydrogen output. Given that hydrogen flow is proportional to cell current [71], the electrochemical physics can be represented using an I-V/polarisation curve.
2. Thermal: Temperature significantly impacts overall electrolysis performance. Therefore, proper assessment of temperature influence, coupled directly with the electrochemical model, is crucial.

2.3. Alkaline water electrolysis modelling

Over the past few decades, numerous researchers have explored the domain of numerical modelling, leading to the development of around 50 models, as documented in a review by Olivier et al. [72]. These models collectively contribute to a comprehensive understanding of alkaline water electrolysis.

These models can be categorised based on their adopted approach to tackling physical phenomena, which is summarised in Fig. 2.2. As for the electrochemical behaviours, the models can be classified as follows:

- Empirical: Meaning that the model is purely driven by experiments, and the parameters included in the model are purely data-driven, in order to better fit the experimental data, without providing any physical meaning to the parameters. An example of it, is the model developed by Ulleberg in 2003 [73], which adopts six parameters to describe the polarisation curve of the electrolysis process, these parameters have to be tuned based on the pre-acquired experimental data. These models are the most adopted ones as they are easy to implement, but their performance is strongly dependent on the quality of experimental data.
- Pure physical: When all physics are solved within a multiphysics software such as Ansys[®] or Comsol[®]; Hammoudi et al. [74] has adopted this solution by coupling MATLAB-Simulink[®] with SimPowerSystems[®], validating it using a Hydrogen Research Institute electrolyser [75]. These models allow considering many aspects of the electrolysis process, however with an expense of deeper knowledge of electrolysis and more time to set it up properly.
- Analytic or semi-empirical: These are based on the physical law equations, therefore all parameters have a physical meaning, even though some of them are computed through empirical correlations, often due to the lack of technical details. These models represent a good trade-off of the previous ones, preserving the physical meaning while having an easy-to-implement model.

Whereas for thermal physics, the following approach has been adopted in literature:

- Lumped parameter models: where the stack is considered as unique thermal capacitance and its temperature to be homogenous, due to its simplicity, it is the most common approach adopted by the researchers [72, 73, 76, 77].
- Distributed parameters models: These models are based on the resolution of Differential Equations of discretized thermal balances and can be either solving Partial Differential Equations (PDEs) or Ordinary Differential Equations (ODEs). They are crucial to understanding the thermal behaviour of an electrolysis cell and studying conception modifications in order to optimise its operation and control [58].

Each modelling approach is viable and already validated by other researchers, therefore, the decision to pursue one modelling pathway rather than another depends

on the application and the objective of the case study, which has to be properly considered.

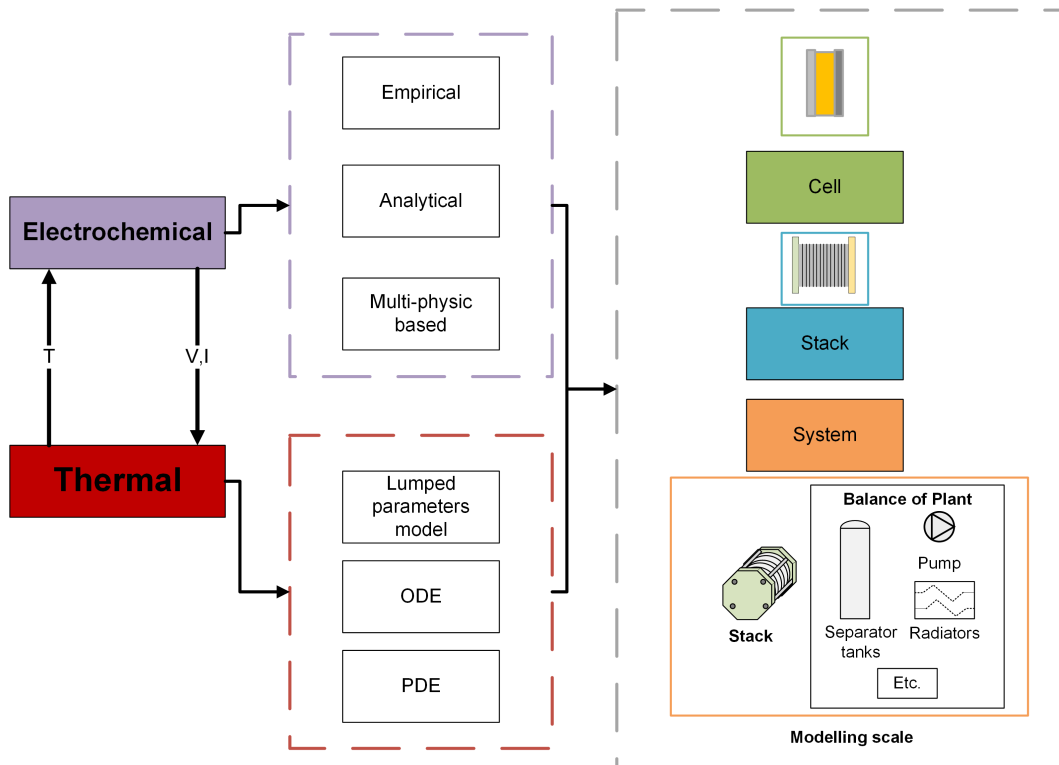


Figure 2.2.: Classification of alkaline electrolysis models

2.4. Alkaline electrolyser: modelling and temperature control effects

The temperature highly influences the operating conditions of the alkaline electrolyzers. To maintain it within the opportune range, several techniques can be used to control it. One approach is to use the water flow rate within the liquid electrolyte to maintain the desired temperature, such that the heat generated by the cell is efficiently dissipated or absorbed. When considering the techno-economic performance of an alkaline electrolysis system, it is crucial to carefully analyse the impact of temperature on the overall efficiency and cost of the system. For instance, Jang et al. [78] have built a model assessing electrolyte flow rate, needed as a temperature control measure, using a polynomial correlation, proposed by the same authors, based on temperature and current density, analysing effects at various temperature differences, between inlet and outlet, of 1-3-5-10°C.

The aim of this section is to illustrate a research output carried out, that effectively answered the research question 1 and 2 (Section 1.4.)²:

²Work carried out during the visiting period in DTU energy, under supervision of Prof. Henrik Lund

2.4. Alkaline electrolyser: modelling and temperature control effects

- **How to capture the technological details of the Power-to-Hydrogen process?**
- **How to model the integration of Power-to-Hydrogen and all its related auxiliaries?**

Moreover, it has the objective to cover such gap by understanding the temperature dependencies of the alkaline electrolyser system, solving the temperature evolution along the cells, and hence within the electrolyser, based on a validated zero-dimensional/lumped model, extended to a one-dimensional model solving for mass and energy conservation, obtaining the electrolyte flow rate information by the physical meaning of the water electrolysis process, allowing to unlock the assessment of system performance at any temperature difference.

The main contributions of this research are the following:

- Propose and validate, with literature data, a novel semi-empirical alkaline water electrolysis model, capable of being applied to different types of electrolyser, with only four parameters, while the other models adopt six or more parameters [73, 79, 80], thus allowing a much easier parameter fitting process. Moreover, the required experiments is also minimised.
- Formulation of a one-dimensional water electrolysis model, based on the physical process, solving ordinary differential equations. Which can assess the evolution of all operating parameters, such as temperature and pressure, illustrating its comparison with other dimensions models.
- Techno-economic assessment of the temperature control, by the sense of heating mass (electrolyte flow rate) variation, at a continuous range of gap temperatures.

The rest of this section is structured as follows, Subsection 2.4.1 describes the methodology adopted in this work, highlighting the novel semi-empirical model, validated and extended to a one-dimensional model, while Subsection 2.4.3 describes the results obtained and finally the conclusion of the work is reported in Subsection 2.4.4.

2.4.1. Semi-empirical model

As previously mentioned, the electrochemical phenomena of alkaline electrolysis are described through the polarisation curve, which in its general form, can be described as follows:

$$V_{cell} = V_{rev} + V_{act} + V_{ohm} + V_{bubble} \quad (2.1)$$

Frandsen (2022)

Where the V_{cell} is the voltage of a single electrolysis cell, V_{rev} is the reversible voltage, meaning the minimum electrical potential to have the electrolysis process going, V_{ohm} the ohmic overvoltage comprising both electrolyte and electrodes overpotential, V_{act} the activation overpotential of both electrodes and finally V_{bubble} is the overpotential, caused by bubble formation from the liquid electrolyte, which starts to be significant when approaching a current density limit, as stated in the research of Hammoudi et al. [74], such limit, based on the reseaches carried out by Vogt et al. [81], such limitation is set as 300 kA/m².

Each term of the Eq. 2.1 can be modelled in different ways, based on the approach and researchers' decisions, the ones adopted in this work are described in the following paragraphs, using the analytical model approach, using four parameters. The review carried out by Olivier et al. [72] has explained each possible approach present in the literature in detail.

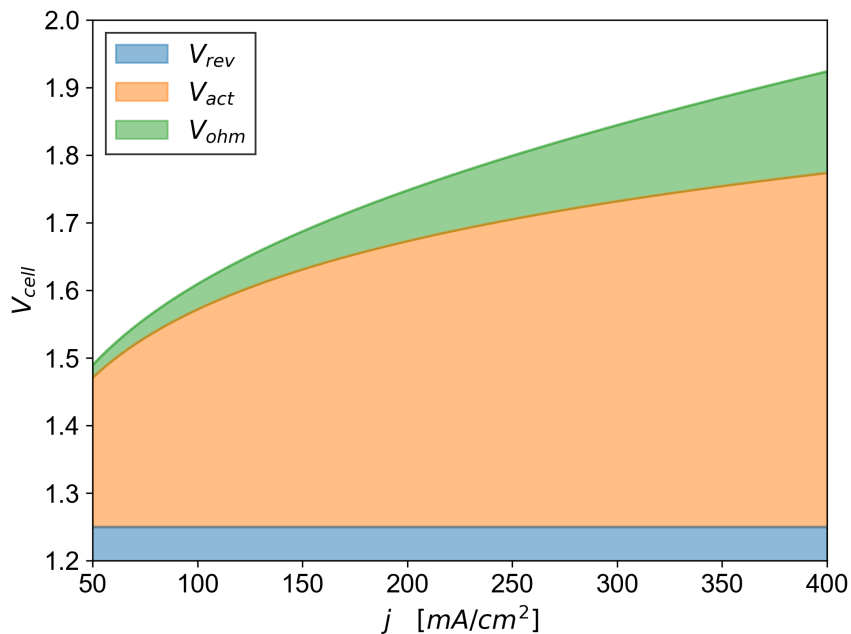


Figure 2.3.: Electrolysis polarisation curve, distinguished into its components. The bubble formation overpotential is not presented as it is for high current densities, where alkaline electrolyzers commonly do not operate.

Almost all commercial alkaline electrolyzers adopt bipolar electrical configurations, meaning the cells are electrically connected in series since it allows to have higher utilisation of the cell area, as reported in [79], therefore the whole electrolyser has the same current of the cell level, while the overall voltage of the stack is the sum of all the cell's voltages. Therefore, the whole electrolyser stack current and voltage can be easily calculated using the following equations:

$$I_{stack} = I_{cell} \quad (2.2a)$$

2.4. Alkaline electrolyser: modelling and temperature control effects

$$V_{stack} = V_{cell} \cdot N_{cell} \quad (2.2b)$$

Furthermore, the polarisation curve provides insights into hydrogen production as well as conversion efficiency due to the following reasons:

- Direct relationship between current and hydrogen production: The amount of hydrogen produced is directly related to the current of the electrolysis cell, in accordance with Faraday's law:

$$\dot{n}_{H_2} = \frac{j}{2F} \cdot A_{cell} \quad (2.3)$$

Here, the molar flow rate of produced hydrogen (\dot{n}_{H_2}) is determined by the ratio of the cell current (a product of the current density and the cell area) and the product of the stoichiometric ratio (which is 2 for hydrogen) of the reaction and the Faraday constant (96500 [C/mol]).

- Assessment of power losses and thermal energy generation: The power losses that occur due to the voltage gap between the cell voltage and the thermoneutral value are converted into thermal energy, causing the electrolysis stack to heat up. The generated thermal power (\dot{Q}_{gen}) can be expressed as follows:

$$\dot{Q}_{gen} = (V_{cell} - V_{th}) \cdot j \cdot A_{cell} \quad (2.4)$$

Here, the thermal power is the product of the electrical power due to the overvoltage between the cell voltage and the thermoneutral value (V_{th}). The thermoneutral value represents the voltage that can be entirely absorbed by the cell without leading to excessive heat. It can be calculated as:

$$V_{th} = \frac{\Delta H}{2F} \quad (2.5)$$

The variation of enthalpy (ΔH) is specific to the chemical process. For electrolysis, it is associated with the following reaction:



$$\Delta H = H_{H_2} + \frac{1}{2}H_{O_2} - H_{H_2O} \quad (2.6b)$$

All enthalpy values are temperature-dependent and can be obtained using empirical equations from databases such as the NIST Chemistry WebBook [82].

Reversible voltage

The reversible voltage can be determined using the following equations, based on the work conducted by Gambou et al. [64]:

$$V_{rev} = V_{rev,T} + \frac{RT}{2F} \ln \left(\frac{(P - P_{v,KOH}^{3/2})}{\alpha_{H_2O}} \right) \quad (2.7a)$$

$$V_{rev,T} = 1.5174 - 1.5421 \cdot 10^{-3}T + 9.523 \cdot 10^{-5}T \cdot \ln(T) + 9.84 \cdot 10^{-8} \cdot T^2 \quad (2.7b)$$

$$P_{v,KOH} = \exp(2.302 \cdot a + b \cdot \ln(P_{v,H_2O})) \quad (2.7c)$$

$$a = -0.0151 \cdot m - 1.6788 \cdot 10^{-3} \cdot m^2 + 2.2588 \cdot 10^{-5} \cdot m^3 \quad (2.7d)$$

$$b = 1 - 1.2062 \cdot 10^{-3} \cdot m + 5.6024 \cdot 10^{-4} \cdot m^2 - 7.8228 \cdot 10^{-6} \cdot m^3 \quad (2.7e)$$

$$P_{v,H_2O} = \exp \left(81.6179 - \frac{7699.68}{T} - 10.9 \cdot \ln(T) + 9.5891 \cdot 10^{-3} \cdot T \right) \quad (2.7f)$$

$$\alpha_{H_2O} = \exp \left(-0.05192 \cdot m + 0.003302 \cdot m^2 + \frac{(3.177 \cdot m - 2.131 \cdot m^2)}{T} \right) \quad (2.7g)$$

Here, V_{rev} is calculated using the Nernst equation, which comprises the standard reversible potential ($V_{rev,T}$) and the pressure influence expressed in [bar] as $V_{P,T}$. The remaining equations involve empirical correlations that have already been validated by other researchers to determine the thermal properties. It's important to note that all these empirical correlations are dependent on temperature ([K]) and the molality of the liquid electrolyte ([mol/kg]), and for this specific case, the KOH solution is considered as the electrolyte.

Activation overpotential

Activation overpotential is the effect of the water electrolysis process happening in both electrodes, Such a phenomenon can be expressed with the Butler-Volmer equation, which for both alkaline electrolysis electrodes (Anode and Cathode) can be expressed as follows:

$$i = i_0 \left[\frac{C_{OH}}{C_{OH,ref}} \exp \left(\frac{\alpha_- F}{RT} \cdot V_{an} \right) - \frac{C_{O_2}}{C_{O_2,ref}} \exp \left(-\frac{\alpha_- F}{RT} \right) \cdot V_{an} \right] \quad (2.8a)$$

$$i = i_0 \left[\frac{C_{OH}}{C_{OH,ref}} \exp \left(\frac{\alpha_+ F}{RT} \cdot V_{ca} \right) + \frac{C_{H_2}}{C_{H_2,ref}} \exp \left(+\frac{\alpha_+ F}{RT} \right) \cdot V_{ca} \right] \quad (2.8b)$$

These equations are not easy to solve, since it is also expressed in an implicit way (current expressed in function of overpotential), Moreover, it has been observed that the second term of the Butler-Volmer equation has a smaller influence, therefore it is common to use the Tafel approximation, which ignores completely the second part. That is valid as long as the operation current density is higher than the exchange

2.4. Alkaline electrolyser: modelling and temperature control effects

current (i_0) of the electrode; which for the alkaline water electrolysis, is always true, due to the limitation on the lower partial load threshold (15-20%). Therefore the general expression of the activation overpotential, for both electrodes can be expressed as:

$$V_{act} = \left(\frac{1}{\alpha}\right) \frac{RT}{2F} (\ln(j) - \ln(j_0)) \quad (2.9)$$

which derives from the Eq. 2.8, with a further simplification of using current densities (j) instead of current (i), Furthermore, quite often is not possible to have separate electrodes' information, thus, for the sake of the similarity, their activation overpotential can be grouped together. For the other terms of the Eq. 2.9:

- α is the charge transfer coefficient, which is an experimental-based parameter, that depends on the electrode material, which is quite often information not accessible; indeed this is the first parameter of the model. [-]
- j_0 is the exchange current density, which is also variable, based on the electrode's material, expressed as [mA/cm²] or [A/m²].
- j is the current density of the cell, expressed as [mA/cm²] or [A/m²].
- R is the universal gas constant, 8.31 [J/mol K]
- T is the cell working temperature, expressed in [K]

where the exchange current densities (j_0) can be assessed using the Arrhenius dependency:

$$j_0 = k \cdot \exp\left(\frac{E_a}{RT}\right) \quad (2.10)$$

where:

- k is the Arrhenius scale factor, which shares the same unit of the exchange current densities, [mA/cm²] or [A/m²].
- E_a is the activation energy of the electrodes, expressed in [J/mol].

Despite the simplification using Tafel's equation, many parameters remain unknown, therefore the Eq. 2.10 can be adjusted and rewritten as:

$$\ln(j_0) = \ln\left(k \cdot \exp\left(-\frac{E_a}{RT}\right)\right) \quad (2.11a)$$

$$\ln(j_0) = \left(-\frac{E_a}{R}\right) \cdot \frac{1}{T} + \ln(k) = \left(-\frac{E_a}{R}\right) \cdot \frac{1}{T} + B \quad (2.11b)$$

Where the parameters $(-E_a/R)$ and B are additional parameters of the analytic model since they can not be assessed without information from experimental tests. The activation overpotential can be finally expressed as:

$$V_{act} = \left(\frac{1}{\alpha}\right) \frac{RT}{2F} \left(\ln(j) - \left(-\frac{E_a}{R} \cdot \frac{1}{T}\right) - \ln(B)\right) \quad (2.12)$$

Ohmic overpotential

The ohmic overpotential regards all voltages of the electrolyser cell that can be estimated using a linear correlation with the current density. Although different physical phenomena have this behaviour, the most contributing effects come from the liquid electrolyte and the electrolyser diaphragm/separator. Thus the ohmic overpotential can be assessed using the following equations:

$$V_{ohm} = j \cdot \left(\frac{\delta_{el}}{1000 \cdot \sigma_{el}} + \frac{\delta_d}{\sigma_d} \right) \quad (2.13a)$$

$$\sigma_{el} = -2.041M - 0.0028M^2 + 0.005332M \cdot T^2 + 207.2 \frac{M}{T} + 0.001043M^3 - 3 \cdot 10^{-7} M^2 T^2 \quad (2.13b)$$

where j is expressed in [mA/cm²], the δ_{el} and δ_d are effective reaction distance and diaphragm thickness, both expressed in [cm]. And σ_{el} and σ_d are ionic conductivities of the electrolyte and the diaphragm ([S/cm]).

As regards the electrolyte ionic conductivity, Gilliam et al. [83] have built the empirical equation, through the experimental tests, that depends on the molarity ([mol/l]) of the solution, which is KOH based, and the operating temperature, as reported in Eq. 2.13b. Yet, the reaction distance δ_{el} is not possible to assess it. Regarding the diaphragm ionic conductivity, Vermeiren et al. [84] have performed tests on a 0.5 mm thick Zirfon-based diaphragm with KOH solution with 30% weight concentration, from their results, is possible to have an empirical correlation for the σ_d at the temperature range of 20-80°C, however, the diaphragm material can vary, therefore the empirical equation developed by Vermeiren is not suitable to all alkaline electrolysers. Hence, in the proposed model, for the sake of the simplicity and their similar behaviour, to the overall cell voltage, the term δ_{el} , considered as an empirical parameter, includes both electrolyte and diaphragm ohmic contribution. Thus:

$$V_{ohm} = j \left(\frac{\delta_{el}}{1000 \cdot \sigma_{el}} \right) \quad (2.14)$$

Bubble overpotential

The bubble overpotential is caused by the formation of bubbles from the liquid electrolyte, and such bubbles cause two main effects:

1. Modification of the activation area of the cell, as the bubbles would cover a portion of it.
2. Change of the electrolyte ionic conductivity.

From the modelling perspective, it is still a challenging task to capture its phenomena properly, as it considers two different phases of the electrolyte (liquid+gas), despite many researchers' ongoing work [74, 75, 81]. Nevertheless, since it contributes to

2.4. Alkaline electrolyser: modelling and temperature control effects

the variation of the activation overpotential (effect 1) and ohmic overpotential (effect 2), where both of them are assessed through empirical parameters, meaning that they are tuned based on the electrolyser operating data, the bubble overpotential is implicitly included, thanks to the empirical approach.

Overall polarisation curve

To sum everything up, the overall four parameters semi-empirical model developed is the following:

$$V_{cell} = V_{rev,T} + \frac{RT}{2F} \ln \left(\frac{(P - P_{v,KOH}^{3/2})}{\alpha H_2O} \right) + \left(\frac{1}{\alpha} \right) \frac{RT}{2F} \left(\ln(j) - \left(-\frac{E_a}{R} \cdot \frac{1}{T} \right) - \ln(B) \right) + j \left(\frac{\delta_{el}}{1000 \cdot \sigma_{el}} \right) \quad (2.15)$$

Where the four parameters, that have to be assessed are the following:

- α : Parameter for the charge transfer assessment, [-]
- $\left(-\frac{E_a}{R}\right)$: Parameter that comprises the ratio of the activation energy and the gas constant, [K]
- $\ln(B)$: Parameter that captures the exchange current density influence, indeed has the units based on the current density, [$\ln(\text{mA}/\text{cm}^2)$]
- δ_{el} , parameter that takes both electrolyte and diaphragm ohmic overpotentials, [cm]

Moreover, the whole polarisation curve depends on only three operating parameters, which are:

1. P , operating pressure of the electrolysis cell, [bar]
2. wt , weight concentration of the KOH-based electrolyte, [0-1]
3. T , electrolysis cell Temperature, [K]

Furthermore, both molarity (m) and molality (M) can be assessed with the wt information:

$$\rho_{el} = f(wt, T), \quad [kg/m^3] \quad (2.16a)$$

$$m = wt \cdot MW_{KOH} \cdot 1000, \quad [mol/kg] \quad (2.16b)$$

$$M = wt \cdot \rho_{el} \cdot MW_{KOH}, \quad [mol/l] \quad (2.16c)$$

With the electrolyte density as an empirical correlation of weight concentration and the temperature, reported in [83], and MW_{KOH} as the molecular weight of the potassium hydroxide, equal to 56.1 g/mol.

Thermal modelling

The thermal behaviour of electrolysis directly influences the efficiency of hydrogen production. Hence, an exhaustive thermal model is essential to accurately capture the electrolysis thermal process. While lumped models treat the entire cell as a single unit and cannot adequately capture temperature evolution (Fig. 2.4), a more advanced approach is needed. In this study, the Ordinary Differential Equations approach has been employed. This approach is based on a lumped electrochemical model for each element, coupled with mass and energy balances along the flow direction. This refined model enables the assessment of variations in temperature, pressure, and KOH concentration along the flow direction (x axis). Furthermore, this

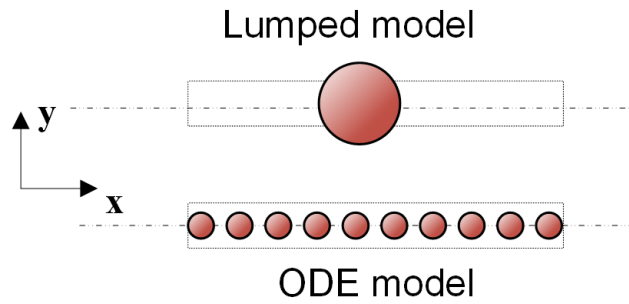


Figure 2.4.: Thermal model differences: Lumped model vs ODE.

model is expanded to the stack level, built upon the electrical arrangement of the cells, as depicted in Fig. 2.7.

To maintain a relatively simple model, so it can be applied at the system level, a reasonable assumption is made. Indeed, it is assumed that all thermo-electrical properties vary exclusively along the electrolyte flow direction (x axis), with their variations along other axes neglected. Consequently, the mass and energy balance differential equations are solved along the electrolyte flow axis, element by element:

$$\frac{d\dot{n}_{H_2}}{dx} = \frac{j_i}{2F} \cdot w_{cell} \quad (2.17a)$$

$$\frac{dT}{dx} = \frac{(V_{cell} - V_{th}) \cdot j_i}{\dot{n}_e \cdot cp_e + \dot{n}_{H_2} \cdot cp_{H_2} + \dot{n}_{O_2} \cdot cp_{O_2}} \cdot w_{cell} \quad (2.17b)$$

$$i = 1, 2, 3, \dots, n_{elements}; \quad w_{cell} = constant \quad (2.17c)$$

In each element (i), the molar flow rate and thermal balance are determined, considering a rectangular cell shape with a constant width (w_{cell}). As depicted, both

2.4. Alkaline electrolyser: modelling and temperature control effects

equations rely on inputs from the electrochemical calculations. Moreover, the temperature outcomes from these equations are subsequently used in the next element, as boundary conditions, for electrochemical assessments, as demonstrated earlier in Fig. 2.2.

When considering standard chemical species, their thermodynamic properties, including specific heat (c_p), can be derived using empirical correlations available in databases such as NASA [85]. However, for the KOH-based electrolyte, its properties vary considerably with weight fraction, as demonstrated in experiments reported by Bideau et al. [86]. For this study, the Zaytsev empirical relationship has been employed to account for these variations [87].

$$c_{p_{el, mass}} = 4.236 \cdot 10^3 + 1.075 \cdot \ln\left(\frac{T_{Celsius}}{100}\right) + (-4.831 \cdot 10^3 + 8 \cdot wt + 8 \cdot T_{Celsius}) \cdot wt \quad (2.18)$$

The temperature is expressed in Celsius, and the specific heat obtained is expressed in [J/kg K]. As all the balances are molar-based, it's necessary to convert this specific heat into molar-based specific heat [J/mol K]. This conversion can be achieved using the following equations:

$$C_{p_{el}} = c_{p_{e, mass}} \cdot \frac{MW_e}{1000} \quad (2.19a)$$

$$wt_i = \frac{n_i \cdot MW_i}{m_{tot}}; m_{tot} = n_{tot} \cdot MW_{tot}; n_{tot} = \sum n_i \quad (2.19b)$$

$$\sum \frac{wt_i}{MW_i} = \frac{1}{MW_{tot} \cdot n_{tot}} \cdot \frac{n_i \cdot MW_i}{MW_i} \quad (2.19c)$$

$$MW_{tot} = \frac{1}{\sum \frac{wt_i}{MW_i}} \rightarrow MW_e = \frac{1}{\frac{wt}{MW_{KOH}} + \frac{(1-wt)}{MW_{H_2O}}} \quad (2.19d)$$

The flowchart of the proposed 0D/lumped electrochemical model, along with its extension to the 1D cell model using the ODE approach for thermal behaviour, and further into the 1D stack model, is illustrated in Fig. 2.7.

2.4.2. Semi-empirical model validation and comparison

The proposed model is further tested and validated, using the experiments presented in the literature by different researchers, to represent different types of alkaline electrolysers with different set-ups of operating conditions. Such operating conditions are namely i) temperature, ii) KOH concentration, and iii) pressure. Additionally, the model's robustness, i.e. its ability to have reasonable accuracy, dealing with the minimum quantity of the data available, has been also tested.

The procedure of calibration of the model, based on the type of the electrolyser with its results, is illustrated in Fig. 2.5, which can be divided into 3 phases:

1. Experimental data processing, ensuring at least 6 data points are present,

ensuring a good accuracy of the model. If more data is available, they can be also included, however, not all available data should be used, to prevent the over-fitting problem.

2. The pre-processed data is then inserted into a curve-fitting framework, commonly used ones are Matlab and Python, adopting the proposed model, assessing 4 calibrating parameters (α , $(-\frac{E_a}{R})$, $\ln(B)$, δ_{el}).
3. As a consequence of the previous step, the model is now defined, and as such, polarisation curves at different temperatures can be obtained.

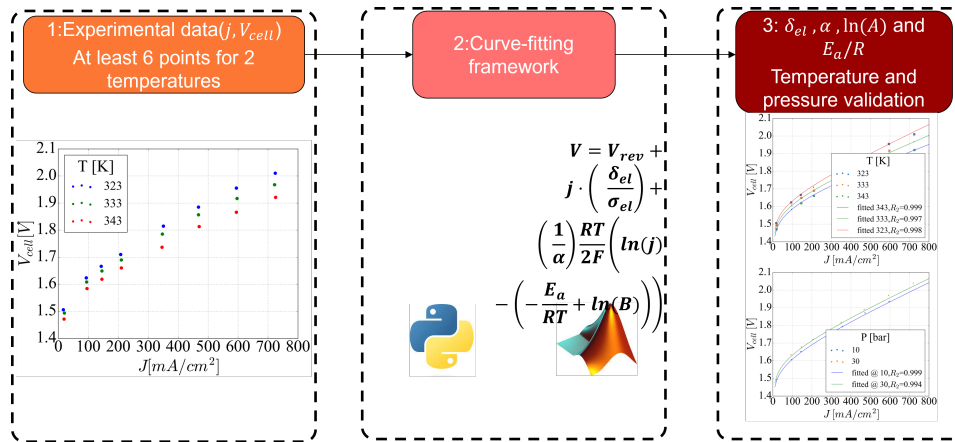


Figure 2.5.: Parameters estimation procedure. Divided into three steps: 1) collection of experimental data at different temperatures, 2) parameter estimation, and 3) temperature and pressure influence validation.

The results regarding the validation of different literature-based datasets, in order to test its robustness, meaning the capability of adopt different electrolyzers and operational conditions. Four different datasets have been used, namely Sakas [88], Ulleberg [73], Sanchez [80] and De Groot [65].

During the parameter estimation process, the dataset is split into two separate datasets. Namely train and test datasets, to prove the model's robustness. Indeed, the training dataset, i.e. the data used to find parameters, is randomly selected, with the only constraint that they need to be at least six data points, from at least two different operating temperatures. The results of the estimation, illustrating the model's wide applicability, are reported in Fig. 2.6.

Whereas the temperature dependence is explicitly highlighted, in activation overpotential, other operating conditions influence, namely KOH weight concentration and pressure are implicitly considered, through the ohmic overpotential and reversible voltage, respectively.

As shown in Fig. 2.6, the proposed model demonstrates exceptional performance (with an R^2 score exceeding 0.98) despite being applied to significantly different electrolyzers [58]. Moreover, it's important to note that not all available experimental

2.4. Alkaline electrolyser: modelling and temperature control effects

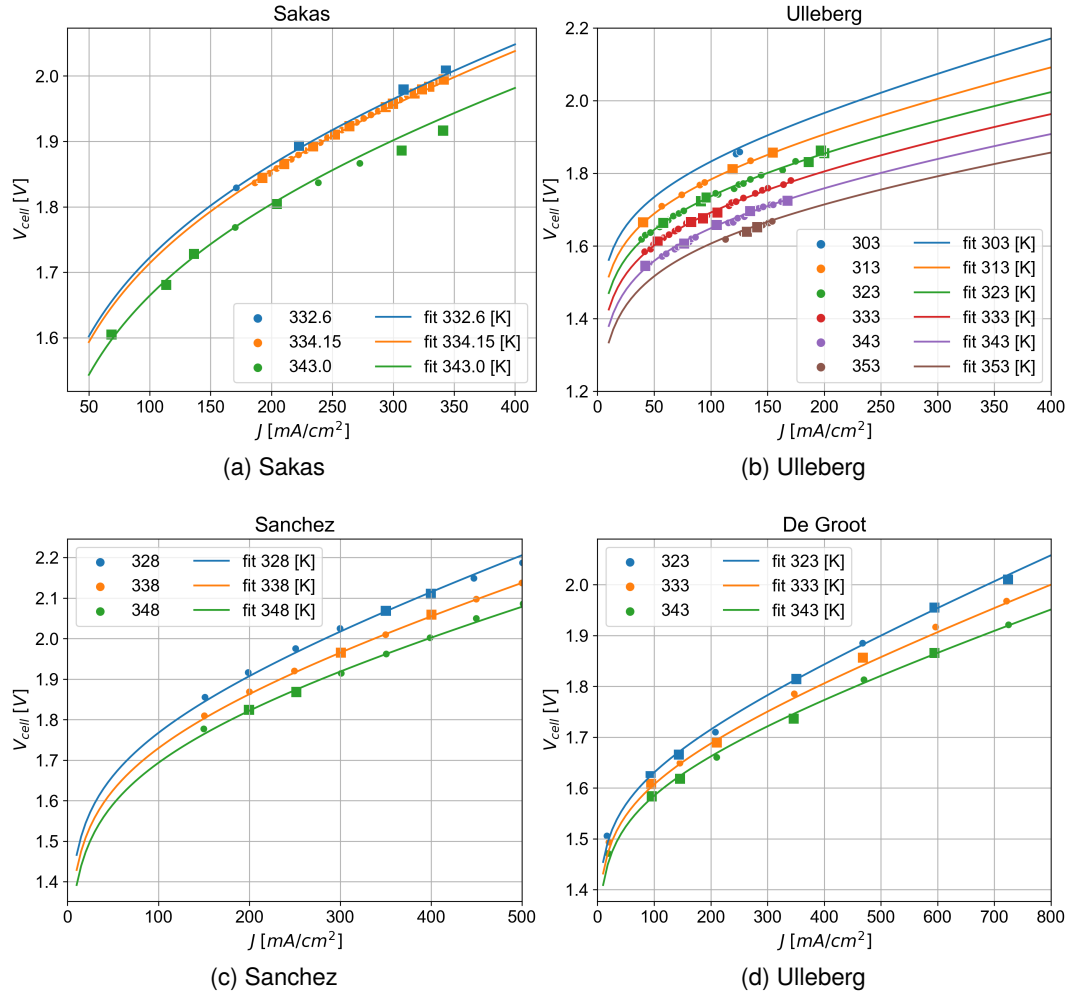


Figure 2.6.: Parameter estimation and validation with temperature variation. Where squared-dotted data are from the training dataset while the circle ones are from the test dataset.

data were utilised for parameter determination, and the training dataset was randomly selected. This indicates the robustness of the model.

In an extreme scenario, even with just four data points (two for each of two distinct temperatures), the model exhibits good performance (with an R^2 score > 0.8). With only six data points, the model achieves an R^2 score exceeding 0.90.

Various comparisons of thermal models at different scales have been conducted, encompassing three distinct domain-scale models. These models were developed utilising the potentiostatic approach, which involves providing the cell's voltage as input data.

- 0D model, or lumped model, only a single point is considered for the whole cell, defined as follows:

$$0D : T_{in}; j = j_{in} = f(T_{in}, V, wt, P) \quad (2.20)$$

Table 2.2.: Semi-empirical model validation: Despite different operational conditions (temperatures and pressures), parameters for the different datasets are similar.

	Experimental conditions			Calibrated parameters			
	p [bar]	T [°C]	wt [-]	δ_{el} [cm]	α [-]	$\frac{-E_a}{R}$ [K]	$\ln(B)$ [$\ln(\frac{mA}{cm^2})$]
Sakas	16	59.6-61.15-70	0.25	0.39	0.1253	-6330	13.11
Ulleberg	7	30-40-50-60-70-80	0.30	0.66	0.1726	-5331	9.18
Sanchez	7	55-65-75	0.35	0.5711	0.12	-3592	4.77
Groot	30	50-60-70	0.28	0.2716	0.28	-3906	3.86

- 1/2 D model, it is a trade-off between the lumped and the ODE model, where inlet and outlet points are considered, however, it is often not possible to know the outlet conditions, thus, it generally needs an iterative loop; for this case, the outlet data is taken from 1D model, in order to have the same conditions.

$$1/2D : T_{in}, T_{out} : j = j_{avg} = \frac{j_{in} + j_{out}}{2} \quad (2.21)$$

- 1D model is the model using ODE previously mentioned, allows having information for discrete points of assessment along the cell:

$$1D : T_i; i = 1, \dots, n_{elements}; j = j_{avg} = \frac{\int j_i dx}{n_{elements} \cdot \Delta x} \quad (2.22a)$$

$$Area = x \cdot w_{cell}; x = (1 \dots n_{elements}) \cdot \Delta x \quad (2.22b)$$

For the sake of the comparison, a 30X30 cm squared cell is considered, in other means 0.3m of width and the x axis can reach a maximum of 0.3 m. Moreover in Fig. 2.8 reported the results of the 1D model of a such cell, working at 1.8V, with an outlet temperature fixed at 80 °C with different gap temperatures, namely 1-2-10 °C.

Fig. 2.9 illustrates a comparison of models with varying dimensionality. The 1D model serves as the reference due to its considered accuracy. The current density is compared at a fixed potential of 1.8 V. This comparison is conducted under various electrolyte flow rates through the stack for cooling, leading to different temperature increases across the stack.

The results of the comparison indicate that the 0D model consistently underestimates the current density and, consequently, the hydrogen production rate. Conversely, the 1/2D model tends to overestimate both. Furthermore, operating at 80°C (353 K) with a voltage of 1.8 V and a 5°C temperature difference between inlet and outlet, the half-dimensional model exhibits a nearly negligible deviation (0.75%). However, the zero-dimensional model showcases a substantial deviation, significantly underrating hydrogen production by approximately 11% when compared to

2.4. Alkaline electrolyser: modelling and temperature control effects

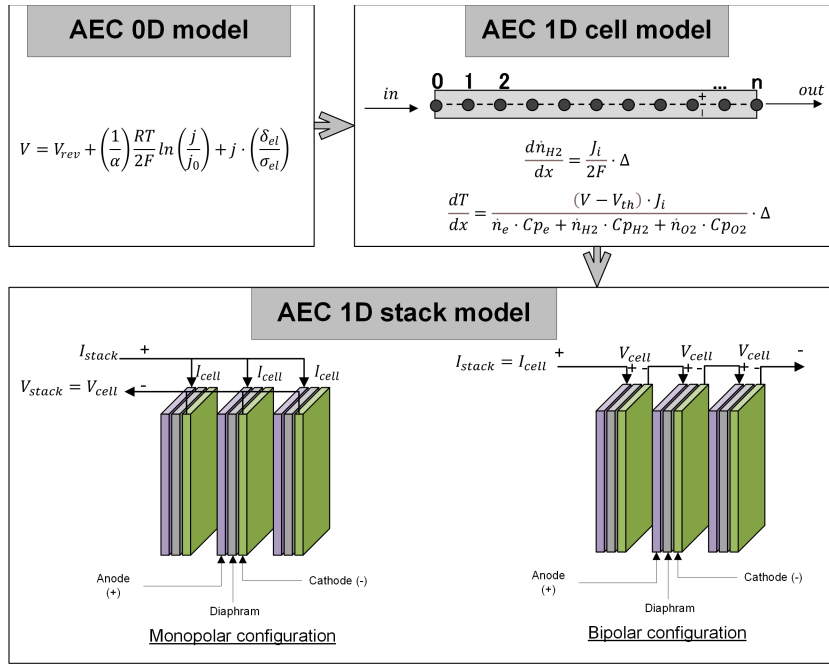


Figure 2.7.: Alkaline 1D stack model flowchart. Starting with the single cell 0D model, extended to the 1D cell model, solving mass and thermal balance, and finally 1D stack model, based on the electrical configuration among cells.

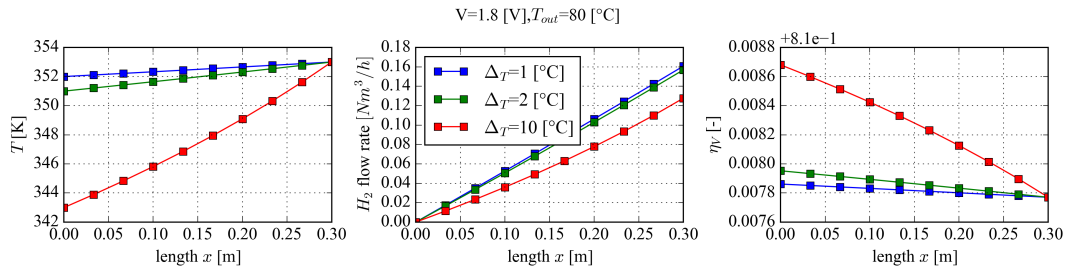


Figure 2.8.: 1D model at 1-2-10 °C temperature difference. Illustrating namely i) temperature, ii) hydrogen production, and iii) voltage efficiency along the cell. Where the outlet temperature is kept constant. Despite having a higher temperature difference and achieving a higher efficiency, the produced hydrogen flow is lower.

the benchmark set by the one-dimensional model.

2.4.3. System level temperature control effects

Another key perspective of having such a model is the possibility of seeing its integration with other technology components and gaining also insights about its optimal operational strategy. For this study, temperature control and its effects on both technological and economical perspectives, have been assessed. Indeed the whole alkaline electrolyser stack can be connected with all necessary auxiliary

Chapter 2. Hydrogen as energy storage

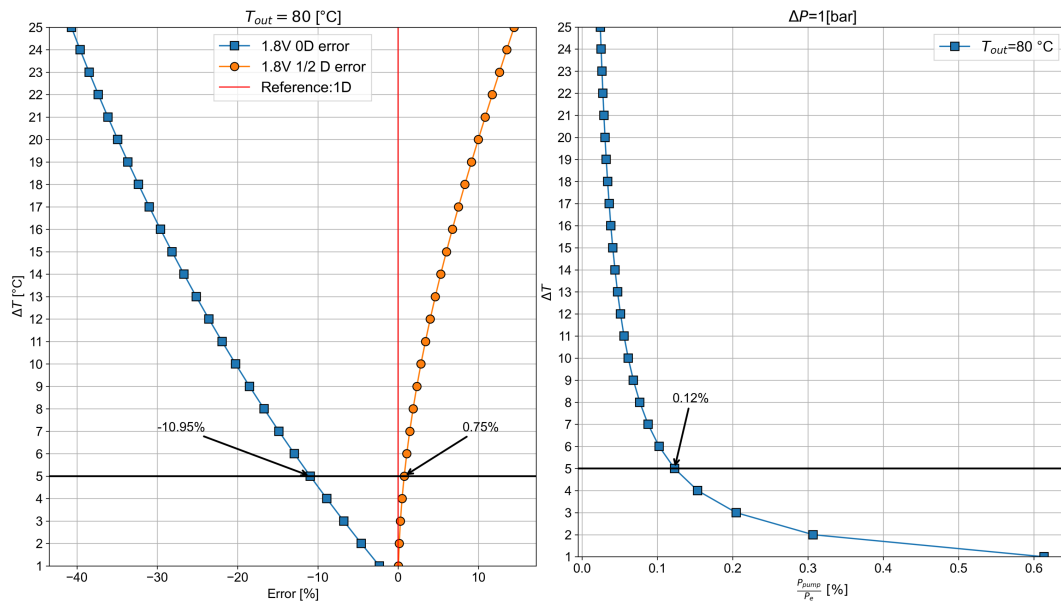


Figure 2.9.: Different scales of electrolyzer models' comparison, at different temperatures increase over the stack. Where error is the difference between the models' average current density, compared with the 1D model's average current density, in percentage.

technologies, as illustrated in Fig. 2.10.

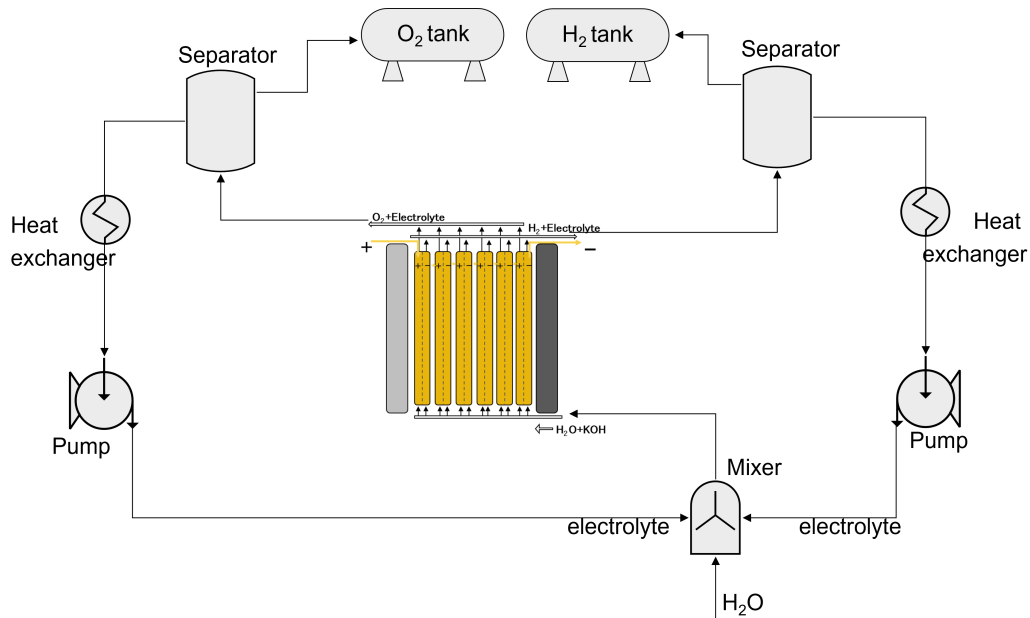


Figure 2.10.: Systems connections. Illustrating auxiliary systems to be coupled with electrolyzer stack.

As evaluation indicators, exploiting the temperature effects, system-level efficiency and the levelised cost of the produced hydrogen are adopted. These indicators

2.4. Alkaline electrolyser: modelling and temperature control effects

criteria are assessed using the following equations:

$$\eta_{tot} = \frac{N_{cells} \cdot n_{H_2,cell} \cdot LHV_{H_2}}{p_{stack} + p_{pump}} \quad (2.23a)$$

$$LCOH = \frac{CAPEX_{stack,a} + CAPEX_{HEX,a} + CAPEX_{pump,a} + LCOE \cdot E_{el}}{m_{H_2}} \quad (2.23b)$$

Where all investment costs ($CAPEX$), that depend on the nominal size of each technology, are actualised in annual costs, while E_{el} is the electrical energy required to produce the mass of the hydrogen m_{H_2} .

In terms of technical implications, when the temperature difference between the inlet and outlet of the electrolyser stack exceeds 1°C, the overall efficiency remains relatively stable at around 0.69, as shown in Fig. 2.11. Since the model keeps the voltage fixed as an input, these results indicate that, beyond this threshold, the impact of energy consumption by the water pump, which is dependent on the water flow rate required for temperature control, becomes nearly negligible when compared to the energy absorbed by the electrolyser.

From an economic perspective, as depicted in Fig. 2.12, there exists a distinct zone (referred to as the "2° zone") where the Levelised Cost of Hydrogen (LCOH) reaches its minimum value. This optimal range aligns with a gap temperature of approximately 1°C, regardless of the specific LCOE (see appendix A.1) used. However, the rate of decrease or increase in LCOH varies in the two cases. In contrast, LCOH is higher in the other two zones (referred to as the "1° zone" and "3° zone"). In the 1° zone, this is due to the elevated operational cost attributed to the energy consumption of the water pump. In the 3° zone, the higher gap temperature leads to a reduction in current density, resulting in lower hydrogen production efficiency overall.

2.4.4. Model limitations and opportunities

In this section, a model that covers different scales of the alkaline water electrolysis is proposed and validated, effectively addressing the first two research questions posed (1.4):

- **Technological details of the Power-to-Hydrogen process**
- **The integration of Power-to-Hydrogen and all its related auxiliaries**

The model not only captures details at the cell-stack-system technology level but also evaluates auxiliaries connected with an electrolysis stack, particularly exploring the effects of temperature control.

The proposed model was carefully fitted to a range of data from existing literature and demonstrated excellent fits across all considered measurements. With just four parameters, a combination of physical and empirical parameters describing specific physical phenomena, the model effectively represents complex behaviours.

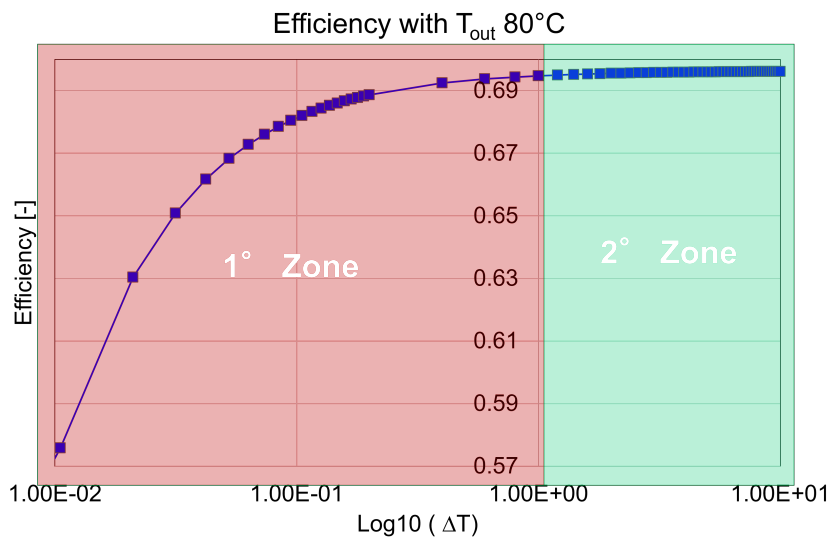


Figure 2.11.: Influence of temperature difference (inlet to outlet) in system efficiency. Where the outlet temperature is set as 80°C.

To gauge the impact of model accuracy on system-level representations, a comparison of different model refinements was conducted, encompassing 0D, 1/2D, and 1D models. Notably, the 0D model significantly underestimates hydrogen production (-11%), while the 1/2D model exhibits a minor overestimation (+0.75%) compared to the more precise 1D model.

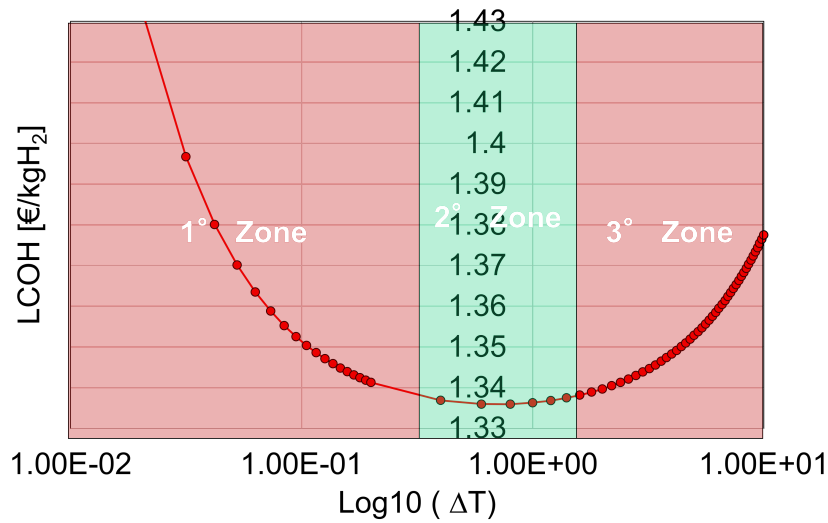
Furthermore, the effect of electrolyte flow rate on overall efficiency and economic standpoints is evaluated. An intriguing observation is that there are clear advantages to increasing the electrolyte flow rate, which helps maintain a temperature increase over the stack close to 1°C. While efficiency may decrease with higher flow rates, it remains steady when the temperature increase is maintained above 1°C. Economically, an optimal flow rate exists where losses from electrolyte pumping and stack losses due to higher resistance at lower temperatures are harmonized.

While the proposed model holds significant potential, it's important to acknowledge its limitations. Notably, the model does not account for Faraday's efficiency due to the lack of a consistent approach in the literature. Additionally, the formation of water vapour has not been comprehensively addressed. It's worth noting that these limitations are unlikely to alter the results discussed in this study. However, they certainly provide avenues for future investigation and refinement.

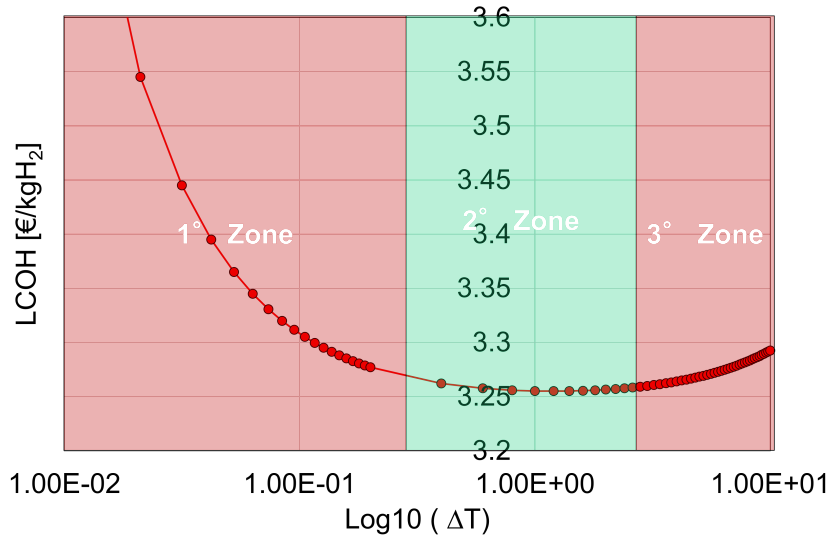
2.5. Innovative hydrogen storage: Metal hydrides

Hydrogen storage presents a significant challenge due to its extremely low density, approximately 0.089 kg/Nm³, which is nearly 10 times lower than that of natural gas. As a result, achieving reasonable storage volumes becomes a critical bottleneck.

2.5. Innovative hydrogen storage: Metal hydrides



(a) LCOH with minimum LCOE



(b) LCOH with maximum LCOE

Figure 2.12.: Influence of temperature difference (inlet to outlet) in the levelised cost of hydrogen. Where the outlet temperature is set as 80°C.

Hydrogen can be stored in three phases matter: gas, liquid, and solid, as illustrated in Fig. 2.13.

When it comes to storing hydrogen in its gaseous form, it must be stored at extremely high pressures, and the standard pressure levels can vary based on the application, as indicated in Tbl. 2.3. However, apart from safety concerns related to managing high-pressure gases, an energy cost is associated with achieving and maintaining such pressure levels. For example, raising hydrogen from standard conditions to 70 bars would require approximately 7% of the energy contained in the hydrogen itself [67]. Liquid hydrogen storage, on the other hand, does not have the

Chapter 2. Hydrogen as energy storage

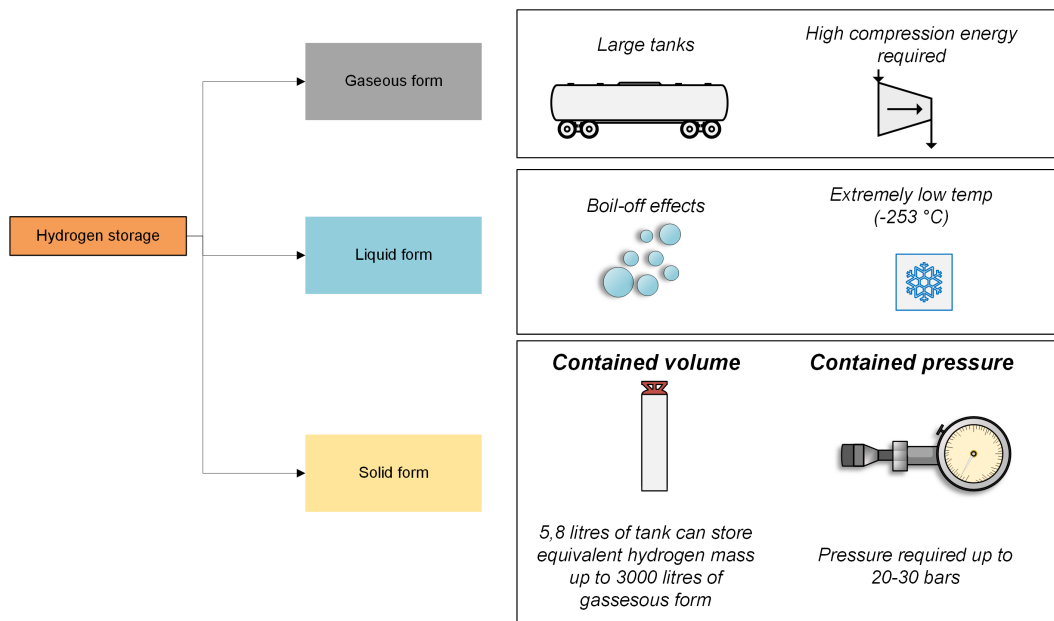


Figure 2.13.: Hydrogen storage pathways: Gas, liquid, solid.

high-pressure limitation. However, to liquefy hydrogen, it needs to be cooled to a frigid temperature of -253°C . As a result, a substantial amount of energy, around 30% [89], is expended in the liquefaction process. Additionally, liquid hydrogen is susceptible to the boil-off effect, which involves its gradual evaporation [90]. Finally, solid storage of hydrogen can be achieved through the use of Metal Hydrides (MH). This approach minimizes safety risks associated with high-pressure hydrogen storage and reduces the energy expenditure required for containment.

Table 2.3.: Hydrogen pressure standard for different applications

Application	Pressure [bar]
Gas pipelines	70
Underground gas storage	200
Busses and trucks	350
Passenger vehicles	700
Tanks	1000

As a crucial component of the Power-to-Hydrogen pathway, this section addresses research question 2 (1.4), which inquires:

*"How to model the integration of Power-to-Hydrogen and all its **related auxiliaries**?"*

Specifically, this section delves into solid hydrogen storage. Its objective is to investigate the technology specifics of solid hydrogen storage for modelling purposes, alongside its integration with other auxiliary systems, including hydrogen compressors

and conditioning systems³.

2.5.1. Metal hydrides working principle

Hydrogen can be stored in metal hydrides, which involve certain metals and alloys and enable solid-state storage under moderate temperatures and pressures. While this approach offers safety and volume efficiency, it has limitations due to the low hydrogen concentration in metal hydrides. This limitation necessitates a large quantity of metal mass to store a significant amount of hydrogen, making it suitable mainly for stationary applications.

There are two possible methods for hydriding a metal: direct dissociative chemisorption and electrochemical splitting of water. This thesis primarily focuses on the former method, which is more commonly used and does not require water input. This process is described as follows:



Where M represents the metal and Q is the heat produced/ absorbed during the process.

Metal hydrides are composed of metal atoms that constitute a host lattice and hydrogen atoms. Metal and hydrogen usually form two different kinds of hydrides, α -phase at which only some hydrogen is absorbed and β -phase at which hydride is fully formed, as illustrated in Fig. 2.14. The absorption and desorption of the

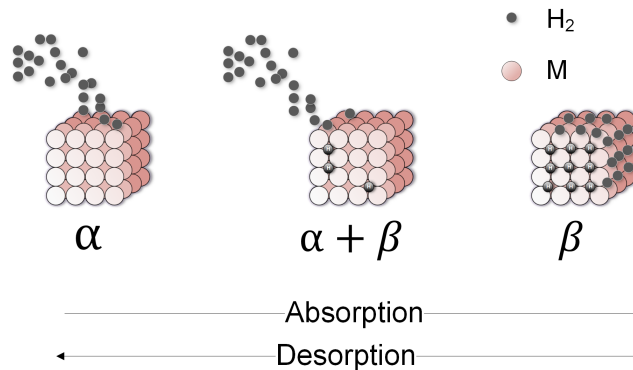


Figure 2.14.: Metal hydrides: different phases

hydrogen, are driven by the pressure difference between the gaseous hydrogen, and the equilibrium pressure of the metal hydride (solid).

During the absorption phase, gaseous hydrogen has a higher pressure than the equilibrium pressure of the metal hydrides. This pressure difference drives the hydrogen to bond with the metal, where it is absorbed. Conversely, during the desorption stage, the MH equilibrium pressure is higher than the pressure of the

³Work already published [57]

released hydrogen, allowing the release of hydrogen. In both cases, the magnitude of the pressure difference directly influences the kinetics of the process. For stationary applications, fast kinetics are expected, resulting in complete hydrogen uptake and release in less than 3 mins [91].

The MH equilibrium pressure depends on the hydrogen concentration and temperature and is typically represented using Pressure-Concentration-Temperature (P-X-T) diagrams. It is associated with the enthalpy of the formation of the hydride (ΔH) and the associated entropy (ΔS). These relationships can be assessed using the Van't Hoff plot [92], which follows the equation:

$$\ln(P_{eq}) = \frac{\Delta H}{RT} - \frac{\Delta S}{R} \quad (2.25)$$

Where R is the universal gas constant and T is the absolute temperature. Furthermore, the relationship among the P-X-T curves and material-based properties, are addressed in Fig. 2.15.

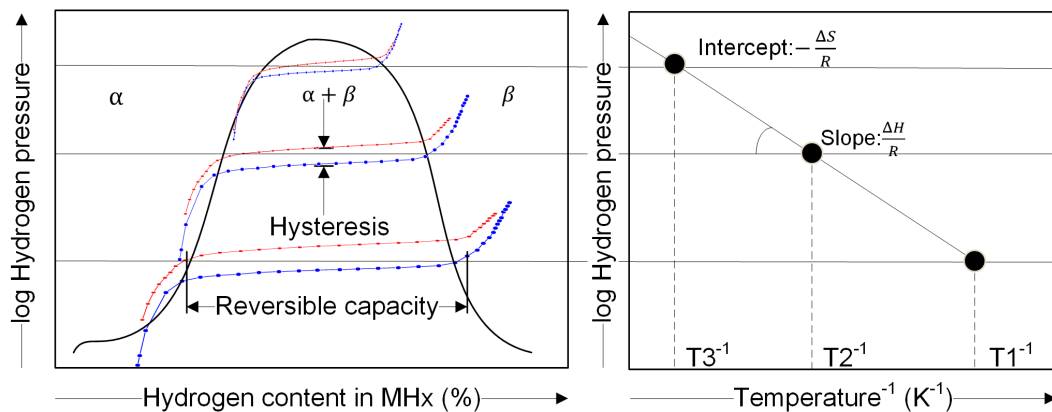


Figure 2.15.: P-X-T diagram and Van't Hoff plot

As depicted in Fig. 2.15, the P-X-T curves provide insight into the state of the metal hydrides based on their operating pressure and temperature. In an ideal scenario, within the biphasic zone ($\alpha + \beta$), the pressure remains constant. However, under real working conditions, a slight slope of pressure increase can be observed. Additionally, there is a pressure gap between absorption (which occurs at higher pressure) and desorption stages due to hysteresis phenomena. For the evaluation of the Van't Hoff plot, the plateau pressure is generally approximated as the average value between the pressures of the two stages within the biphasic zone.

The solid hydrogen storage systems and the proper materials have been reported in numerous studies [93, 94, 95]. Indeed, different types of metal alloys can be adopted for hydrogen storage, as highlighted by the review done by Modi et al. [91], where metals operating at room temperatures ($-50\text{ }^{\circ}\text{C} \div 100\text{ }^{\circ}\text{C}$) are further discussed. The most adopted alloys are the intermetallic compounds, which can be divided into different families, as illustrated in Tbl. 2.4 with some examples.

Table 2.4.: Intermetallic compounds families for metal hydrides [96].

Family	Metal	Metal hydrides	hy- Concentration limit [wt%]	Enthalpy of formation [kJ/mol]
AB ₅	LaNi ₅	LaNi ₅ H ₆	1.3	30.1
AB	FeTi	FeTiH _{1.95}	1.7	28.1
AB ₂	ZrMN ₂	ZrMN ₂ H ₄	1.7	53.2
A ₅ B	Mg ₂ Ni	Mg ₂ NiH ₄	7.0	53.2

While there is rather extensive research on the hydrogenation-dehydrogenating process, there is still a lack of systematic analyses of these technologies integrated with other energy systems. Therefore, the focus of this thesis section is to present an overview of metal hydride system control strategies, and their effects coupled with a hydrogen source, as well as a hydrogen compressor, and a conditioning system to adjust pressure and temperature properly. By examining these aspects, a more comprehensive understanding of the potential of metal hydride systems for hydrogen storage in energy applications.

2.5.2. Metal hydrides and ancillary systems

The solid hydrogen storage system is typically a pressurized tank filled with metal powders. Based on the pressure of the gaseous hydrogen at the inlet and outlet sections, the system is either in the charging or discharging mode (refer to Fig. 2.17). Ancillary systems, such as hydrogen compressors and the conditioning system, are connected to it as needed.

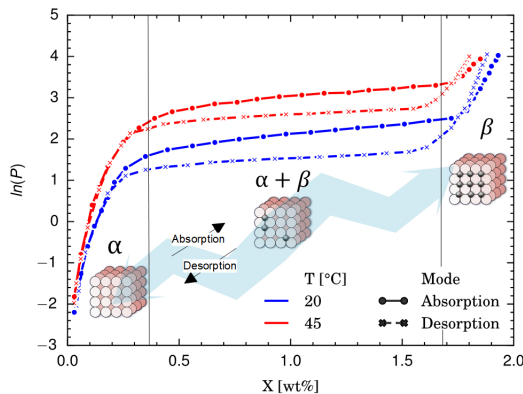


Figure 2.16.: Metal hydride phases: i) solid solution phase, ii) metal-hydrogen solution phase, and iii) hydride phase.

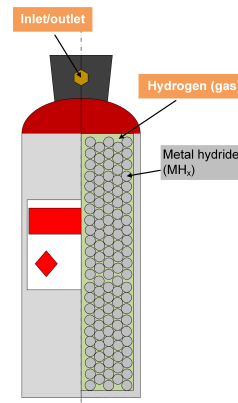


Figure 2.17.: Metal hydrides hydrogen storage system: pressurized hydrogen is injected into the tank where the metal powder is contained.

The layout for both charging and discharging stages is shown in Fig. 2.18 and it can be divided into three zones:

1. Hydrogen pressure control zone: in the charging phase, the pressure is managed by the hydrogen compressor, while the pressure in the discharging phase is set based on the hydrogen consumption request (fuel cell).
2. Metal hydride system: it presents an exothermic behaviour in the charging phase and an endothermic one in the discharging phase.
3. Temperature control zone: this area involves the conditioning system of the metal hydride system, which has to cool the metal hydrides down during the charging and warm them up during the discharging stage. The application of the heat pump is used to supply both heating and cooling energy when required.

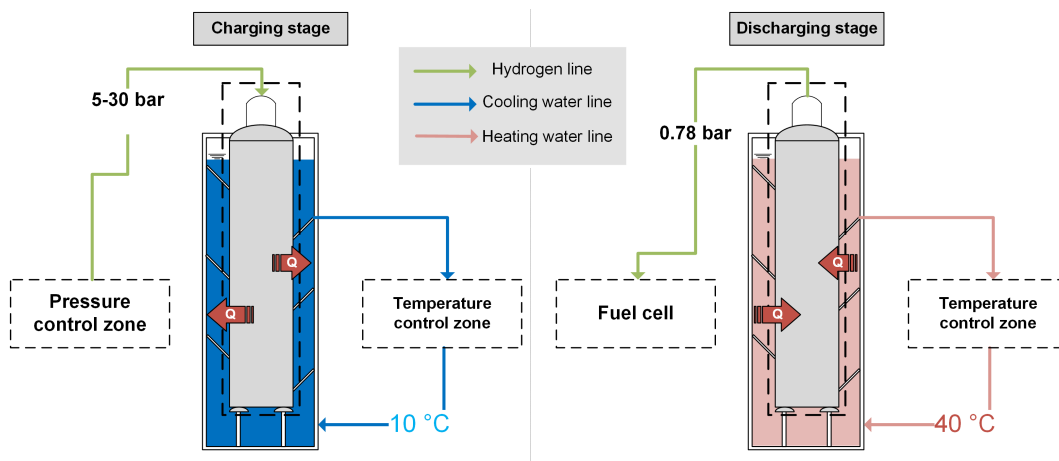


Figure 2.18.: Systems' layout for both charging and discharging stages.

2.5.3. Metal hydride system modelling and testing

To gain an extended overview of the control strategies, different scenarios varying the operating pressures and temperatures have to be included. For this study, the operational parameters' ranges are listed in Tbl. 2.5 where the conditioning water temperature is set as 10 °C during the absorption phase, and 40 °C in the desorption one. The system's temperature is chosen from a predefined set.

As the core of this analysis, the metal hydrides numerical modelling has been investigated deeper, which is divided into two steps:

1. The parameterization of experimental data, provided by the manufacturer of the metal hydride system, involves assessing the metal's technical properties using a polynomial fitting method. This method determines the equilibrium

Table 2.5.: MH numerical testing: Operation parameters' range and conditions.

	Absorption	Desorption
X [%]	0.2→ 1.5	1.6→ 0.2
Pressure [bar]	15, 20, 25	0.78
Setting temperature [°C]	15, 20, 25	20, 25, 30, 35
Water temperature [°C]	10	40
Heat pump refrigerant type		R134a
Heat pump refrigerant temperature [°C]	5-15	50-70
Overall heat exchangers efficiency [-]		0.8
Hydrogen compressor efficiency [-]	0.8	n.a.

pressure function concerning changes in concentration (X) and temperature, thereby providing information about its value at operating conditions not directly obtained in the experiments. Similar approaches have been employed by Hariyadi et al. [97] and Talagañis et al. [98].

To facilitate dynamic evaluation, specific technical parameters of the material, such as enthalpy variation, must be known in advance. Thus, a parameterisation process using the P-X-T diagram and the Vant'hoff plot (as described in Dornheim's work [99]), which is also reported in Hariyadi's work [97], is employed with the relationship stated in Eq. 2.26.

Regarding the kinetic parameters of the metal, they cannot be derived from the P-X-T curve due to the absence of the time variable. Therefore, in this study, the kinetic parameters are sourced from the scientific literature [98].

$$\ln(P) = \frac{\Delta H}{RT} - \frac{\Delta S}{R} \quad (2.26)$$

2. The numerical modelling of the kinetics of the metal hydride system relies on ordinary differential equations to establish mass and energy balances. The equations used in this work are based on the by various researchers (Gambini et al. [100, 101] and Talagañis et al. [98]).

The mass concentration variation within the solid is described by the following equation with its upper limit occurring during the charging phase, specifically when the β phase has been reached, while for the discharging stage, such limit is equal to zero.

$$\frac{dX}{dt} = K_{a,d} e^{-\frac{E_{a,d}}{RT}} \cdot \ln\left(\frac{P}{P_{eq}}\right) \cdot |X_{lim} - X| \quad (2.27)$$

This can be converted into solid hydrogen mass using the definition of X , which

Chapter 2. Hydrogen as energy storage

is defined as the mass ratio:

$$X = \frac{m_{H_2}}{m_{H_2} + m_s} \quad (2.28)$$

therefore, the mass balance of the gaseous hydrogen is expressed as follows:

$$\frac{dm_{H_2,g}}{dt} = -\frac{d(X \cdot (m_{H_2} + m_s))}{dt} + \dot{m}_{H_2,in} - \dot{m}_{H_2,out} \quad (2.29)$$

Under the assumption of an ideal scenario, where the mass of the gaseous form of hydrogen within the metal hydrides system remains constant, the hydrogen mass flow balance is defined as follows:

$$\dot{m}_{H_2,in} - \dot{m}_{H_2,out} = \frac{d(X \cdot (m_{H_2} + m_s))}{dt} \quad (2.30)$$

Finally, the energy balance can be expressed by Eq. 2.31, where the specific heat capacity of the system includes both solid and gaseous hydrogen (see Eq. 2.34).

$$C \frac{dT}{dt} = -\frac{\Delta H}{MW_{H_2}} \frac{d(X \cdot (m_{H_2} + m_s))}{dt} + \dot{m}_f c_f \epsilon (T_f - T) + \dot{m}_{H_2,in} \cdot h_{in} - \dot{m}_{H_2,out} \cdot h_{out} \quad (2.31)$$

$$C = (m_{H_2,g} \cdot cp_{H_2} + (m_{H_2} + m_s) \cdot cp_s) \quad (2.32)$$

It is assumed to have a constant supply pressure; as a consequence, the temperature of the system must remain constant over time:

$$\dot{m}_f c_f \epsilon (T_f - T) = \frac{\Delta H}{MW_{H_2}} \frac{d(X \cdot (m_{H_2} + m_s))}{dt} - \dot{m}_{H_2,in} \cdot h_{in} + \dot{m}_{H_2,out} \cdot h_{out} \quad (2.33)$$

Additionally, since the solid mass of the hydrogen (m_{H_2}) can reach up to 1.6 -2% of the metal mass (for AB₂-type metals), its contribution to the overall mass can be neglected.

$$(m_{H_2} + m_s) \approx m_s \quad (2.34)$$

For the evaluation of different sets of operational parameters (pressure and temperature), the following indicators have been used to evaluate both economic and control perspectives:

- The time required to reach the pre-defined weight concentration condition, indicating the amount of hydrogen stored or discharged (Tbl. 2.5), is considered as one performance indicator.

2.5. Innovative hydrogen storage: Metal hydrides

- Another set of indicators is the energy consumption of the heat pump and the hydrogen compressor during the capture and release of hydrogen. These indicators are linked together and provide preliminary insights into the operating cost of the entire process.

2.5.4. Evaluation of operational strategies

The results of the dynamics in both stages are presented Fig. 2.19. In the charging stage, the hydrogen gas is injected at the inlet with the set pressure. The exothermic nature of the absorption process, along with the gaseous hydrogen inlet, leads to an increase in the system temperature, but the conditioning system compensates for it by controlling the water mass flow rate (heat transfer fluid) flowing through the storage system. Conversely, in the discharging stage, the dynamics are similar but reversed with the conditioning system working to recover the temperature drop. Moreover, the concentration variations differ between the absorption and desorption stages that are influenced by the kinetic and activation energy parameters. As a consequence, the required thermal energy varies significantly between the two phases with the desorption one requiring a lower thermal energy.

Numerous combinations of the operational parameter sets are explored to provide a comprehensive understanding of the performance indicators as shown in Figures 2.20a and 2.20b. When only one controllable parameter is considered, the influence of changing operational conditions is straightforward. Indeed, for the desorption phase, the dynamic indicator and the energy indicator form a Pareto-curve shape where both indicators cannot be minimised at the same time. However, the absorption phase presents a more complex situation due to the presence of multiple controllable parameters, including temperature and pressure. Additionally, their associated energy consumption is connected with the dynamics. It is observed that to store the same amount of mass, the dominant parameter for the dynamics is the pressure; indeed, over a certain pressure threshold (e.g., 15 bar), the set temperature would not affect the charging time considerably. Moreover, under such a pressure threshold, the system cannot reach the targeted charged mass due to the low-pressure gap. By reducing the system set temperature, not only the energy dedicated to the heat pump compressor is reduced, but the hydrogen compressor would benefit from it since the charging time lowers.

2.5.5. Study's potential and limitation

This section of the thesis delves into the exploration of dynamic control strategies for a metal hydride (AB_2 type) system employed in solid hydrogen storage. The numerical modelling relies on experimental data characterizing the P-C-T diagram provided by the system's supplier. In the absorption stage, it becomes evident that hydrogen pressure significantly influences the process time, surpassing the

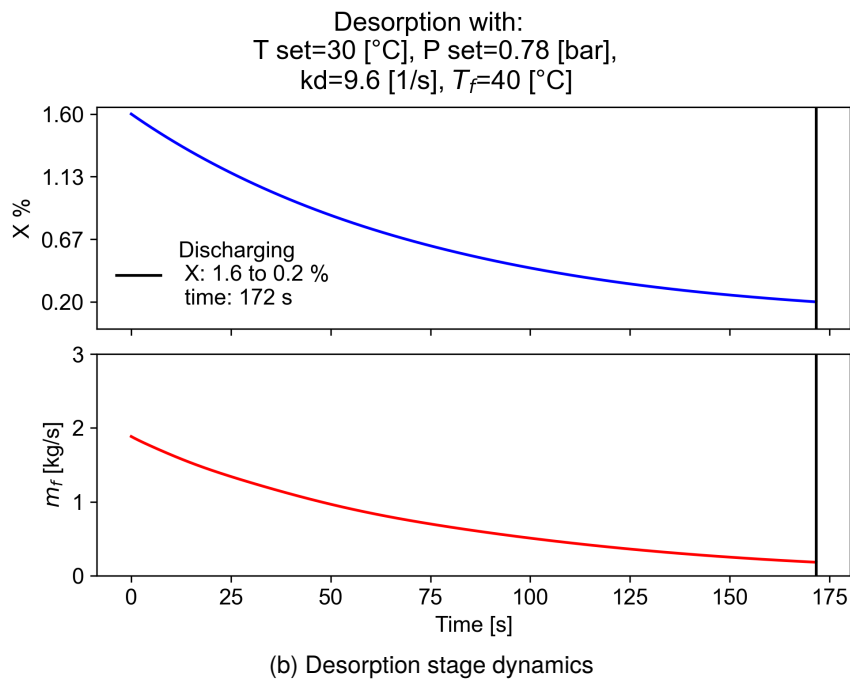
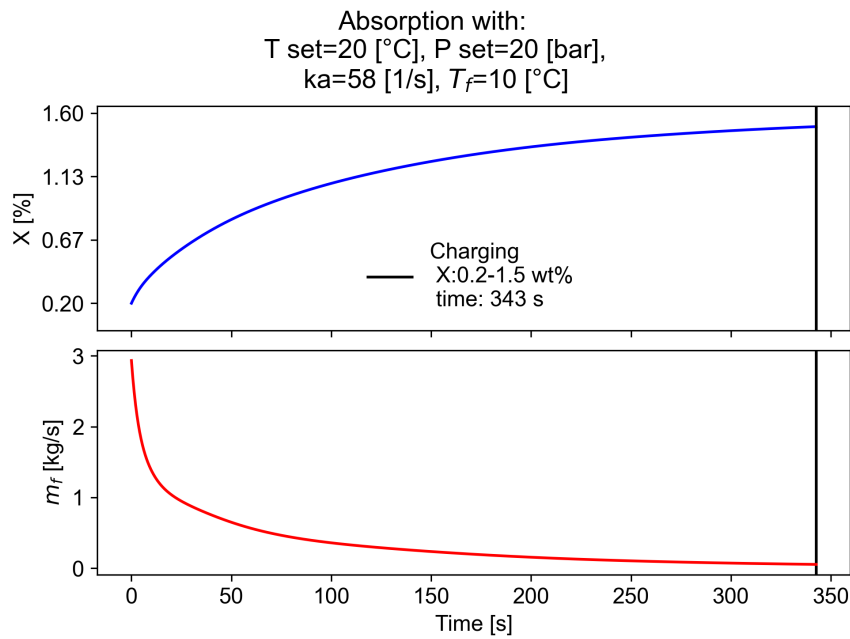
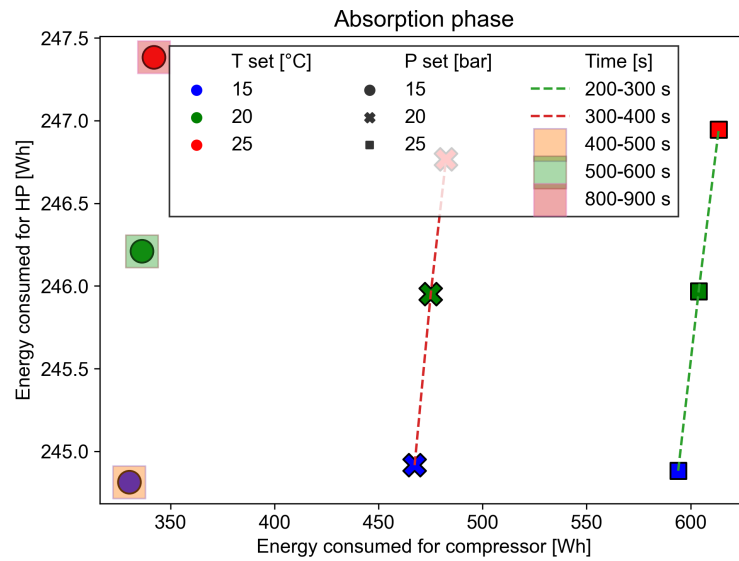


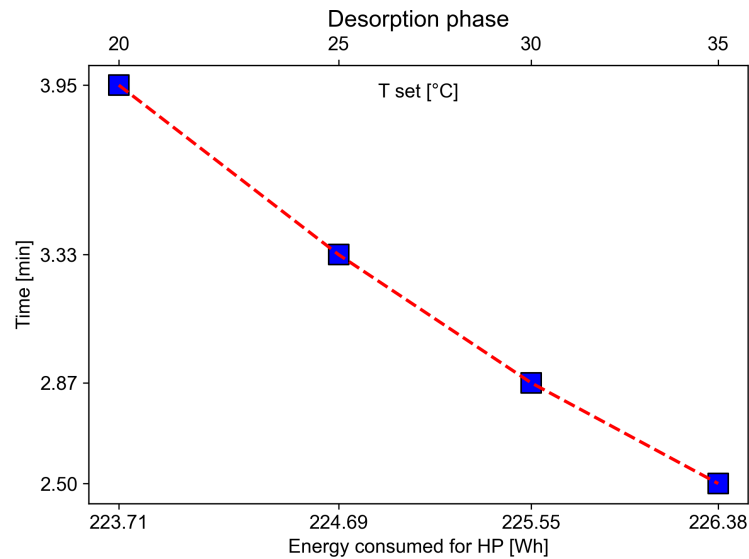
Figure 2.19.: Examples of metal hydrides hydrogenation and de-hydrogenation kinetics.

impact of conditioning temperature. However, this does lead to increased energy consumption by the hydrogen compressor. To counterbalance the energy costs of the hydrogen compressor, one approach could involve reducing the system's set temperature, despite the consequent increase in heat pump power. Nevertheless, the overall energy consumption is reduced due to the process's shorter duration. In

2.5. Innovative hydrogen storage: Metal hydrides



(a) Performance indicators in the absorption phase. Various colours representing different set temperatures (blue, green, and red), shapes indicating setting pressures (●, ✕, and ■), and dotted lines denoting the time needed for charging.



(b) Performance indicators during desorption.

Figure 2.20.: Performance indicators for the evaluation of metal hydrides operational strategy.

the desorption stage, achieving faster hydrogen release would come at the expense of higher conditioning energy supply costs. Determining an optimal operational strategy for both phases is no easy task, and future investigations may explore the following directions:

1. System controllers into the model, such as partial integral differential ones, to explore the response time of the system.

Chapter 2. Hydrogen as energy storage

2. Conducting experimental tests to ascertain material kinetic parameters and activation energy.

Chapter 3.

Battery Energy Storage Systems: Li-ion battery

A clever person solves a problem. A wise person avoids it.

Albert Einstein

Rechargeable lithium-ion batteries are currently the leading choice for Battery Energy Storage Systems (BESS) in mobile applications, including electric vehicles, thanks to their impressive energy and power density. Furthermore, they are also extensively employed in stationary applications.

Despite their high energy/power density, these batteries are subject to performance degradation in terms of both capacity and power over time. Furthermore, issues like electrolyte leakage and micro-short circuits may arise, potentially leading to battery failure and even triggering thermal runaway, as discussed in [102]. As a result, the implementation of an advanced battery management system becomes crucial for monitoring and optimizing battery behaviour and safety, preventing its accelerated degradation, throughout the entire electrification system, as emphasized in [103].

The Battery's State of Health (SOH) serves as a critical indicator of its overall condition and longevity. It assesses the battery's health in terms of its capacity (in Ah) and its current performance compared to its initial state.

Unlike other battery parameters, SOH cannot be directly measured. Its determination relies on various factors, including the battery's usage history, external conditions like current rates (C-rates), temperature, and operating range. These variables collectively influence the battery ageing process, resulting in diverse ageing paths. Consequently, accurately estimating SOH remains a subject of ongoing research [104, 105, 106]. Numerous research efforts have been dedicated to exploring the mechanisms underlying battery deterioration, all of which contribute to the degradation of Li-ion batteries. Based on a comprehensive review conducted by Edge et al. [105], the most influential factors include:

1. Solid Electrolyte Interface (SEI) layer growth.
2. Lithium plating.

3. Particle fracture.
4. Loss of Active Material (LAM).

Moreover, these mechanisms are interconnected, making it challenging to isolate their effects, thereby adding to the complexity of SOH estimation.

Over the years, extensive research has been dedicated to numerical modelling of Li-ion batteries, primarily aimed at assessing SOH, particularly for automotive applications to promote electric vehicle adoption [104]. Broadly, there are two main branches of battery models: Equivalent Circuit Models (ECM) and Physical-Based Models (PBM), as highlighted in Zhao et al.'s review [107]. ECMs represent batteries using an equivalent electrical circuit, employing essential electrical components like resistors and capacitors to simulate battery behaviour. While ECMs are relatively easy to implement and offer fast solutions, they often lack the accuracy needed for real-world battery applications, especially in dynamic scenarios. On the other hand, PBMs delve deeper into battery physics, encompassing phenomena such as Butler–Volmer kinetic equations [108, 109]. PBMs provide insights into internal battery dynamics, including Li-ion diffusion, ohmic effects, and electrochemical kinetics. Consequently, they enable a more comprehensive assessment of battery degradation. To enhance the accuracy of PBMs further, an increasing number of researchers are incorporating data-driven and machine-learning techniques [106]. As the level of physical detail increases, so does the computational burden, as illustrated in Fig. 3.1. The available PBMs include the Single Particle Model (SPM) [110], Single Particle Model with electrolyte (SPMe) [110], and Doyle-Fuller-Newman Model or Pseudo Two Dimensional (PS2D) [108].

From the perspective of energy systems, particularly in the context of stationary applications like local energy communities, a comprehensive assessment of SOH offers several advantages:

- **Preventing Premature Battery Depletion:** Assessing SOH helps prevent situations where the battery's lifetime expires before the intended design time. Such scenarios often lead to discrepancies between the planning phase of the LEC and its actual operation.
- **Reducing Capital Expenditure:** By extending the battery's lifespan through proper BMS, LECs can reduce their overall capital expenditure, thus achieving cost savings.
- **Facilitating Accurate Comparisons:** SOH assessment enables more precise comparisons with alternative energy storage solutions. Battery degradation, although complex, is often not considered in energy planning and optimisation models, allowing batteries with extended lifespans to outperform other options.

Therefore, this chapter of the thesis focuses on highlighting the efforts done during the Ph.D. study to investigate both types of numerical models of Li-ion battery

3.1. Li-ion modelling: Equivalent Circuit Models' robustness

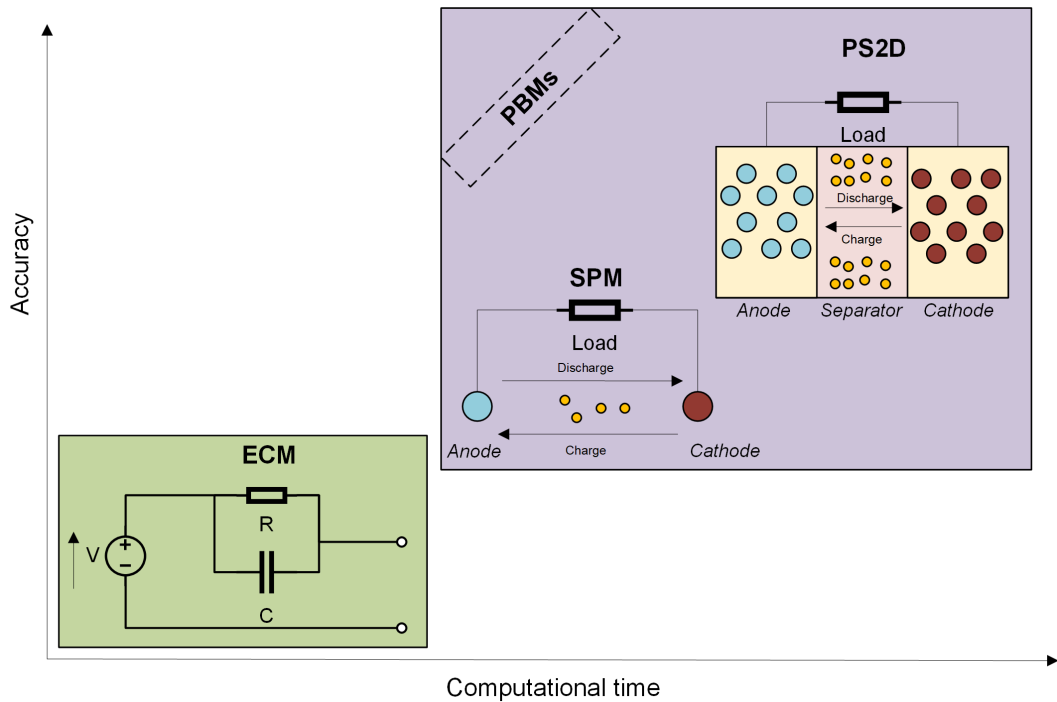


Figure 3.1.: Battery models comparison

degradation, from a different perspective¹, with the objective to answer research question 4 (1.4):

How to capture the degradation phenomena of Lithium-ion batteries?

This chapter is structured as follows:

1. Firstly, a study that assesses different ECM data-driven models' sensitivity, aiming to provide an exhaustive overview of the robustness of the most commonly adopted data-driven models is presented.
2. Next, a section involves the application of physical modelling of the battery using *Pybamm*, to evaluate the SOH of the battery. This evaluation is based on multi-objective multi-energy system scheduling, ultimately providing the optimal solution from the Pareto frontier.

3.1. Li-ion modelling: Equivalent Circuit Models' robustness

Microscopic ageing mechanisms in batteries are closely tied to the storage conditions, whether the battery is at rest or undergoing cycling. These conditions give rise to two distinct types of ageing: calendar ageing and cycle ageing. While both ageing modes

¹Works described in this chapter is published in [111], or under revision.

occur throughout the battery's life, investigating their combined effects presents a non-trivial challenge, and thus, the scientific community often studies them separately. Calendar ageing includes all the mechanisms that take place when the battery is at rest, stored under fixed conditions. It directly depends on the storage temperature and the State of Charge (SOC) level of the battery. Conversely, cycle ageing is characterized by the battery's cycling operational conditions, influenced by factors such as temperature (e.g., ambient, pack, or cell temperature), Depth of Discharge (DOD), charge or discharge current (C-rate), and the total number of cycles [112]. Fig. 3.2 illustrates the relationships between these two distinct ageing modes and highlights the key parameters influencing each mode.

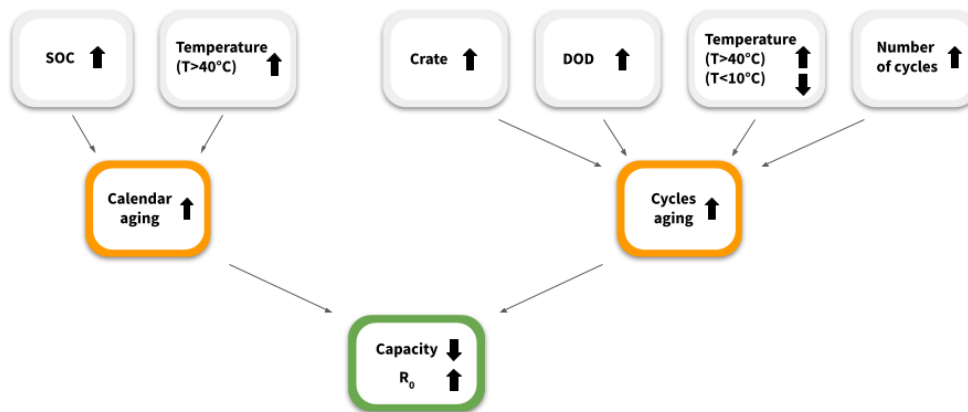


Figure 3.2.: Relation between calendar and cycle ageing: as a result, the capacity drops and the resistance increases.

The internal resistance, often denoted as R_0 , plays a critical role in determining the energy dissipated as heat due to the Joule effect. It's important to note that R_0 cannot be measured directly, but its nominal value is typically provided in the datasheets. R_0 differs significantly from the resistance that can be estimated from the electrical model, and it depends on the amount of current injected into the battery.

Apart from ageing effects, R_0 is generally influenced by both temperature and the State of Charge (SOC) level. Its resistance decreases promptly as the temperature increases and vice versa [113]. Operating batteries at high temperatures is unfavourable as it can lead to substantial battery degradation due to the Joule effect. However, the impact of SOC level on R_0 in Li-Ion batteries is considered minor compared to its variations caused by ageing processes and operating temperature changes [114].

The maximum capacity of a battery denoted as C , and its residual capacity, denoted as C_{res} , represent the maximum amount of charge the system can store and release,

3.1. Li-ion modelling: Equivalent Circuit Models' robustness

respectively. These values cannot be directly measured and must be estimated by the BMS, which calculates the amount of energy transferred into or out of the system. Estimating residual capacity can be challenging and may become more accurate after deeper operational cycles, while it can present difficulties in the case of short charge and discharge cycles. Similar to R_0 , residual capacity depends on both ageing and temperature factors [115]. Since there is a strong relationship between the residual capacity and the ageing of the BESS, the residual capacity is considered the main parameter to define the SOH of a battery. Typically, the SOH of a battery is defined as the ratio between the residual C_{res} and the rated capacity C_0 according to Eq. 3.1:

$$SOH(t) = \frac{C_{res}(t)}{C_0} \quad (3.1)$$

Moreover, R_0 plays a key role in defining the SOH, albeit with less prominence in the scientific literature. Thus, the specific formula that relates R_0 with the SOH has not been provided in this work since it is out of the scope of the current study. The SOH value is the determining factor to define the EOL, and it is specifically tailored for each application according to the minimum operative conditions required by the storage system. For instance, the EOL for automotive applications is usually set equal to 80% since the residual capacity reflects the vehicle range. A similar metric to EOL is the remaining useful life (RUL) which defines the residual operating life of a BESS, which is usually expressed in the number of cycles.

Despite an extensive review of the scientific literature on BESS' ageing models, using the ECM approach, where the machine-learning techniques are adopted, that the models are firstly trained based on controlled experiments. None of them investigated so far incorporate a sensitivity analysis to assess the models' response to input variations post-training. Indeed, this is a crucial aspect that still remains unexplored, which is the focus of this thesis section.

3.1.1. Sensitivity analysis

The sensitivity analysis, which aims to evaluate the robustness of models and how these deal with an unexpected variation in the input variables compared to the training dataset, is conducted. This analysis allows the identification of which parameters have the greatest impact on model predictions and determines the range of values over which a specific model is most accurate. This study considers the variation of both temperature and current since they represent the principal cycling factors that impact the battery life [116].

Univariate and multivariate analyses are performed to study how the variation of a single quantity, or both quantities simultaneously, affects the model response. Each ageing model is described by a parametric equation, which changes based on the model selected, reported in the dedicated appendix section (B.1). The analysis comprises firstly a training phase to compute model parameters that are then tested

on another dataset. Simulated data are obtained with an algorithm based on a least-squares support-vector machines model, which has been trained using experimental data obtained by [117]. As a result, a simulated dataset of 160 Ah BESS is used in these analyses.

Regarding the univariate analysis, data are obtained by changing the temperature and keeping the current and vice versa. Temperature and current values for the univariate analysis are changed as shown in Table 3.1.

Table 3.1.: Operating conditions of simulated data through the univariate analysis.

Temperature	20 °C	25 °C	30 °C	35 °C	
C-rates	0.1C	0.25C	0.5C	0.75C	1C

A residual capacity curve is generated per each value as shown in Fig. 3.3 and 3.4.

The models are trained considering current values of 0.1C and 1C and, temperature values of 20 °C and 35 °C; then, each model previously trained is tested to the excluded values, namely 0.25C, 0.5C, and 0.75C concerning the current and 25 °C and 30 °C regarding the temperature. Conversely, the dataset used for

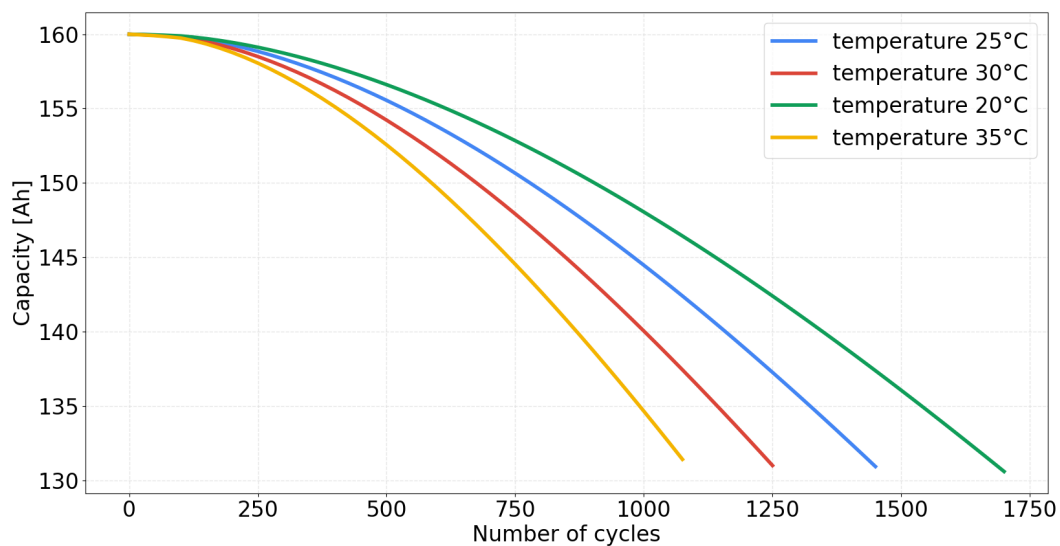


Figure 3.3.: Simulated dataset used for the temperature sensitivity analysis: the residual capacity of the battery is plotted as a function of the number of cycles. Temperature values range from 20 °C to 35 °C.

the multivariate analysis is composed of degradation curves that are generated using different temperatures and currents as reported in Fig. 3.5. The value pairs reported in Table 3.2 are the operating conditions simulated to resemble the ageing phenomena for the multivariate analysis. It is worth noting that only the pairs (0.1C, 20° C) and (1C, 35° C) have been used for the training process, while the remaining

3.1. Li-ion modelling: Equivalent Circuit Models' robustness

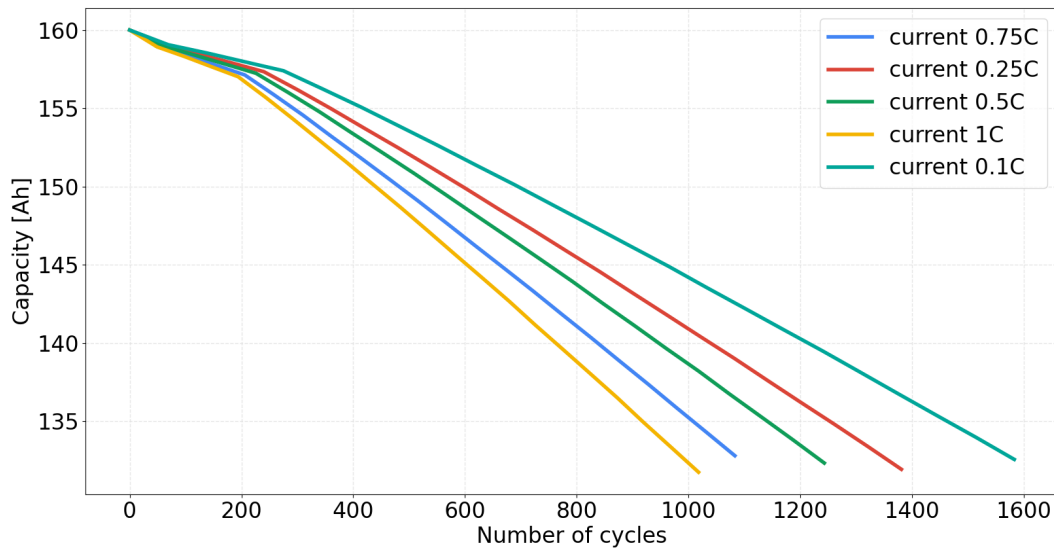


Figure 3.4.: Simulated dataset used for the current sensitivity analysis: the residual capacity of the battery is plotted as a function of the number of cycles. Current values range from 0.1C to 1C.

Table 3.2.: Variation in operating conditions of simulated data for the multivariate analysis. Temperature and current are simultaneously changed

Temperature	C-rate
20°C	0.1C
24°C	0.25C
27.5°C	0.5C
31°C	0.75C
35°C	1C

ones have been employed for the model testing. The values used for the testing phase are those that have not been used in the training process of both univariate and multivariate analyses. The other parameters that affect an ageing degradation are kept fixed as reported in Tbl. 3.3.

The Particle Swarm Optimisation algorithm [118] is used to get the optimum model parameters due to its effectiveness in dealing with non-linear functions.

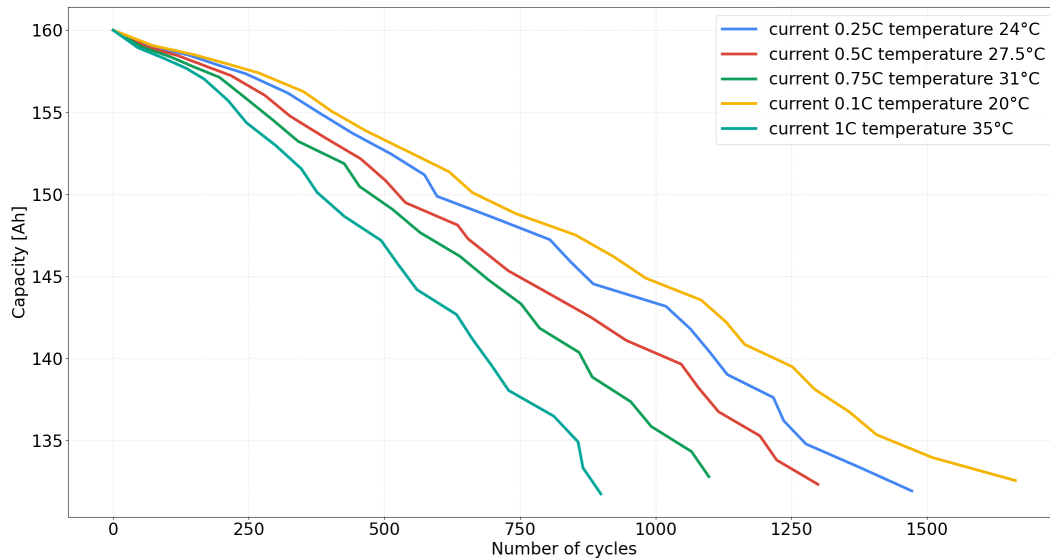


Figure 3.5.: Dataset used for the multivariate sensitivity analysis: the residual capacity of the battery is plotted as a function of the number of cycles. Temperature values range from 20° C to 35° C, while the current ones between 0.1C and 1C.

Table 3.3.: Other parameters used in the testing process

Fixed input	Values	Notes
DOD	85%	Depth Of Discharge in each cycle
SOC average	50%	Average SOC level in each cycle
C-rate	0.1C	Current fixed in the univariate temperature analysis
T	20 °C	Temperature fixed in the univariate current analysis

3.1.2. Selected models

For this study, three models described in the scientific literature have been selected to assess the ageing phenomena of the simulated 160 Ah BESS, that are namely:

- Omar et al's [117].
- Wang et al's. [119].
- Baghdadi et al.'s [120].

These models have been chosen due to their completeness in terms of inclusion of the principal macroscopic quantities affecting the ageing phenomena (e.g., temperature, charge/discharge current, DOD, SOC, easiness of training, and frequent employment in the scientific literature).

Omar et al. [117] used four mathematical equations to describe the data acquisition separately based on the variation of the principal quantities affecting the ageing

3.1. Li-ion modelling: Equivalent Circuit Models' robustness

phenomena. Since the input variables are treated individually, these models can be easily trained. Wang et al. [119] used an exponential model that is widely employed when dealing with cumulative degradation dynamics due to its robustness and easier identification procedure of the parameters [121]. The authors of [120] implemented both calendar and cycle ageing using only one model, thus improving its application when dealing with several conditions. The selected models are further discussed in Appendix B.1.

3.1.3. Comparison metric

The main metric used to compare the effectiveness of the used models is the Mean Average Percentage Error (MAPE) as described in Eq. 3.2. This parameter provides a coherent comparison between the models of [119] and [120] because the outputs are the same (e.g., capacity), while it represents an error indication in all the models of [117] whose outputs are expressed in terms of number of cycles at a different scale.

$$MAPE = \frac{100\%}{n} \sum_{t=1}^n \left| \frac{y_t - \hat{y}_t}{y_t} \right| \quad (3.2)$$

3.1.4. Comparison results

Different data of temperature and current are employed in the training and evaluation phase to define which model provides a more reliable and robust characterisation. In particular, both temperature and current are varied either singularly or simultaneously while keeping the other quantities unchanged, as reported in Tbl. 3.4.

Table 3.4.: Training & test sets

	Train	Test
Temperature varying univariate	20°C 35°C	25°C 30°C
Current varying univariate	0.1C 1C	0.25C 0.25C 0.75C
Multivariate	(0.1C, 20°C) (1C, 35°C)	(0.25C, 25°C) (0.5C, 27.5°C) (0.75C, 31°C)

Temperature univariate analysis

For the temperature-varying univariate analysis, the model's performances are reported in Tbl. 3.5. Among the studied models, the most robust one when dealing

with temperature variations is Baghdadi's model. A slightly worse performance is obtained by using Omar's model, particularly at the 30 °C curve. Conversely to the other models, Omar's one is not a viable solution as it solely considers a single quantity and requires a more complex parameter computation, making it unfeasible in practical applications. Although both Baghdadi and Wang's models cannot significantly discriminate the ageing evaluation among the two values of the temperature, Baghdadi's model is slightly more robust and represents the best choice when considering temperature variations. However, experimental data reported by Omar et al. [117] indicate that 20°C is the optimal temperature condition that ensures a greater Remaining Useful Life, whereas a decrease of the life cycles is expected with a temperature lower and greater than 20 °C. Conversely to Omar's model which describes each residual capacity point at different temperatures with a concave downward parabola, Baghdadi and Wang's models are not able to reproduce that behaviour, unless a training curve with temperatures lower than 20 °C is used. Therefore, further models should be investigated for possible future development.

Table 3.5.: MAPE computed in the temperature sensitivity analysis

<i>Temperature</i>	Wang	Baghdadi	Omar
25°C	1.19 %	1.05 %	14 %
30°C	1.79 %	1.54 %	14 %

Current univariate analysis

The MAPE calculated during the current sensitivity analysis to compare the performance of all models is presented in Tbl. 3.6. Wang's model exhibits the highest robustness across all C-rate values. The poorest performance was observed with Omar's model, particularly at 0.25C. Furthermore, considering that Omar's model does not account for other variables and involves a more complex training phase, resulting in a set of parameters for each capacity value, it is not a practical choice compared to the others. Baghdadi's model does not perform as effectively as Wang's model. Consequently, Wang's model is the most robust and represents the optimal choice when accounting for current variations.

Table 3.6.: MAPE computed in the current sensitivity analysis.

<i>C-rate</i>	Wang	Baghdadi	Omar
0.25 C	0.85 %	4.83 %	16.53 %
0.5 C	0.96 %	4.84 %	13.46 %
0.75 C	1.26 %	3.09 %	10.18 %

3.2. Li-ion battery degradation modelling: State of health as Pareto frontier indicator

Multivariate analysis

The MAPE values computed for the multivariate analysis, used to compare model performance, are presented in Tbl. 3.7. Wang's model demonstrates the highest robustness when considering variations in both temperature and current. Omar's model has been excluded from this analysis because each of its equations assesses ageing based solely on the variation of a single input variable, rendering it unsuitable for multivariate analysis.

Table 3.7.: MAPE computed for the multivariate sensitivity.

<i>C-rate, Temperature</i>	Wang	Baghdadi	Omar
0.25C, 24°C	0.55 %	4.43 %	NA
0.5C, 27.5°C	0.76 %	4.49 %	NA
0.75C, 31°C	0.73 %	2.79 %	NA

3.1.5. Study's remarks and limitations

The study presented in this section presents a sensitivity analysis of data-driven ECMs for battery ageing, to evaluate how a model deals with the variation of the BESS operating conditions. Three different ECMs have been included in the study, using the data of a 160 Ah battery.

Regarding the univariate analysis of temperature, the best model is represented by Baghdadi et al. [120] when dealing with both temperature values of 25°C and 30°C. Differently, the model of Wang et al. [119] is the most robust solution when dealing with current variation for values of 0.25 C, 0.5 C and 0.75C.

The results of the sensitivity analysis showed that all three models were able to predict battery ageing under various operating conditions. However, some models were more sensitive to the variation of certain factors than others. The inclusion of other mathematical or data-driven models in a future sensitivity analysis of battery ageing could provide interesting results. Particularly, data-driven models such as neural networks use deep learning algorithms to identify patterns and non-linear relationships in data, and can often provide more accurate predictions than mathematical models, particularly when working with complex systems such as batteries.

3.2. Li-ion battery degradation modelling: State of health as Pareto frontier indicator

In the energy system modelling sector, When there are multi-objectives to optimise, a trade-off among them has to be found, and there are different techniques to find

the set of the trade-off solutions, among them, ϵ -constraint method proposed by Mavrotas [48], and weighted sum method, are the most adopted ones by scientific community [122]. And as a result of both methods, the Pareto curve or Pareto frontier is obtained.

The Pareto curve is a graphical representation of the set of non-dominated solutions in a multi-objective optimisation problem. Each point on the curve represents a solution that is optimal in the sense that no other solution is better for all objectives. However, selecting the "ultimate" solution from the Pareto front depends on the decision maker's preferences and priorities among the different objectives. One way to select the best solution from the Pareto front is to use a decision-making method that incorporates the decision maker's preferences, such as weighting coefficients for objective functions or a utility function approach [123]. Another way is to use an interactive method where the decision maker provides feedback on the solutions presented and the algorithm generates new solutions based on this feedback. Ultimately, the "best" solution is subjective and depends on the decision maker's priorities and preferences.

The aim of this section is², to propose a novel approach, that assesses the battery'SOH, through a Li-ion battery physical modelling framework (*Pybamm* [124]), characterized by the battery manufacturer datasheet data, i.e. no experimental testing on the battery is required, due to different multi-objective scheduling operational strategies, each of them is a solution from Pareto curve, assessed from Home Energy Management System (HEMS), of a smart home case, where four distinct energy carriers and its related systems are included. It represents the smallest scale of the multi-carrier energy community. therefore the same methodology can be up-scaled to a bigger scale of energy communities. Finally, by using such an approach, the best solution is automatically identified, without any additional input from modellers. Indeed, compared to the previous sections' methodology, although ECMs are easy to implement and fast to solve, compared to PBMs, as previously illustrated in Fig. 3.1, they are data-driven, meaning the vast amount of the experimental data, under different operating conditions, have to be present [106], which quite often is not possible to have, the reason why for this study, physically based modelling is applied.

3.2.1. Pybamm framework and battery parameterization

PyBaMM (Python Battery Mathematical Modelling) is an open-source battery simulation package written in Python, and developed by a team of experts, funded by the British funding scheme, the Faraday Institution [125]. The whole repository of the framework can be found on the GitHub page at [126]. It solves physics-based electrochemical models of various types, like Doyle-Fuller-Newman (DFN) and also the Single Particle Model with Electrolyte, proposed by Marquis et al. [110], using

²Work carried out during the visiting period in Technical University of Eindhoven, under the supervision of Prof. Christina Papadimitriou (2023)

3.2. Li-ion battery degradation modelling: State of health as Pareto frontier indicator

state-of-the-art automatic differentiation and numerical solvers, such as CasADi [127], indeed multiple scientific papers are produced by the same developers, describing the framework modelling process [110, 128, 129, 130, 131, 132]. All models are implemented in a flexible manner, and a wide range of models and parameter sets are available. It is also possible to set specified drive cycles of the battery, using user-defined current, voltage, or power curves.

The parameterization of the Li-ion battery is the process of including the Li-ion battery characteristics into the Pybamm framework so that it can reproduce the battery's operational properties accurately, even under different operating conditions. Parameterization, therefore, has a fundamental role in the methodology, and it is divided into two steps, initialization and parameters tuning, which is based on the experimental data, that can be retrieved by the battery manufacturer.

Cell level model initialisation

The first step of the parameterization is the initialization of the Pybamm model using the datasheet's operational data, reported by Li-ion battery manufacturers:

1. Battery chemistry, which can be Lithium iron phosphate (LFP), Nickel Manganese Cobalt oxide (NMC) or Nickel-cobalt-aluminum (NCA). And based on the chemistry, the Modelers can select among the built-in parameter sets from the Pybamm framework, all of them can be consulted at [133].
2. Charging mode, although almost every manufacturer is adopting Constant Current-Constant Voltage (CC-CV) mode, it is possible to have some exceptions.
3. Electrode geometry, which is crucial to assess the electrical properties such as current densities, however, this information is not often reported in the datasheet.

From the modeller's perspective, the numerical model for the battery has to be selected, among different available ones, with the increasing physics details, but also the computational burden, as illustrated in Fig. 3.1. The ones based on physics are the Single Particle Model [110], Single Particle Model with electrolyte [110], Doyle-Fuller-Newman Model or Pseudo Two Dimensional [108].

The entire initialisation process is reported in Fig. 3.6, and once completed, it is already possible to perform experiments and assess the operational behaviour of the Li-ion battery, however, since the parameter set is based on the built-in ones, some of the properties may differ from the ones from the datasheet, the reason why the second step of the parameterization is needed.

Parameters tuning

As the second step of the parameterization, different parameters of the model have to be tuned, to fit the experimental data, provided by battery manufacturers. The

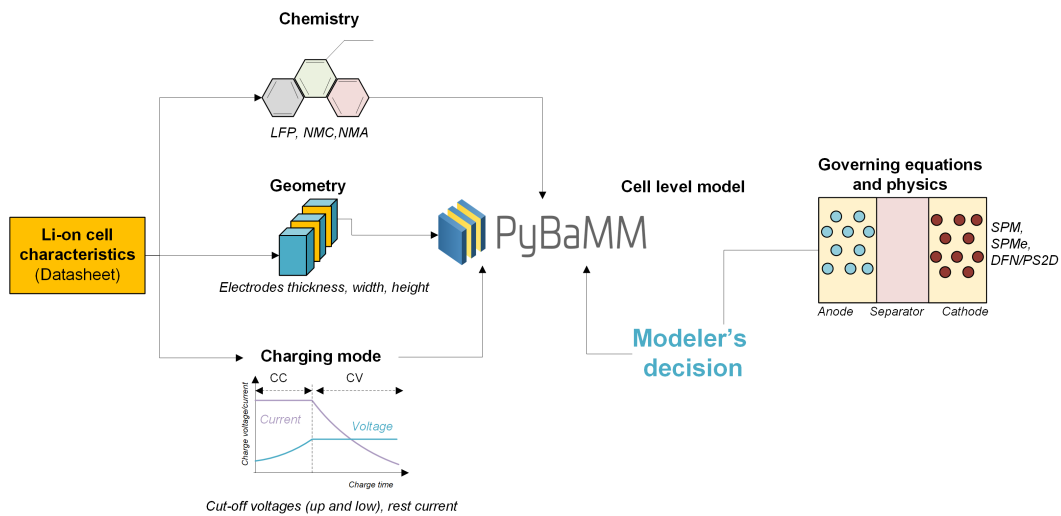


Figure 3.6.: Workflow of the initialization of Pybamm model.

whole workflow is represented graphically in Fig. 3.9.

From the datasheet provided by battery manufacturers, the following lab test results are usually reported:

1. Discharge curves at different C-rates.
2. Discharge curves at different temperatures.
3. Aging/degradation curves at 1-C cycles.

The parameters tuning is not trivial, since it is not straightforward which parameters to tune in order to have the best accuracy, compared with the experimental data. Additionally, thermal and electrical properties are strictly connected, by the kinetics of the electrode, governed by the Butler-Volmer equation, hence, making the parameters tuning even more arduous and complex. However, it is not impossible, and in this work, a data-driven technique, through the use of Mean Absolute Error (MAE) as an index, widely adopted in the machine learning research field, has been adopted. The process is illustrated in Fig. 3.7, and it has two steps:

1. Sensitivity analysis, of all tunable parameters, changing them from the default value and twice its original value, and observing the variation of MAE; Generally speaking, for proper sensitivity analysis, more data points of the parameters should be assessed, yet, with the vast amount of parameters to be evaluated, the computational effort would be enormous.
2. Selection of the most important parameters based on the previous step, and through the grid-search method, where all selected parameters are defined within their range, based on the physical meaning of the parameter, to finally obtain the values of the selected parameters, that minimise the MAE.

3.2. Li-ion battery degradation modelling: State of health as Pareto frontier indicator

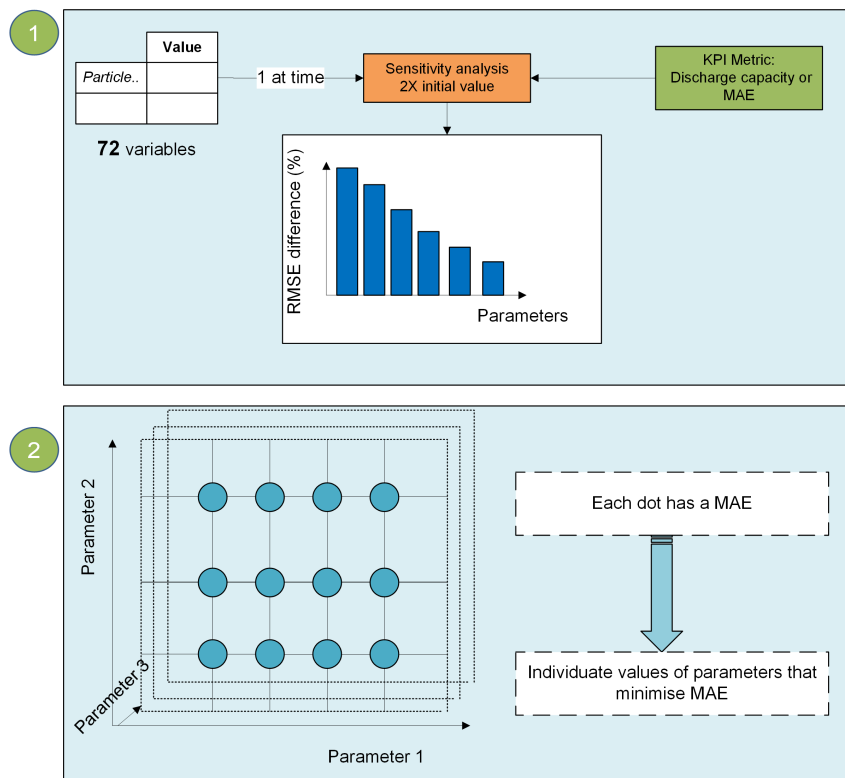


Figure 3.7.: Parameters selection and tuning process

Despite the intrinsic link between electrochemical and thermal properties, their parameterization can be decoupled, making the whole process easier. Indeed, the electrochemical experiments are done at a constant, standard temperature of 25°C/298 K, where the thermal properties are not subject to any variation. Subsequently, ageing parameterization can proceed as it requires the outputs of the electrochemical one. Furthermore, the ageing part requires an extended experiment, i.e. more than 2000 cycles of charging and discharging, meaning that it requires more computational time, compared to the other two parameterization steps. Thus, the whole parameters tuning is sequential consisting of the following steps: 1) electrochemical parameterization, 2) thermal parameterization, and finally 3) aging parameterization.

3.2.2. State Of Health assessment

In addition to the battery physical model (Section 3.2.1), the power curve of the battery, for each of the Pareto curve solutions from HEMS, is obtained. The complete workflow is depicted in Fig. 3.9. Where the battery cell power assessment module serves the purpose of converting power at the module level, sourced from HEMS, into the cell level. This distinction is vital as Pybamm operates at the cell level. On top of that, the electrical design of the battery cell-to-module must be carried out, with the already known cell characteristics (voltage, current, and capacity), provided

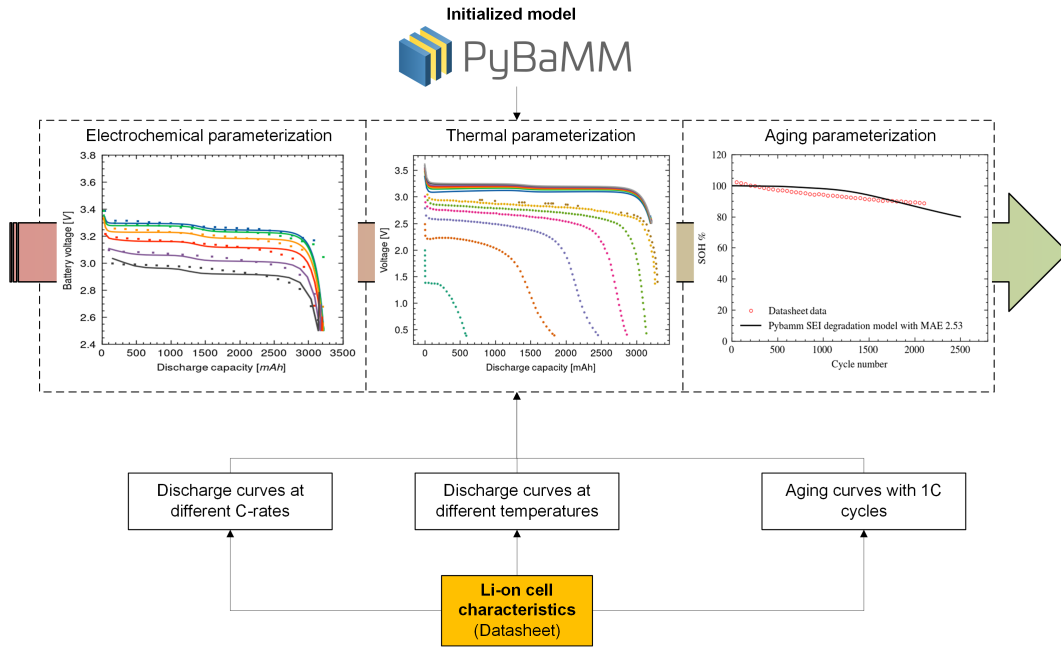


Figure 3.8.: Workflow of the parameters tuning for Pybamm model: 1) electrochemical parameterization, 2) thermal parameterization, and 3) ageing parameterization

by the manufacturer datasheet and already parameterized previously. The design process is initiated by selecting the nominal voltage of the battery module, which, based on market standards, can typically be 12, 24, or 48 V. Following this, the capacity of the module is determined. However, for the sake of simplicity and given that designing the battery management system is not within the scope of this work, it is assumed that the battery power is equally distributed across each cell.

$$N_{cells,series} = \frac{V_{batt}}{V_{cell}} \quad (3.3)$$

$$N_{cells,parallel} = \frac{E_{batt}}{V_{batt} \cdot C_{cell}} \quad (3.4)$$

$$P_{cell}(t) = \frac{P_{batt}(t)}{N_{cells,series} \cdot N_{cells,parallel}} \quad (3.5)$$

For each Pareto curve solution, there's a distinct power curve, meaning a distinct experiment for the parameterized model, with its own SOH indicator of the battery at the end of the evaluation time.

3.2.3. Results of the case study and limitation of the approach

LFP-type battery cells are adopted for the case study, with fifteen Pareto curve solutions based on two objectives, which are economical and environmental, for a

3.2. Li-ion battery degradation modelling: State of health as Pareto frontier indicator

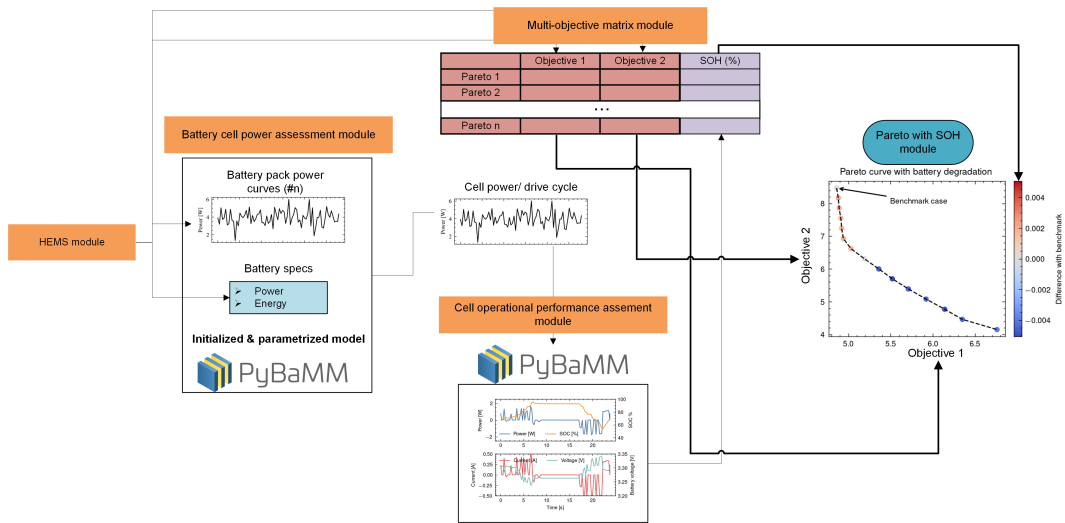


Figure 3.9.: Workflow of assessing the Pareto curve using SOH as indicator

four-energy-carrier energy system.

Thus, fifteen different experiments are performed using Pybamm, obtaining different SOH at the end of the evaluation time frame. Notably, due to the choice of a constrained evaluation window lasting 24 hours, this duration was insufficient to induce substantial battery degradation. To facilitate a comparative analysis of these solutions, it is established a benchmark case.

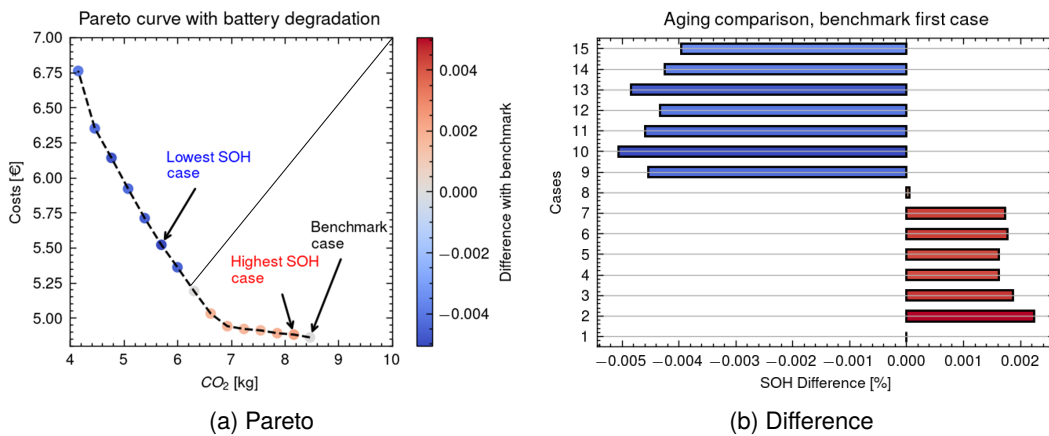


Figure 3.10.: SOH as Pareto indicator. The differences among the different cases are extremely low due to the limited time frame of the study.

The process of automatically selecting the ultimate case using a portable computer took approximately 10 minutes. Detailed specifications regarding computational resources and the case study are provided in the Appendix section, Tbl. B.4. While the results are visually depicted in Fig. 3.10. Fig. 3.10a presents a colour map illustrating the SOH difference among the 15 Pareto frontier solutions, using it as a KPI. In general, solutions without PV integration tend to have higher SOH compared to the

benchmark case. Notably, Case 8 represents a solution that effectively divides the Pareto frontier into two distinct zones. However, it's not a straightforward relationship where more PV penetration necessarily means lower SOH. In fact, Case 2 has the maximum SOH despite not having the least PV integration. Therefore, from a real-time scheduling perspective, the operational strategy employed in Case 2 emerges as the ultimate solution among all optimal scenarios. This strategy ensures the maximum health of the battery at the end of the evaluation time.

The results affirm the suitability of the proposed methodology for automatically determining the optimal solution, employing SOH as a performance metric. Overextended operational periods, such as 10 years, with consistent scheduling strategies, this approach can yield savings of up to 26.67% in battery lifespan. This is particularly significant in the context of multi-energy systems economics, given the frequency of battery replacements and their related investment costs. It is worth noting that while integrating PV systems can accelerate battery degradation due to increased usage, it is not immediately evident that the highest PV integration (case 15) leads to the worst SOH. In fact, the 10th scenario in the case study represents the worst SOH case, as illustrated in Fig. 3.10a. Therefore, the utilisation of SOH as a key indicator provides valuable insights.

The process of parametrizing the Li-ion cell is undeniably time-consuming, and its duration cannot be precisely estimated due to its inherent complexity. However, the Python-based architecture of Pybamm offers a practical advantage: once the parameters are determined and stored, they can be readily applied to any number of experiments involving the same type of cells. This eliminates the need to repeat the entire parameterization process for each subsequent study.

One-day evaluation time window was chosen to validate the methodology, primarily for computational efficiency. Nonetheless, it's important to note that this relatively short timeframe has a limited impact on battery degradation. Simulations over a more extended period should be performed for a proper analysis. While this will entail greater computational demands, it will provide a more comprehensive understanding of battery behaviour over time. Moreover, although the proposed approach has the novelty of automatic selection of the best solution from the Pareto curve, it also establishes a connection between battery operational parameters, such as SOH, and the optimization and scheduling problem of energy modelling. Nevertheless, it is important to acknowledge that the approach remains passive, in the sense that the SOH assessment and scheduling are conducted independently. Thus, there is a possibility to look for active integration, whereby the SOH derived from the Pybamm model serves as an indicator directly considered during the energy modelling optimization problem. With active integration, it would provide information that can directly influence the outputs of the optimisation process.

Part II.

**System approach: energy
planning**

Chapter 4.

Energy systems planning

The best way to predict the future is to create it.

Abraham Lincoln

Peter Drucker

The optimal planning of Local Energy Communities is a challenging task. Due to the presence of multiple energy technologies operating with different carriers, that interact with each other to satisfy the time-varying end-users energy demands. In addition, economic aspects are not sufficient to be considered for the optimal planning problem, whereas environmental constraints should be also taken into account. In summary, the most convenient LEC configuration and related operation strategies should be identified in terms of the choice of the energy technologies, their sizes, and their operation by ensuring both the economic and the environmental sustainability of the system.

The selection of the right model for designing a local multi-carrier energy system from scratch, while finding a trade-off between model accuracy and computation efforts, is not a minor task. Therefore, it is preferable to design LECs starting from a baseline scenario and then analyse further ones with different design possibilities and objectives to be compared with the baseline one. Indeed, since the analysed scenarios share the same level of detail for the modelling approach, their differential evaluation eliminates the uncertainty of the results.

To achieve energy policy's goals, storage and sector coupling technologies are essential. However, they are still economically expensive compared to other fossil fuel-based technologies. Furthermore, technological details of the energy storage systems of interest have been elaborated upon in previous chapters (2 and 3). These details can be integrated into the energy system modelling process, unlocking the possibility of predicting, optimising, and analysing future energy system scenarios.

However, there are several research gaps that remain unexplored. As previously discussed in Section 1.4, the following research questions, from the system level remain unanswered:

- ***How to effectively include these technologies into a system modelling and assess their impact?***

• ***How to include the dynamic variation and investment stages of parameters in medium-term energy planning?***

Therefore, this chapter is dedicated to displaying the efforts undertaken during this Ph.D. study to address these critical questions.

The chapter is structured into two sections, each dedicated to answering one of the research questions. First, potential solutions for determining optimal alternatives, rather than relying solely on a single optimal solution, are explored. This approach helps mitigate uncertainties associated with modelling parameters. Second, the chapter delves into the dynamic evaluation of parameter variations, such as technological cost reductions over planning horizons, as well as the inclusion of various investment stages throughout the planning process¹.

4.1. Energy planning: Optimal alternatives

Energy planning is inherently reliant on input parameters, encompassing both technological and economic aspects. Notably, financial investments are susceptible to significant fluctuations, influenced by technological advancements and unforeseen circumstances. To address this challenge, many researchers have turned to stochastic programming approaches [136, 137, 138]. However, these approaches often demand extensive computational resources and expertise in operational research, a skill set not always possessed by energy modellers.

With the aim to answer the following research question (1.4):

How to effectively include these technologies into a system modelling and assess their impact?

This thesis section aims to explore an innovative methodology for medium-term energy planning within a multi-energy carrier system, where besides the optimal solution, also other alternatives are presented. The case study revolves around the Marche Polytechnic University campus in Ancona, Italy, towards carbon neutrality, specifically a 50% reduction in carbon emissions, while maintaining economic viability.

The university campus exemplifies the concept of a multi-carrier LEC, incorporating various technologies such as PV systems, Combined Heat and Power units, gas-fired boilers, and absorption and electric chillers, all aimed at fulfilling the energy needs of its users. Building upon this foundational scenario, different combinations of existing and new technologies, including electrolysers, fuel cells, heat pumps, and electric/thermal/hydrogen storage, are explored for medium-term planning. The objective is to ensure both environmental sustainability and economic feasibility within the LEC.

¹Some work described in this chapter has been previously published in [134] and [135]

4.1. Energy planning: Optimal alternatives

To tackle the challenges posed by oscillating investment costs, the Spatially-explicit Practically Optimal REsultS (SPORES) mode within the Calliope framework [139] is employed. This approach offers an alternative to stochastic programming, reducing the computational complexity while maintaining effectiveness.

4.1.1. Calliope framework and scenario analysis

Calliope is an open-source multi-energy system modelling framework: it is user-friendly and highly customisable [139]. Indeed, *Calliope* allows an evaluation of energy systems with user-defined spatial and temporal resolutions, besides their modelling at different levels using a scale-agnostic mathematical formulation based on the power nodes modelling framework which has been proposed by Heussen et. Al. [140]. *Calliope* executes many runs based on the same base model and has a clear separation of the framework (code) and model (data). *Calliope* adopts a bottom-up approach and a MILP optimisation problem formulation to minimize the overall user-defined costs of the whole scenario (Eq. 4.1), which is the sum of each technology cost considering multiple energy balance restrictions per each energy carrier. The mathematical modelling of the energy systems and the energy balance constraints can be found in [141].

$$\min : z = \sum_{loc,tech,k} (cost(loc : tech, cost = cost_k)) \quad (4.1)$$

where $loc, tech, k$ represents three levels of the model: (i) locations/sites, (ii) technology, and (iii) type of costs, whereas $loc : tech, cost = cost_k$ refers to a specific cost voice related to a specific technology installed in a determined location.

Calliope accepts types of costs, namely (i) investment costs related to the capacity of the technology and (ii) Operation and Maintenance (O&M) costs, which are expressed as a fraction of the investment cost or/and an annual capacity-based cost. Furthermore, the depreciation rate is adopted to compare various technologies' investments as defined in Eq. 4.2.

$$d_r = \frac{i \cdot (i + 1)^{lt}}{(1 + i)^{lt} - 1} \quad (4.2)$$

where d_r is the depreciation rate, lt is the lifetime of the technology (expressed in years), and i is the interest rate. The depreciation rate enables the comparison of all the technologies considering the same equivalent year, different lifetimes, and interest rates. Hence, the overall cost of a single technology considering a year of reference is the sum of all the cost types:

$$C_{tot} = S \cdot d_r(1 + O\&M\%) + S \cdot O\&M_{year} \quad (4.3)$$

where S is the capacity of the technology and the design variable of the optimisation

Chapter 4. Energy systems planning

model. Regarding the constraints, all the energy carriers coming from the modelled technologies are balanced at each time step and they are mainly divided into five families of systems [141]:

1. Energy supply;
2. Energy demands;
3. Energy storage;
4. Energy transmission;
5. Energy conversion.

for the purpose of this work, as output data, Calliope provides the following ones:

- Costs of each technology (CAPEX and OPEX).
- Technologies size.
- Levelised Cost of Energy, which is calculated as the ratio between the costs for the energy carrier production (CAPEX and OPEX) and the amount of energy produced in the planning horizon.

Considering that the costs can assume different natures, as defined by the modeller, it is possible to have different types of levelised costs. Precisely, in this work, there are economic (€/kWh) and environmental levelised costs ($\text{g}_{\text{CO}_2}/\text{kWh}$), where the latter considers the achievement of 50% emissions reduction.

It is worth noting that the stochastic behaviour is not included in *Calliope* due to its complexity and computational efforts; however, this can be evaluated using other energy modelling tools such as *Temoa* [142]. Furthermore, it is possible to obtain any number of optimum alternatives through SPORES mode [143] where not only the best configuration is based on a predefined objective, but also any defined number of alternatives within a range of optimal cost solutions are obtained. Each alternative is called “spore”, whereas the range of acceptance is called “slack”: this mode considers the variability of the costs and provides also a wider perspective of the analysed scenario.

4.1.2. Three phases analysis and the case study

The analysis is divided into three phases, achieving a comprehensive overview of the energy system scenarios, which is divided into (i) the Business As Usual (BAU) case, where its environmental cost is used as input for an additional constraint to obtain the (ii) optimal economic scenario for energy transition, where the expansion of the existing energy system with sustainable technologies is considered. Furthermore, the economical result from (ii) is the starting point to assess the (iii) optimal alternatives

4.1. Energy planning: Optimal alternatives

scenario, where each alternative is a case scenario with the same environmental constraint but different economic costs, i.e., different technology types and/or sizes.

These three phases must be performed sequentially since each phase result is used as input data for the following one. For each phase, both economic and environmental costs are the results of the optimisation problem; indeed, the environmental cost of the first phase (BAU) is used as an additional constraint for the second and third phases.

$$C_{CO_2} \leq 0.5 \cdot C_{CO_2,BAU} \quad (4.4)$$

where C_{CO_2} is the environmental cost of scenarios after the first phase, which must be lower than 50% of the first phase's one ($C_{CO_2,BAU}$).

After the second phase (optimal economical solution), the economic costs are used as input for the third phase (optimal alternatives) and updated at each alternative based on Eq. 4.5 :

$$C_{e,i} \leq C_{e,0} \left[i \cdot \frac{(1+m)}{n} \right]; i \in \mathbb{Z}, i = 1, \dots, n \quad (4.5)$$

where $C_{e,0}$ is the economic cost from the second phase, while m and n are the acceptance range and the number of optimal alternatives, respectively. The flowchart of all three phases, which highlights the required input data and results together with the additional constraints between phases, are reported in Fig. 4.1, Fig. 4.2, and Fig. 4.3, respectively.

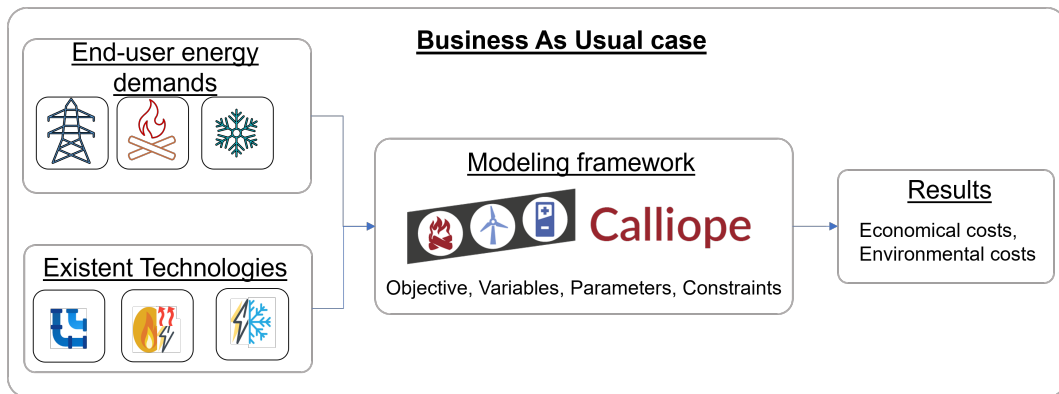


Figure 4.1.: First phase flowchart.

Thanks to the three-phase methodology, the expansion plan of the energy system toward the carbon reduction mission of the LEC is well defined, thus providing a differential comparison with the BAU scenario (first phase). Furthermore, the best economic configuration (second phase), together with different alternatives (third phase), provides a wide range of possible solutions, including the possibility of assessing the correlation among the technologies.

However, despite the similarity, the proposed methodology is not stochastic, meaning that it does not provide the statistical probability of each alternative. Indeed, the

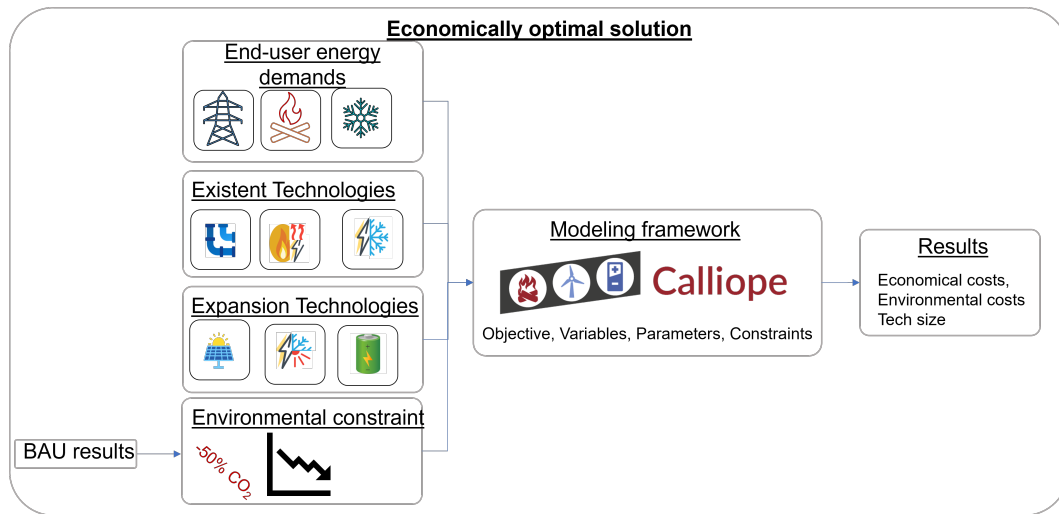


Figure 4.2.: Second phase flowchart.

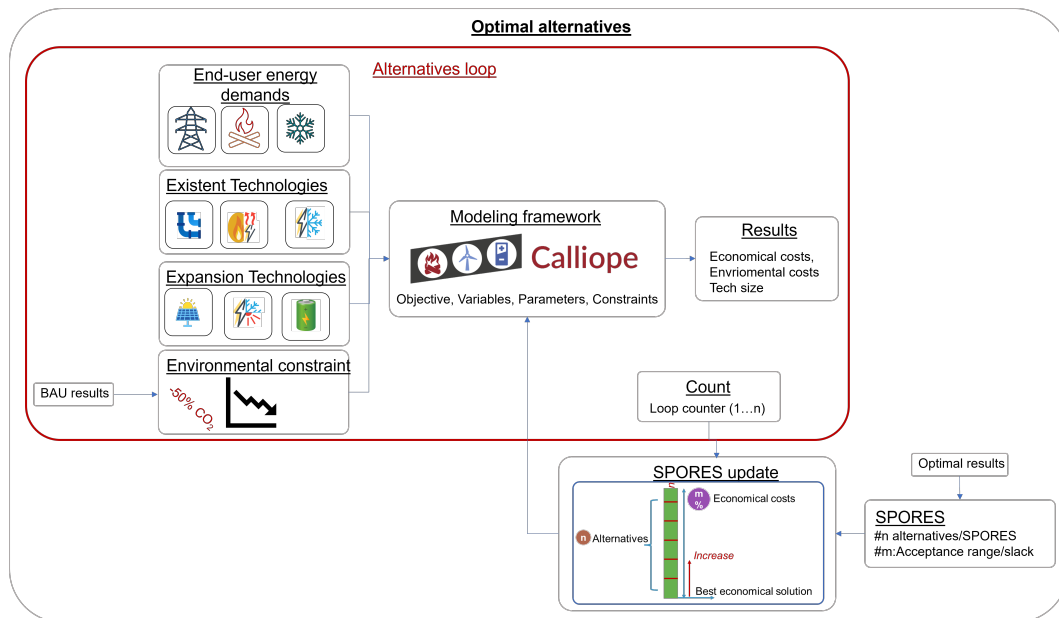


Figure 4.3.: Third phase flowchart.

number of alternatives and the acceptance range are user-defined. Both parameters directly impact the possible solutions; however, there is no proper guideline on how to choose them besides the modeller’s experience.

The case study under investigation is the university campus of “Marche Polytechnic University” (UNIVPM) located in Ancona (Italy). It is a medium-scale campus that accounts for almost 17’000 people among students and academic, administrative, and technical staff.

It hosts different faculties, namely Engineering, Agriculture, and Natural Sciences. The UNIVPM campus is divided into several buildings that are dedicated to offices,

4.1. Energy planning: Optimal alternatives

classrooms, and laboratories that are shown in Fig. 4.4 and covers an area of around 31'000 m². The UNIVPM campus is connected to the national electrical grid with a medium voltage cabin, being a single node of connection with the local distribution system operator, and one connection node for the natural gas network.

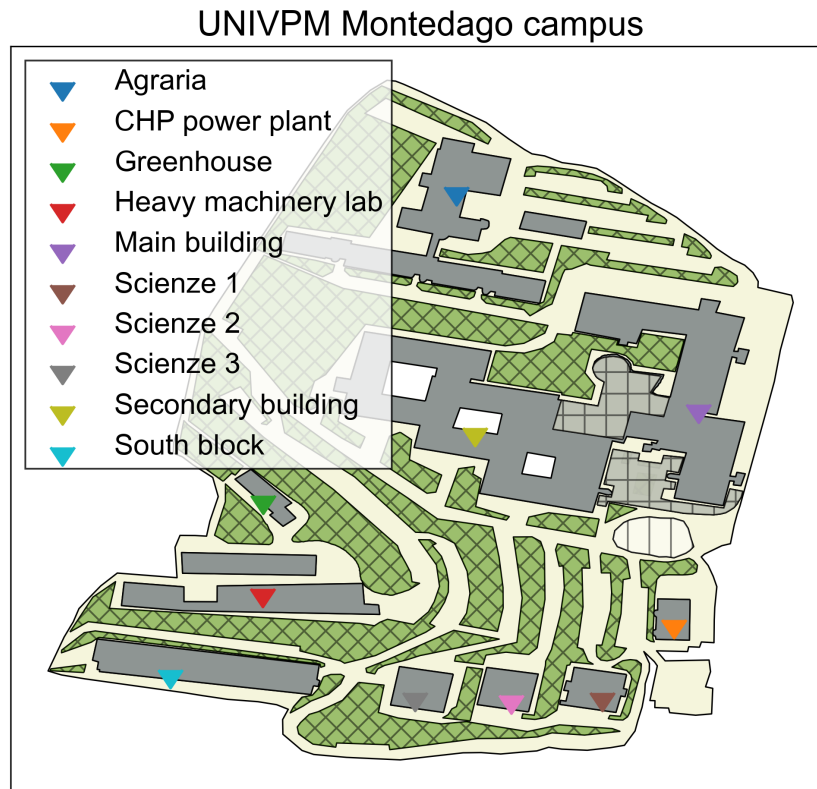


Figure 4.4.: UNIVPM Campus map, recreated with Geopandas [144].

The UNIVPM campus is configured as a multi-energy LEC where several types of energy demands must be satisfied; in particular, there are (i) electrical energy demands for office appliances, lighting, and laboratory equipment plus (ii) thermal energy and cooling demands for the space heating and space cooling. The electrical energy demand is satisfied by distributed energy resources and the national electrical grid, while the thermal energy demand is fulfilled by natural gas boilers located in the thermal power plant.

Currently, the energy technologies already installed in the UNIVPM campus are:

- A PV system with a peak power of 20 kW_p.
- A CHP system, which is fed by the natural gas coming from the national network, with a rated power of 575 kW_{el}/610 kW_{th} connected to the district heating network. Its yearly average electrical and thermal efficiency are equal to 0.415 and 0.44, respectively.
- Eight natural gas boilers, each of them having a rated capacity of 1 MW_{th} and

Chapter 4. Energy systems planning

an average thermal efficiency of 0.91.

- Two absorption chillers with an overall capacity of 500 kW_{th} and an average efficiency of 0.80.
- Three electrical chillers with 900 kW_{th} of total capacity and an average Coefficient Of Performance (COP) of 3.

In 2019, the overall electrical energy consumption was equal to 5.0 GWh with a peak power of 1,368 MW as reported in Fig. 4.5a. The thermal energy demand was related to space heating purposes only in the cold months; in particular, around 4.0 GWh of thermal energy was consumed with a power peak request of 4.4 MW, which occurred on the 4th of January as reported in Fig. 4.5b. This power peak was due to the “rebound effect” caused by powering up the space heating infrastructure that remained inactive during the Christmas holidays; thus, a considerable amount of heat was needed to restore the temperature set-point of the internal spaces. On the other hand, the cooling energy demand was present only in July-September when 0.5 GWh of cooling power was consumed with a power peak of 1.3 MW as shown in Fig. 4.5c.

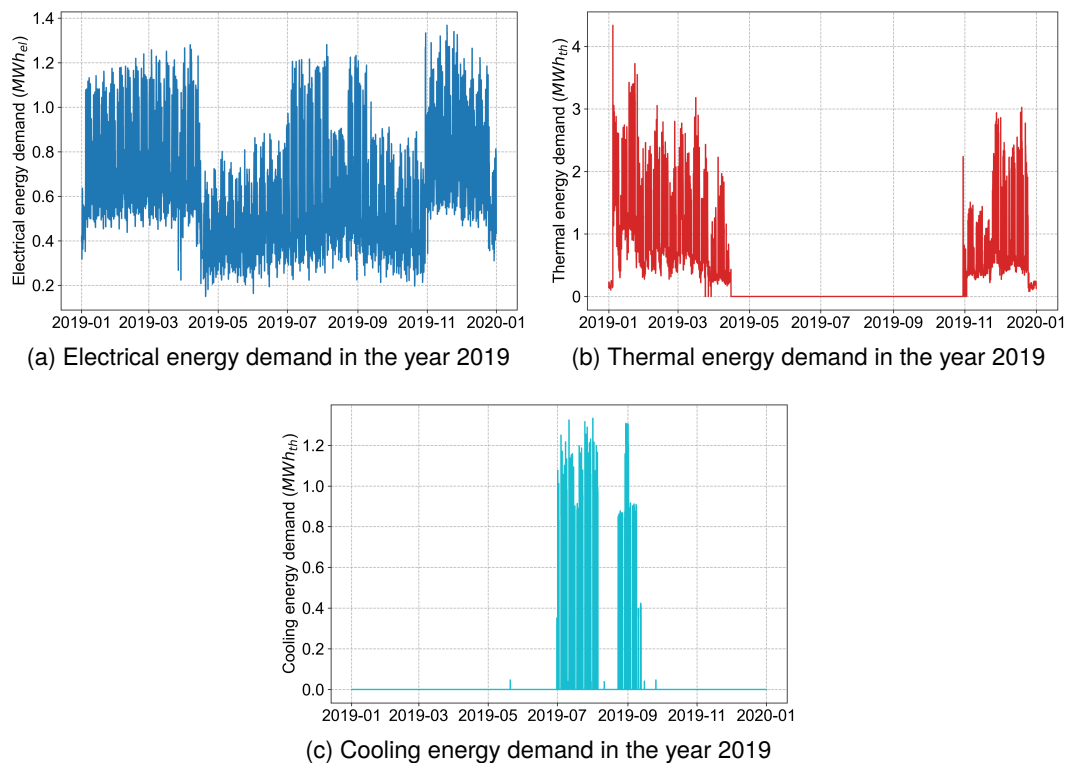


Figure 4.5.: Multiple energy demands with hourly resolution.

The planning horizon is based on a typical year. The current technologies and the new ones considered for the potential expansion plans sorted by the energy nature are the following:

4.1. Energy planning: Optimal alternatives

- Energy supply: national electric network and natural gas grid.
- RES: PV systems whose input is the solar irradiance. The irradiance data, which are adjusted with the panel efficiency, has been reconstructed with RenewablesNinja [145] that is an online tool that allows to perform an estimation of the PV system production based on the location of the installation site.
- Energy conversion technologies: CHP unit, natural gas boilers, PEM electrolyser (EZ), PEM fuel cell (FC), absorption chiller, electrical chiller (EC), and heat pump (HP).
- Energy storage technologies: thermal and cooling energy storage, battery, and hydrogen storage.
- A mixer is a conversion system that allows to have natural gas-hydrogen blending. This energy carrier, named “blend”, can be used as input for the CHP unit and boilers. It is worth noting that the mixer is a figurative conversion system with no financial cost and with 100% efficiency since its function is to supply hydrogen-natural gas blends.

The functional scheme of all the technologies is reported in Fig. 4.6. This scenario presents six energy carriers and a RES plant, two energy supply technologies, eight conversion technologies, four types of ESSs, and three kinds of energy demand. Once the energy technologies involved in the baseline scenario have been estab-

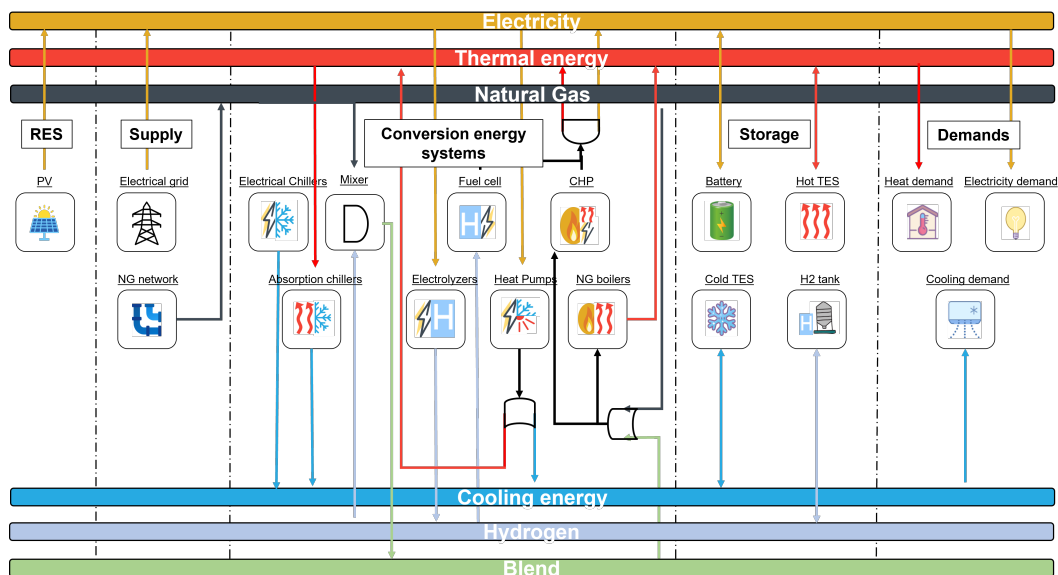


Figure 4.6.: Functional scheme of the energy carriers and technologies involved in all the scenarios

lished, their technical and cost parameters must be defined, which are reported in the Appendix section C.1.

4.1.3. Results and limitations of the approach

Baseline results

In the baseline scenario, which refers to the case with the technologies already installed, the UNIVPM campus must withstand 1.39 M€ due to the import of the energy carriers from the national supply, and therefore it has an annual carbon emission of 2.4 tons. In this scenario, the UNIVPM campus is dependent on the supply grids despite the DERs installed on site; however, the CHP unit plays a crucial role in the energy demand fulfilment.

As reported in Fig. 4.7, the CHP unit does not only contribute to 38.5% of the overall electricity production, but it also provides thermal energy that covers 54.8% of the overall thermal energy demand. As for the cooling energy, both the absorption and the electric chillers share almost the same percentage of energy production.

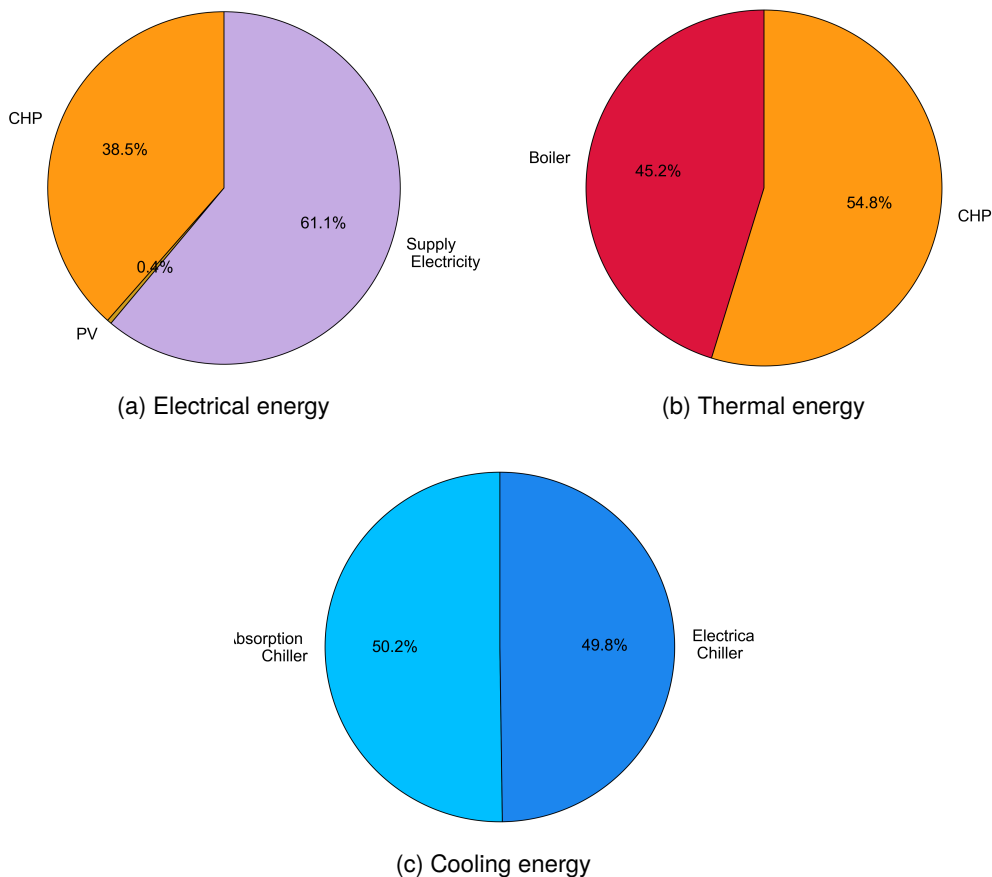


Figure 4.7.: Energy share of the baseline scenario.

Both the monetary and environmental LCOEs are reported in Fig. 4.8, where both thermal and electrical energy depend on the cost of natural gas and electricity supply, in addition to the technical efficiencies of the CHP plant, which is equal to 0.33 and 0.25 €/kWh, respectively.

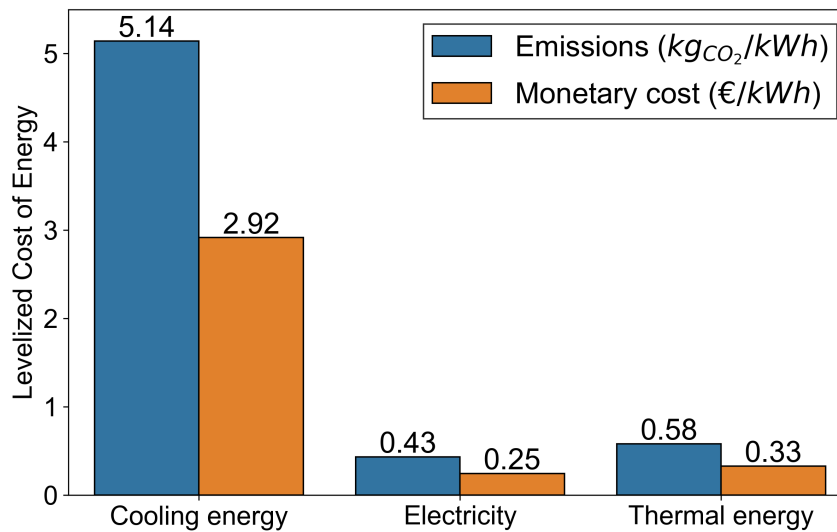


Figure 4.8.: LCOE of the energy carriers in the baseline scenario

Economical optimal scenario

The economically optimal scenario is based on the constraint of reaching the pre-set environmental goal, i.e., 50% of carbon emissions reduction in the multi-carrier LEC. Such a goal is based on the baseline results; thus, the scenario must have annual carbon emissions lower than 1.2 kton_{CO_2} . The best economic solution has been reached by installing new energy technologies: positive results are obtained not only from an environmental point of view (-50% of CO_2 emissions) but also from an economical point of view (-6%). Indeed, the LCOEs of every single carrier face a significant decrease: such changes are due to the use of new technologies that allow for drastically lower supply dependence. As can be noticed in Fig. 4.9, the energy demand matrix experiences an important change compared to the baseline scenario. For instance, the supply of both electricity and natural gas, which have both considerable economic and environmental expenses, is drastically reduced compared to the baseline scenario due to the use of newly installed technologies. The natural gas supply value can be derived by the share of the CHP unit and natural gas boilers for thermal energy production since they are only natural gas consumers.

Compared to the BAU case, the configuration of the technologies involved in this scenario includes i) a wider expansion of the already installed technology (PV) and ii) the inclusion of new ones like heat and cooling energy storage, fuel cell, electrolyser, hydrogen storage, and heat pumps: this information can be found in Fig. 4.10. Furthermore, the levelised cost of each energy carrier is notably dropped compared to the baseline scenario (see Fig. 4.8), while the cooling energy is the most expensive carrier with monetary and emission expenses of 2.5 €/kWh and $2.1 \text{ kg}_{CO_2}/kWh$, respectively.

Chapter 4. Energy systems planning

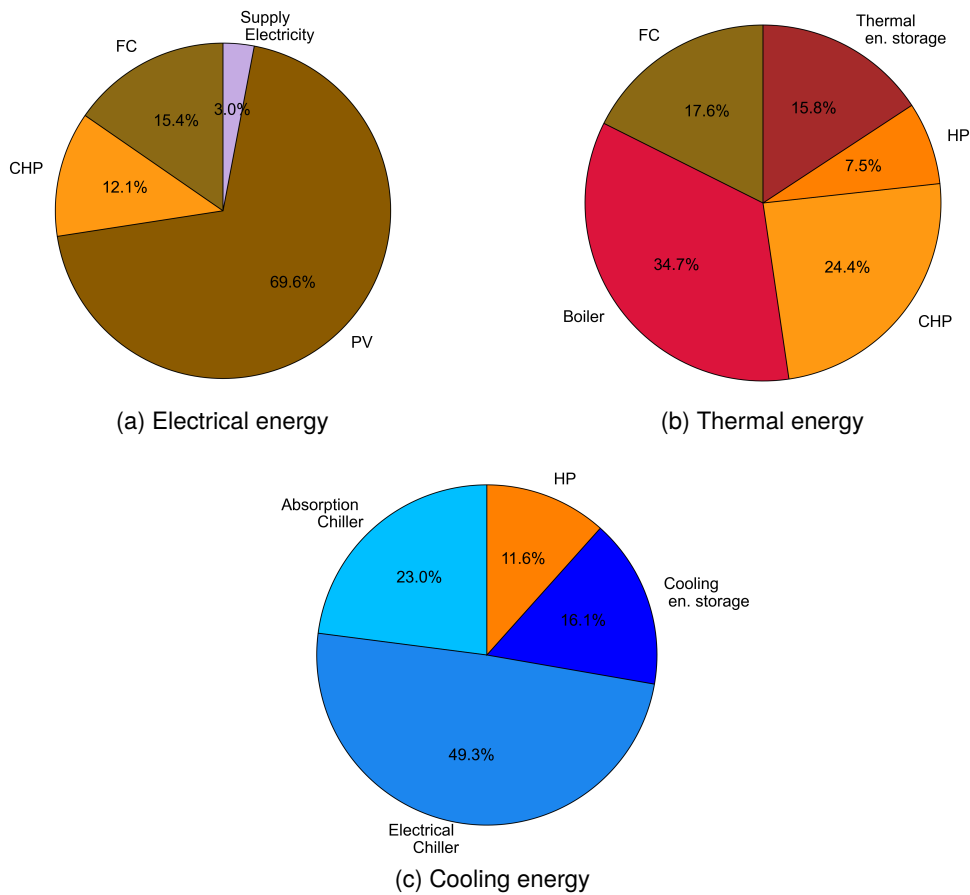


Figure 4.9.: Energy matrix of the optimal scenario.

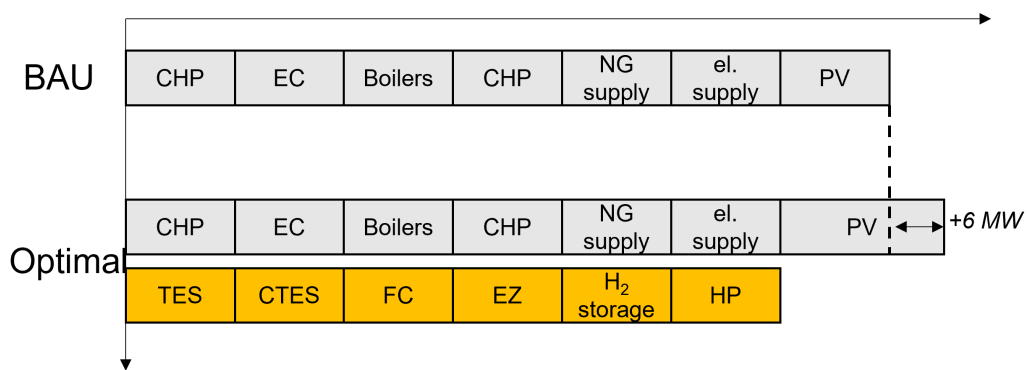


Figure 4.10.: Technologies difference between the optimal and baseline scenario.

Optimal alternatives

Starting from the optimal scenario, twenty alternatives have been analysed. In particular, the objective of the problem is still economically driven by the environmental limitations and the acceptance range of the objective value (monetary costs), which is set equal to 50% to consider the variability of the costs of the different systems.

4.1. Energy planning: Optimal alternatives

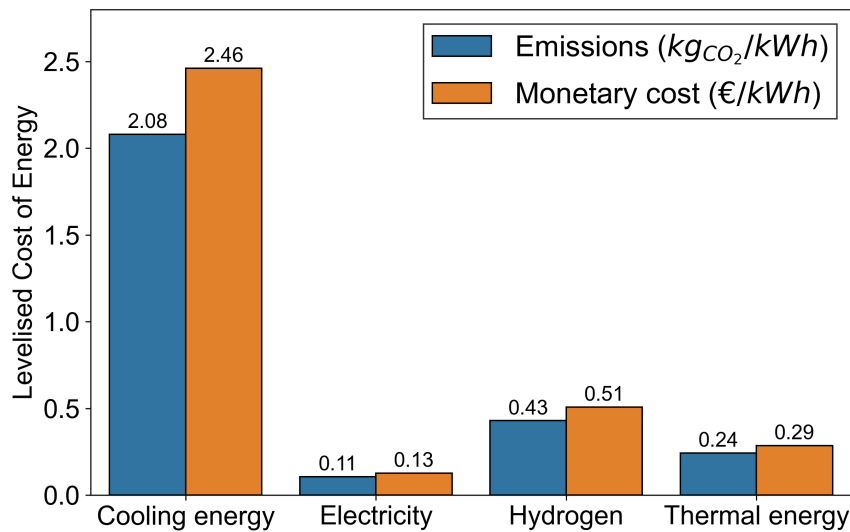


Figure 4.11.: LCOE of the optimal scenario

Each alternative can have different results of planning if they do not exceed 50% of the economic costs addressed to the optimal scenario. The large acceptance range is required to assess the large cost variability of the different energy systems; indeed, these alternatives can assume a wide range of size values since the equipment has not been installed yet and the objective is to find their optimal size, whereas the existent technologies cannot vary.

Precisely, the technologies that are allowed to vary their size in the different scenarios are:

- Electrolyser.
- Fuel cell.
- Hydrogen storage.
- Battery.
- Cooling energy storage.
- Heat pumps.
- Photovoltaic systems.
- Thermal energy storage.
- Mixer.

No solution has shown the use of a mixer, meaning that the blended energy carrier is not economically feasible in the acceptance range due to the lower density of hydrogen. Indeed, a 15% of natural gas-hydrogen blending volume leads to a 5.13% emissions reduction as already stated in [59]. For this reason, rather than using

the natural gas-hydrogen blend, the model chooses a more economically efficient decarbonisation path using hydrogen or heat pumps. Among these alternatives, the results regarding both the emissions and the economic levels are the same and equal to 1.11 kton_{CO₂} and 1.96 M€, respectively, where the latter value corresponds exactly to the maximum allowable cost that is 1.5 times higher than the one obtained in the optimal scenario. However, the size of the technologies can change significantly because of the high slack (50%).

The analysis of different alternatives allows us to assess the dependency among the energy technologies, which is carried out through the Spearman correlation, depicted in Fig. 4.12. It is a correlation indicator of the monotonic relationship for two generic parameters (x and y), ranging from -1 to +1, where 0 stands for no correlation. Correlations of -1 or +1 imply an exact monotonic relationship, while positive correlations indicate that, as the parameter x increases, the parameter y increases as well. On the contrary, negative correlations suggest that as x increases, y decreases. The correlation indicator is considered significant only if the absolute

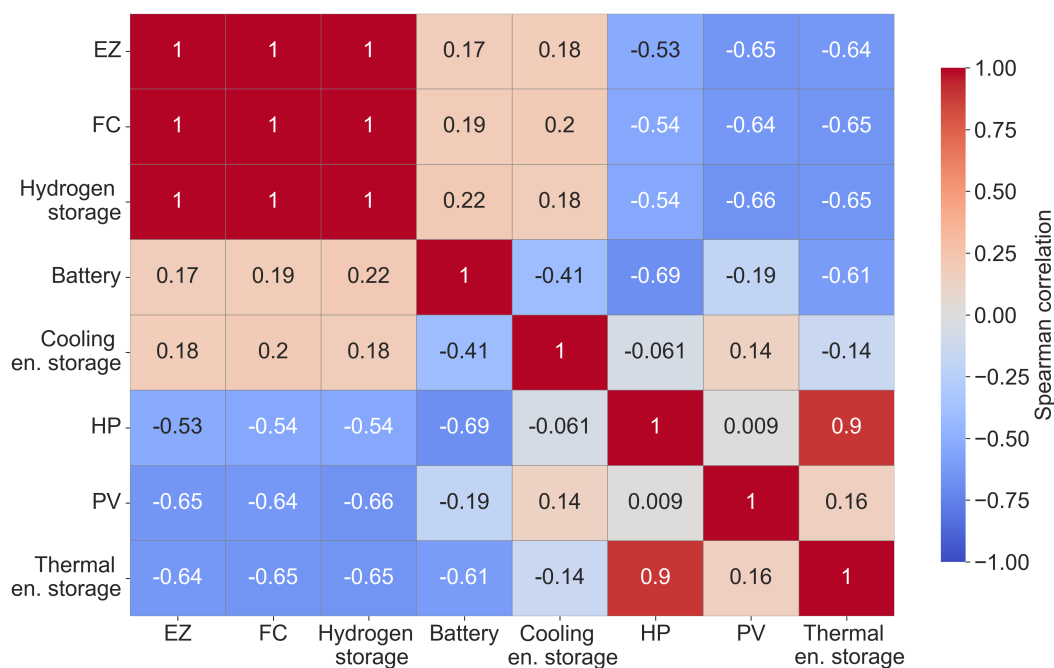


Figure 4.12.: Spearman correlation matrix of technologies from twenty optimal alternatives.

value of the correlation indicator exceeds the value of 0.4. Indeed, three hydrogen technologies are strictly connected. The same behaviour occurs for the heat pumps and thermal energy storage with a correlation of 0.9. Furthermore, the whole hydrogen infrastructure has a notable negative correlation with PV, heat pumps, and thermal storage. The increase of the battery capacity does not only allow a slight reduction of the PV system size but also the deployment of heat pumps and thermal energy storage capacity as well.

Approach's potential and limitation

With the approach presented in this thesis section, a multi-carrier LEC planning problem has been established and solved to achieve the goal of 50 % emissions reduction without neglecting the crucial economic factor. Furthermore, twenty optimal alternatives have also been analyzed.

Results show that, to reach the environmental goal, the energy matrixes face a quite radical change due to the new technologies installation and, as a result, the levelised costs of each energy carrier dropped.

The optimal alternative result assesses (i) the variability, (ii) the priority, and (iii) the correlation among the new technologies. Indeed, to achieve the modelling goal, the PV system capacity increases from 3 MW_p to 6.3 MW_p, and then battery, heat pumps, and thermal storage are embedded since they are technologies downstream of the PV system. The electricity surplus generated by the PV system can be either stored in the battery or used in heat pumps to produce thermal energy. Lastly, thermal storage has the role of absorbing the excess thermal energy from heat pump production.

Moreover, different technical solutions of the expansion plan can be assessed: they are highly dependent on the number of alternatives and the acceptance range, and this represents a limitation of the presented methodology. Thus, the use of other technologies has to be taken into account. The integration of stochastic aspects (statistical distributions) is also not included in this approach. Therefore, this approach is important for analysing possible energy cost fluctuation, thanks to the numerous optimal alternatives, with a reasonable computational time and complexity. Achieving a possible overview of a LEC to cut down the costs and be as much as possible self-sufficient from an energy point of view.

4.2. Energy planning: Dynamic medium-term energy planning

As already discussed in previous sections, different types of energy systems modelling inputs are subjected to high variability like the investment cost, especially those having a low TRL like hydrogen systems. In addition, the degradation rate of the technology and the energy demands variability over the years are important aspects to be aware of.

To deal with these uncertainties, Piao et al. [146] developed an optimization model that considers the oscillation of the electricity demand in Shanghai, China. The stochastic simulation-optimisation model not only managed to predict the electricity demand perfectly, but it also allowed us to assess uncertainties such as interval values and probability distributions. Mavrotas et al. [147] combined both MILP and Montecarlo approaches to consider the deviation of financial parameters (e.g., interest

rate). Several probability functions have been obtained and provided to the decision-makers; as a result, the stochastic programming came out to be more time-consuming due to the additional complexity given by the statistical behaviour of the model.

For the time being, methodology addressing multiple energy carriers at the level of district energy communities and with multiple financial decision stages, which is able to support the investment decisions coherent with the dynamic of the energy market, the technology degradation, and the demand growth has not been deeply investigated so far. Moreover, most of the energy modelling approaches assume continuous design variables that require a customisation of the equipment, with a consequent increase in costs or possible infeasible solutions. A more realistic, or at least less expensive, design of energy systems should require the use of integer decision design variables (e.g., power/capacity) able to capture the modular nature of the equipment of real energy systems; indeed, equipment and technologies are provided by manufacturers in distinct variants, each one with detailed specifications. Thus with the aim to answer the research question (1.4):

How to include the dynamic variation and investment stages of parameters in medium-term energy planning?

In this section, an approach for the integrated short and long-term (decades) district-level planning of multi-energy carriers is introduced. In particular, a MILP-based two-step iterative method dealing with multi-stage investment decisions over the whole planning horizon of 30 years is proposed. Investment costs, energy demands, and each time-dependent data are assumed over the whole planning horizon. Such a time period is discretised into stages, one year each, and an energy system expansion plan is computed for each stage. In the first step, a MILP formulation is solved to set long-term investment decisions (the changes over time of the energy system configuration), while the short-term decisions (e.g., the operations on the technologies) are kept on a coarse-grained yearly scale. In the second step, a modified version of the MILP formulation provides the best scheduling of the deployed technologies in representative weeks of the time horizon, each one discretized into intervals of one hour. The MILPs employed in the two steps interact through linking inequalities, and they are embedded in an iterative scheme that leads to good integrated long/short-term solutions.

The robustness and the computational efficiency of the proposed approach have been tested and validated with data coming from the case study of the UNUIVPM campus, same as the one presented in the previous section 4.1.2. Historical multi-energy carrier demands have been used to compute optimal energy plans over 30 years in three different scenarios: i) BAU, ii) *sector-coupling* scenario, and, finally, iii) *hydrogen deployment*, the latter being the most-likely energy scenario in the future since, according to the European REPowerEU strategy targets, 20 million tons of hydrogen will be needed by 2030, whose 10 million tons will be produced

4.2. Energy planning: *Dynamic medium-term energy planning*

in Europe and the other 10 million tons will be imported. Then, this thesis section proposes an efficient computational approach for obtaining effective energy plans in the context of multi-energy carrier communities that consider dynamic multi-stage investments, fluctuating parameters, and realistic technology design. In particular, the main novelties of this study are:

1. **Dynamic multi-stage investments:** the proposed method takes considers the entire energy system at each year of the planning horizon, thus allowing for changes and expansions in response to ever-changing conditions. The objective function and operational conditions are the drivers of such adjustments.
2. **Variation of parameters over time:** time fluctuating parameters, such as technology degradation and energy demand growth, are embedded into the model to ensure a more comprehensive and realistic energy planning process.
3. **Realistic modular design:** the proposed approach adopts integer selection variables typical of the modular design instead of continuous variables describing the device features. Indeed, according to a more realistic representation of the technology deployment, the selection variables model the choice of a suitable device among a given number of available variants, each of them described by manufacturers' datasheets.
4. **Two-step iterative approach:** the solution of MILPs within the proposed iterative scheme, on the one hand, trades off between the computational effort and the solution accuracy while, on the other hand, it makes viable the integrated long- and short-term planning over a wide time horizon of 30 years.

4.2.1. Methodology

The optimisation approach described in this work aims to find solutions for multi-energy systems planning problems. A system layout is designed throughout the whole planning horizon, and selected technologies operate with technical constraints to fulfil the energy demand using different energy carriers. To explore multi-carrier energy communities, electricity, gas, heat, and cooling are considered as energy carriers along with water and hydrogen that are used only in the hydrogen deployment scenario.

Decisions are taken to minimise the overall economic cost, which is composed of investment, maintenance, and operative ones. A preliminary version of this approach has been described in [148] where it has been tested and validated for the energy planning of a residential district in the United States considering a multi-year horizon. The methodology has been further developed and refined to:

- Make use of integer variables in the MILP approach for modelling investment choices.

Chapter 4. Energy systems planning

- Includes the efficiency degradation of technologies over time and the discount rate of expenditures at present values.
- improve the exchange of information between the long- and short-term optimisation by means of refined constraints.
- Integrate hydrogen systems with the other considered technologies.

Dynamic variation of parameters

The proposed approach considers the variations of several parameters over a planning horizon of 30 years. This time horizon has been chosen to reach 2050 when the net zero global targets should be achieved according to [3]. The following list provides an overview of the parameters involved in this study and explains how they have been chosen/considered:

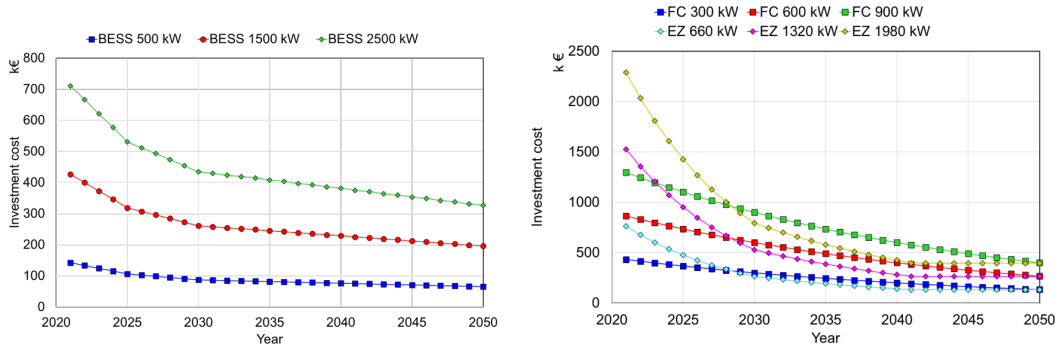
- Energy demand, where according to [149] and in line with the European Commission vision [150], the electricity one increases by 0.32 %/year due to the electrification process, whereas other demands, e.g., natural gas, are kept constant according to [151].
- Battery technology where both investment cost reduction and ageing phenomena (e.g., capacity loss over time of 0.2%/day) have been modelled according to [152].
- Efficiency degradation of technologies where all the involved technologies are subjected to a 1%/year of energy efficiency degradation, except Photovoltaic (PV) which has a degradation rate of 0.3%/year.
- Hydrogen technology whose investment cost is based on the outcomes of [152].

The investment cost reduction of the involved technologies plays a key role in the analyses carried out in this work since the objective of the model is economic-driven. Fig. 4.13 shows that 2030 will be the turning point for the investment cost reduction of most of the involved technologies according to [149, 150, 152].

MILP-based two-step scheme

Solution models for multi-energy systems planning problems can be broadly divided into monolithic and decomposition-based approaches [153]. The former typically aims at finding optimal, or nearly optimal, solutions by relying on a single and very detailed description of the whole problem. However, since the related mathematical formulations typically embed time-indexed (binary) variables and constraints, such an approach rapidly becomes infeasible as the size of the problem increases due to

4.2. Energy planning: Dynamic medium-term energy planning



(a) Cost forecast of BESS equipment available in the 3 variants of 500-1500-2500 kW. (b) Cost forecast of hydrogen technologies: electrolyser and fuel cell devices are considered in 3 available variants of size.

Figure 4.13.: Outlook of the trends of investment costs: BESS and hydrogen technologies.

a wide time horizon and/or a refined time discretisation. As an example, a planning horizon of 10 years discretised in intervals of one hour corresponds to roughly 87600 hours. A formulation for a multi-energy system with 3 energy carriers and 20 technologies has at least $20 \times 87600 = 1752k$ variables and $3 \times 20 \times 87600 = 5256k$ constraints. Clearly, MILP solvers may struggle in such instances of only a moderate-size planning horizon. Decomposition-based techniques, as the two-step MILP approach described in this work, overcome such limits by leveraging in several possible ways the separation between the long-term decisions (investment stage) and the short-term ones (operative stage), still providing good quality solutions.

While the general structure of the approach is reported in Fig. 4.14, the whole mathematical formulation, and the algorithm are reported in detail in of appendix section C.2.1. Furthermore, Tbl. C.7 in the Appendix reports the details of the mathematical notation.

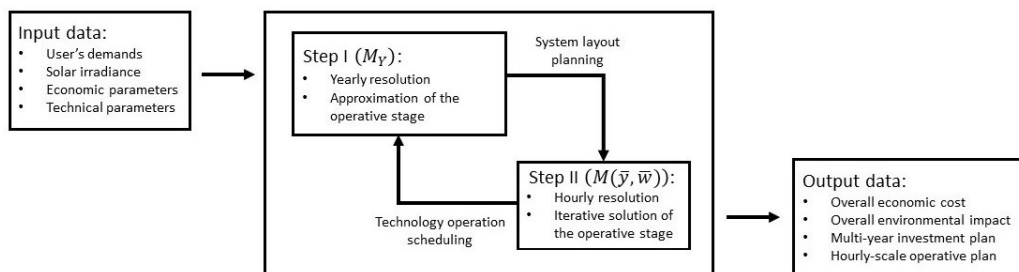


Figure 4.14.: Flowchart of the iterative MILP-based two-step approach

Scenarios definition

While the case study is the same as the previous section one, namely the UNIVPM Montedago campus (subsection 4.1.2), different scenarios have been analysed to assess different future perspectives of the present case study from energy, environmental, and economic points of view. However, it is worth recalling that the MILP approach is economic-driven and does not optimise the environmental costs. The analysis started with the BAU scenario, which was validated with real data and then used as a reference scenario before carrying on the other two studied scenarios, namely the *Sector-coupling* and the *Hydrogen deployment*. The former scenario provides insights into the impact of PV and ESSs, whereas the latter is more focused on the employment of hydrogen technologies along with their viability. In particular:

- *BAU*: this case consists of forecasting the energy planning based on the BAU scenario from today over 30 years, meaning that the energy will be mainly provided by the grid connection and already installed DERs. These technologies will be replaced with the same technologies once their lifetime will run out;
- *Sector-coupling*: in this scenario, a higher share of PV is introduced, which is constrained by the available surface area. Additionally, different types of ESSs are incorporated, including batteries and thermal energy storage, to mitigate PV production fluctuations. Heat Pumps (HPs) are also included as cross-carrier sector coupling solutions to enhance the performance of the overall system;
- *Hydrogen deployment*: this scenario provides insights into the economical feasibility of the deployment of hydrogen technologies within the UNIVPM campus considering its production only with water electrolysis. Various ELs are available in the market such as Alkaline (ALK), PEM, Anion Exchange Membrane, and Solid Oxides. Among them, the PEM technology has been chosen for the proposed scenario due to its maturity and good performance in managing part-load operating conditions, which is warmly suggested when dealing with variable loads like in the present case study. The produced hydrogen is then stored in a pressurised tank and subsequently used to generate electricity through a PEM FC.

4.2.2. Results of the case study

In this section, the results of both the planning (long-term) and the operational (short-term) perspective are reported and discussed. The assessment of the proposed approach has been performed by an analysis of the three scenarios previously mentioned. In particular, the capability of making multi-stage investments over the entire planning horizon and achieving an energy balance by a refined operational control has been evaluated.

4.2. Energy planning: Dynamic medium-term energy planning

Regarding the computational aspects, the MILP-based two-step algorithm was implemented with AMPL (version 20221013, MSVC 19.29.30146.0, 64-bit) and solved by Cplex (version 12.10.0) with an integrality gap relative tolerance set to $2 \cdot 10^{-3}$ in the first step and to the default (i.e., 10^{-4}) in the second step. Each MILP was solved optimally within the time limit of 600 seconds. Experiments were carried out on an Intel® Core™ i7-7500U 2.90 GHz with 16GB RAM.

Planning results and scenarios comparison

Numerical results of all three scenarios are presented. Where Fig. 4.15 reports the results of the BAU scenario, highlighting both the economic and environmental LCOE of each energy carrier. In particular, cooling energy is expensive in both economic and environmental terms since its demand is lower than other involved energy carriers. The economic LCOE of heat is higher than that of the electricity because it also includes the costs of locally installed equipment for energy conversion, while the electricity can be obtained from the national grid. However, the environmental LCOE of heat is lower because of (i) the high efficiency of energy conversion systems and (ii) the lower environmental impact of primary sources for its production. The investment plan over the entire planning horizon is reported in Fig. 4.15b, where all the technologies are deployed in the first year and replaced once their lifetime runs out. The investment decisions beyond the 1st year have been strictly considered to satisfy the technical constraints rather than pursuing the economic strategies.

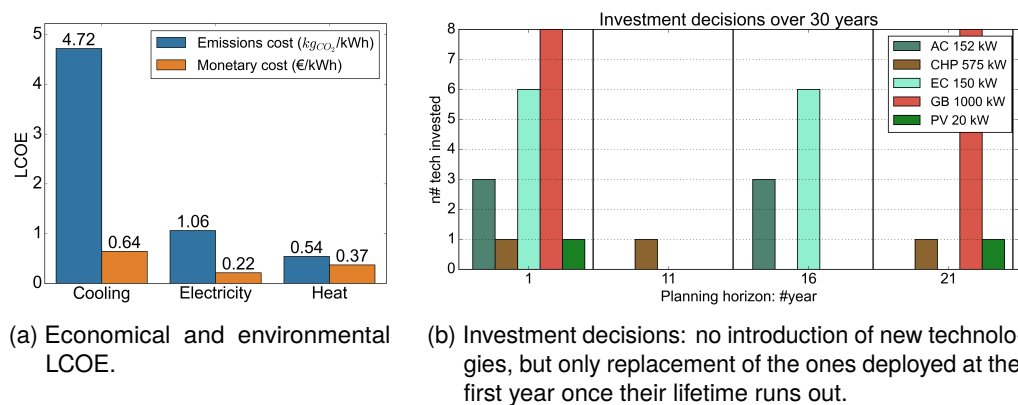


Figure 4.15.: BAU: levelised costs and investment stages

As for the *Sector-coupling scenario*, the maximum PV capacity is limited by the rooftop area, and it reaches a maximum value of 3300 kW_p. The optimal investment (actually replacement) plan considers a high share of PV and different types of BESS solutions, as reported in Fig. 4.16 where the economic-driven objective has been chosen to adopt the highest deployable PV installation capacity. Furthermore, the whole energy system fleet supports more diversified technologies to cover the energy demand; among them, different types of environmentally beneficial technologies have

Chapter 4. Energy systems planning

been selected such as HPs with sizes of 270 and 380 kW together with electric and cooling/thermal energy storage. Multi-stage investments have been also highlighted in Fig. 4.16; indeed, different changes occurred in the technologies deployment during the planning horizon. As evidence, not all the technologies deployed in the first year are replenished when their lifetime runs out. Some of these technologies are replaced with different ones that can accommodate the required energy demands together with the investment of battery at the 11th year, which is the year 2031 when its investment cost is significantly lower than it was in the first year.

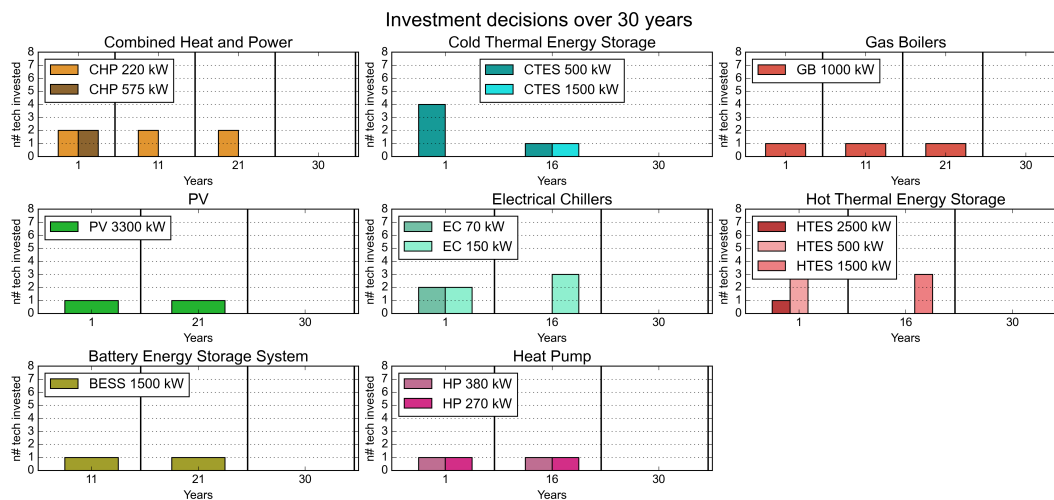


Figure 4.16.: Sector coupling scenario: multi-stage investment decisions.

Finally, The results of the *Hydrogen deployment* scenario are similar to those of the Sector-coupling one (see Fig. 4.16). The hydrogen infrastructure is deployed in the 10th year (2030) when its cost will reach a rather low relative level. In particular, the whole hydrogen infrastructure, namely PEM EZ, hydrogen storage (SH), and PEM FC, are deployed starting at 10th year as shown in Fig. 4.17, when their investment costs will reach a threshold value that is economically and environmental convenient. Furthermore, both EZ and FC must be re-bought every 10 years because of their 10-year lifetime. A key behaviour proving the model capability of capturing the dynamic conditions over the years is the decision of progressively increase the number of 500 kW ESSs devices to take advantage from the technology cost reduction and, at the same time, to pursue a more sustainable impact of the system since the copies of the natural gas boilers are contextually reduced (see Fig. 4.13a.)

The differential assessment has been done on the BAU benchmark scenario, using LCOEs as indicators, while the different investment decisions have been previously reported. Indeed, the economic levelised cost of electricity in the sector-coupling scenario grows by 43% compared to the BAU case, while the levelised cost of both heat and cooling energy reduces by 61 and 73%, respectively, thanks to the presence of Cold and Heat Thermal Energy Storage (CTES and HTES), see Figure 4.18 and Table 4.1. Furthermore, such a scenario, which introduces new and

4.2. Energy planning: Dynamic medium-term energy planning

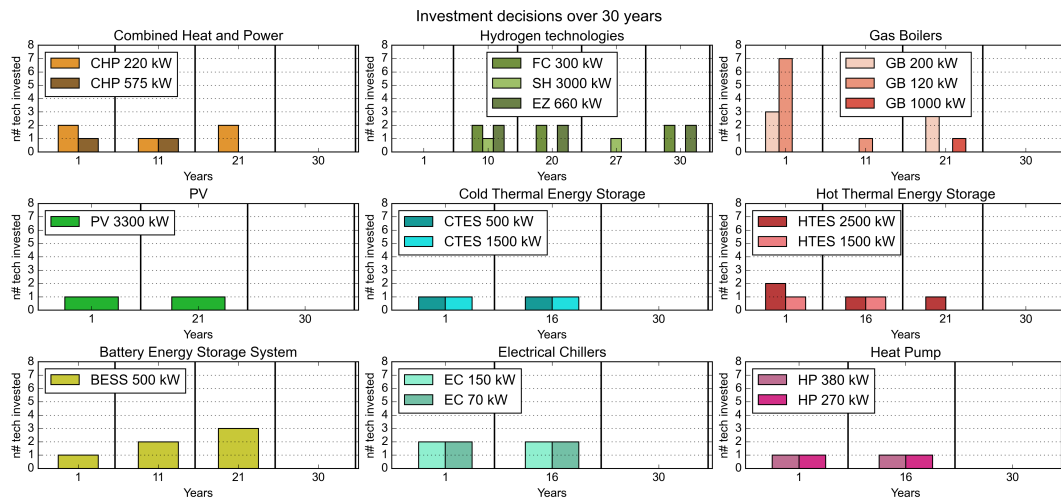


Figure 4.17.: Hydrogen deployment scenario: multi-stage investment decisions

sustainable solutions, has a positive impact from an environmental point of view, reaching a minimum environmental levelised cost reduction of 51% per each involved energy carrier. A higher reduction of the carbon footprint (80% compared to the BAU scenario) is reached by the hydrogen deployment scenario since the hydrogen technologies integration is directly affected by the electricity. On the other hand, it leads to an increase of the economic cost by 89%.

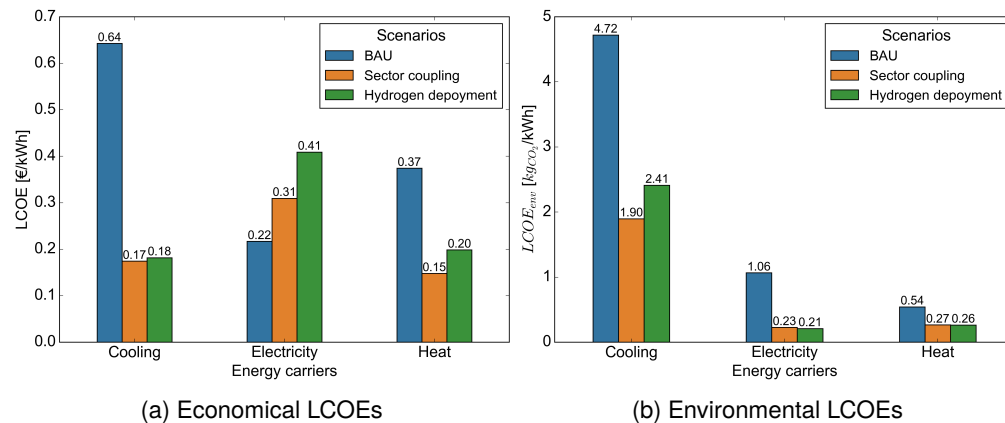


Figure 4.18.: Scenarios comparison: LCOEs of different energy carriers.

Fig. 4.19 reports the overall costs of all the analysed scenarios over the whole planning horizon. It is observed that the hydrogen deployment scenario exhibits the minimum economic cost due to its higher independence from the grid. As a result, expenses related to grid imports are minimised. As regards the environmental benefits, the high share of PV and BESS integration together with the hydrogen deployment scenarios have similar effects, with the latter having a slightly further reduction; indeed, both of them have reached the maximum decarbonisation allowable

Table 4.1.: Scenarios analysis: LCOEs variation

Scenarios	Energy carrier	Values	Variation (%)
Economic LCOE (€/kWh)			
BAU	Cooling	0.64	n.a.
	Electricity	0.22	n.a.
	Heat	0.37	n.a.
Sector coupling	Cooling	0.17	-73
	Electricity	0.31	+43
	Heat	0.15	-61
Hydrogen deployment	Cooling	0.18	-72
	Electricity	0.41	+89
	Heat	0.20	-47
Environmental LCOE (kg _{CO2} /kWh)			
BAU	Cooling	4.72	n.a.
	Electricity	1.06	n.a.
	Heat	0.54	n.a.
Sector coupling	Cooling	1.89	-60
	Electricity	0.23	-79
	Heat	0.27	-51
Hydrogen deployment	Cooling	2.41	-49
	Electricity	0.21	-80
	Heat	0.26	-52

level that is constrained by the available surface for the PV.

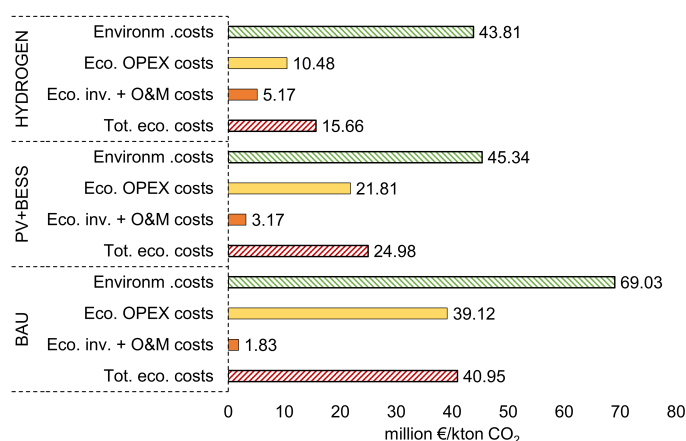


Figure 4.19.: Scenarios comparison with overall costs of the entire planning.

Operational results

Results on various aspects of the case study operation’s planning, such as hourly scheduling and energy balance, are illustrated in the following figures. For the sake of clarity and conciseness, only operational decisions of a day randomly selected are reported, instead of the complete 30-year span.

Figure 4.20 displays the hourly energy balance for all the energy carriers being examined. Where all the energy carriers maintain a flawless balance, demonstrating the validity and robustness of the mathematical constraints of the model.

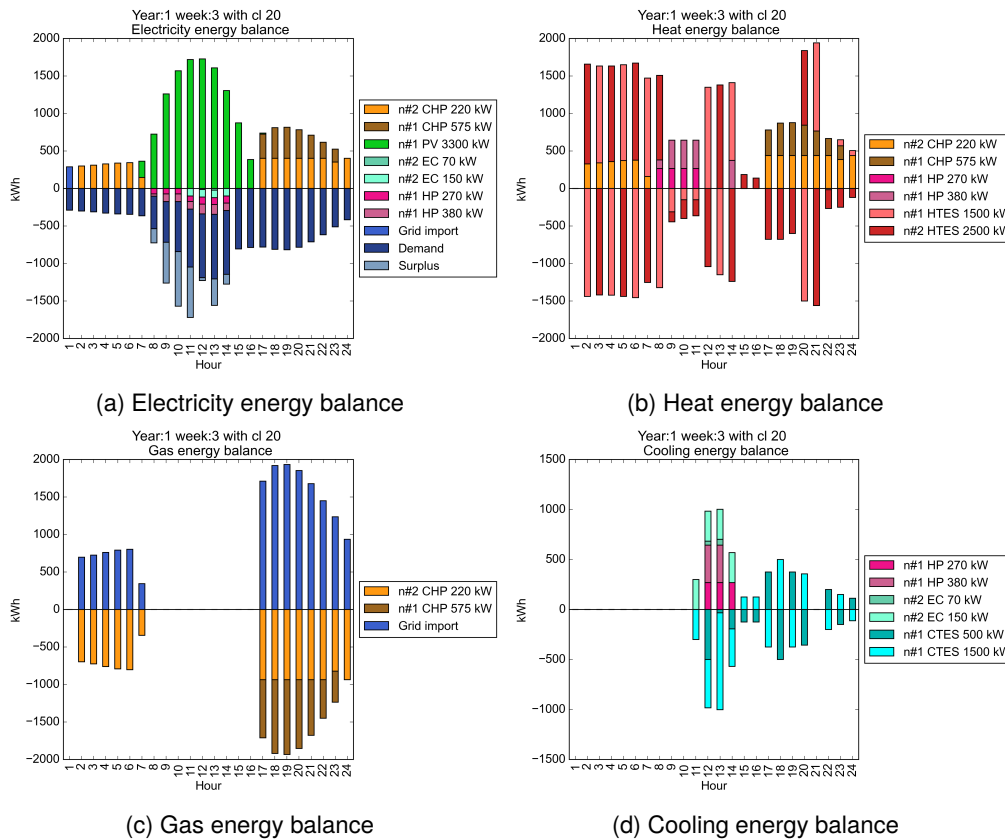
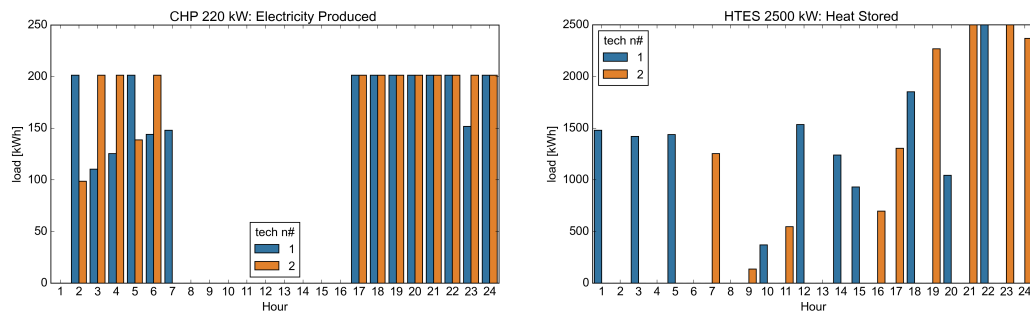


Figure 4.20.: Operations’ results. To illustrate energy balances during the scheduling.

Load distribution over technological devices

Figure 4.21 shows how the loads of the conversion and storage systems are distributed among the discrete set of available variants of each technological device. The mathematical model does not exhibit any preference for prioritizing the operations of one variant over those of others. Instead, the load distribution is scheduled randomly, while still adhering to all constraints, including size limitations.

Chapter 4. Energy systems planning



(a) Conversion systems (CHPs production): No preference for any specific copies over others is exhibited. However, a slight rotating behaviour among copies can be observed between 2:00 and 7:00. It is worth noting that this behaviour is not explicitly accounted for in the mathematical model.

(b) Storage systems (HTES): No preferences for one copy over another can be observed.

Figure 4.21.: Examples of load distribution among the same technologies. Data taken from the *Hydrogen deployment* scenario, year 1, week 2.

4.2.3. Methodology's potential and limitation

This thesis section has the objective of answering the research question (1.4):

How to include the dynamic variation and investment stages of parameters in medium-term energy planning?

With this perspective, a MILP-based two-step iterative approach for medium/long-term (30 years) multi-energy systems planning is presented. The approach suggests multi-stage investment decisions by taking into account the dynamic of different parameters throughout the planning horizon, as well as the modular design, and hence the availability of devices in a limited number of variants, of the involved technologies.

In the first step of the algorithm, each year of the planning horizon is considered as an investment stage where the new technologies procurement can be applied. In the second step, the operations of the designed system are then scheduled on an hourly basis along the whole planning horizon. The optimisation is devoted to the overall minimisation of economic costs. Such a methodology has been applied and validated using the same case study of the previous section's study (section 4.1). Yet, with significant differences in methodology, such as:

- All 30 years are considered and analysed in this approach, rather than using a typical year planning;
- Multiple investment stages, one per each year;
- Dynamic variation over the planning horizon.

4.2. Energy planning: Dynamic medium-term energy planning

The results obtained on three different scenarios have been analysed to gain an extended assessment of the model's capabilities and limitations under different conditions. Considering the overall planning horizon (30 years), the BAU case needs 40.95 million € of financial investment with a carbon footprint of 69.03 kton CO₂, while the two other analysed scenarios, namely the *Sector-coupling* and the *Hydrogen deployment*, have significantly reduced both economic and environmental costs, namely 24.98 million € and 45.34 kton_{CO₂} for the former and 15.66 million € and 43.81 kton_{CO₂} for the latter. In particular, a different study on the same case (Presented in the previous section 4.1), where however the planning horizon is traditionally modelled by representative year, led to comparable results of LCOEs for the BAU scenario (0.22 €/kWh vs. 0.25 €/kWh obtained in section 4.1 (Fig. 4.8) for the electricity and 0.37 €/kWh vs. 0.33 €/kWh for the heat energy), so validating the proposed approach.

Indeed, the results show that it has not only captured different stages of investments, but it also handled well all dynamic variations of the involved parameters, e.g., an increasing number of ESSs devices are purchased over the years in the hydrogen deployment scenario, according to their investment costs reduction. Furthermore, hydrogen-related technologies become economically viable by acting as a cross-sector coupling solution in the 10th year based on the forecast of the investment cost reduction. Additional results on the operational side, such as the dynamic balance of all the energy carriers and the load distribution among the technologies, show the effectiveness of the method in capturing the expected behaviours of the energy system.

On the computational side, the proposed methodology efficiently provided optimised solutions in reasonable running time by leveraging the separations among investment and operation scheduling stages.

However, contrary to all-encompassing single-step MILPs, the two-step algorithm may lose effectiveness because of the heuristic decomposition. Moreover, parameters reported in Appendix section C.2.3 (C.23)-(C.24), are partially sensitive to the case study features and hence require accurate tuning to allow the computation of high-quality solutions. Further investigations on the algorithmic side are needed to identify the settings of the well-performing parameters, possibly based on inference and/or learning. On the modelling side, several aspects of the energy systems have been simplified or neglected. Also input data, e.g., costs and demands, which clearly are neither deterministic nor completely predictable, require a more precise estimation and/or an explicit handling by, e.g., stochastic programming, which can be investigated in future studies.

Another promising direction lies in linear programming decomposition schemes (e.g., Dantzig-Wolfe decomposition, Benders decomposition) that can provide useful duality gaps and optimal-guaranteed solutions while keeping the computational viability.

Other aspects, like a detailed description of the environmental impact, the balancing

Chapter 4. Energy systems planning

of the same technologies' loads (and therefore prioritise one copy over another) and among the loads of interconnected multi-energy systems can be addressed as future research directions.

Part III.

Energy storage details into systems approach: case studies

Chapter 5.

Bi-level interconnection case studies

Today's scientists have substituted mathematics for experiments, and they wander off through equation after equation and eventually build a structure that has no relation to reality.

Nikola Tesla

Energy system analysis is a multidisciplinary field encompassing the examination of energy systems and their various components, behaviours, and interactions. This area of study bridges the disciplines of engineering and economics, offering valuable insights into the complex world of energy. Energy system analysis operates at different tiers, with a primary distinction between technology-level and system-level analysis. Technology level analysis involves the study of individual energy technologies, such as PV panels, wind turbines, and batteries, and their performance characteristics, costs, and environmental impacts [154, 155], as discussed in Part I of this thesis. System-level analysis, on the other hand, involves the study of entire energy systems, including their components, such as power plants, transmission lines, and distribution networks, and their interactions, such as energy flows, demand patterns, and environmental impacts, already discussed in Part II.

Energy system analysis is important for understanding the complex interactions between different components of energy systems and for identifying opportunities for improving their performance, reducing their costs, and mitigating their environmental impacts. It is also important for informing policy decisions related to energy, such as the development of renewable energy targets, the design of energy efficiency programs, and the regulation of energy markets [156].

Both levels of analysis, technology, and system, offer unique insights, as depicted in Fig. 5.1, complementing each other. However, they are often treated as distinct studies. While technology-level analysis investigates the physical details of energy systems, exploring multi-physical phenomena, system-level analysis emphasizes the interconnections and synergies among various systems, sometimes relying on simplified linear equations.

The characteristics details at the technology level, owing to their nonlinear behaviour, cannot be integrated into system-level analyses, typically characterized

by linear models. Nevertheless, leveraging the comprehensive analysis previously conducted, it becomes feasible to capture and incorporate these nonlinear effects, instead of directly including multi-physical details into the system-level models, often after linearisation. This approach serves to mitigate the complexity of the bi-level interconnection and has been embraced by other researchers in the field [157].

The preceding chapters of this thesis have delved into both levels of analysis, with a particular focus on energy storage technology. Nonetheless, these analyses have largely operated in isolation, and this chapter aims to bridge this gap.

Furthermore, it is essential that the applications are grounded in real-world case studies, amplifying the practical relevance and usability of the thesis work. This chapter introduces two distinct case studies. Each case study provides a unique vantage point on the integration of technology details into the broader system level, all while pursuing specific research objectives. With the aim to answer the following research questions (1.4):

- **How to deal with fluctuation in power supply for Power-to-Hydrogen?**
- **Which is the best solution for long-term storage?**

In the initial section of this chapter, the coupling of hydrogen production technology (already described in Chapter 2) and its related auxiliary systems, with an intermittent renewable source, is investigated ¹. The second section, on the other hand, has the objective of including the degradation effects of the Li-ion batteries, to properly compare their performance with the hydrogen storage solutions, dedicated to seasonal applications, in the context of the Local Energy Communities².

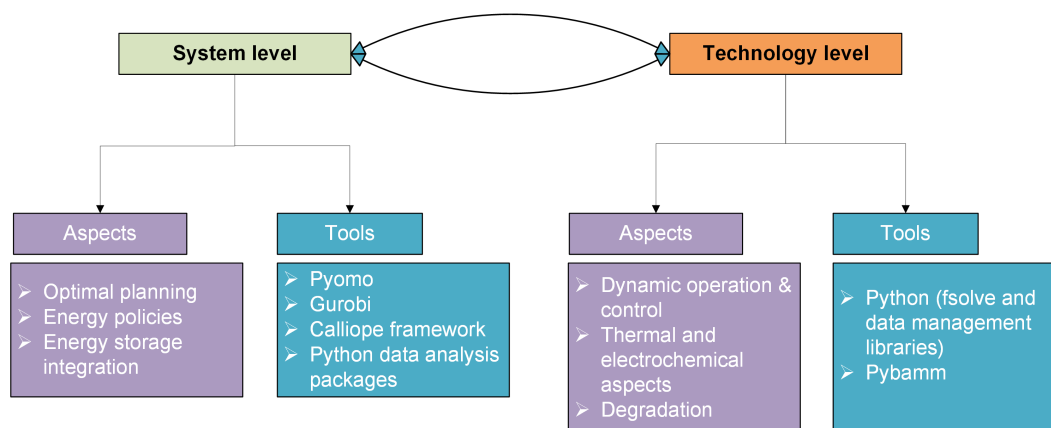


Figure 5.1.: Approach adopted for connecting two levels of energy systems analysis.

¹Work carried out in collaboration with DTU colleagues, during the visiting period in DTU Energy, Lyngby in Denmark, 2022.

²Some of the work described in this chapter has been previously published in [158, 159].

5.1. Case study 1: Wind turbine design optimisation for hydrogen production

A year ago (March 2022), the European Council agreed to phase out dependence on Russian natural gas and become independent before 2030. Each year, the EU uses 10 Mt of natural gas to produce hydrogen for fertilizers, refining, and other chemical applications [160]. The main alternative to "grey" hydrogen from natural gas is "green" hydrogen produced using electrolysis and zero-carbon electricity. Green hydrogen may be a path for the EU to reduce import dependence and support the green transition. As green hydrogen requires about 55 kWh/kg_{H₂}, it also represents a potential 120 GW market for the wind industry (at a capacity factor of 0.5) just for this use case alone.

While placing electrolyzers and Power-to-X plants on land provides the highest possible integration with other energy sources [161], placing them offshore close to the power source may still be an advantage. The main reason is that electrical cables are far more expensive than hydrogen pipes, and energy transportation becomes cheaper. [162] show that importing hydrogen to Germany is more affordable than producing it locally. This will be even more evident with the establishment of the European Hydrogen Backbone [163], which will provide a cost-effective option for long-distance hydrogen transport.

The costs and constraints of electrical infrastructure determine the boundary conditions for today's offshore wind turbine design. Changing the energy transportation to hydrogen eliminates electrical components and power conversion losses of traditional grid-connected electrolyser facilities and potentially allows for a simpler and cheaper wind turbine design. On a Hydrogen Wind Turbine (HWT), the electrolysis stack is integrated with the WT generator and operates off-grid. As the H₂ production requires water as feedstock, it is natural to think of offshore concepts that include a seawater desalination system [164, 165].

One of the main design choices for an HWT is the rating of the electrolysis stack (P_e) compared to the generator (P_g). Since the efficiency of the considered alkaline electrolyser stack drops at high loads [166], [167] suggest that it may be beneficial to "oversize" the electrolyser compared to the generator. They find that an electrolyzer rating 20% higher than the generator results in a drop of the LCOH of about 5%. However, the oversizing ratio is sensitive to the efficiency curve of the electrolysis system, which is not explicitly modelled by [167]. If the generator output exceeds the electrolyser capacity, it may be curtailed. Having battery storage can reduce the curtailment, but its size needs to be chosen wisely to minimise the LCOH.

Another critical parameter in the HWT design is the specific power, which is the ratio of the rated power to the swept area. Modern wind turbines have a relatively low specific power, designed to reach maximum rated power at relatively low wind speeds to maximise the capacity factor. However, [168] argues that an HWT should

have a high specific power to increase electrolyser efficiency and lower the LCOH.

This thesis section, therefore presents a first case study of integrating different scales of the energy system analysis, with the objective of dealing with the following research question:

How to deal with fluctuation in power supply for Power-to-Hydrogen?

In particular, the design of an HWT is discussed. where the first conceptualise an electrolyser system for the IEA 10 MW reference wind turbine [169]. Next, the evaluation of how the size of the alkaline electrolysis stack and the battery would impact the LCOH. Finally, a parametric study of the main wind turbine design parameters (specific power) is conducted to investigate the potential of reducing LCOH by optimising the wind turbine design. Such a study tries to answer the following specific questions:

1. How should an electrolyser system for an HWT be designed?
2. Does hydrogen production change the boundary conditions for wind turbine design?
3. How does changing the main HWT components affect the LCOH?

5.1.1. The HWT model

The HWT modelling framework consists of three main elements:

1. The wind climate,
2. The wind turbine (WT),
3. and the electrolysis system (ES).

A battery is also included to provide the grid-forming service for off-grid operation and to reduce curtailment when WT power exceeds the electrolyser rating. Each subsystem provides the input for the next subsystem until pressurised H_2 is finally output (Figure 5.2). As the paper focuses on the design of an isolated HWT, it does not consider the integration with the remaining energy system. The H_2 production is, therefore, not constricted to follow a demand profile and is simply exported when produced. Consequently, costs and losses due to wind farm infrastructure, H_2 transport and storage are not considered. The following sections describe each of the subsystems, followed by a section that describes how we evaluate the system's performance.

5.1. Case study 1: Wind turbine design optimisation for hydrogen production

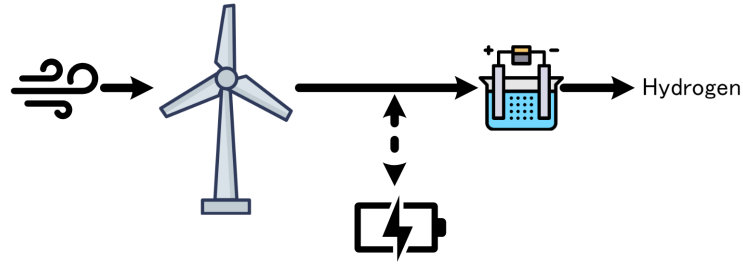


Figure 5.2.: The subsystems of HWT model: the wind climate, the wind turbine with an integrated battery, and the electrolysis system.

The Wind climate

The location of the planned energy island in the North Sea in Denmark was selected to get a realistic wind climate for the simulations. The hub-height wind climate for 2021 was estimated using the ERA5-GWA2 method [170] with the resulting all-sector Weibull parameters given in Table 5.1. The Weibull distribution represents the frequency distribution of wind speed,

$$f(v) = \frac{k}{A} \left(\frac{v}{A}\right)^{k-1} \exp\left(-\left(\frac{v}{A}\right)^k\right) \quad (5.1)$$

where $f(v)$ is the frequency of occurrence of the wind speed v . The wind climate is assumed to represent the lifetime average conditions of the wind turbine, e.i. no long-term correction of the wind climate has been performed. To estimate the wind climate for varying hub heights, the Weibull- A is a scaled parameter using a logarithmic velocity profile with a roughness length of 0.0002 m. The Weibull- k parameter and the air density are kept fixed.

Table 5.1.: Parameters of the reference wind climate

V_{ref}	Reference mean wind speed	9.78	m/s
z_{ref}	Reference height	119	m
k	Weibull shape parameter	2.28	-
A	Weibull scale parameter	11.0	m/s
z_0	Roughness length	0.0002	m
ρ	Air density	1.225	kg/m ³

Wind turbine

The IEA 10-MW off-shore WT [169] is used as a reference wind turbine (RWT). It has a rated power of 10 MW, a rotor diameter of 198.0 m, and a hub height of 119.0 m giving it a specific power of $SP = 325 \text{ W/m}^2$. To evaluate the effects of optimising the main WT parameters (Tbl. 5.2), we model the wind turbine as a simple parametric power curve. The power in the full load region is equal to the rated power, while we

use the power equation in the partial load region, assuming optimal power coefficient ($C_p=0.49$):

$$P(V) = \frac{1}{2}\rho V^3 C_p \cdot \pi \left(\frac{D}{2}\right)^2 \quad (5.2)$$

Knowing the wind turbine power curve and the wind climate, the gross Annual Energy production (AEP) and the capacity factor (C_f) can be calculated. Since this work only analyses a single wind turbine, the wake effects are ignored, and the RWT has a high capacity factor of 0.628 and an AEP of 55.0 GWh.

The electrical system for an HWT is very different to traditional WTs. The WT generator and a battery are connected to a DC bus through separate converters. The primary role of the battery is to provide grid-forming services necessary for the HWT to operate in off-grid/island mode [171]. However, the battery also serves as a reserve for "cold" upstarts and reduces curtailment in situations where power production exceeds the rating of the electrolysis system. The optimal battery capacity (E_b) is investigated in the following subsection 5.1.3.

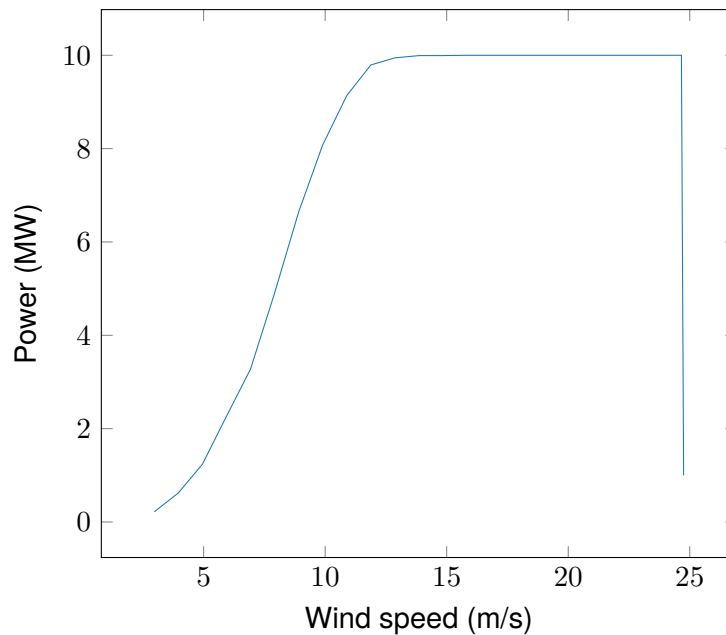


Figure 5.3.: The power curve of the reference wind turbine

Knowing the wind turbine power curve $P(v)$ and the Weibull parameters, the Annual Energy production (AEP) can be calculated:

$$AEP = \int_0^{\infty} P(v) f(v) dv \quad (5.3)$$

The wind turbine capacity factor (C_f) is the ratio of the actual energy production to the theoretical maximum production:

5.1. Case study 1: Wind turbine design optimisation for hydrogen production

Table 5.2.: The main parameters of the reference wind turbine including the design parameters.

V_{rated}	Rated wind speed	11	ms^{-1}
V_{in}	Cut-in wind speed	4	ms^{-1}
V_{out}	Cut-out wind speed	25	ms^{-1}
C_p	Optimal power coefficient	0.49	-
Ω_r	Rated rotational speed	8.68	rpm
Design parameters:			
P_g	Generator rating	10	MW
D	Rotor diameter	198	m
H_H	Hub height	119	m

$$C_f = \frac{AEP}{P_{rated} \times 8760} \quad (5.4)$$

Since the current work only analyses a single wind turbine and wake effects are ignored, the RWT has a high capacity factor of 0.628 and an AEP of 55.0 GWh.

An electrical system for HWT is proposed, which is very different to traditional WTs. The WT generator is connected to an AC/DC converter and a battery is connected to the DC bus through a separate DC/DC converter. The primary role of the DC/DC converter to which the battery is connected is to provide grid-forming services, which is essentially required since the external grid is unavailable. The battery also serves as a reserve for “cold” upstarts and to reduce curtailment in situations where power production exceeds the rating of the electrolysis system. For the RWT, a battery capacity of 1.25 MWh is determined by minimising the LCOH. When optimising the WT design parameters the battery capacity is chosen as $E_b = 0.125P_g$.

The AC/DC converter is used to control the active power output of the WT and helps meet the dynamic requirements of the electrolysis system. A super-capacitor could have been connected to the system to mitigate the high-frequency fluctuations from the wind as there is a risk that the fluctuating power will negatively influence hydrogen production and result in a shorter lifetime of the electrolyser system [164]. This work focuses on how the fluctuating power influences hydrogen production and the potential lifetime reduction has not been analysed. To analyse the most severe case the super-capacitor has been omitted. Instead, a 1-second resolution WT generator time series was simulated as described by [172] and used directly as input for the electrolyser system without applying any low-pass super-capacitor filter.

Electrolysis system

Based on the model developed and discussed in thesis section 2.4, an alkaline electrolysis stack operating at nominal conditions of 30% wt. KOH, 80 °C, 7 bar, is

adopted.

Once produced, hydrogen is separated from the electrolyte and compressed in a multi-stage process to a pipeline, which is kept pressurized at 70 bar [67]. A desalination unit (based on the reverse osmosis process) constantly replaces the water consumed in the electrolyser and the cooling towers. The proposed design for the electrolysis system is illustrated in Fig. 5.4 and the main modelling assumptions are summarized in Tbl. D.1, reported in a dedicated Appendix section.

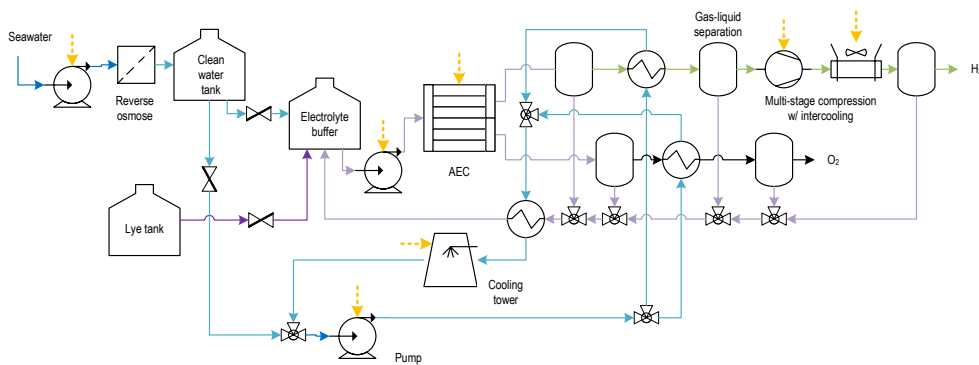


Figure 5.4.: Flowsheet of the electrolysis system

It is important to highlight that the electrolysis system does not follow a H_2 -demand profile, but it is assumed that all hydrogen produced is purchased by an off-taker and, therefore, hydrogen storage and onshore transport are not considered. The thermodynamic model for the electrolysis system was developed using Python with the libraries Numpy [173] and Scipy [174], and the system is solved using a MILP optimisation algorithm using Julia with the JuMP modelling framework [175] and the Gurobi solver [176].

The cell voltage model is based on the equations proposed by Ulleberg [73], which were modified to reduce the number of calibrated parameters (i.e. from 6 down to 4) and to be more physically consistent, previously described in section 2.4.1.

The fitted values and the model results compared with experimental data ([73]) can be observed in Tbl. 5.3 and Fig. 5.5, respectively. It can be observed that despite having only four parameters, the model can replicate the experimental values very closely ($R^2 = 0.9967$). Moreover, the model results are as fitted as those reported by [73], which used 6 parameters for calibration. A similar procedure is made for the Faraday efficiency, in which the parameters f_1 and f_2 were re-calibrated to assure their accuracy ($R^2 = 0.9989$). The comparison with experimental data and fitted values are shown in Fig. 5.6 and Tbl. 5.4, respectively.

5.1. Case study 1: Wind turbine design optimisation for hydrogen production

Table 5.3.: Parameters fitted for experimental data reported by [73].

Parameter	Value	Unit
δ_{el}	0.6637	cm
α	0.17255	-
k	$1.0267 \cdot 10^{-4}$	A/cm ²
E_a	44'324	J/mol K

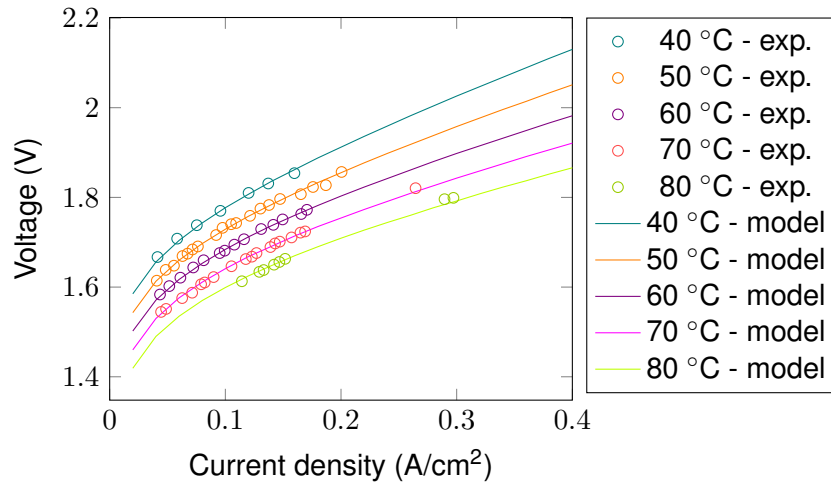


Figure 5.5.: Comparison of cell voltage model results with experimental data reported by [73].

Table 5.4.: Faraday efficiency parameters fitted for experimental data reported by [73].

Parameter	Value	Unit
f_1	0.9945	-
f_2	$1.015 \cdot 10^{-4}$	A ² /cm ⁴

5.1.2. System evaluation

To evaluate the HWT performance for different configurations of electrolyser rating, generator rating, and rotor diameter, different key performance indicators (KPI) are defined.

Energy curtailment:

If the power supply from the wind turbine generator exceeds the rating of the electrolysis system, the oversupply can charge the battery; otherwise, it must be curtailed. Energy curtailment may also occur when the power generation is less than the minimum power load of the AEC stack (15% of P_e). Curtailment is presented as a fraction of AEP, where E_c is the annual energy curtailed:

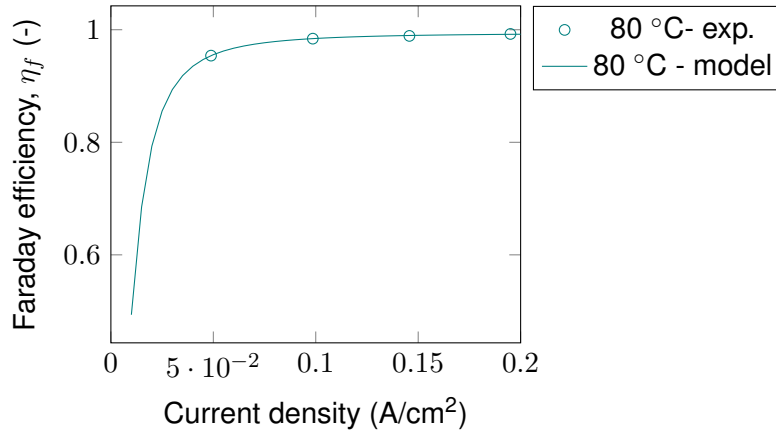


Figure 5.6.: Comparison of Faraday efficiency model results with experimental data reported by [73].

$$\phi_c = \frac{E_c}{AEP} \quad (5.5)$$

Energy efficiency:

The overall energy efficiency of the HWT system compares the energy content of the produced H_2 to the total energy supplied by the WT. LHV is the lower heating value of H_2 (33.33 kWh/kg):

$$\eta = \frac{AHP \times LHV}{AEP} \quad (5.6)$$

Levelised cost of hydrogen:

The LCOH measures the H_2 cost per unit H_2 produced:

$$LCOH = \frac{\sum_{i=1}^t (CAPEX + OPEX) / (1 + r)^i}{\sum_{i=1}^t AHP / (1 + r)^i}, \quad (5.7)$$

where, $CAPEX$ is the capital cost and $OPEX$ is the yearly operational cost, t is the project duration (20 years), and r (8%) is the discount rate.

To evaluate the costs, The DTUs off-shore wind farm cost model [177] implemented in the TOPFARM Python package [178]. The model includes the CAPEX and OPEX of the wind turbine, foundation, and balance of the plant (BOP). For this work, simple cost models for the electrolyser and battery were added (reported in the appendix chapter, in Tbl. D.2). The model inputs include the wind climate (Table 5.1), the WT configuration (Tbl. 5.2), and the BOP (water depth, distance to shore, number of turbines). The analysis aims to investigate the trade-offs between efficiency and costs for different design choices rather than precisely estimating the cost of hydrogen. Thus, the AHP and LCOH are normalized relative to the results of a base case

5.1. Case study 1: Wind turbine design optimisation for hydrogen production

condition: the reference wind turbine with a 10 MW electrolysis stack system and no battery support. The normalized results are calculated as described in Eqs. (5.8) and (5.9).

$$AHP_n = \frac{AHP}{AHP_{base}} \quad (5.8)$$

$$LCOH_n = \frac{LCOH}{LCOH_{base}} \quad (5.9)$$

5.1.3. Results of the case study

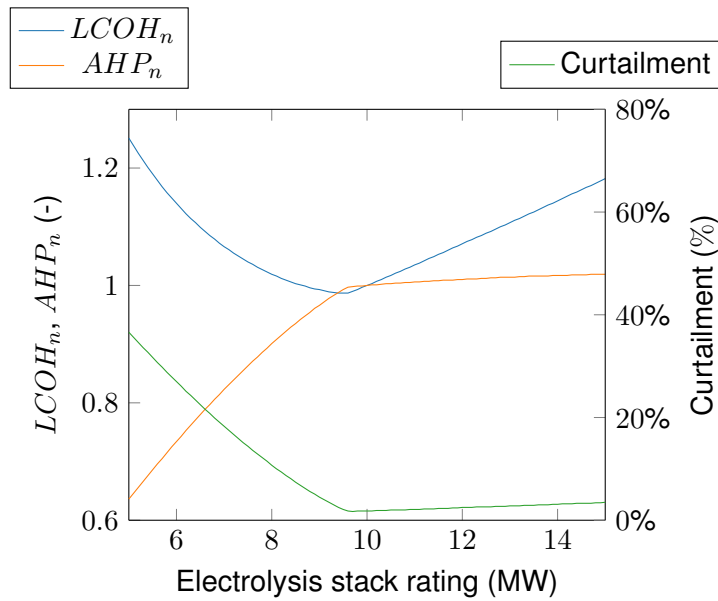
Optimisation of the electrolysis system

To determine the optimal size of the electrolysis system, the KPIs (Subsection 5.1.2) for different ratings of the electrolysis stack are assessed while keeping wind climate (Tbl. 5.1) and the WT configuration (Table 5.2) fixed. The results in Figure 5.7a indicate that the electrolysis system's optimal size depends on the chosen KPI. For instance, a minimal $LCOH_n = 0.987$ may be obtained for a 9.5 MW stack size, although lower curtailment (1.7% for 9.7 MW) and higher AHP_n (1.019 for 15.0 MW) can be achieved for larger systems. The relationship between the cost of the electrolysis system and the WT determines the optimum. Even though the AHP increases for larger electrolysis systems, the cost becomes too high as the design surpasses the minimal curtailment point. A similar trend is observed for different battery capacities (Figure 5.7b), where the minimum LCOH is estimated to be 97.6% of the base case for a storage capacity of 1.25 MWh and stack size of 9.5 MW.

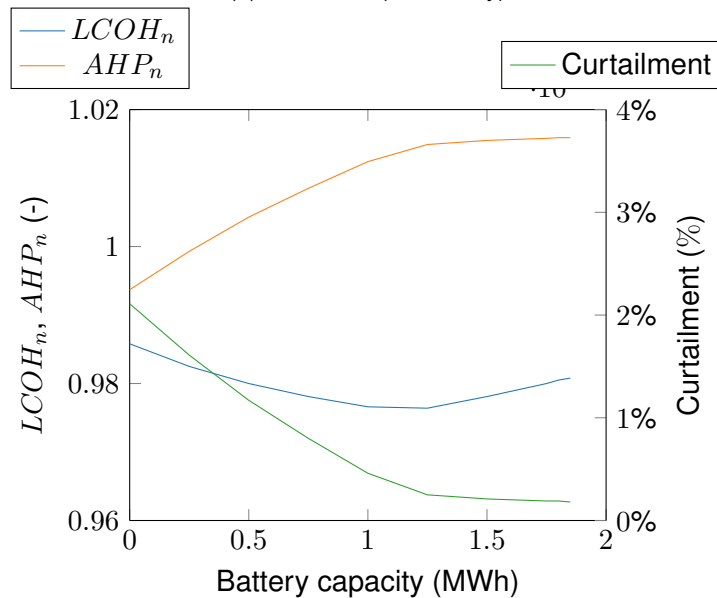
Optimisation of the wind turbine

This section explores the optimal wind turbine design for hydrogen production for the electrolysis/battery configuration derived from the previous section. The sensitivity of the wind turbine production and cost to the main top-level design parameters is studied. The main parameters comprise the rated power, rotor diameter and hub height. The range of parameters explored corresponds to realistic modern offshore wind turbine designs, although certain combinations result in infeasible designs. When optimising the main WT parameters, the electrolyser rating is set to $P_e = 0.9 P_g$, and the battery capacity is set to $E_b = 0.125 P_g$. The parameters and their range are shown in Table 5.5.

In Fig. 5.8 left, the resulting LCOH is shown as a function of rated power and rotor diameter for a hub height of 110 m. The optimal design gives the minimum LCOH of 1.48 €/kg, for $P_g = 11$ MW, $D = 240$ m and $H_H = 110$ m. Compared to the initial design of the RWT ($P_g = 10$ MW, $D = 198$ m and $H_H = 119$ m) with an LCOH of 1.56 €/kg, this results in a 5% LCOH reduction. It is seen that, for the given design assumptions, the LCOH-optimised design moves towards a larger rotor. The specific



(a) Stack size (No battery)



(b) Battery capacity (9.5 MW stack)

Figure 5.7.: Impact of the electrolysis stack rating (upper) and battery capacity (lower) on AHP, curtailment and LCOH. The battery capacity and battery rating are assumed to be the same.

power for the LCOH-optimised WT is $SP = 243\text{W/m}^2$ compared to $SP = 325\text{W/m}^2$ of the RWT.

It is interesting to compare the optimal design trends with the ones for a traditional LCOE-optimised wind turbine. In Figure 5.8 right, the resulting LCOE is shown as a function of rated power and rotor diameter for a hub height of 90 m. The optimal

5.1. Case study 1: Wind turbine design optimisation for hydrogen production

Table 5.5.: Range of wind turbine design parameters

Parameter	Range
Rated power	5:2:15 [MW]
Diameter	130:10:240 [m]
Hub height	90:20:150 [m]

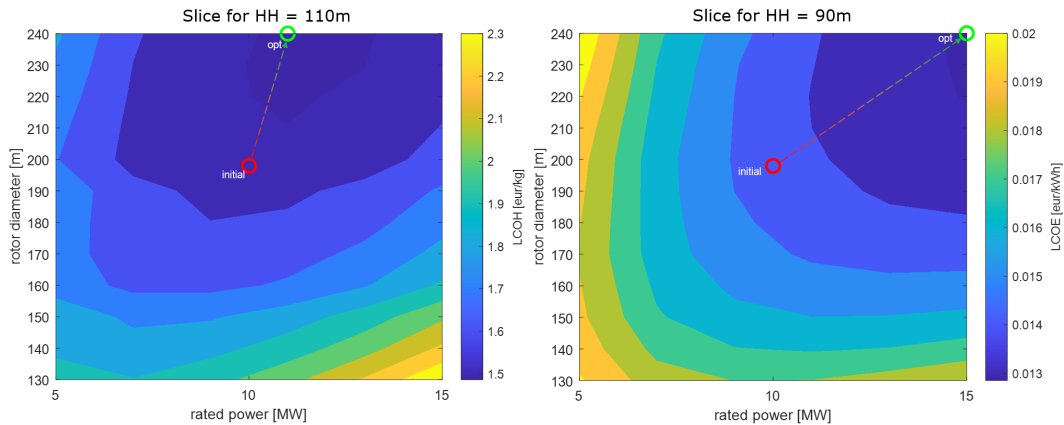


Figure 5.8.: Left: LCOH as a function of rated power and rotor diameter for a hub height of 110m. The initial (RWT) and optimal (min LCOH) points are also indicated. Right: LCOE as a function of rated power and rotor diameter for a hub height of 90m.

design gives the minimum LCOE of 0.0129 €/kW for $P_g = 15$ MW, $D = 240$ m and $H_H = 90$ m. Although this design combination is infeasible due to the low hub height, results are comparable to the closest feasible design for a hub height of 130 m. Compared to the initial design of the RWT ($P_g = 10$ MW, $D = 198$ m and $H_H = 119$ m) with an LCOE of 0.0144 €/kW, this results in a 10% LCOE reduction.

The specific power for the LCOE-optimised WT ($SP = 332$ W/m²) is close to the one of the RWT ($SP = 325$ W/m²), indicating that the RWT is an LCOE-optimised design, as expected. For the given design assumptions, the LCOH-optimised design moves towards a smaller generator than the LCOE-optimised design. This indicates that HWTs should have lower specific power ($SP \approx 240$ W/m²) than traditional LCOE-driven WT designs ($SP \approx 330$ W/m²). This is different from [168], who argues that an HWT should have a high specific power to increase electrolyser efficiency and lower the LCOH.

5.1.4. Approach's potential and case study's results

This study represents a milestone in the interconnection of both system and technology-level analysis of the energy systems. It includes:

- The design of different energy systems, including an optimisation problem,

which is a typical system approach,

- Alkaline electrolyser operational details, including the non-linear behaviour of the polarisation curves.

These efforts have been instrumental in addressing the research question 1.4:

How to deal with fluctuation in power supply for Power-to-Hydrogen?

It's imperative to highlight that this investigation owes its depth and effectiveness to prior exhaustive technology-level studies (Section 2.4). These earlier studies have provided invaluable insights into:

1. Dynamic response due to input fluctuations
2. Non-linearities due to multi-physical phenomena.

Case study's conclusion

Specifically, this work investigated how an off-shore wind turbine designed for hydrogen production differs from a traditional WT. The analysis is based on a modelling framework that can estimate the hydrogen production and cost of an HWT for a given wind climate. The work includes a detailed thermodynamic model of the electrolysis system that can calculate the system efficiency at different stack loads. Using the IEA 10 MW WT as a reference, the main parameters of the HWT system (generator rating, rotor diameter, electrolyser rating and battery capacity) were changed to minimise the levelised cost of hydrogen and then compared the design to an LCOE-optimised WT. The following conclusions can be drawn:

1. The analysis revealed an optimal electrolyser rating of 9.5 MW and a battery capacity of 1.25 MWh for the 10 MW RWT. This finding aligns with the research by Gea Bermudez et al. [161], who identified an optimal electrolyser-to-generator ratio of 0.92. In contrast, Mehta et al. [167] propose an 'oversizing' strategy for the electrolyzer compared to the generator and suggest a suitable ratio of 1.2. The choice between these ratios hinges on the efficiency and cost of the electrolysis system. Increasing the system's cost tends to result in a lower electrolyzer-to-generator ratio, all other factors being equal. In the proposed electrolysis system, the alkaline electrolysis cell stack accounts for 96.3% of the total power consumption, while H₂ compression contributes 2.6%, and the remaining 1% is attributed to cooling and desalination.
2. The impact of varying the rotor diameter and rated power of the RWT ($P_g = 10$ MW, $D = 198$ m) on both LCOH and LCOE was investigated. Within the permissible parameter range, the LCOE optimisation results in a shift towards larger generators and rotor diameters ($P_g = 15$ MW, $D = 240$ m). However, it's

5.2. Case study 2: Storage solutions comparison

noteworthy that the specific power for the LCOE-optimised design ($SP = 332 \text{ W/m}^2$) remains in proximity to that of the RWT ($SP = 325 \text{ W/m}^2$), signifying that the RWT is indeed LCOE-optimised, as anticipated. On the other hand, when optimising for hydrogen production, the design veers towards a smaller generator ($P_g = 11 \text{ MW}$, $D = 240 \text{ m}$) and a reduced specific power ($SP = 243 \text{ W/m}^2$). This observation suggests that HWTs should ideally possess lower specific power ($SP \approx 240 \text{ W/m}^2$) compared to conventional LCOE-driven WT designs ($SP \approx 330 \text{ W/m}^2$). This finding contrasts with [168], which argues for a high specific power in HWTs to enhance electrolyser efficiency and lower the LCOH.

3. The findings suggest that the incorporation of a 9.5 MW electrolyser and a 1.25 MWh battery leads to a 2.4% reduction in LCOH when compared to a configuration utilizing a 10 MW electrolysis stack without a battery. Additionally, optimisation of rotor diameter and generator rating yielded an extra 4.6% reduction in LCOH. These outcomes collectively indicate the presence of viable opportunities for cost reduction in hydrogen production through the design of wind turbines tailored for optimal hydrogen production.

5.2. Case study 2: Storage solutions comparison

Among ESSs, the Battery Electric Storage System is one of the most known and commonly used. However, BESSs present relevant self-discharge phenomena due to the crossover reactions and material degradation that limit their long-term storage capabilities; indeed, they can present a 5% loss of stored energy in a month [179]. Furthermore, the BESS's degradation phenomena have been also partially investigated, in the Chapter 3.

On the other hand, long-term chemical-based ESSs (e.g., hydrogen storage) are promising solutions due to the higher energy density and stability over time compared to BESSs [60]. At the same time, although the energy loss in the round-trip conversion is considerable, the hydrogen storage solution is suitable for long charging/discharging periods due to the high energy density per unit of mass and long-term stability in its stored form. Since the hydrogen storage solution is based on open conversion systems (e.g., electrolyser and fuel cell), the stored energy volume depends only on the storage capacity, and it does not affect the power rating of the conversion systems; in this way, substantial increases in the investment costs can be avoided [180].

Generally, Battery energy storage and hydrogen storage systems are being used for short- and long-term periods, respectively; thus, their comparison in terms of both the design and the usage is crucial for properly assessing their optimal operation. For sure, the characteristics of the renewable source affect considerably the choice of the two previous technologies, providing an advantage of one of them over the other

[181]. Indeed, BESSs and hydrogen storage systems have been already defined by other researchers as mutual alternatives to be embedded in the energy systems [182]. However, both ESSs have been identified as attractive solutions in different combinations to enhance the reliability and resiliency of national grids and energy systems.

This thesis section presents the second case study carried out for bi-level interconnection, including both BESS energy loss over time and the hydrogen technologies, with the aim of investigating different ESSs, namely the BESS and the hydrogen storage system, coupled with an existent 220 kW small-scale hydropower plant, for fulfilling the electricity demand of a LEC completely.

Indeed this section of the thesis has the aim to unveil the answers to the following research question (1.4):

Which is the best solution for long-term storage?

Specifically applied to the context of local energy community perspective. Where both technologies (BESS and hydrogen) are analysed over a year to achieve an off-grid, decarbonised LEC. Using the scenario analysis approach, all the scenarios are analysed with a model-based approach by implementing the energy modelling framework *Calliope*, already illustrated in subsection 4.1.1, which is based on a MILP algorithm, to minimise the user-defined objective.

Furthermore, with the implementation of this case study, by assessing the seasonal application of this ESS integration to provide a fully grid-independent operated LEC, several contributions to the scientific literature can be delivered:

- Provides an investigation on the loss of BESSs' stored energy when dealing with long-term storage;
- Assess the hydrogen storage benefits in LECs since it is not subjected to stored energy loss over time;
- Investigate energy-power coupling issues due to the ESSs' integration;
- Compare the Levelised Cost Of Storage (LCOS) of both ESS technologies in seasonal storage applications.

5.2.1. Methodology adopted

The method adopted, to compare BESS and hydrogen storage systems coupled with a small-scale hydropower plant for the off-grid operation of a LEC is described in detail in the following paragraphs. Based on historical data of i) the small-scale hydropower plant's power production, ii) Italian energy price, and iii) the LEC's electricity demand, all of them with an hourly resolution, a two-stage study is performed with the *Calliope* framework (already described in section 4.1.1).

5.2. Case study 2: Storage solutions comparison

The description of both stages, as well as the connection between the involved energy systems, are reported; then, the case study under investigation is described by reporting all operational data required for the analysis.

Description of the two-stage analysis

As previously mentioned, the analysis is divided into two distinct stages, namely baseline and off-grid operation. Their main characteristics are described as follows:

1. The baseline stage (Fig. 5.9) is the case where no energy storage is present. In this case, the overall energy demand is mainly provided by the national grid and, when available, from the small-scale hydropower plant. The use of hydropower electricity over the one withdrawn from the national grid is driven by the market cost, which is different in the two cases. When the small-scale hydropower plant's production is higher than the LEC's energy demand, the energy surplus is injected into the grid. Such a stage represents the benchmark scenario that allows having a reference case of the current situation (on-grid operation) and a base for carrying out the analysis with the implementation of ESSs.

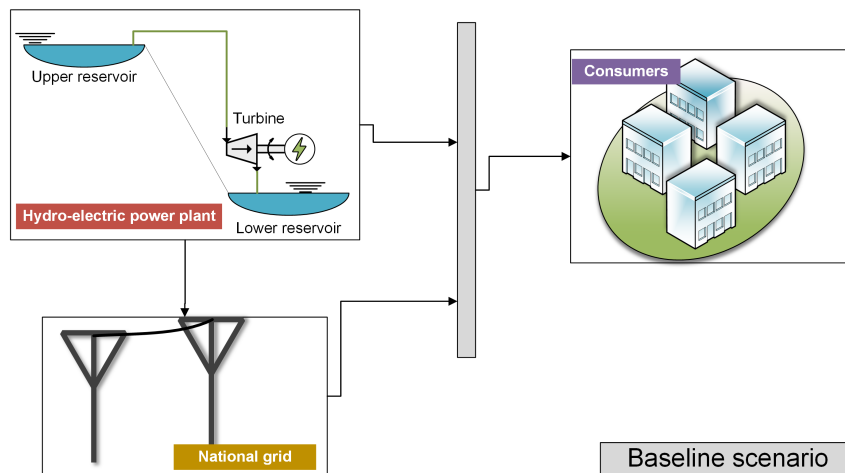


Figure 5.9.: Baseline scenario (on-grid operation of consumers).

2. Off-grid operation stage assesses the grid independence of the LEC, and it is further divided into two scenarios:
 - The BESS scenario (Fig. 5.10) assesses the off-grid operation of the LEC with a battery, where both capacity and energy management are considered. Technological barriers, such as self-discharge losses, are also included;
 - The hydrogen scenario (Fig. 5.11) assesses the Power-to-Power (P2P) route for the off-grid operation of the LEC. This stage is devoted to the

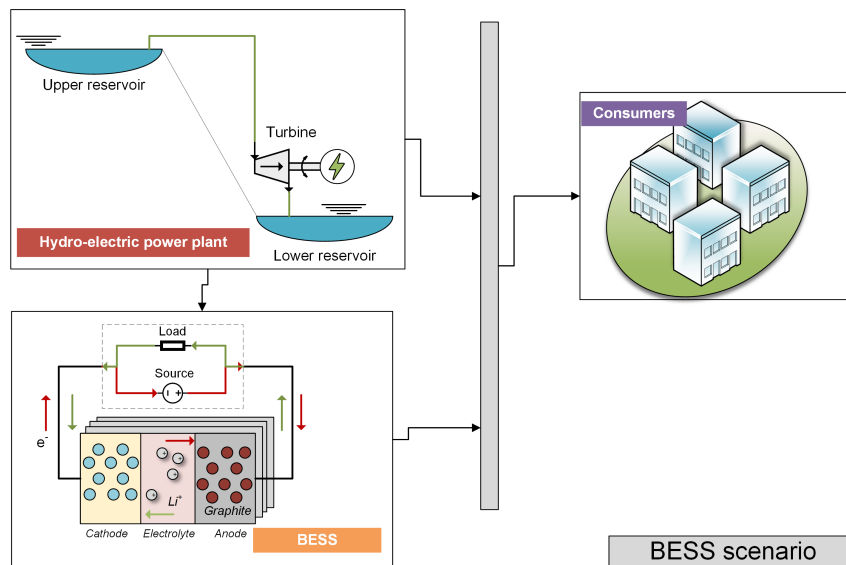


Figure 5.10.: BESS scenario (off-grid operation of consumers).

design of the electrolyser, the hydrogen storage, and the fuel cell, stressing the energy (hydrogen storage) - power(electrolyser/fuel cell) decoupling.

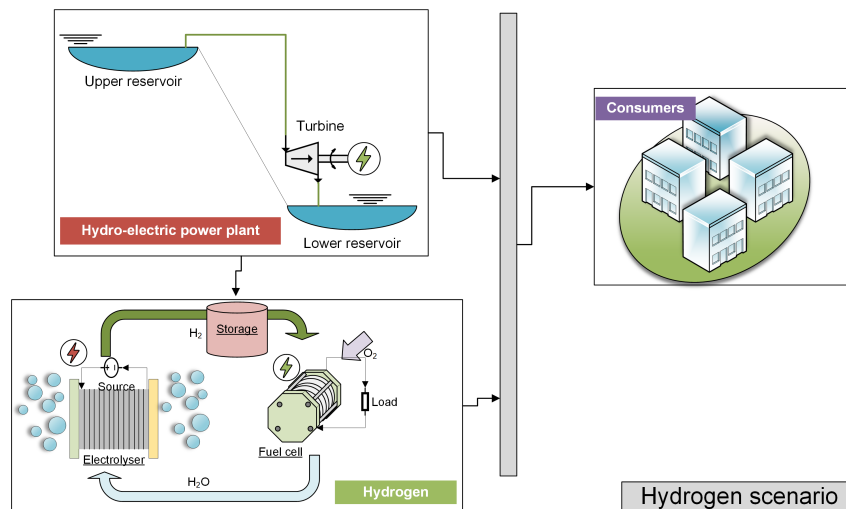


Figure 5.11.: Hydrogen system scenario (off-grid operation of consumers).

In the off-grid operation, a seasonal energy storage strategy has to be considered to provide the off-grid operation of the LEC because of the fluctuation of the small-scale hydropower production in some months of the year. Precisely, this strategy consists in storing the energy surplus produced by a RES system into an ESS for an extended period of time and using it afterwards, when the RES system is not operating, to fulfil the energy demand of the LEC completely. Thus, the national grid has been excluded in this stage; indeed, the main three elements involved in the analysis are (i) the small-scale hydropower plant, (ii) the end-user's demand, and (iii)

5.2. Case study 2: Storage solutions comparison

the ESS.

As reported in Fig. 5.10, the BESS is modelled as a single component. On the other hand, even though the hydrogen storage system can be considered a single energy storage solution, it has been divided into two conversion systems (e.g., electrolyser and fuel cell) plus one storage (e.g., hydrogen tank) to evaluate the power and energy decoupling nature of this solution. It is worth noting that both the BESS and the hydrogen storage system have been analysed separately. For hydrogen, only the re-electrification through a fuel cell is studied to compare two Power-to-Power storage routes; by doing this, it is possible to perform a comparative analysis of the two ESSs by addressing their technical and economic differences.

The single national price of the Italian energy market

In the case of the on-grid operation of the LEC, the electricity cost takes the name of the "Single National Price" (PUN), which is the wholesale reference price of the electricity that is purchased from the electric market. The PUN represents the national weighted average of the zonal sales prices of the hourly electricity day, and it considers both quantities and prices formed in the different areas of Italy and at different day times. The historical values of the PUN (hourly resolution) are publicly accessible on the National Energy Market Operator named *Gestore dei Mercati Energetici* database [183]. In this work, the historical data of the PUN, regarding the year 2019, have been adopted, ensuring the time-horizon alignment with the hydropower plant production data.

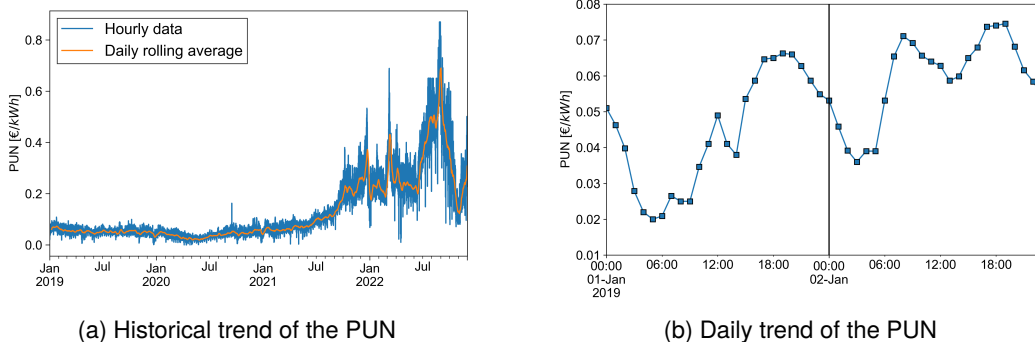


Figure 5.12.: Single National Price/PUN trend

In 2019, as reported by Figure 5.12, the PUN values varied between 0.01-0.12 €/kWh and its daily trend is recurrent throughout the year. As it is highlighted by the same figure, its value has skyrocketed, starting in 2021, due to the energy crisis. Indeed, from 0.05 €/kWh in January 2019, it achieved a value of 0.4 €/kWh in December 2022, thus further enhancing the economic importance of operating in off-grid mode. The period between 3-6 am is characterised by the lowest PUN value of that day, while it increases during the day at 10-12 am until the maximum daily value is achieved at 6 pm.

Small-scale hydropower plant

The case study consists of a 220 kW small-scale hydropower plant (e.g., run-of-the-river) in the Center of Italy. It is constituted by a Kaplan turbine with movable runner blades to adjust their operating point according to the available flow rates. The main characteristics and performance curves of the Kaplan turbine are shown in Table 5.6 and Figure 5.13, respectively. In particular, the Best Efficiency Point (BEP) is obtained at 417 rpm with a flow rate of 3.04 m³/s and a head of 4.05 m with an overall efficiency of 90%. An inverter is also connected to the electric generator of the hydraulic turbine to provide more flexibility to the machine operation by shifting the operating point while changing the rotational speed: indeed, this procedure allows the hydraulic turbine to operate in a wider range of flow rates keeping high hydraulic efficiency.

Hydropower generation implies variable power production throughout the year since it depends on the occurrences of rainfalls, and thus on the flow rate of the water resource. Fig. 5.13 shows the measured data of the power output of the hydraulic turbine in 2019. The seasons characterised by a lack of hydropower production are usually the spring and the summer when the water shortages do not allow the hydropower plants to operate at their rated operating conditions. The minimum vital flux defined by the legislation of each country, which must be guaranteed to preserve both the local flora and fauna [184], affects the variability of the hydropower plants' production. The average power output recorded in 2019 was equal to 70.07 kW considering the shutdown of the small-scale hydro-power plant in two periods of the year (e.g., March-April and July-November), as previously mentioned, where the second extended shutdown lasts more than 140 days.

Table 5.6.: Main characteristics of the Kaplan turbine

Parameter	Value	Unit of measure
Diameter	0.9	m
Rotational speed	417	rpm
#n of blades	5	—
Head	4.05	m

5.2. Case study 2: Storage solutions comparison

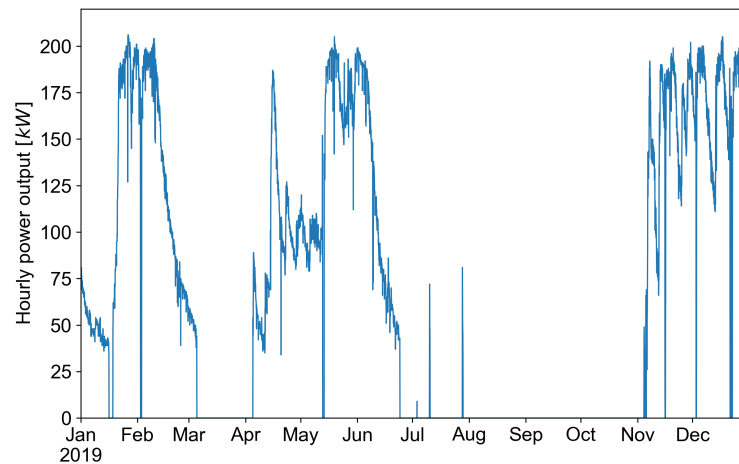


Figure 5.13.: Trend of the hourly power output of the small-scale hydropower plant in 2019

Energy demand of the Local Energy Community

The electricity demand of the end-users is required to obtain the design requirements of the ESSs. Due to the lack of data related to the end-users close to the small-scale hydropower plant, the energy demand has been obtained using the “mid-rise apartment” dataset of the *Building Energy Codes Program*, which is a database widely used in the scientific literature by assuming the characteristics of the loads [185]. The “mid-rise apartment” from BECS is a non-industrial, multi-use building (both residential and offices) divided into 4 floors with 32 small apartments that cover an overall area of nearly 3400 m². The electric load is reconstructed through (i) the occupancy of the end-users and the electrical activities during the day (e.g., appliances and lighting), (ii) the rated surface, and (iii) the specific electric power consumption by lighting and appliances as shown in Fig. 5.14. It is possible to modify the data of the 32 small apartments of the single building with 32 stand-alone houses and offices, thus constituting a small-scale LEC to analyse a more common urban environment in Italy. Furthermore, this modification does not affect the overall electricity consumption and the model output since the total energy demand is taken as a whole as input of the model.

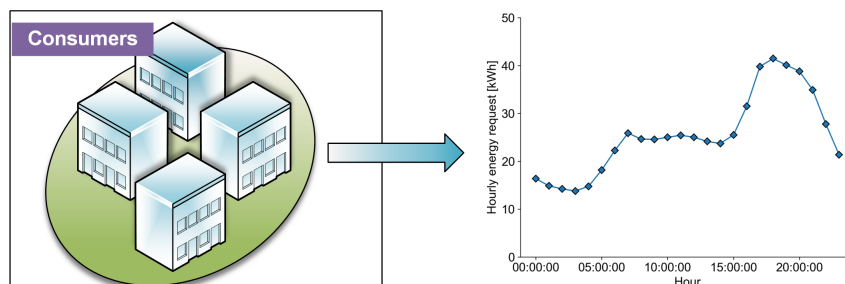


Figure 5.14.: Daily electrical load of the LEC [185].

The yearly electric load is simulated with a recurrent daily trend (hourly resolution). During the day, the trend follows the occupancy and the people's behaviour at work/home. Finally, the energy is equal to 614 kWh/day, thus resulting in a maximum stored energy requirement of 85 MWh for the maximum hydropower plant shutdown (about 140 days as described previously in 5.2.1).

5.2.2. Calliope set-up

All scenarios of the work are investigated through a system-level simulation using the energy modelling framework *Calliope*, which allows modelling energy systems at different levels through a scale-agnostic mathematical formulation based on the power nodes modelling framework proposed by Heussen et. al [140]. As already presented in section 4.1.1, *Calliope* is based on a bottom-up approach; indeed, every single energy system (j) is modelled with its own characteristics and constraints based on the type of technology (e.g., supply, conversion, storage, demand, and transmission).

For all stages of the study, the optimisation problem is to find the best economic system design to provide the energy request during the entire planning horizon. Such a problem can be described by the following equations, where the objective is:

$$\min : z = \sum_j^J C_j \quad (5.10)$$

where C_j are the costs of each energy system involved in the study. Additionally, the problem is subjected to the following technical constraints:

$$\sum_{j,h}^{J,H} E_{prod(j,h)} = \sum_{j,h}^{J,H} E_{cons(j,h)} \quad (5.11)$$

$$E_{prod(j,h)} + E_{cons(j,h)} \cdot \eta_j = 0 \quad (5.12)$$

$$E_{prod(j,h)} \leq S_j \quad \forall h \in H \quad (5.13)$$

$$E_{stored(j,h)} = E_{stored(j,h-1)} \cdot (1 - \epsilon_j) - E_{cons(j,h)} \cdot \eta_j - \frac{E_{prod(j,h)}}{\eta_i} \quad (5.14)$$

$$S_j \cdot \delta_j \leq E_{stored(j,h)} \leq S_j \quad \forall h \in H \quad (5.15)$$

$$E_{prod} \geq 0; E_{cons} \leq 0 \quad (5.16)$$

While the overall systems energy balance is described in Eq. (5.11), Equation

5.2. Case study 2: Storage solutions comparison

(5.12) describes the energy conversion process and Equation (5.13) sets the technology size constraint (S_j). Finally, storage technical characteristics, including the self-discharge behaviour (ϵ), are present in the hourly balance in Eq. (5.14) as well as the minimum State Of Charge (δ_j) reported in Eq. (5.15).

The national grid is modelled as an unlimited supply, meaning that it is an energy system that has only E_{prod} , which is variable and associated with both economic (PUN, time-dependent) and environmental costs, where the latter is set equal to 281.4 gCO₂/kWh as reported by the Italian energy and climate regulatory agency [186]. The small-scale hydropower plant, instead, is an energy system with already known E_{prod} over the entire planning horizon since its historical production data is known. Finally, the energy demand is modelled as an energy system with only E_{cons} , which is time-dependent but known as input data.

As an economic evaluation, *Calliope* allows defining different costs that are divided into fixed (e.g., investment costs related to the capacity of the technology and the Operation and Maintenance (O&M) ones that are expressed as a fraction of the investment cost) and variable. Furthermore, the depreciation rate is adopted to compare different types of technologies:

$$d_r = \frac{i \cdot (i + 1)^{lt}}{(i + 1)^{lt} - 1} \quad (5.17)$$

where d_r is the depreciation rate, lt the lifetime of the technology expressed in years, and i is the interest rate. The depreciation rate allows comparing all the technologies into an equivalent year considering the different lifespans and interest rates as well. Hence, the overall cost for a single technology is the sum of all of the costs previously mentioned:

$$C_j = C_{fix} + C_{var} = S_j \cdot CAPEX \cdot d_r(1 + O\&M) + c_{var} \cdot E_{prod(j)} \quad (5.18)$$

that is divided into fixed costs (C_{fix}) and variable ones (C_{var}). While the fixed part is strictly dependent on the technology size S , which is the design variable of the optimisation model, $CAPEX$ represents the investment cost of the technology expressed either in €/kW or €/kWh, and O&M is the operation and maintenance costs of the technology expressed as a ratio of the investment cost. Regarding the variable part, it depends on the operational strategy; indeed, it is based on the energy produced and the cost per kWh of produced energy (c_{var}).

Based on the case study's characteristics, only supply technology (e.g., national grid and small-scale hydropower plant), conversion technology (e.g., electrolyser and fuel cell), storage (either Li-ion battery or hydrogen tank), and energy demands are included in the analysis. Still, *Calliope* offers more advanced and complex modelling in terms of both technology types and constraints; however, since this is not the focus of the study, further details can be found in [141]. The techno-economic parameters of the BESS and the hydrogen storage system (e.g., PEM electrolyser, PEM fuel cell,

and compressed hydrogen tank) are listed in Tbl. D.3 and Tbl. D.4 (in a dedicated Appendix section), which have been taken as a reference for the inputs of the *Calliope* model [187]. It is worth noting that PEM electrolyser and fuel cell have been chosen due to their high technology readiness level and availability in the market. Furthermore, the good performance at a low current density makes them suitable for managing transient loads as in the case of the hydropower plant under investigation. These parameters are not included for the small-scale hydropower plant yet since it is an already existent installation with previously monitored data. Regarding the BESS, the technical parameters such as round-trip efficiency and minimum SOC have been taken from the scientific literature [187]. The self-discharge rate, which is defined as the hourly loss of the stored energy over time and expressed as a percentage of the previously stored energy, was adjusted to have a calendar ageing (without BESS operation) of 5% in a month, which is aligned with the data available in the scientific literature [188]. On the other hand, the conversion efficiencies of the two systems (e.g., PEM electrolyser and fuel cell) are considered separately in the hydrogen storage system. It is worth noting that the minimum SOC and the self-discharge rate of the compressed hydrogen tank are not applicable. Indeed, it has been assumed that the charging and discharging phases occur via a mass transfer of the hydrogen with no losses.

Evaluation indicators

Both off-grid operating stages' designs are assessed to further compare them both technically and economically. Additionally, the LCOS has been calculated to evaluate and compare the competitiveness of the two ESSs to store energy over a fixed time period. The LCOS analysis is performed daily and for a period of 140 days. In particular, the analysis of the LCOSs trend with increasing storage periods from a day up to 180 days (e.g., stored energy volumes) allows evaluation of the storage duration limit that indicates the competitiveness of each ESS. The rated BESS capacity per scenario is obtained considering the self-discharge calculated on an operational basis. The LCOS analysis is carried out with the same economic parameters reported in Tbl. D.4, in the dedicated Appendix section (D.2), thus evaluating the number of cycles that the ESS can sustain with an overall time horizon of 20 years. The LCOS is calculated as follows:

$$LCOS = \frac{C_{ESS,y}}{E_{stored,y}} \quad (5.19)$$

where $C_{ESS,y}$ is the annualised cost of the selected scenario obtained with the economic parameters reported in Tbl. D.4, and $E_{stored,y}$ is the total energy volume that could be annually stored in the ESS. The latter considers the number of charging/discharging cycles according to the storage period, where the charging duration is assumed to be equal to the discharging one.

5.2.3. Results of the case study

The configuration of the *Calliope* framework and the modelling parameters employed for this case study can be found in Appendix Section D.2. The results of the two-stage scenarios under analysis are presented subsequently.

Initially, the results of the baseline scenario provide insights into the grid-connected stage. This is followed by an examination of the off-grid operational mode, elucidating the consequences of this choice.

Baseline scenario

As previously mentioned, the first stage refers to the standard operation mode where no energy storage is used. As it can be noticed in Fig. 5.15, the LEC cannot operate in off-grid mode using only the electricity produced by the small-scale hydropower plant due to its discontinuous energy production throughout the year.

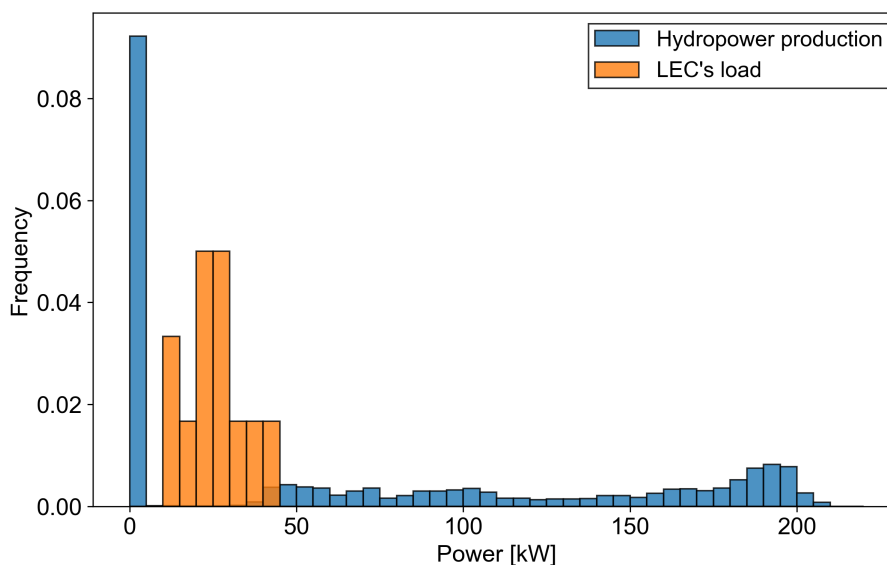


Figure 5.15.: Production and load frequencies (sorted by power).

Figure 5.16 shows that, in a single year, about 104 MWh of electricity from the grid (46%) and about 122 MWh of electricity from the small-scale hydropower plant (54%) is required by the LEC to fulfil its overall energy demand. In this case, there are both economic and environmental costs due to the dependence of the LEC on the national grid.

Off-grid operation mode

The cost-optimal model determines the lowest values of the design parameters of the BESS and the hydrogen storage system to supply the energy demand of the LEC in the whole period of the small-scale hydropower plant shutdown by exploiting

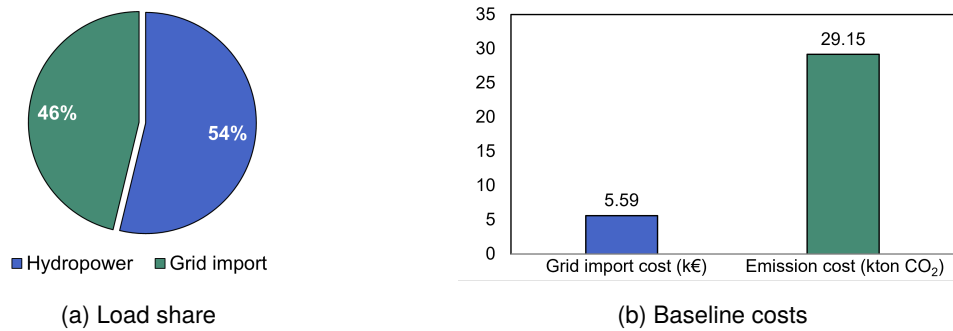


Figure 5.16.: Baseline scenario results

the surplus of the stored energy. Results for the design parameters of both the ESSs to meet the long-term storage requirements, including the characteristics of the technologies, are reported in Table 5.7 and Table 5.8 as follows:

- BESS storage: 280 MWh (capacity) and 193 kW (maximum power rating during the charging phase);
- Hydrogen storage: 137 kW electrolyser, 5'247 kg of hydrogen tank capacity (175 MWh, based on the Lower Heating Value of hydrogen), and 42 kW fuel cell.

Table 5.7.: BESS scenario results

BESS scenario	Value	Unit of measure
BESS capacity	280	MWh
BESS power	193	kW
BESS energy-to-power ratio	1'451	–
Min charge	56	MWh
Min SOC	20	%
Annualized BESS cost	3.38	M€/year
Overall cost	5.61	M€/year
LCOS	50'271	€/MWh

While the BESS capacity sizing is mainly driven by the energy rating (e.g., a larger stored energy volume implies a larger capacity), the sizing of the hydrogen system follows the power rating for the conversion systems and the energy rating for the hydrogen tank. Following the power production profile of the small-scale hydropower plant, the operational SOC of the ESSs (Fig. 5.17) reaches its peak at the end of the producibility before using the stored energy capacity to cover the lack of the small-scale hydropower plant operation. Due to the minimum SOC constraint (e.g., 20% of the capacity), high efficiency (91%), and modest self-discharge, the

5.2. Case study 2: Storage solutions comparison

Table 5.8.: Hydrogen scenario results

Hydrogen scenario	Value	Unit
Electrolyser capacity	137	kW
Hydrogen storage tank capacity	5'247	kg _{H₂}
Hydrogen storage tank capacity	175	MWh
Fuel cell capacity	42	kW
Annualized electrolyser cost	14.2	k€/year
Annualized hydrogen storage tank cost	290.5	k€/year
Annualized fuel cell cost	5.9	k€/year
Overall annualized cost	0.31	M€/year
LCOS	258	€/MWh

BESS capacity is discharged during the lack of small-scale hydropower production (July-November), but it is not completely depleted. Furthermore, due to the higher charge efficiency, its energy capacity remains higher than the one of the hydrogen tank during the subsequent start-up of the small-scale hydropower plant after the long period where it did not operate (e.g., November-December).

It is worth noting that a cyclic SOC (e.g., the SOC at the end of the evaluation time) for this case study cannot be achieved due to the characteristics of the plant since there is a gap between the yearly hydropower production and consumption; therefore, there is an abundant excess of hydrogen (i.e. 4'155 kg_{H₂}) stored in the hydrogen tank or electrical energy stored in the BESS (i.e. 280 MWh) at the end of the year.

The electrical energy that can be delivered from both ESSs to the LEC is reported in Fig. 5.17. It is possible to spot that, with the inclusion of the battery self-discharge loss, the available electrical energy has a steeper slope and decreases much faster than the hydrogen storage system. For larger stored volumes, the possibility of decoupling the power and energy rating allows sustaining moderate sizes of the conversion systems (e.g., electrolyser and fuel cell) that are the most expensive components. For this reason, the total cost and LCOS of the hydrogen solution (0.31 M€/year; 3 k€/MWh) is significantly more competitive with respect to the BESS (5.61 M€/year; 50 k€/MWh) as an effect of the high energy-to-power ratio, thus leading to an uneconomical result in terms of BESS investment cost.

By analysing the LCOS trend reported in Fig. 5.18, it can be observed that, with increasing storage periods, the hydrogen storage system is more competitive when dealing with periods greater than 30 h (e.g., between 1-2 days) and energy volumes greater than nearly 1 MWh. The intersection of the LCOS curves related to the two ESSs occurs at around 400 €/MWh. For energy volumes higher than 1 MWh, the additional cost for a larger BESS exceeds the CAPEX of the hydrogen conversion system, while the hydrogen storage tank only marginally contributes to the LCOS.

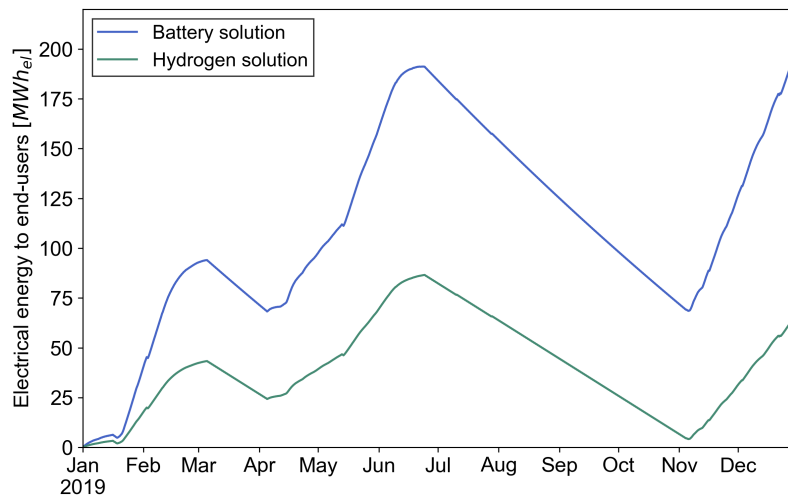


Figure 5.17.: Available electrical energy to end-users from the two ESS solutions

For storage periods beyond 1'000 h (about 40 days), the LCOS of the BESS storage (about 10 k€/MWh) is one order of magnitude higher than the LCOS of the hydrogen storage (about 1 k€/MWh). The LCOS trends are coherent with what has been previously discussed regarding the sizing of the hydrogen storage system and the scientific literature as reported in [189].

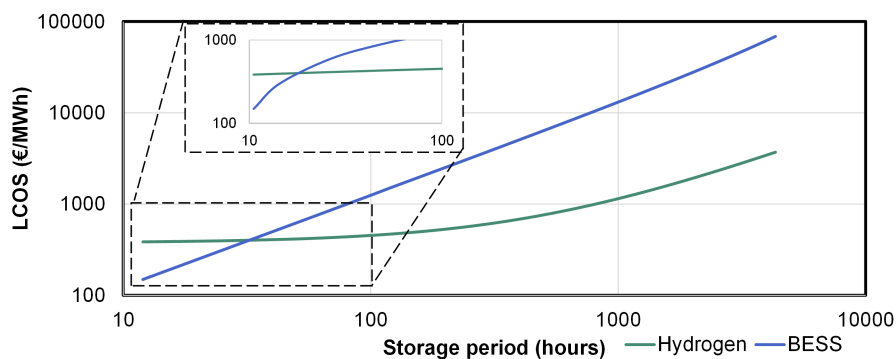


Figure 5.18.: LCOS as a function of the storage period

5.2.4. Case study's insights

This work is the second case study of the interconnecting of both technology and system level of energy systems analysis, using as input the historical RES data, with the objective to assess the following research question:

Which is the best solution for long-term storage?

5.2. Case study 2: Storage solutions comparison

Specifically, in this work, the integration of different ESSs coupled with a 220 kW small-scale hydropower plant (e.g., run-of-the-river) is investigated to provide an off-grid operated 48 kW LEC. In particular, a BESS and a hydrogen storage system are used as a Power-to-Power route and their energy and economic performance are compared. In particular, the study consisted of three stages, where firstly the baseline scenario is analysed to be then followed by other two stages related to the off-grid operation of the LEC with two different ESSs (e.g., BESS and hydrogen storage system).

Despite the difference in the rated power between the small-scale hydropower plant and LEC's energy demand, the former satisfies 54% of the LEC's energy demand, while the rest is covered by the electricity withdrawn from the national grid with an expense for power purchasing of 5.59 k€ and a carbon footprint of 29.15 kton_{CO₂} per year. However, such expenses can be avoided with a LEC operating completely off-grid.

Off-grid operation requires the prerequisite of seasonal storage integration, meaning storing the energy surplus produced by the small-scale hydropower plant into the ESS for an extended period of time (months)). Afterwards, this stored energy is used to fulfil the LEC's energy demand completely when the small-scale hydropower plant is not running. With the focus on achieving a fully electrically sustainable LEC (e.g., complete off-grid operation), the ESS technologies have been considered separately.

While the hydrogen storage can meet the storage requirements through 137 kW of electrolyser, 42 kW of the fuel cell, and a 5'247 kg capacity hydrogen tank (173 MWh), the BESS must have 280 MWh of energy capacity. The inclusion of the BESS self-discharge loss behaviour makes its discharging slope much steeper than the hydrogen discharging one. Furthermore, it has a higher round-trip efficiency but, since it is an energy-power coupled into a single energy system, it is not more economically convenient compared to hydrogen when a high imbalance among such parameters (e.g., extremely high Energy-to-Power ratio) is present.

Indeed, by analysing the LCOS trend, it can be observed that, with increasing storage times, hydrogen is more competitive when dealing with periods greater than 30 h (e.g., between 1-2 days) and energy volumes greater than nearly 1 MWh. For energy volumes higher than 1 MWh, the additional cost for a larger BESS exceeds the CAPEX of the hydrogen conversion system, while for storage periods beyond 1'000 h (about 40 days), the LCOS of the BESS (about 10 k€/MWh) is one order of magnitude higher than the LCOS of the hydrogen storage (about 1 k€/MWh).

Finally, the study has proven hydrogen storage systems as viable solutions when dealing with long periods of RES plant shutdowns. Indeed, although battery storage allows to achieve a higher round-trip efficiency, it suffers several limitations when operating for long-term storage periods, not to mention the bottleneck of having energy and power coupled which is not a limitation with hydrogen solutions as they are separated systems.

Chapter 6.

Conclusions, recommendations and future developments

The only thing that is constant is change.

Heraclitus

Energy system analysis, from both technologies and system levels, is crucial for reaching energy transition goals. However, they are seldomly integrated each over. This thesis has the objective of answering the following research question:

"Within the context of energy storage integration, how to bridge both technical and system perspectives of the energy system modelling, where the subsystem's critical properties are included at the system level, as well as systematic limitations?"

The thesis begins by identifying the technological limitations and key aspects of energy storage solutions considered (hydrogen and Li-ion battery). Subsequently, a thorough investigation of systematic limitations is undertaken. The ultimate goal is to integrate the critical aspects of energy storage into the energy planning and optimization stages, particularly in the context of multi-carrier energy communities.

6.1. Conclusions

In this section, firstly technological and system perspective conclusions are presented, highlighting the results obtained, to be followed by a discussion of their integration, assessed with two case studies. Furthermore, the final remarks of the thesis are discussed at the end of this section.

Power to hydrogen: alkaline electrolysis

A four-parameter semi-empirical model for alkaline cells has been successfully developed, demonstrating its accuracy through validation against four distinct sets

of experimental data obtained from various literature sources. Furthermore, the model's robustness was tested, revealing its capability to provide reasonably accurate predictions with only six input data points.

This model was further expanded by incorporating ordinary differential equations to explore the impact of various properties throughout the cell. Using this extended cell model, the study delved into the effects of temperature control, particularly its optimization through water flow rate adjustments, from both technological and economic perspectives.

Key findings from this research include:

1. The numerical model has the R^2 score higher than 0.90 for four different datasets, coming from different types of electrolysers.
2. In terms of efficiency evaluation, the 1/2 D model strikes a reasonable balance between capturing cell details and maintaining model simplicity.
3. Temperature control plays a significant role in overall efficiency. Optimal temperature regulation not only enhances electrolyser efficiency but also impacts the cost of hydrogen production, which reaches its lowest point when the temperature gap between the stack inlet and outlet is approximately 1°C.

Hydrogen storage: metal hydrides

Solid hydrogen solutions are being explored as innovative alternatives to address the limitations posed by the low density of gaseous hydrogen storage.

A numerical modelling framework has been devised to facilitate the integration of auxiliary systems with metal hydride-based hydrogen storage. Furthermore, this study delves into both the kinetics and economics of this storage approach under varying operating conditions, specifically focusing on pressure and temperature. The principal findings are as follows:

1. In stationary applications, metal hydrides emerge as viable contenders when compared to alternative hydrogen storage methods.
2. Notably, the control of pressure exerts a substantial influence on hydrogen charging and discharging kinetics, while thermal control exhibits a relatively minor impact.
3. Material properties, encompassing activation energies and kinetic parameters, are pivotal for a comprehensive assessment.
4. A trade-off is observed between minimizing energy consumption and optimizing hydrogen charging/discharging kinetics.

Li-ion battery degradation

This thesis has examined both Equivalent Circuit Models and Physics-Based Models from various angles.

- ECMs, while capable of achieving accuracy with a substantial dataset, tend to lack robustness when faced with unforeseen conditions.
- PBMs, on the other hand, display an advantage in that they can be tuned with a relatively limited amount of data, often obtainable from readily available commercial datasheets.

Moreover, this research has explored the robustness of ECMs using data from a 160 Ah battery and discussed the application of PBMs as inputs for determining optimal solutions in a multi-objective scheduling problem within a smart home case study. Key findings include:

1. In the univariate analysis of temperature, the model proposed by Baghdadi et al. [120] stands out as the best performer, while Wang et al.'s model [119] proves to be the most robust solution when dealing with variations in current.
2. State of Health can effectively serve as an automatic selection criterion for identifying the best solution on the Pareto frontier. This is achieved through the utilization of PBMs, which can accurately determine SOH across various battery working schedules.
3. It's worth noting that the parametrization of PBMs can be exceedingly time-consuming, representing a critical aspect of accurately assessing SOH.
4. Over extended operational periods, when employing consistent scheduling strategies based on SOH as the indicator for selecting the best solution, potential lifespan savings of up to 26.67% in battery lifespan are obtainable.

Energy planning

Two distinct energy planning methodologies have been developed and rigorously tested using the same case study. Remarkably, both approaches share similar results, mutually validating their accuracy and robustness. Furthermore, each approach has thoughtfully addressed specific limitations found in current energy planning tools, such as:

- Optimal alternatives, besides the optimal solution.
- Inclusion of the dynamic variations of the input data.

In the context of the same case study, both methodologies offer valuable insights:

1. Optimal alternatives give key insights, such as the technologies deployment priority, and technologies correlations. Moreover, the assessment of different alternatives allows the stakeholders to have an extended overview of possible solutions.
2. The consideration of multiple investment stages throughout the entire planning horizon can be enabled. This flexibility empowers decision-makers to explore various expansion plans for the energy system.
3. By accommodating changes in input parameters over time, such as reductions in technology investment costs, these methodologies accurately reflect the evolving landscape of energy planning.

Bi-level integration studies

This thesis encompasses two enlightening case studies dedicated to the integration of technological details into the broader energy system context:

1. **Alkaline electrolyser system dynamics:** This case study has the primary objective to optimise the design of an offshore wind turbine in conjunction with this electrolyser system.
2. **Seasonal storage comparison for an independent energy community:** The second case study focuses on comparing seasonal storage solutions for an energy-independent community.

The key findings derived from these case studies are as follows:

- Alkaline electrolyser operational details, including the non-linear behaviour of the polarisation curves, can be effectively included.
- Optimal electrolyser-to-wind generator ratio is around 0.92.
- With increasing storage times, hydrogen is more competitive, compared to the Li-ion battery solution.
- While Li-ion battery energy and power are coupled, representing a limitation in sometimes, hydrogen solutions can prevail, as they are separated systems.

Final remarks

As illustrated by previous subsections, both energy storage solutions have still many technological limitations. Especially for hydrogen, where both its production and storage need proper assessment, including thermal-electrochemical phenomena as they play a significant role in efficiency identification. Moreover, their behaviours are far from linear, which has to be considered for their integration at the system

level. Furthermore, although Li-ion batteries have already reached the technology readiness and are widely adopted, their degradation still can't be accurately assessed, especially in stationary applications such as energy communities, where they play a passive role, as a support measure of other services, instead of having a degradation prevention control, and as result of this, the battery life could be mismatched from the initial energy community planned.

Also at the system level, many opportunities and research gaps are there. Due to the high fluctuation of the input parameters, and as a result of this, the outputs can't be considered exact, therefore having optimal alternatives would give a much clearer picture allowing the energy planners to consider different possibilities. Moreover, when medium-long-term energy planning is considered (i.e. >20 years), multi-investment stages planning is beneficial, to include different kinds of oscillations and respond to them.

Finally, the integration of the technology details into the energy planning stage has the potential of unlocking new horizons, obtaining a more accurate financial assessment, new design strategies, and assessing different energy storage solutions integration.

6.2. Recommendations

Several extensions and deepening of the research presented in this work are possible. A non-exhaustive list of possible directions are following:

1. The semi-empirical alkaline electrolyser proposed in this work, designed with a focus on computational efficiency, currently does not incorporate considerations for Faraday's efficiency. Furthermore, the comprehensive treatment of water vapour formation within the system has not been addressed. Both of these aspects represent potential areas for further investigation and refinement.
2. To ensure the accuracy and reliability of the results obtained through numerical evaluation, it is imperative to conduct experimental validation of the temperature control system within the alkaline electrolyser. This experimental validation will serve to confirm the performance of the temperature control mechanisms under real-world conditions, adding an important layer of verification to the research.
3. To conduct a more comprehensive analysis of the metal hydride system, the inclusion of advanced system controllers, such as partial integral differential controllers, would be beneficial. These controllers can provide a deeper understanding of the system's response time and behaviour, allowing for a more detailed examination of its dynamics and performance characteristics. This addition would enhance the overall analysis of the metal hydride system and provide valuable insights into its operation.

4. Conducting experimental tests on the materials involved in metal hydride systems is essential to evaluate material-specific kinetic parameters and activation energy. These experimental data are crucial inputs for numerical models and simulations. Enhancing the precision and validity of the numerical models used in the analysis of metal hydride systems.
5. In the evaluation of Li-ion batteries, particularly when considering them from a module perspective where each cell is assessed independently, effective thermal management emerges as a critical factor. This is essential not only for preventing thermal runaway but also for mitigating degradation issues. Further research into this aspect, with a focus on advanced thermal management techniques and strategies, can be a valuable area for future investigation.
6. The inclusion of the State Of Health of the battery in the energy planning and scheduling stage is a promising avenue for future research. This goes beyond the passive consideration discussed in this work, where the SOH could assume an active role in influencing energy planning decisions. Investigating how SOH can be integrated into decision-making processes and optimising energy systems accordingly is certainly a possible research direction.
7. The proposed two-step algorithm designed for energy planning, particularly regarding the inclusion of dynamic input parameters, may face a reduction in effectiveness due to its heuristic decomposition. Therefore, future research can delve into refining the algorithmic aspects. This could involve identifying optimal parameter settings through techniques like inference or learning, aiming to enhance its performance and robustness.
8. In the context of system-level studies presented, it's essential to recognize that certain aspects of energy systems have been simplified. For instance, factors such as costs and demands, which exhibit non-deterministic and often unpredictable characteristics, call for more accurate estimation and explicit treatment. One avenue for addressing this challenge is the utilization of stochastic programming methods, which can provide a more robust and comprehensive analysis of these dynamic system elements.
9. While this thesis has successfully captured numerous technical and system-level details, it's important to note that not all intricacies have been integrated into the analyzed case studies. The bi-level integration case studies presented here represent initial attempts at interconnection, incorporating only a limited set of technical details. This future work can leverage the research foundation established in this work to expand the scope and depth of such interconnections, thereby enhancing our understanding of these complex energy systems.

6.3. A glimpse of the future

By conducting incremental research activities focused on both energy storage technologies and the development of advanced management, all supported by supportive energy policies, it's possible to foresee a reduction in investment costs. This effort will enhance accessibility and enable wider deployment of these energy storage solutions within local energy communities. To conclude the thesis, several directions, about energy storage integration in energy communities, and their efficient management during the planning stage, are listed.

More intensive R&D efforts are required to make hydrogen competitive, in particular:

- Effective thermal management of electrolyzers plays a decisive role in the production of hydrogen, and its proper control can lead to a substantial reduction in the overall cost associated with hydrogen production [190, 191].
- One of the most critical limitations of hydrogen storage is its low density. To address this limitation, metal hydrides can be adopted, leading to the following key directions:
 - While metal hydride solutions can be suitable for stationary applications, their limitation in terms of low hydrogen concentration (typically ≤ 7.6 wt%) makes them unsuitable for use in vehicles and dynamic operations. Therefore, there is a need for ongoing research and development to discover materials that can absorb higher levels of hydrogen content [91].
 - Material degradation in various types of metal alloys will be thoroughly investigated to advance the TRL of metal hydride technology [192].
- Dynamic assessments of the power-to-hydrogen system, encompassing the balance of the plant, will undoubtedly contribute to determining the optimal operational stages, including shutdown and stand-by phases, in alignment with the constraints of the electrolyser [193, 194].

In the case of Li-ion batteries, with a specific emphasis on degradation assessment:

- Additional experimental data needs to be collected to account for the wide array of possible Li-ion battery chemistries. This will streamline the parameterization process, making it less time-consuming. Furthermore, it is essential that this data is openly accessible to the broader research community [195, 126, 196].
- Research into stationary applications for second-life batteries will be undertaken to prolong their lifespan. These batteries have typically reached 80% of their SOH, making them unsuitable for electric vehicles [197, 198].

When focusing on energy system planning, an ideal modelling tool should possess the following characteristics:

Chapter 6. Conclusions, recommendations and future developments

- **Adaptable:** The modelling tool should be flexible enough to accommodate an expanding array of energy carriers and associated technologies effectively [199].
- **Diverse output solutions:** The modelling tool should be capable of generating multiple output solutions to offer a comprehensive view of the expansion plan.
- **Incorporation of diverse objectives:** The tool should be able to handle different objectives and facilitate multi-objective evaluations.

The above list is not exhaustive, as new concepts and potential research directions continue to be explored and tested by researchers globally.

Appendices

Appendix A.

Hydrogen technologies

In this part all supplementary information for the chapter 2 is reported.

A.1. Alkaline system level modelling parameters

This section reports all the modelling parameters used in the work described in section 2.4, regarding the temperature control in alkaline water electrolysis. All parameters are reported in Tbl. A.1.

Table A.1.: Modelling parameters for alkaline water electrolysis temperature control

Pheobus electrolyser	
Cell area [m ²]	0.25
#n of cells	21
Nominal pressure [bar]	7
Nominal power [kW]	26
Unitary cost [€/kW]	830
Stack lifetime [years]	10
Water pump	
Efficiency	0.7
Input power	$P = \eta_{pump} \cdot \Delta P \cdot Q_e$
ΔP	1
Investment cost [€/kg/s]	60
Heat exchanger	
Investment cost [€]	$C = C_1 \left(\frac{A_{HEX}}{0.093} \right)^{0.78}$
C_1 [€/m ²]	110
U [W/m ² K]	700
ΔT_{HEX} [K]	5
A_{HEX} [m ²]	$A_{HEX} = \frac{\dot{n}_{H_2O} \cdot MW_{H_2O} / 1000 \cdot c_{pH_2O} \cdot \Delta T_{H_2O}}{U \cdot \Delta T_{HEX}}$
Lifetime [years]	15
Levelised Cost of Electricity	
min-max [€/MWh]	20-60

A.2. Metal Hydride and ancillary systems model's parameters

This section provides an overview of all the modelling parameters related to solid hydrogen storage used in this thesis work. These parameters are described in Section 2.5 and are associated with the effects of temperature and pressure control on the system's kinetics.

Table A.2.: MH Modelling parameters

	Values	Description
R	8.31	Universal gas constant [J/mol K]
T	15-35	System initial temp [°C]
$P_{charging}$	5-30	System charging pressure [bar]
$P_{discharging}$	0.78	System discharging pressure [bar]
k_a	58	Absorption kinetics [s^{-1}]
k_d	9.6	Desorption kinetics [s^{-1}]
x_d	1.6	Initial state of discharging [%]
x_a	0.2	Initial state of charging [%]
m_s	15500	Metal alloy mass [g]
cp_s	355	Specific heat of metal [J/kg K]
cp_{H_2}	14300	Specific heat of gaseous hydrogen [J/kg K]
MW_{H_2}	0.002	Molecular weight of hydrogen [kg/mol]
c_f	4181.3	Specific heat of the conditioning water [J/kg K]
T_f	10 or 40	Fluid temperature [°C]
E_a	21.17	Absorption activation energy [kJ/mol]
E_d	16.42	Desorption activation energy [kJ/mol]
ϵ	0.8	Heat transfer efficiency [-]

Appendix B.

Li-ion battery

B.1. ECMs

In this section all three models used for the study described in section 5.2, assessing the robustness of numerical models for SOH forecast, are reported.

B.1.1. Baghdadi

This model is the most comprehensive among the selected methods, but it also tends to be the most complex, which introduces a higher risk of overfitting.

In essence, this method provides an estimate of the maximum available capacity at a given point in time while taking into account both cycle and calendar ageing effects. It relies on the computation of two key parameters, denoted as k_{cyc} and k_{cal} , which are associated with cycle and calendar ageing, respectively. Consequently, this method can be applied effectively in various real-world contexts, considering the interplay between these ageing phenomena.

$$k_{cal}(T, SOC) = \exp\left(k_1 \frac{SOC}{R}\right) \cdot \exp\left(\frac{k_2}{R}\right) \cdot \exp\left(-\frac{k_3}{RT}\right) \quad (\text{B.1})$$

$$a(T) = \exp\left(\frac{k_4}{RT} + k_5\right) \quad (\text{B.2})$$

$$k_{cyc} = \exp\left(a(T) \cdot \frac{I}{I_0}\right) \quad (\text{B.3})$$

$$k_{tot} = k_{cal} \cdot k_{cyc} \quad (\text{B.4})$$

$$C(t) = C_0 \cdot \exp\left(-k_{tot} t^{k_6}\right) \quad (\text{B.5})$$

Application: energy and power intensive contexts.

Input: SOC [%], temperature [K], time [d], and current [A].

Parameters: k_1, k_2 [$\text{J mol}^{-1} \text{K}^{-1}$], k_3, k_4 [J mol^{-1}], k_5, k_6 dimensionless

Coefficients: I_0 , reference current A; C_0 , rated capacity expressed in Ah; R, universal

Appendix B. Li-ion battery

gas constant expressed in $\text{J mol}^{-1} \text{K}^{-1}$.

Outputs: $C(t)$ that is the capacity at a specific time expressed in Ah.

Storage size: validated with two storage at 5.3 Ah and 4.2 V and 7 Ah and 4 V, scalable to other sizes.

Pros: both calendar and cycle ageing are considered.

Cons: the model validation proposed is performed by keeping constant both SOC and temperature; furthermore, the analysis is focused on a single Li-ion cell, thus ignoring the internal resistance variation.

Note: the calendar contribution computation is simplified. Differently from this model that computes the calendar factor as the average of k_{cal} with respect to the SOC interval, the calendar contribution is evaluated using the average SOC of charge and discharge cycles.

B.1.2. Wang

This model assesses capacity loss as a percentage of the current utilised and injected into the electric storage system. It's important to mention that exponential modelling is a well-established approach extensively utilized in the scientific literature for this purpose.

$$Q_{loss} = k_1 \cdot \exp\left(\frac{k_3 + 370 \cdot C_{rate}}{RT}\right) \cdot (Ah)^{k_2} \quad (\text{B.6})$$

Application: energy- and power-intensive contexts.

Inputs: temperature [K], total amount of capacity supplied and extracted to and from the battery [Ah], C-rate.

Parameters: k_1, k_2 dimensionless, k_3 [J mol^{-1}].

Output: Q_{loss} [%] that is the capacity loss in percentage due to the ageing phenomenon.

Storage size: validated with 2.2 Ah with 3.6 V, scalable to other sizes of storage.

Pro: computational efficiency and robustness due to the single exponential equation. Input data is always noted.

Cons: a single exponential model does not adequately describe the high variation of the quantities. Different training is needed based on the operating conditions.

Note: k_3 is an additional parameter that improves the model performance instead of using a constant value as in the original study.

B.1.3. Omar

This model allows defining the degradation of a battery in terms of life cycles (e.g., Remaining Useful Life to achieve 80% of the residual capacity due to the effect of the cycle ageing). Each model is univariate, meaning that it evaluates the ageing effect according to the variation of a single input, while the remaining ones are kept fixed.

B.2. PBM model for SOH assessment

Since the interest of this study is restricted to temperature and current analyses, only the models that include them are here reported.

$$CL(T) = k_1 T^2 + k_2 T + k_3 \quad (\text{B.7})$$

$$CL(I_d) = k_1 \exp(k_2 I_d) + k_3 \exp(k_4 I_d) \quad (\text{B.8})$$

Application field: energy- and power-intensive contexts.

Inputs: temperature [K] and Crate (I_d).

Parameters: k_1 [K^{-2}], k_2 [K^{-1}], $k_i, i = 3, \dots, 5$ dimensionless.

Outputs: Cycle life or RUL of the battery expressed in the number of cycles.

Storage size: 2.3 Ah with 3.3 V. It is scalable to other dimensions.

Pros: it allows to study of multiple parameters regarding aging. It has been also experimentally tested and validated.

Cons: the variables that are not evaluated through equations are considered constant parameters. Since each model equation evaluates the ageing based on the variation of a single input quantity, they are not suitable for performing multivariate analysis. Consequently, Omar's model is not included in the multivariate analysis study.

Note: the polynomial Eq. B.7 is reduced to one degree with respect to the model proposed in the literature. The simplification is introduced to avoid over-fitting and simplify the training phase since the coefficient relative to the third-degree term is evaluated to be close to zero. Since these models estimate the number of cycles executed to reach a specific capacity threshold, many sets of parameters are computed, each for a different residual capacity value, so that the capacity degradation curve can be modelled. Moreover, k_1 is forced to be lower than zero according to data reported in [200] regarding the temperature modelling.

B.2. PBM model for SOH assessment

In this section, all support materials for the work reported in 3.2.1 are presented. These materials include two different types of details:

1. Pybamm parameterization results, including some problems and solutions encountered.
2. Battery design characteristics, the rack design of battery modules, computational efforts, case study specifics, tuned parameters, as well as some experimental results from Pybamm (including voltage, current, and SOH).

B.2.1. Parameterization

The initialization process is done through values from Table B.1, with the Parameter set of *Prada2013* [131], Using SPMe modelling, as the best compromise between

Appendix B. Li-ion battery

the accuracy and computational effort (Figure 3.1). The selection of the parameters is established according to the cell's chemistry, specifically Lithium Iron Phosphate.

Electrochemical parameterization

During the electrochemical parameterization process, two main inconsistencies from the initialized model and test results at different C-rates. i) firstly the dischargeable energy from the cell is different from the nominal value, due to dataset inconsistencies, and ii) the voltage drop slopes (Fig. B.1a).

Addressing the first inconsistency is relatively straightforward. It involves adjusting the electrode geometry to match the required dischargeable capacity. Since dischargeable capacity is directly proportional to current density (A/m^2), and the current is determined by an internal formulation that is not easily accessible, altering the electrode's surface area offers a practical solution to achieve the desired outcome more efficiently. In contrast, resolving the voltage drop slope inconsistency is a more intricate process. It necessitates adopting the comprehensive approach described in section 3.2.1. The key parameters to fine-tune in this case are the porosities of both the electrode and separator, which can vary between 0 and 1. These porosities are critical for ion transport within the battery and have been the subject of study for researchers like Parikh et al. [201]. Importantly, all three porosities are interconnected, making it challenging to isolate the effect of each one. Therefore, a grid search method is indispensable for this optimization process.

The results after the electrochemical parameterization are illustrated in Fig. B.1b, where the MAE is minimised for different C-rates.

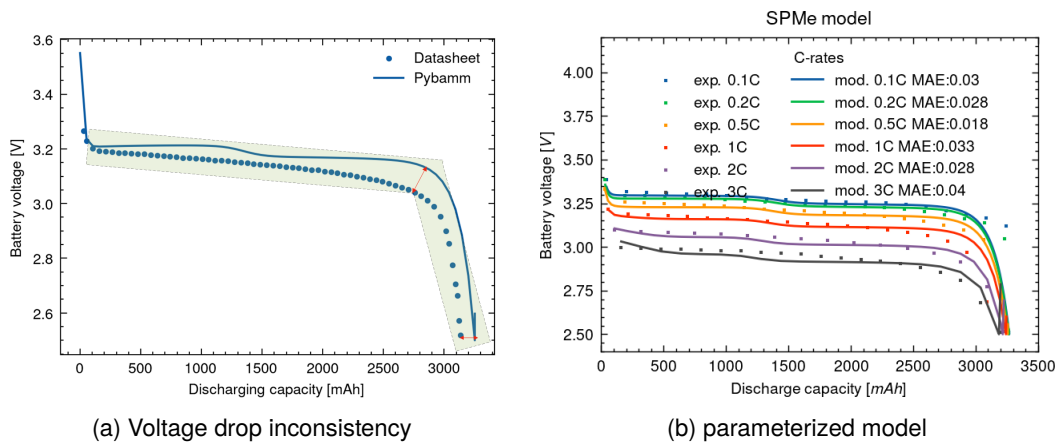


Figure B.1.: Electrochemical parameterization

B.2.2. Thermal parameterization

Regarding thermal parameterization, the "lumped thermal model" is the option selected. where two different natures of the difference between the reported data in the datasheet and the initialized model are observed:

1. The voltage gap, among different discharge curves at different working temperatures, enlarges when it is far from the reference temperature, and as

$$\Delta V = f(T) \quad (\text{B.9})$$

A solution to this is to adopt a new temperature, adjusted with a correction factor that can manage such behaviour so that the model's input temperature is the new modified temperature. Of course, with such a process, the updated temperature does not have a physical meaning, and for temperature variation analysis the initial temperature is referenced.

$$T_{new} = T_{initial} \cdot cf \quad (\text{B.10})$$

$$cf = 1 + m \cdot (T_{initial} - T_{ref}) \quad (\text{B.11})$$

Such inconsistency is fixed using a correction factor (cf), which is a linear interpolation, which depends on the ΔT between the working temperature and the reference temperature ($T_{ref}=298.15$ K)

2. Decreasing trend about the cell available capacity (C), working at low temperatures:

$$\Delta C = f(T) \quad (\text{B.12})$$

In order to take this into account, the available capacity of the cell at different temperatures is gathered to be described through a polynomial function ($f(T)$), and as best polynomial order, i.e. compromise between the accuracy and complexity of it, results to be a 4th order, to describe such variation.

The entire thermal parameterization process is illustrated in Figure B.2, where the comparison is also reported, between the tuned model and the experimental data. As can be seen, although the different correction measures, the model can't accurately describe the discharge curves at low temperatures (≤ 0 °C), where the second part of voltage drop (dV/dC) happens much earlier than the model predicts. Despite such differences, since the objective of the work is not thermal assessment, the cell is set to work at the reference temperature (298K).

B.2.3. Aging parameterization

Ageing parameterization is the most intricate aspect of this study, primarily owing to the inherent complexity of the phenomena involved. The developers of Pybamm

Appendix B. Li-ion battery

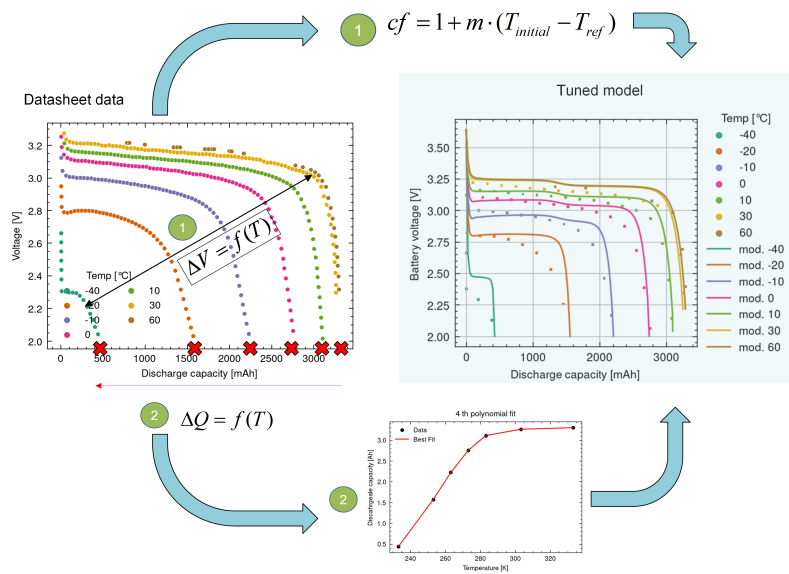


Figure B.2.: Thermal parameterization

have conducted a detailed analysis of ageing phenomena, which encompass the factors contributing to the gradual reduction in a cell's available capacity over time. These insights have been thoughtfully incorporated into the Pybamm framework [202], which are the following ones:

1. SEI layer growth
2. Lithium plating
3. Particle fracture/cracking
4. Loss of active material

It's crucial to begin by understanding which phenomena should be incorporated into the model. This necessitates a comparative analysis of various degradation behaviours to identify the one that aligns most closely with the experimental data. In the case study under consideration, the following ageing phenomena have been taken into account: SEI growth, lithium plating, and alterations in lithium plating porosity. Once these ageing phenomena have been defined, the entire parameterization process is executed in accordance with the method detailed in Section 3.2.1.

The full ageing parameterization process is reported in Fig. B.3, where the tuned model and its comparison with experimental data are also illustrated. Furthermore, calendar ageing is predominant in such cells. Despite the fact that it's not common, calendar ageing can prevail over cycle ageing, which was also analyzed by other researchers previously [203, 204], especially when cycle depths and current rates are low.

B.2. PBM model for SOH assessment

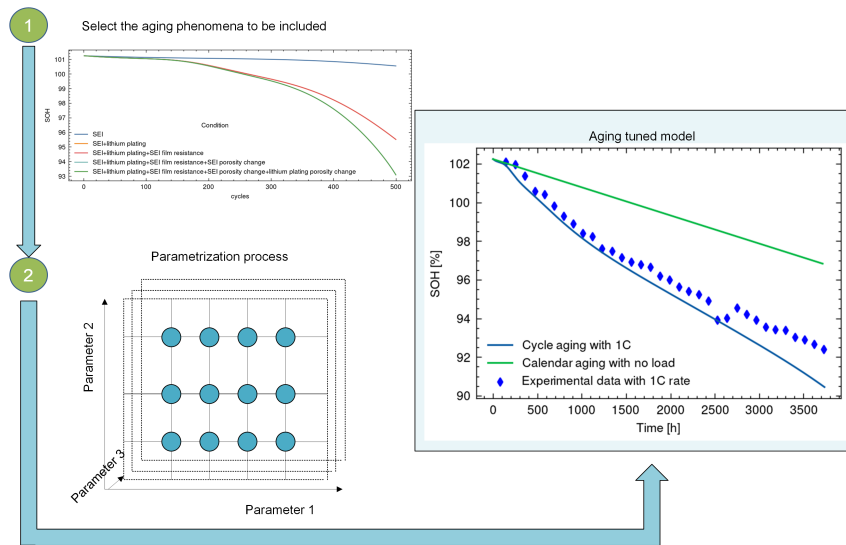


Figure B.3.: Ageing parameterization

B.2.4. HEMS results

From the HEMS, a total of 15 optimal solutions are derived from the Pareto front, each employing distinct scheduling strategies.

The Pareto curves generated by HEMS are visually represented in Fig. B.4. This graphical representation allows the identification of, based on the battery power curves, which solutions effectively utilize PV production. Notably, solutions (1-7) do not absorb the PV production, resulting in increased carbon emissions during the day. Conversely, in other cases, reducing emissions necessitates higher economic expenses.

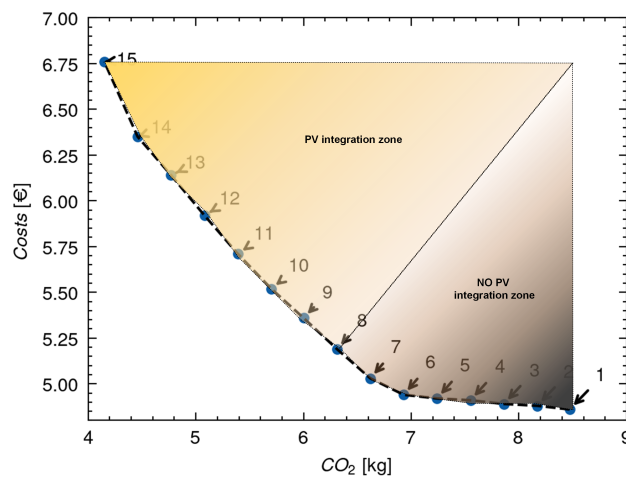


Figure B.4.: Pareto curve from HEMS

B.2.5. Battery design characteristics

Battery design characteristics, battery modules, computational efforts, case study specifics, and tuned parameters are reported in the following tables. Where the cells selected are from *CEGASA PORTABLE ENERGY*, available at [205].

Table B.1.: LFP Li-ion battery specifications

Parameter	Value	Units
V_{nom}	3.2	V
$V_{up,cut}$	3.65	V
$V_{low,cut}$	2.5	V
I_{nom}	1.6	A
Q_{cell}	3.2	Ah
T_{op}	-20 ÷ 60	°C
$Crat_{max}$	3	-

Table B.2.: HEMS results: battery

Parameter	Value	Units
Energy	15	kWh
Nominal power	3	kW
Minimum SOC	20	%
Maximum C-rate	0.25	C

Table B.3.: Battery design

Rack configuration	
#10 modules in parallel	
Module specs	
Configuration	4S40P
Voltage	12V
Capacity	128 Ah

Table B.4.: Computational specs for the case study

Computation specs	
Model	Dell G5 15
CPU	Intel(R) Core(TM) i7-8750H CPU @ 2.20GHz
RAM	8 Gb
Computation time	9 min 56 seconds

Case study details	
#n of scenarios	15
Time resolution	15 mins
Time horizon	24 hours

Table B.5.: Pybamm model tuned parameters

Parameter	Value	units
Initialization dataset Prada2013	-	-
<i>Electrochemical parametrization</i>		
Positive electrode porosity	0.85	-
Separator porosity	0.04	-
Negative electrode porosity	0.3	-
<i>Thermal parametrization</i>		
	$Q = aT^4 + bT^3 + cT^2 + dT + e$	
a	2.005 e-07	-
b	-2.25933 e-04	-
c	9.443 e-02	-
d	-1.732 e+01	-
e	1.177 e+03	-
	$T_{new} = cf \cdot T_{initial}$	
	$cf = 1 + m \cdot (T_{initial} - T_{ref})$	
m	0.006	-
T_{ref}	298.15	K
<i>Aging parametrization</i>		
	SEI : ec reaction limited	
SEI growth activation energy	0	J/mol
EC initial concentration in electrolyte	4541	mol/m ³
SEI open-circuit potential	0.4	V
SEI resistivity	200000	ohm/m
Initial outer SEI thickness	0.5e-9	m
Initial inner SEI thickness	2.5 e-9	m
EC diffusivity	2e-18	m ² /s
Inner SEI reaction proportion	0.5	-
SEI reaction exchange current density	1.5e-07	A/m ²
Inner SEI partial molar volume	9.585e-05	m ³ /mol
Ratio of lithium moles to SEI moles	2.0	-
Outer SEI partial molar volume	9.585e-05	m ³ /mol
SEI kinetic rate constant	8.45e-17	m/s
Positive electrode active material volume fraction	0.295	-
	Lithium plating : irreversible	
Exchange-current density for plating	0.00205	A/m ²
Typical plated lithium concentration	1000.0	mol/m
Initial plated lithium concentration	0	mol/m
Lithium plating transfer coefficient	3.0	-
	Lithium plating porosity change : true	
Lithium metal partial molar volume	1.3e-05	m ³ /mol

Appendix C.

Energy Planning

C.1. Optimal alternatives

In this section, all modelling parameters adopted in the study of the section 4.1 are reported here, including:

1. Baseline technologies.
2. Baseline supply costs.
3. Technologies investment costs.
4. Energy systems efficiencies.

Table C.1.: Baseline technologies

	Size	Efficiency
Cogeneration plant	575 kW _{el} /611kW _{th}	0.415(el)/0.44(th)
Natural gas boilers	8 MW	0.91
Electrical chillers	900 kW _{th}	3
Absorption chillers	455	0.8

Table C.2.: Supply costs

	Import cost	Emission cost
Electricity	0.2 €/kWh	281.4 gCO ₂ /kWh
Natural gas	0.095 €/kWh	201 gCO ₂ /kWh

Table C.3.: Energy conversion technologies costs

Technology	Efficiency/COP	Lifetime [years]	Investment cost [€/kW]	O&M cost
PV	N.A.	30	1473	10 €/kW
Heat pump	3(heat)/3.5 (cold)	20	1600	4% CAPEX
Electrolyser	0.71	15	1295	3.5%CAPEX
Fuel cell	0.5(el)/0.34(th)	14	1500	3.8% CAPEX

Table C.4.: Storage technologies parameters

Technology	Efficiency	Lifetime [years]	Investment cost [€/kWh]	O&M cost [%CAPEX]	Minimum SOC [%]
Battery	0.95	15	1000	2	20
Hot TES	0.81	24	10	1.5	0
Cold TES	0.81	24	10	1.5	0
H ₂ tank	0.99	23	10	2.3	0

C.2. Dynamic modelling

In this section all informative material regarding the analysis performed in section 4.2, where firstly the mathematical description of the algorithm is illustrated, followed by the modelling parameters and input data.

C.2.1. Two-step algorithm

The algorithm is divided into two steps, focusing on both levels (planning and operation) problems.

First step: design of the system layout and planning of investments

In the first step, a MILP (M_Y) is solved to define the investment actions. Each year of the planning horizon represents a decision stage for the installation or the renewal of technological devices. The variables of M_Y decide the system layout (e.g., indicate which and how many devices, generally of different types and sizes) are selected among a set of available ones as well as the operation management. The latter (e.g., supply of external energy, device activation, energy conversion and storage) are controlled on an aggregated scale of one year by the constraints of M_Y .

In particular, let Y be the set of intervals in a multi-year planning horizon K the set of available energy carriers, and $\hat{K} \subseteq K$ the subset of energy carriers (e.g., heat, cooling, and hydrogen in this case study) that cannot be fed from an external supply

due to the lack of infrastructure. Moreover, let Q be the collection of deployable technological devices including both conversion and storage equipment and, in particular, let $S \subseteq Q$ be the set of storage devices. Finally, let ℓ_q be the expected lifetime of the technological device $q \in Q$. The model M_Y is defined upon the following variables for each year $y \in Y$ (notice: the amounts of energy are expressed in kWh):

- $x_{qy}, z_{qy} \in \mathbb{N}_0$: the number of devices of type $q \in Q$ purchased and active in year y , respectively;
- $p_{qy}^k \in \mathbb{R}^+$: the amount of energy by carrier $k \in K$ and produced by the conversion device $q \in Q \setminus S$ in year y ;
- $r_{qy}^{lk} \in \mathbb{R}^+$: the amount of energy by carrier l converted into energy by carrier k through the conversion device $q \in Q \setminus S$ in year y ;
- $s_{qy}^k \in \mathbb{R}^+$: the amount of energy by carrier k accumulated into the storage device $q \in S$ in year y ;
- $f_y^k \in \mathbb{R}^+$: the amount of energy by carrier k and supplied from external sources at year y .

Variables are defined as non-negative because of the scenario, which corresponds to the case study where the energy system is one-way connected to the national grid and thus no surplus of energy can be sold. Moreover, alternative profitable strategies involving the sale of energy, possibly from non-dispatchable sources, to the external grid (e.g., *feed-in* or *net metering*) generally make ESS technologies economically disadvantageous. Clearly, $f_y^k = 0$ for energy of type $k \in \hat{K}$, see constraint (C.8).

According to the yearly granularity of the model, each parameter expresses a yearly aggregated value. In particular, the values of parameters \bar{d} , \bar{b} , \bar{U} , and \bar{C} are computed as the rated hourly value times the total number $T_h = 8760$ of hours in one year. The model M_Y reads as follows:

Appendix C. Energy Planning

$$\min \sum_{k \in K} \sum_{y \in Y} c_y^k f_y^k \cdot \frac{1}{(1+r)^y} + \Gamma \quad (\text{C.1})$$

$$\begin{aligned} \bar{d}_y^k + \sum_{q \in S} s_{qy}^k + \sum_{q \in Q \setminus S} \sum_{l \in K \setminus \{k\}} r_{qy}^{kl} = \\ \sum_{q \in S} e_q^k s_{qy-1}^k + \sum_{q \in Q \setminus S} p_{qy}^k + f_y^k \end{aligned} \quad \forall k \in K, \forall y \in Y \quad (\text{C.2})$$

$$z_{qy} = \sum_{\tau=\max\{1, y-\ell_q+1\}}^y x_{q\tau} \quad \forall q \in Q, \forall y \in Y \quad (\text{C.3})$$

$$\begin{aligned} p_{qy}^k = \sum_{l \in K \setminus \{k\}} \phi_q^{lk} r_{qy}^{lk} + \bar{b}_{qy}^k \cdot \\ \left(x_{qy} + \sum_{\tau=\max\{1, y-\ell_q+1\}}^{y-1} (1-\delta_q)^{(y-\tau)} x_{q\tau} \right) \end{aligned} \quad \forall q \in Q \setminus S, \forall k \in K, \forall y \in Y \quad (\text{C.4})$$

$$p_{qy}^k \leq \bar{U}_q^k z_{qy} \quad \forall q \in Q \setminus S, \forall k \in K, \forall y \in Y \quad (\text{C.5})$$

$$\begin{aligned} s_{qy}^k \leq \\ \bar{C}_q^k \cdot \left(x_{qy} + \sum_{\tau=\max\{1, y-\ell_q+1\}}^{y-1} (1-\delta_q)^{(y-\tau)} x_{q\tau} \right) \end{aligned} \quad \forall q \in S, \forall k \in K, \forall y \in Y \quad (\text{C.6})$$

$$s_{q0}^k = 0 \quad \forall q \in S, \forall k \in K \quad (\text{C.7})$$

$$f_y^k = 0 \quad \forall k \in \hat{K}, \forall y \in Y \quad (\text{C.8})$$

$$x_{qy}, z_{qy} \in \mathbb{N}_0 \quad \forall q \in Q, \forall y \in Y \quad (\text{C.9})$$

$$p_{qy}^k, r_{qy}^{lk} \in \mathbb{R}^+ \quad \forall q \in Q \setminus S, \forall l, k \in K : l \neq k, \forall y \in Y \quad (\text{C.10})$$

$$s_{qy}^k, f_y^k \in \mathbb{R}^+ \quad \forall q \in S, \forall k \in K, \forall y \in Y \quad (\text{C.11})$$

Constraints (C.2) are the flow balancing equalities that hold for each energy carrier k and year y : the total amount of energy by carrier k and given by the user's annual demand plus the possible surplus of energy stored for being used afterwards when required plus the energy converted into a different energy carrier must correspond to

the total quantity given by the available charge of storage devices (e.g., heat thermal, electrical energy storage) at the previous year plus the production of installed devices plus the amount of energy purchased from external sources.

The parameter e_q^k is the round-trip efficiency of the storage device q when accumulating the energy of type k , and assuming that both charging and discharging dynamics of ESSs are linear. Eq. (C.3) link the number of operative devices to the number of those purchased in the past, also considering the device lifetime. For each energy carrier k and year y , the equality (C.4) sets the output of the conversion device q to the sum of two contributions. The former is the overall quantity of energy of type k obtained by the conversion from other kinds of energy carriers involved in the system, linearly weighted with the conversion efficiency ϕ_q^{lk} of the technology. The latter, instead, refers to the conversion from exogenous energy carriers that depends on exogenous factors that are all embedded into the annual base production value \bar{b}_{qy}^k (e.g., renewable technologies like PV or wind farms are strongly dependent on weather conditions). The latter term also incorporates the parameter δ_q that expresses the annual degradation of the energy production efficiency (clearly, the contribution of δ_q increases as far as the device q gets older). Although the loss of efficiency also affects the conversion from energy carriers involved in the system, it has not been considered in the former contribution to avoid non-linearities, and therefore p_{qy}^k only approximates the output of the (set of) device: an exact expression is used in the MILP of the second step). In any case, the production of each conversion device is limited by the scaled upper rated power \bar{U}_q^k as prescribed by constraints (C.5).

Inequalities (C.6) bound the aggregated annual capacity of storage devices from above: the amount of energy of type k accumulated in one year by the storage device $q \in S$ must be no higher than the scaled rated capacity \bar{C}_q^k amortised by the obsolescence of q . Moreover, all the operating storage devices are assumed to be empty at the beginning of the planning horizon, which is a constraint as reported in (C.7). Since BESSs are generally used to absorb the peaks of production and because of the coarse-grained time resolution of the model, the s variables naturally would take the zero value (there is no economic convenience to store energy from one year to the other). To promote the investment and exploitation of energy storage devices, the model M_Y is fed by the linking constraints (see Sub-subsection C.2.1), with refined weekly-based data provided from the second step of the algorithm. Finally, besides the constraints (C.9)-(C.11) on the variables domains, further constraints are added to M_Y for modelling features and constraints of specific technologies employed in the case study (see Sub-section C.2.2). The objective function (C.1) minimises the overall yearly costs with a discount rate at present value r for the whole planning horizon of $|Y| = 30$ years. The first term refers to the buying costs of external energy supply (c_y^k is the cost of energy per kWh). The analytical expression of Γ is the following:

Appendix C. Energy Planning

$$\Gamma = \sum_{\substack{q \in Q \\ y \in Y}} v_{qy} x_{qy} \cdot \frac{1}{(1+r)^{y-1}} + \sum_{\substack{q \in Q \\ y \in Y}} m_{qy} z_{qy} \cdot \frac{1}{(1+r)^y} - \sum_{\substack{q \in Q \\ y \geq |Y|+1-\ell_q}} \left[v_{qy} x_{qy} \cdot \frac{1 - (1+r)^{|Y|+1-y-\ell_q}}{1 - (1+r)^{-\ell_q}} \right] \quad (\text{C.12})$$

Investment v_{qy} and maintenance costs m_{qy} are summed up over the planning horizon for all the operating devices. The last term gives the total residual value of the owned equipment at the end of the planning horizon. Due to the features of the addressed case study (e.g., UNIVPM campus in Italy) and the choice of an economic-driven optimisation, revenues due to energy sales, costs for energy storage, and environmental costs have not been included in Γ . However, alternative/additional cost terms could be included in the objective function, or addressed by relying on multi-criteria optimisation methods (e.g., lexicographic, linear scaling, and ϵ -constraint), if relevant for case studies with different characteristics and/or located in different economic zones (e.g., environmental costs or costs in the U.S. market related to the maximum demand-based charge).

Second step: system operations scheduling

A solution sol^Y provided by M_Y gives a full description of the system layout for the whole planning horizon. The second step of the optimisation computes a refined time scale schedule of the components chosen by M_Y , evaluates the actual total operative costs of the system, and assesses the operative feasibility of the layout. As reported in [206], a common approach adopted in energy systems modelling to control the computational viability consists in extracting a set of weeks through a κ -means clustering procedure [207], which is representative of the average weekly demands per each energy carrier and the average PV production. Therefore, a set W_y of representative weeks for each year $y \in Y$ of the planning horizon is considered in the second step. The weeks W_1 of the first year are directly obtained by clustering the historical data of the case study, whereas the representative weeks of the following years are obtained by considering the estimated data variations. After tuning the parameter κ , $|W_y|$ was set equal to 6. Each week in W_y is composed of 168 hours and represents n_w original weeks.

For each year $\bar{y} \in Y$ and week \bar{w} in $W_{\bar{y}}$, a second MILP formulation $M(\bar{y}, \bar{w})$ computes the hourly schedule of the energy system operations at minimum cost. Let $H_{\bar{w}}$ be the set of hours composing the week \bar{w} , $Q^{\bar{y}}$ the set of operating devices that sol^Y indicates for year \bar{y} , and i_q the year of installation for each device $q \in Q^{\bar{y}}$. The set $Q^{\bar{y}}$ is obtained by adding a number $z_{q\bar{y}}$ of copies of the device q for conversion and storage operations at year \bar{y} , whereas i_q is given from the values of $x_{q\bar{y}}$ in sol^Y .

C.2. Dynamic modelling

Finally, let $S^{\bar{y}} \subseteq Q^{\bar{y}}$ be the set of storage devices operating in year \bar{y} .

MILP $M(\bar{y}, \bar{w})$ does not perform investment decisions, thus design variables x_{qy} and the corresponding constraints are not used. Variables z_{qy} are restricted to be binary and re-indexed as z_{qh} to model the use of the device $q \in Q^{\bar{y}}$ at hour $h \in H_{\bar{w}}$. All the other variables (and constraints) are similarly re-indexed (e.g., $f_y^k \rightarrow f_h^k$). The formulation $M(\bar{y}, \bar{w})$ reads as:

$$\min \Omega_{\bar{y}\bar{w}} = \sum_{k \in K, h \in H_{\bar{w}}} c_{\bar{y}}^k f_h^k \cdot \frac{1}{(1+r)^{\bar{y}}} \quad (\text{C.13})$$

$$\begin{aligned} d_h^k + \sum_{q \in S^{\bar{y}}} s_{qh}^k + \sum_{q \in Q^{\bar{y}} \setminus S^{\bar{y}}} \sum_{l \in K \setminus \{k\}} r_{qh}^{kl} = \\ \sum_{q \in S^{\bar{y}}} e_q^k (1 - \rho_q) s_{qh-1}^k + \sum_{q \in Q^{\bar{y}} \setminus S^{\bar{y}}} p_{qh}^k + f_h^k \quad \forall k \in K, \forall h \in H_{\bar{w}} \end{aligned} \quad (\text{C.14})$$

$$\begin{aligned} p_{qh}^k = \\ \sum_{l \in K \setminus \{k\}} \phi_q^{lk} (1 - \delta_q)^{(\bar{y}-i_q)} r_{qh}^{lk} + \\ b_{qh}^k (1 - \delta_q)^{(\bar{y}-i_q)} z_{qh} \quad \forall q \in Q^{\bar{y}} \setminus S^{\bar{y}}, \forall k \in K, \forall h \in H_{\bar{w}} \end{aligned} \quad (\text{C.15})$$

$$L_q^k z_{qh} \leq p_{qh}^k \leq U_q^k z_{qh} \quad \forall q \in Q^{\bar{y}} \setminus S^{\bar{y}}, \forall k \in K, \forall h \in H_{\bar{w}} \quad (\text{C.16})$$

$$s_{qh}^k \leq C_q^k (1 - \delta_q)^{(\bar{y}-i_q)} z_{qh} \quad \forall q \in S^{\bar{y}}, \forall k \in K, \forall h \in H_{\bar{w}} \quad (\text{C.17})$$

$$s_{qh_1}^k = s_{qh_{168}}^k \quad \forall q \in S^{\bar{y}}, \forall k \in K \quad (\text{C.18})$$

$$f_h^k = 0 \quad \forall k \in \hat{K}, \forall h \in H_{\bar{w}} \quad (\text{C.19})$$

$$z_{qh} \in \{0, 1\} \quad \forall q \in Q^{\bar{y}}, \forall h \in H_{\bar{w}} \quad (\text{C.20})$$

$$p_{qh}^k, r_{qh}^{lk} \in \mathbb{R}^+ \quad \forall q \in Q^{\bar{y}} \setminus S^{\bar{y}}, \forall l \neq k \in K, \forall h \in H_{\bar{w}} \quad (\text{C.21})$$

$$s_{qh}^k, f_h^k \in \mathbb{R}^+ \quad \forall q \in S^{\bar{y}}, \forall k \in K, \forall h \in H_{\bar{w}} \quad (\text{C.22})$$

The objective function (C.13) is the total discounted cost of the purchased energy, which is computed by considering the cost $c_{\bar{y}}^k$ per kWh of energy of type k at year \bar{y} . Constraints (C.14) are the balancing equations specifying the hourly requirements of the system and they refine (C.2) by introducing the hourly capacity loss ρ_q for storage. Constraints (C.15) and (C.17) are the analogous of (C.4) and (C.6), respectively, for

Appendix C. Energy Planning

a fixed year and equipment. However, the efficiency degradation δ_q in constraints (C.15) is considered in both the conversion efficiency ϕ_q^{lk} and base production b_{qh}^k . If the conversion devices q is operating at hour h (e.g., if $z_{qh} = 1$), inequalities (C.16) bound the energy output p_{qh}^k between the upper hourly rated power U_q^k and the lower partialisation bound L_q^k ; otherwise, if the device q is not active (i.e., if $z_{qh} = 0$), p_{qh}^k will be set equal to zero. Finally, (C.18) ensures that during the week \bar{w} , which is only representative, the energy storage and consumption are balanced. Further constraints are considered on the basis of specific technologies used. (for the work analysed see Sub-section C.2.2). A solution sol^W of the whole second step will be feasible if $M(\bar{y}, \bar{w})$ is feasible for each $\bar{y} \in Y$ and $\bar{w} \in W_{\bar{y}}$. In this case, its cost Ω is the sum of the costs $\Omega_{\bar{y}\bar{w}}$ of all the solutions $sol(\bar{y}, \bar{w})$ of $M(\bar{y}, \bar{w})$, each one multiplied by $n_{\bar{w}}$. subsubsectionLinking inequalities The information obtained from the solutions of the $M(\bar{y}, \bar{w})$ programs is used through a feedback loop, which is implemented by the linking constraints (C.23) and (C.24), to guide M_Y towards different system layouts. A solution $sol(\bar{y}, \bar{w})$ of $M(\bar{y}, \bar{w})$ can be either:

1. Infeasible due to the impossibility of satisfying the demand by exploiting the operating devices in case of shortage of external supply (e.g., k belongs to \hat{K} and (C.19) hold), or
2. Feasible: in this case, it describes the hourly schedule of the device operations in the current week.

In the former case, a *feasibility cut* constraint of M_Y , which pursues the operative feasibility of the system layout on hourly scale (see line 22 in Algorithm 1), is updated. This constraint is defined for each non-purchasable energy carrier $k \in \hat{K}$ that do not fulfill the demand at a given hour \hat{h} in at least a representative week of $W_{\bar{y}}$ for some years \bar{y} :

$$\hat{d}_{\bar{y}}^k \leq \sum_{q \in Q \setminus S} \left[(1 - \theta) U_q^k z_{q\bar{y}} + b_{q\hat{h}}^k (z_{q\bar{y}} - \sum_{\tau=\max\{1, \bar{y}-\ell_q+1\}}^{\bar{y}-1} \delta_q^{(\bar{y}-\tau)} x_{q\tau}) \right] + \theta \sum_{q \in S} C_q^k (z_{q\bar{y}} - \sum_{\tau=\max\{1, \bar{y}-\ell_q+1\}}^{\bar{y}-1} \delta_q^{(\bar{y}-\tau)} x_{q\tau}). \quad (C.23)$$

In particular, considering the energy of type $k \in \hat{K}$ and year $\bar{y} \in Y$, let $\hat{d}_{\bar{y}}^k$ be the parameter indicating the largest demand per hour. $\hat{d}_{\bar{y}}^k$ is initialised to d_w^k and increased by $\hat{u}_{\bar{y}}^k$ (see lines 3 and 20 in Algorithm 1), where d_w^k is the largest demand per hour among the weeks in $W_{\bar{y}}$, \hat{h} is the hour when the unmet demand of the infeasible solution is maximum, and $\hat{u}_{\bar{y}}^k$ is the value of such unmet demand. In (C.23), technical parameters of devices have an hourly scale, and the estimated base production b of renewable technologies is set to its value at hour \hat{h} . The hourly demand $\hat{d}_{\bar{y}}^k$ must be

met by using renewable technologies together with a convex combination of the rated power U_q^k of energy conversion technologies producing k and the storage capacity C_q^k for k . Parameter $\theta \in [0, 1)$ defines the weight of each term of the combination and balances the ratio between conversion and storage. After preliminary experiments and tuning, its value was set equal to 0.4. Such a tuning made the investments into ESSs more profitable, hence overcoming the lack of convenience in storage technologies because of the aggregated annual scale of M_Y .

Moving to feasible solutions $sol(\bar{y}, \bar{w})$, a constraint of M_Y which promotes the autonomy of the energy system by reducing the incoming supply from external sources, such as the national grid, and it is updated (line 23 in Algorithm 1). The inequality for a purchasable energy carrier $k \in K \setminus \hat{K}$ in year \bar{y} reads as:

$$\tilde{d}_{\bar{y}}^k \leq \frac{f_{\bar{y}}^k}{T_h} + \sum_{q \in Q \setminus S} \left[U_q^k z_{q\bar{y}} + b_{q\tilde{h}}^k (z_{q\bar{y}} - \sum_{\tau=\max\{1, \bar{y}-\ell_q+1\}}^{\bar{y}-1} \delta_q^{(\bar{y}-\tau)} x_{q\tau}) \right] + \sum_{q \in S} C_q^k (z_{q\bar{y}} - \sum_{\tau=\max\{1, \bar{y}-\ell_q+1\}}^{\bar{y}-1} \delta_q^{(\bar{y}-\tau)} x_{q\tau}). \quad (C.24)$$

The parameter $\tilde{d}_{\bar{y}}^k$ represents the request of energy linked to the peak of purchased external energy of type k recorded at year \bar{y} . It is initialised to zero at the beginning of the two-step algorithm. Then, the procedure looks for the hour \tilde{h} of the feasible solutions $sol(\bar{y}, \bar{w})$ when the maximum quantity of energy of type k ($\tilde{f}_{\bar{y}}^k$ in Algorithm 1) is bought, and updates the parameter $\tilde{d}_{\bar{y}}^k$ if its current value is quite smaller than $\tilde{f}_{\bar{y}}^k + d_{\tilde{h}}^k$ (see line 21 in Algorithm 1). The updating threshold is modulated by the parameter γ , which has been set equal to 0.6 after the parameter tuning. The idea of the constraint is to guide M_Y towards the selection of a set of devices able to meet the expected hourly residual demand, thus enhancing the autonomy of the system. The constraint (C.24) imposes the fulfilment of the energy request $\tilde{d}_{\bar{y}}^k$ by using only the mean value $f_{\bar{y}}^k/T_h$ of the annual external supply, thus limiting the peak of purchase. Similarly to (C.23), the presence of the terms associated to storage devices implicitly promotes the installation of ESSs in the system.

The whole procedure

A solution sol of the overall multi-energy system planning problem consists of both the long-term investment variables $sol^Y[x]$ and the short-term operative variables $sol^W[z, p, r, s, f]$. Its total cost \mathcal{C} is given by the sum $\Gamma + \Omega$. If the current solution sol has the smallest cost obtained so far, the best total cost \mathcal{C}^* and the best solution sol^* are then updated (see lines 22-24 in Algorithm 1). The two step procedure is repeated for a fixed number N of iterations (e.g., 5 in the experiments). The algorithm returns the best solution sol^* and the corresponding total cost \mathcal{C}^* (see line 25 in

Algorithm 1).

The pseudo-code of the whole procedure is the following:

Algorithm 1 MILP-based two-step iterative algorithm

```

1: Initialise sets, parameters and variables;
2: Set  $\mathcal{C}^* = +\infty$ ;
3: Set  $\tilde{\mathbf{d}} = \mathbf{0}$  and  $\hat{d}_y^k$  to the largest hourly demand, for each  $k \in \hat{K}$  and  $y \in Y$ ;
4: for  $N$  times do
5:   Solve  $M_Y$ , update solution  $sol^Y$  and  $\Gamma$ ;
6:   Set  $sol^W = \emptyset$  and  $\Omega = 0$ ;
7:   for  $\bar{y} \in Y$  do
8:     Initialise  $Q^{\bar{y}}, S^{\bar{y}}$  from  $sol^Y[z_{\bar{y}}]$ ; ▷ used technologies at year  $\bar{y}$ 
9:     Set  $i$  from  $sol^Y[x_{\bar{y}}]$ ; ▷ year of installation per technology
10:    Set  $\hat{\mathbf{u}}_{\bar{y}} = \mathbf{0}$  and  $\tilde{\mathbf{f}}_{\bar{y}} = \mathbf{0}$ ;
11:    for  $\bar{w} \in W_{\bar{y}}$  do
12:      Solve  $M(\bar{y}, \bar{w})$ ;
13:      if  $sol(\bar{y}, \bar{w})$  is infeasible then
14:        Update  $\hat{u}_{\bar{y}}^k$  if hour  $\hat{h} \in H_{\bar{w}}$  has the largest unmet demand, for each
         $k \in \hat{K}$ ;
15:        Set  $\Omega = +\infty$ ;
16:      else
17:        Update  $\tilde{f}_{\bar{y}}^k$  if hour  $\tilde{h} \in H_{\bar{w}}$  has the largest quantity of purchased
        energy, for each  $k \in K \setminus \hat{K}$ ;
18:        Set  $\Omega = \Omega + n_{\bar{w}} \cdot \Omega_{\bar{y}\bar{w}}$ ;
19:        Set  $sol^W = sol^W \cup sol(\bar{y}, \bar{w})$ ;
20:      Set  $\hat{\mathbf{d}}_{\bar{y}} = \hat{\mathbf{d}}_{\bar{y}} + \hat{\mathbf{u}}_{\bar{y}}$  and update (C.23);
21:      Set  $\tilde{\mathbf{d}}_{\bar{y}} = \max\{\gamma \cdot (\mathbf{d}_{\hat{h}} + \tilde{\mathbf{f}}_{\bar{y}}), \tilde{\mathbf{d}}_{\bar{y}}\}$  and update (C.24);
22:      if  $\mathcal{C}^* > \Gamma + \Omega$  then
23:        Set  $\mathcal{C}^* = \Gamma + \Omega$ ; ▷ update best solution cost
24:        Set  $sol^* = sol^Y[x] \cup sol^W[z, p, r, s, f]$ ; ▷ update best solution
25: return ( $sol^*, \mathcal{C}^*$ )

```

C.2.2. Technology-dependent constraints

Some of the technologies available in the case study under investigation need specific constraints to coherently model the requirements in M_Y and/or $M(\bar{y}, \bar{w})$; in particular:

- The CHP unit needs a couple of equalities to model the simultaneous production of electricity (index el) and heat (index th) from the same natural gas supply with different conversion efficiencies. Let Q^{CHP} be the subset of deployable CHP devices in model M_Y ; then, per each year $y \in Y$ the following equalities are imposed:

$$p_{qy}^{el} = \phi_q^{gas,el} r_{qy}^{gas,el} \quad (C.25)$$

$$p_{qy}^{th} = \phi_q^{gas,th} r_{qy}^{gas,el} \quad (C.26)$$

Constraints are also included in $M(\bar{y}, \bar{w})$ after re-indexing on $h \in H_w$ when CHP units operate in a week represented by the model. An analogous formalisation is used to model the operations of a PEM Fuel Cell, which exploits hydrogen for the simultaneous production of electricity and heat;

- The size of the PV systems is constrained to an upper bound due to physical occupation, which is translated into a maximum deployable rated power in the system at each year $y \in Y$ for M_Y :

$$\sum_{q \in Q^{PV}} U_q^{el} z_{qy} \leq U_{\max}^{PV} \quad (C.27)$$

where Q^{PV} is the collection of the PV systems of different sizes that can be installed;

- The Heat Pump provides alternative heating and cooling outputs. Let Q^{HP} be the collection of available HP technologies. Each $q \in Q^{HP}$ is differentiated as follows: q_1 can only generate heat, whereas q_2 generates the cooling energy. The different $q \in Q^{HP}$ share the same year of installation, and each of them contributes to half of the total costs of the device in the objective function of M_Y . For each $y \in Y$, the following equalities are added to M_Y to model the operation choice while observing the lifetime of the system:

$$z_{q_1 y} + z_{q_2 y} = \sum_{\tau=\max\{1, y-\ell_q+1\}}^y x_{q\tau} \quad (C.28)$$

Given the binary nature of variables z_{qh} , a constraint for each hour $h \in H_w$ is introduced in $M(\bar{y}, \bar{w})$:

$$z_{q_1 h} + z_{q_2 h} \leq 1; \quad (C.29)$$

- The PEM ELectrolyser operates with electricity and water as inputs (index *wat*) for producing hydrogen (index *hyd*). The inequalities used to model its operations in M_Y are:

$$p_{qy}^{hyd} = \phi_q^{el,hyd} r_{qy}^{el,hyd} \quad (C.30)$$

$$\frac{\sum_{q \in Q^{EZ}} p_{qy}^{hyd}}{\phi_q^{wat,hyd}} \leq f_y^{wat} \quad (C.31)$$

per each $y \in Y$ (or $h \in H_w$ in $M(\bar{y}, \bar{w})$), with Q^{EZ} subset of available EZ technologies.

C.2.3. Modelling parameters

In this section, tables recalled throughout the section 4.2 are reported with exhaustive details about the mathematical notation (Tbl. C.7) and economic/technological parameters used in the discussed scenarios (Tables C.5-C.9).

Table C.5.: Scenario parameters employed in the case study.

Parameters		CO ₂ emission factors	
Electricity price [€/kWh]	0.195	Grid electricity [gCO ₂ /kWh]	281.4
Natural gas price [€/kWh]	0.0695	CHP [gCO ₂ /kWh]	353.3
Water price [€/m ³]	3.79	GB [gCO ₂ /kWh]	231.1
Electrical demand per year increment	0.32%		
Discount rate r	5%		

Table C.6.: Performance characteristics and cost coefficients of PV technology.

PV characteristics	
Rated power [kW _p]	20, 500, 1000, 1500, 2000, 2500, 2700, 3300
Efficiency factor	17%
Efficiency degradation per year	0.3%
Lifetime [y]	20
Investment cost [€/kW _p]	1200
Maintenance cost factor	1.3%

Table C.7.: Sets, parameters and variables common to the two formulations, exclusive of M_y and M_w .

Sets	
Common	
K : energy vectors in the system	
M_y	M_w
\bar{T} : yearly planning horizon	T : hourly scheduling horizon
Q : deployable technologies	$Q^{\bar{t}}$: installed technologies in year \bar{t}
$S \subseteq Q$: deployable storage devices	$S^{\bar{t}} \subseteq Q^{\bar{t}}$: installed storage devices in year \bar{t}
$Q^{CHP} \subseteq Q$: deployable CHP technologies	W : representative weeks in the planning horizon
$Q^{PV} \subseteq Q$: installable PV systems	
$Q^{HP} \subseteq Q$: deployable HP engines	

Parameters	
Common	
c_t^k : cost per kWh of energy vector k at time t	
e_q^k : round-trip efficiency of storage technology q accumulating energy vector k	
ϕ_q^{hk} : conversion efficiency from energy vector h to k of technology q	
δ_q : efficiency degradation of technology q	
b_q^k : estimated base production in kWh of energy vector k of technology q at hour t	
U_q^k : maximum rated power in kW of energy vector k of technology q	
C_q^k : rated capacity in kWh of storage technology q accumulating energy vector k	
l_q : lifetime of technology q	
r : discount rate at present value	
M_y	M_w
\bar{d}_t^k : aggr. demand in kWh of energy vector k in year t	d_t^k : demand in kWh of energy vector k at hour t
\bar{b}_{qt}^k : aggr. base production in kWh of energy vector k of technology q in year t	ρ_q : hourly capacity loss of storage technology q
\bar{U}_q^k : aggr. maximum rated power in kWh of technology q producing energy vector k	L_q^k : lower partialisation limit of power in kWh of technology q producing energy vector k
\bar{C}_q^k : aggr. rated capacity in kWh of storage technology q accumulating energy vector k	n_w : number of weeks clustered in representative week w
v_{qt} : investment cost in technology q at year t	
m_{qt} : maintenance cost of technology q in year t	
T_y : number of years in the planning horizon	
H_y : number of hours in a year	
\hat{d}_t^k : estimated peak of unmet demand in kWh of energy vector k at year t	
θ : sensitivity of constraint (C.23)	
\tilde{d}_t^k : estimated peak in kWh of requested energy vector k at year t	
γ : sensitivity of parameter \tilde{d}_t^k	

Variables	
Common	
$f_t^k \in \mathbb{R}^+$: flow of energy vector k purchased at time t	
$s_{qt}^k \in \mathbb{R}^+$: energy vector k accumulated in storage of type q at time t	
$p_{qt}^k \in \mathbb{R}^+$: energy vector k produced by technologies q at time t	
$r_{qt}^{kh} \in \mathbb{R}^+$: energy vector k required for producing energy h by technologies q at time t	
M_y	M_w
$z_{qt} \in \mathbb{N}_0$: number of devices q operating in year t	$z_{qt} \in \{0, 1\}$: number of devices q operating at hour t
$x_{qt} \in \mathbb{N}_0$: number of devices q installed at year t	

Appendix C. Energy Planning

Table C.8.: Performance characteristics and cost coefficients of conversion technologies.

Common					
Efficiency degradation per year	1%				
Partialisation limit of power	30%				
Conversion technologies	Rated power [kW]	Conversion efficiency	Lifetime [y]	Investment cost [€/kW]	Maintenance cost factor
CHP	110	39% <i>el</i> (49% <i>th</i>)	10	900	2%
	220	43% <i>el</i> (47% <i>th</i>)		600	
	575	42% <i>el</i> (44% <i>th</i>)		321	
HP	160	2.80	15	124	1%
	270	2.88		127	
	380	2.80		119	
AC	131	80%	15	174	1%
	152				
	316				
EC	70	2.74	15	121	1%
	120	2.71		124	
	150	3.00		125	
GB	120	88%	20	90	1.5%
	200	88%			
	1000	91%			
FC	300	50% <i>el</i>	10	Table C.9	Table C.9
	600				
	900				
EL	660	71%	10	Table C.9	Table C.9
	1320				
	1980				
Storage technologies	Rated capacity [kWh]	Round-trip efficiency	Lifetime [y]	Investment cost [€/kWh]	Maintenance cost factor
HTES/CTES	500	75%	15	40	2%
	1500				
	2500				
EES	500	90%	10	Table C.9	1%
	1500				
	2500				
SH	1000	99%	18	30	2.3%
	2000				
	3000				

Table C.9.: Dynamic costs of storage technology EES, PEM conversion technologies FC and EL for the 30-year planning horizon.

Years	EES Investment cost [€/kWh]	FC		EL	
		Investment cost [€/kWh] rate [%/y]	Maintenance cost factor rate [%/y]	Investment cost [€/kWh] rate [%/y]	Maintenance cost factor rate [%/y]
		-3.97	-2.21	-11.12 (-6.05)	12.84
2021	284	1309	3.91	1155	6.21
2022	267	1257	3.83	1027	7.00
2023	248	1207	3.74	913	7.90
2024	231	1159	3.66	811	8.92
2025	212	1113	3.58	721	10.06
2026	204	1069	3.50	641	11.35
2027	197	1027	3.42	570	12.81
2028	189	986	3.35	506	14.45
2029	182	947	3.27	450	16.31
2030	174	909	3.20	400	18.40
2031	172	873	3.20	376	18.40
2032	169	838	3.20	353	18.40
2033	168	805	3.20	332	18.40
2034	166	773	3.20	312	18.40
2035	163	742	3.20	293	18.40
2036	161	713	3.20	275	18.40
2037	159	684	3.20	258	18.40
2038	157	657	3.20	243	18.40
2039	154	631	3.20	228	18.40
2040	153	606	3.20	214	18.40
2041	150	582	3.20	201	18.40
2042	148	559	3.20	200	18.40
2043	146	537	3.20	200	18.40
2044	144	515	3.20	200	18.40
2045	141	495	3.20	200	18.40
2046	139	475	3.20	200	18.40
2047	137	456	3.20	200	18.40
2048	135	438	3.20	200	18.40
2049	132	421	3.20	200	18.40
2050	131	404	3.20	200	18.40

Appendix D.

Bi-level case studies

D.1. Hydrogen Wind Turbine

For the study discussed in section 5.1 the i) modelling parameters of the electrolysis system, and the ones used for the assessment of the levelised cost of hydrogen (Tbl. D.1-D.2), are reported.

D.2. Energy Storage Systems comparison

The modelling parameters adopted, for the study related to 5.2, for both technical and economic perspectives, are reported in Tbl. D.3-D.4.

Table D.1.: Modelling assumptions for the electrolysis system

Description	Value
Alkaline electrolysis	
Electrolyte concentration	30% w.t. KOH
Electrolyte max. temperature	80 °C
Electrolyte pressure	7 bar
Average current density	400 mA/cm ²
Max. temperature increase in the stack	1 °C
Min. power load in the stack	15%
Reverse osmosis [208]	
Specific power demand	4 kWh/m ³ water
Cooling tower [209]	
Min. water temperature	30 °C
Max. water temperature	40 °C
Specific power demand	0.6 kJ/kg
Water losses	2%
Gas-liquid separator	
Equilibrium temperature	40 °C
Pumps	
Isentropic efficiency	70%
Equilibrium temperature	95%
Multi-stage compressor	
Number of stages	2
Pressure ratio	3.16
Isentropic efficiency	75%
Mechanical efficiency	95%
Air intercooler	
Temperature increase of air	10 °C
Pressure drop in heat exchanger	800 Pa
Isentropic efficiency	70%
Mechanical efficiency	95%

Table D.2.: Parameters of the LCOH modelling

Battery		
CAPEX 1	160	EUR/kW
CAPEX 2	142	EUR/kWh
OPEX	0.54	EUR/kW/year
Lifetime	10	years
Electrolysis system		
H ₂ rate	0.02	kg _{H₂} /kWh
CAPEX	1000	EUR/kW
OPEX	2	%/CAPEX/year
Lifetime	10	years

D.2. Energy Storage Systems comparison

Table D.3.: Main characteristics of the ESSs

	Value	Unit	ref.
BESS			
Round-trip efficiency	91	%	[187]
Self-discharge ratio	0.007	%/hour	[188]
Minimum SOC	20	%	[187]
Hydrogen			
Electrolyser efficiency	71	%	[187]
Fuel cell efficiency	50	%	[187]

Table D.4.: Cost parameters of the study

Costs	Value	Unit of measure	ref.
BESS investment cost	285	€/kWh	[187] [210]
BESS O&M annual costs	2.2	%	[187] [210]
BESS lifetime	12	years	[187] [210]
Electrolyser investment cost	1'295	€/kW	[187] [210]
Electrolyser O&M annual cost	3.5	%	[187] [210]
Electrolyser lifetime	15	years	[187] [210]
Hydrogen storage tank cost	30	€/kWh	[211] [210]
Hydrogen storage tank O&M cost	2.3	%	[211] [210]
Hydrogen storage tank lifetime	30	years	[211] [210]
Fuel cell investment cost	1'684	€/kW	[187] [210]
Fuel cell O&M annual cost	2	%	[187] [210]
Fuel cell lifetime	14	years	[187] [210]
Interest rate (all systems)	2	%	[187] [210]

References

- [1] IPCC. *Global Warming of 1.5 °C*. URL: <https://www.ipcc.ch/sr15/>.
- [2] *Statistics | Eurostat*. URL: https://ec.europa.eu/eurostat/databrowser/view/NRG_IND_REN/default/table?lang=en&category=nrg.nrg_quant.nrg_quanta.nrg_ind_share.
- [3] *Pathway to critical and formidable goal of net-zero emissions by 2050 is narrow but brings huge benefits, according to IEA special report - News - IEA*. URL: <https://www.iea.org/news/pathway-to-critical-and-formidable-goal-of-net-zero-emissions-by-2050-is-narrow-but-brings-huge-benefits>.
- [4] *Net Zero Coalition | United Nations*. URL: <https://www.un.org/en/climatechange/net-zero-coalition>.
- [5] *Fit for 55 - The EU's plan for a green transition - Consilium*. URL: <https://www.consilium.europa.eu/en/policies/green-deal/fit-for-55-the-eu-plan-for-a-green-transition/>.
- [6] *A European Green Deal*. URL: https://commission.europa.eu/strategy-and-policy/priorities-2019-2024/european-green-deal_en.
- [7] *REPowerEU: affordable, secure and sustainable energy for Europe*. URL: https://commission.europa.eu/strategy-and-policy/priorities-2019-2024/european-green-deal/repowereu-affordable-secure-and-sustainable-energy-europe_en.
- [8] *A first look at REPowerEU: The European Commission's plan for energy independence from Russia - Florence School of Regulation*. URL: <https://fsr.eui.eu/first-look-at-repowereu-eu-commission-plan-for-energy-independence-from-russia/>.
- [9] *Wind energy in Europe: 2022 Statistics and the outlook for 2023-2027 | WindEurope*. URL: <https://windeurope.org/intelligence-platform/product/wind-energy-in-europe-2022-statistics-and-the-outlook-for-2023-2027/#downloads>.
- [10] *Is the European Union on track to meet its REPowerEU goals? – Analysis - IEA*. URL: <https://www.iea.org/reports/is-the-european-union-on-track-to-meet-its-repowereu-goals>.
- [11] *Energy communities*. URL: https://energy.ec.europa.eu/topics/markets-and-consumers/energy-communities_en.

References

- [12] Tohid Nasiri et al. “Energy optimization of multi-carrier energy systems to achieve a low carbon community”. In: *Journal of Cleaner Production* 390 (mar. 2023), p. 136154. ISSN: 0959-6526. DOI: 10.1016/J.JCLEPRO.2023.136154.
- [13] Morteza Nazari-Heris, Behnam Mohammadi-Ivatloo e Somayeh Asadi. “Optimal operation of multi-carrier energy networks with gas, power, heating, and water energy sources considering different energy storage technologies”. In: *Journal of Energy Storage* 31 (ott. 2020), p. 101574. ISSN: 2352-152X. DOI: 10.1016/J.EST.2020.101574.
- [14] Gianfranco Chicco, Marialaura Di Somma e Giorgio Graditi. “Overview of distributed energy resources in the context of local integrated energy systems”. In: *Distributed Energy Resources in Local Integrated Energy Systems: Optimal Operation and Planning* (gen. 2021), pp. 1–29. DOI: 10.1016/B978-0-12-823899-8.00002-9.
- [15] Nima Nasiri et al. “A bi-level market-clearing for coordinated regional-local multi-carrier systems in presence of energy storage technologies”. In: *Sustainable Cities and Society* 63 (dic. 2020), p. 102439. ISSN: 2210-6707. DOI: 10.1016/J.SCS.2020.102439.
- [16] Giulio Raimondi e Giuseppe Spazzafumo. “Exploring Renewable Energy Communities integration through a hydrogen Power-to-Power system in Italy”. In: *Renewable Energy* 206 (apr. 2023), pp. 710–721. ISSN: 0960-1481. DOI: 10.1016/J.RENENE.2023.02.074.
- [17] Subhashree Choudhury. “Review of energy storage system technologies integration to microgrid: Types, control strategies, issues, and future prospects”. In: *Journal of Energy Storage* 48 (apr. 2022), p. 103966. ISSN: 2352-152X. DOI: 10.1016/J.EST.2022.103966.
- [18] Marie Münster et al. “Sector Coupling: Concepts, State-of-the-art and Perspectives”. In: (2020).
- [19] J ; ; Cantor et al. “The Role of Renewable Energies, Storage and Sector-Coupling Technologies in the German Energy Sector under Different CO2 Emission Restrictions”. In: *Sustainability 2022, Vol. 14, Page 10379* 14.16 (ago. 2022), p. 10379. ISSN: 2071-1050. DOI: 10.3390/SU141610379. URL: <https://www.mdpi.com/2071-1050/14/16/10379/htm%20https://www.mdpi.com/2071-1050/14/16/10379>.
- [20] International Renewable Energy Agency. “SECTOR COUPLING IN FACILITATING INTEGRATION OF VARIABLE RENEWABLE ENERGY IN CITIES SECTOR COUPLING IN FACILITATING INTEGRATION OF VARIABLE RENEWABLE ENERGY IN CITIES SECTOR COUPLING IN FACILITATING INTEGRATION OF VARIABLE RENEWABLE ENERGY IN CITIES 2”. In: (2021). URL: www.irena.org.

- [21] Hans Christian Gils, Hedda Gardian e Jens Schmugge. “Interaction of hydrogen infrastructures with other sector coupling options towards a zero-emission energy system in Germany”. In: *Renewable Energy* 180 (dic. 2021), pp. 140–156. ISSN: 0960-1481. DOI: 10.1016/J.RENENE.2021.08.016.
- [22] Mohammad Mohammadi et al. “Energy hub: From a model to a concept – A review”. In: *Renewable and Sustainable Energy Reviews* 80.July (2017), pp. 1512–1527. ISSN: 18790690. DOI: 10.1016/j.rser.2017.07.030.
- [23] Pierluigi Mancarella. “MES (multi-energy systems): An overview of concepts and evaluation models”. In: *Energy* 65 (feb. 2014), pp. 1–17. ISSN: 0360-5442. DOI: 10.1016/J.ENERGY.2013.10.041.
- [24] Behnam Mohammadi-Ivatloo e Farkhondeh Jabari. “Operation, planning, and analysis of energy storage systems in smart energy hubs”. In: *Operation, Planning, and Analysis of Energy Storage Systems in Smart Energy Hubs* (apr. 2018), pp. 1–456. DOI: 10.1007/978-3-319-75097-2/COVER.
- [25] C. N. Papadimitriou et al. “Demand Response schemes in Energy Hubs: A comparison study”. In: *Energy Procedia* 157 (gen. 2019), pp. 939–944. ISSN: 1876-6102. DOI: 10.1016/J.EGYPRO.2018.11.260.
- [26] Mohammad Mohammadi et al. “Optimal management of energy hubs and smart energy hubs – A review”. In: *Renewable and Sustainable Energy Reviews* 89 (giu. 2018), pp. 33–50. ISSN: 1364-0321. DOI: 10.1016/J.RSER.2018.02.035.
- [27] Mohammad Ali Lasemi et al. “A comprehensive review on optimization challenges of smart energy hubs under uncertainty factors”. In: *Renewable and Sustainable Energy Reviews* 160 (mag. 2022), p. 112320. ISSN: 1364-0321. DOI: 10.1016/J.RSER.2022.112320.
- [28] Christina Papadimitriou et al. “A Comprehensive Review of the Design and Operation Optimization of Energy Hubs and Their Interaction with the Markets and External Networks”. In: *Energies* 2023, Vol. 16, Page 4018 16.10 (mag. 2023), p. 4018. ISSN: 1996-1073. DOI: 10.3390/EN16104018. URL: <https://www.mdpi.com/1996-1073/16/10/4018/htm%20https://www.mdpi.com/1996-1073/16/10/4018>.
- [29] Turgut M. Gür. “Review of electrical energy storage technologies, materials and systems: challenges and prospects for large-scale grid storage”. In: *Energy & Environmental Science* 11.10 (ott. 2018), pp. 2696–2767. ISSN: 1754-5706. DOI: 10.1039/C8EE01419A. URL: <https://pubs.rsc.org/en/content/articlehtml/2018/ee/c8ee01419a%20https://pubs.rsc.org/en/content/articlelanding/2018/ee/c8ee01419a>.

References

- [30] Wei He et al. “Technologies and economics of electric energy storages in power systems: Review and perspective”. In: *Advances in Applied Energy* 4.May (2021), p. 100060. ISSN: 26667924. DOI: 10.1016/j.adapen.2021.100060. URL: <https://doi.org/10.1016/j.adapen.2021.100060>.
- [31] Xing Luo et al. “Overview of current development in electrical energy storage technologies and the application potential in power system operation”. In: *Applied Energy* 137 (2015), pp. 511–536. ISSN: 03062619. DOI: 10.1016/j.apenergy.2014.09.081. URL: <http://dx.doi.org/10.1016/j.apenergy.2014.09.081>.
- [32] Edward Barbour et al. “A review of pumped hydro energy storage development in significant international electricity markets”. In: *Renewable and Sustainable Energy Reviews* 61 (ago. 2016), pp. 421–432. ISSN: 1364-0321. DOI: 10.1016/J.RSER.2016.04.019.
- [33] *The 10 Largest Pumped-Storage Hydropower Plants in the World | 2018-04-09 | ENR | Engineering News-Record*. URL: <https://www.enr.com/articles/44302-the-10-largest-pumped-storage-hydropower-plants-in-the-world>.
- [34] *World's largest capacity pumped storage hydropower project to be built in Queensland, Australia*. URL: <https://www.hydropower.org/news/largest-capacity-pumped-storage-project-queensland>.
- [35] Samuele Spedaletti et al. “Energy recovery in gravity adduction pipelines of a water supply system (WSS) for urban areas using Pumps-as-Turbines (PaTs)”. In: *Sustainable Energy Technologies and Assessments* 45 (giu. 2021). ISSN: 22131388. DOI: 10.1016/j.seta.2021.101040.
- [36] Jidai Wang et al. “Overview of Compressed Air Energy Storage and Technology Development”. In: *Energies 2017, Vol. 10, Page 991* 10.7 (lug. 2017), p. 991. ISSN: 1996-1073. DOI: 10.3390/EN10070991. URL: <https://www.mdpi.com/1996-1073/10/7/991/htm%20https://www.mdpi.com/1996-1073/10/7/991>.
- [37] Julian David Hunt et al. “Mountain Gravity Energy Storage: A new solution for closing the gap between existing short- and long-term storage technologies”. In: *Energy* 190 (gen. 2020), p. 116419. ISSN: 0360-5442. DOI: 10.1016/J.ENERGY.2019.116419.
- [38] Md Mustafizur Rahman et al. “Assessment of energy storage technologies: A review”. In: *Energy Conversion and Management* 223.May (2020), p. 113295. ISSN: 01968904. DOI: 10.1016/j.enconman.2020.113295. URL: <https://doi.org/10.1016/j.enconman.2020.113295>.

- [39] *Highview Power to Develop Multiple Cryogenic Energy Storage Facilities in the UK and to Build Europe's Largest Storage System - Highview Power | Highview Power*. URL: https://highviewpower.com/news_announcement/highview-power-to-develop-multiple-cryogenic-energy-storage-facilities-in-the-uk-and-to-build-europes-largest-storage-system/.
- [40] Tristan R. Davenne e Benjamin M. Peters. "An Analysis of Pumped Thermal Energy Storage With De-coupled Thermal Stores". In: *Frontiers in Energy Research* 8 (ago. 2020), p. 538236. ISSN: 2296598X. DOI: 10.3389/FENRG.2020.00160/BIBTEX.
- [41] Shinichi Mukoyama et al. "Development of Superconducting Magnetic Bearing for 300 kW Flywheel Energy Storage System". In: *IEEE Transactions on Applied Superconductivity* 27.4 (giu. 2017). ISSN: 10518223. DOI: 10.1109/TASC.2017.2652327.
- [42] Miguel Chang et al. "Trends in tools and approaches for modelling the energy transition". In: *Applied Energy* 290 (2021). ISSN: 03062619. DOI: 10.1016/j.apenergy.2021.116731.
- [43] Stefan Pfenninger, Adam Hawkes e James Keirstead. "Energy systems modeling for twenty-first century energy challenges". In: *Renewable and Sustainable Energy Reviews* 33 (2014), pp. 74–86. ISSN: 13640321. DOI: 10.1016/j.rser.2014.02.003.
- [44] Henrik Lund et al. "Simulation versus Optimisation: Theoretical Positions in Energy System Modelling". In: *Energies 2017, Vol. 10, Page 840* 10.7 (giu. 2017), p. 840. ISSN: 1996-1073. DOI: 10.3390/EN10070840. URL: <https://www.mdpi.com/1996-1073/10/7/840/htm%20https://www.mdpi.com/1996-1073/10/7/840>.
- [45] L. Suganthi e Anand A. Samuel. "Energy models for demand forecasting—A review". In: *Renewable and Sustainable Energy Reviews* 16.2 (feb. 2012), pp. 1223–1240. ISSN: 1364-0321. DOI: 10.1016/J.RSER.2011.08.014.
- [46] Lisa M.H. Hall e Alastair R. Buckley. "A review of energy systems models in the UK: Prevalent usage and categorisation". In: *Applied Energy* 169 (mag. 2016), pp. 607–628. ISSN: 0306-2619. DOI: 10.1016/J.APENERGY.2016.02.044.
- [47] R. Timothy Marler e Jasbir S. Arora. "The weighted sum method for multi-objective optimization: New insights". In: *Structural and Multidisciplinary Optimization* 41.6 (giu. 2010), pp. 853–862. ISSN: 1615147X. DOI: 10.1007/S00158-009-0460-7/METRICS. URL: <https://link.springer.com/article/10.1007/s00158-009-0460-7>.
- [48] George Mavrotas. "Effective implementation of the ϵ -constraint method in Multi-Objective Mathematical Programming problems". In: *Applied Mathematics and Computation* 213.2 (2009), pp. 455–465. ISSN: 00963003. DOI:

References

- 10.1016/j.amc.2009.03.037. URL: <http://dx.doi.org/10.1016/j.amc.2009.03.037>.
- [49] Hans Kristian Ringkjøb, Peter M Haugan e Ida Marie Solbrekke. “A review of modelling tools for energy and electricity systems with large shares of variable renewables”. In: *Renewable and Sustainable Energy Reviews* 96.July (2018), pp. 440–459. ISSN: 18790690. DOI: 10.1016/j.rser.2018.08.002. URL: <https://doi.org/10.1016/j.rser.2018.08.002>.
- [50] Andrea Herbst et al. “Introduction to Energy Systems Modelling”. In: *Swiss Journal of Economics and Statistics* 148.2 (apr. 2012), pp. 111–135. ISSN: 22356282. DOI: 10.1007/BF03399363/METRICS. URL: <https://sjes.springeropen.com/articles/10.1007/BF03399363>.
- [51] Detlef P van Vuuren et al. “Comparison of top-down and bottom-up estimates of sectoral and regional greenhouse gas emission reduction potentials”. In: *Energy Policy* 37.12 (2009), pp. 5125–5139. ISSN: 03014215. DOI: 10.1016/j.enpol.2009.07.024. URL: <http://dx.doi.org/10.1016/j.enpol.2009.07.024>.
- [52] George B Dantzig. “Linear Programming”. In: *Operations Research* 50.1 (2002). DOI: 10.1287/opre.50.1.42.17798. URL: <http://pubsonline.informs.org/42-47>. <https://doi.org/10.1287/opre.50.1.42.17798><http://www.informs.org>.
- [53] A M Foley et al. “A strategic review of electricity systems models”. In: *Energy* 35.12 (2010), pp. 4522–4530. ISSN: 03605442. DOI: 10.1016/j.energy.2010.03.057. URL: <http://dx.doi.org/10.1016/j.energy.2010.03.057>.
- [54] *Regional Energy Deployment System (ReEDS) | NREL*. URL: <https://www.nrel.gov/analysis/reeds/>.
- [55] Iain Staffell et al. “The role of hydrogen and fuel cells in the global energy system”. In: *Energy & Environmental Science* 12.2 (feb. 2019), pp. 463–491. ISSN: 1754-5706. DOI: 10.1039/C8EE01157E. URL: <https://pubs.rsc.org/en/content/articlehtml/2019/ee/c8ee01157e><https://pubs.rsc.org/en/content/articlelanding/2019/ee/c8ee01157e>.
- [56] *HYDROGEN ROADMAP EUROPE*. 2019.
- [57] Lingkang Jin et al. “Metal hydrides in hydrogen storage: optimization of dynamic control strategies”. In: *Journal of Physics: Conference Series* 2648.1 (dic. 2023), p. 012056. DOI: 10.1088/1742-6596/2648/1/012056. URL: <https://dx.doi.org/10.1088/1742-6596/2648/1/012056>.
- [58] Lingkang Jin et al. “Alkaline Electrolysis for Green Hydrogen Production: Techno-Economic Analysis of Temperature Influence and Control”. In: *36th International Conference on Efficiency, Cost, Optimization, Simulation and Environmental Impact of Energy Systems (ECOS 2023)* (2023), pp. 908–919.

DOI: 10.52202/069564-0082. URL: <https://www.proceedings.com/069564-0082.html>.

- [59] Lingkang Jin et al. "Evaluation of the Impact of Green Hydrogen Blending Scenarios in the Italian Gas Network: Optimal Design and Dynamic Simulation of Operation Strategies". In: *Renewable and Sustainable Energy Transition* 2.April (2022), p. 100022. ISSN: 2667-095X. DOI: 10.2139/ssrn.3957992. URL: <https://doi.org/10.1016/j.rset.2022.100022>.
- [60] M Reuß et al. "Seasonal storage and alternative carriers: A flexible hydrogen supply chain model". In: *Applied Energy* 200 (2017), pp. 290–302. ISSN: 03062619. DOI: 10.1016/j.apenergy.2017.05.050.
- [61] *Hydeploy*. URL: <https://hydeploy.co.uk/>.
- [62] Irfan Ahmad Gondal. "Hydrogen integration in power-to-gas networks". In: *International Journal of Hydrogen Energy* 44.3 (2019), pp. 1803–1815. ISSN: 03603199. DOI: 10.1016/j.ijhydene.2018.11.164. URL: <https://doi.org/10.1016/j.ijhydene.2018.11.164>.
- [63] Changqing Li e Jong Beom Baek. "The promise of hydrogen production from alkaline anion exchange membrane electrolyzers". In: *Nano Energy* 87 (set. 2021), p. 106162. ISSN: 2211-2855. DOI: 10.1016/J.NANOEN.2021.106162.
- [64] Frank Gambou et al. "A Comprehensive Survey of Alkaline Electrolyzer Modeling: Electrical Domain and Specific Electrolyte Conductivity". In: *Energies* 2022, Vol. 15, Page 3452 15.9 (mag. 2022), p. 3452. ISSN: 1996-1073. DOI: 10.3390/EN15093452. URL: <https://www.mdpi.com/1996-1073/15/9/3452/html>
<https://www.mdpi.com/1996-1073/15/9/3452>.
- [65] Matheus T. de Groot, Joost Kraakman e Rodrigo Lira Garcia Barros. "Optimal operating parameters for advanced alkaline water electrolysis". In: *International Journal of Hydrogen Energy* 47.82 (set. 2022), pp. 34773–34783. ISSN: 0360-3199. DOI: 10.1016/J.IJHYDENE.2022.08.075.
- [66] Martín David, Carlos Ocampo-Martínez e Ricardo Sánchez-Peña. "Advances in alkaline water electrolyzers: A review". In: *Journal of Energy Storage* 23 (giu. 2019), pp. 392–403. ISSN: 2352-152X. DOI: 10.1016/J.EST.2019.03.001.
- [67] IRENA. *GREEN HYDROGEN COST REDUCTION*. Rapp. tecn. 2020. URL: https://www.irena.org/-/media/Files/IRENA/Agency/Publication/2020/Dec/IRENA_Green_hydrogen_cost_2020.pdf.
- [68] Marcelo Carmo et al. "A comprehensive review on PEM water electrolysis". In: *International Journal of Hydrogen Energy* 38.12 (apr. 2013), pp. 4901–4934. ISSN: 0360-3199. DOI: 10.1016/J.IJHYDENE.2013.01.151.
- [69] Pierre Millet e Sergey Grigoriev. "Water Electrolysis Technologies". In: *Renewable Hydrogen Technologies: Production, Purification, Storage, Applications and Safety* (2013), pp. 19–41. DOI: 10.1016/B978-0-444-56352-1.00002-7.

References

- [70] Naiying Du et al. "Anion-Exchange Membrane Water Electrolyzers". In: *Chemical Reviews* 122.13 (lug. 2022), pp. 11830–11895. ISSN: 15206890. DOI: 10.1021/ACS.CHEMREV.1C00854/SUPPL{_}FILE/CR1C00854{_}SI{_}001.PDF. URL: /pmc/articles/PMC9284563/%20/pmc/articles/PMC9284563/?report=abstract%20https://www.ncbi.nlm.nih.gov/pmc/articles/PMC9284563/.
- [71] Pierre Baurens, Pierre Serre-Combe e Jean Philippe Poirot-Crouvezier. "Fuel Cells". In: *Low Emission Power Generation Technologies and Energy Management* (feb. 2013), pp. 179–262. DOI: 10.1002/9781118557976.ch5. URL: https://onlinelibrary.wiley.com/doi/full/10.1002/9781118557976.ch5%20https://onlinelibrary.wiley.com/doi/abs/10.1002/9781118557976.ch5%20https://onlinelibrary.wiley.com/doi/10.1002/9781118557976.ch5.
- [72] Pierre Olivier, Cyril Bourasseau e Pr Belkacem Bouamama. *Low-temperature electrolysis system modelling: A review*. 2017. DOI: 10.1016/j.rser.2017.03.099.
- [73] Øystein Ulleberg. "Modeling of advanced alkaline electrolyzers: a system simulation approach". In: *International Journal of Hydrogen Energy* 28.1 (gen. 2003), pp. 21–33. ISSN: 0360-3199. DOI: 10.1016/S0360-3199(02)00033-2.
- [74] M Hammoudi et al. "New multi-physics approach for modelling and design of alkaline electrolyzers". In: *International Journal of Hydrogen Energy* 37.19 (2012), pp. 13895–13913. ISSN: 03603199. DOI: 10.1016/j.ijhydene.2012.07.015.
- [75] Christian Henao et al. "Simulation tool based on a physics model and an electrical analogy for an alkaline electrolyser". In: *Journal of Power Sources* 250 (2014), pp. 58–67. ISSN: 03787753. DOI: 10.1016/j.jpowsour.2013.10.086. URL: http://dx.doi.org/10.1016/j.jpowsour.2013.10.086.
- [76] R. García-Valverde, N. Espinosa e A. Urbina. "Simple PEM water electrolyser model and experimental validation". In: *International Journal of Hydrogen Energy* 37.2 (gen. 2012), pp. 1927–1938. ISSN: 0360-3199. DOI: 10.1016/J.IJHYDENE.2011.09.027.
- [77] P. M. Diéguez et al. "Thermal performance of a commercial alkaline water electrolyzer: Experimental study and mathematical modeling". In: *International Journal of Hydrogen Energy* 33.24 (dic. 2008), pp. 7338–7354. ISSN: 0360-3199. DOI: 10.1016/J.IJHYDENE.2008.09.051.
- [78] Dohyung Jang et al. "Numerical modeling and analysis of the temperature effect on the performance of an alkaline water electrolysis system". In: *Journal of Power Sources* 506 (giu. 2021). ISSN: 03787753. DOI: 10.1016/j.jpowsour.2021.230106.

- [79] Alfredo Ursúa, Luis M Gandía e Pablo Sanchis. “Hydrogen production from water electrolysis: Current status and future trends”. In: *Proceedings of the IEEE*. Vol. 100. 2. Institute of Electrical e Electronics Engineers Inc., 2012, pp. 410–426. DOI: 10.1109/JPROC.2011.2156750.
- [80] Mónica Sánchez et al. “Semi-empirical model and experimental validation for the performance evaluation of a 15 kW alkaline water electrolyzer”. In: *International Journal of Hydrogen Energy* 43.45 (giu. 2018), pp. 20332–20345. ISSN: 03603199. DOI: 10.1016/j.ijhydene.2018.09.029.
- [81] H Vogt e R J Balzer. “The bubble coverage of gas-evolving electrodes in stagnant electrolytes”. In: *Electrochimica Acta* 50.10 (2005), pp. 2073–2079. ISSN: 00134686. DOI: 10.1016/j.electacta.2004.09.025.
- [82] *NIST Chemistry WebBook*. URL: <https://webbook.nist.gov/chemistry/>.
- [83] R J Gilliam et al. “A review of specific conductivities of potassium hydroxide solutions for various concentrations and temperatures”. In: *International Journal of Hydrogen Energy* 32.3 (2007), pp. 359–364. ISSN: 03603199. DOI: 10.1016/j.ijhydene.2006.10.062.
- [84] Ph Vermeiren et al. “Evaluation of the zirfon® separator for use in alkaline water electrolysis and Ni-H₂ batteries”. In: *International Journal of Hydrogen Energy* 23.5 (1998), pp. 321–324. ISSN: 03603199. DOI: 10.1016/S0360-3199(97)00069-4.
- [85] Bonnie J McBride, Michael J Zehe e Sanford Gordon. “NASA Glenn coefficients for calculating thermodynamic properties of individual species: National Aeronautics and Space Administration”. In: *John H. Glenn Research Center at Lewis Field* September (2002), p. 295. URL: <https://ntrs.nasa.gov/search.jsp?R=20020085330%202020-05-03T03:42:36+00:00Z>.
- [86] Damien Le Bideau et al. “Review of necessary thermophysical properties and their sensitivities with temperature and electrolyte mass fractions for alkaline water electrolysis multiphysics modelling”. In: *International Journal of Hydrogen Energy* 44.10 (2019), pp. 4553–4569. ISSN: 03603199. DOI: 10.1016/j.ijhydene.2018.12.222. URL: <https://doi.org/10.1016/j.ijhydene.2018.12.222>.
- [87] Ivan Dmitrievich Zaitsev e G G Aseev. “Properties of Aqueous Solutions of Electrolytes”. In: *undefined* 30.08 (giu. 1992), pp. 30–4415. ISSN: 0009-4978. DOI: 10.5860/CHOICE.30-4415.
- [88] Georgios Sakas et al. “Dynamic energy and mass balance model for an industrial alkaline water electrolyzer plant process”. In: *International Journal of Hydrogen Energy* 47.7 (giu. 2022), pp. 4328–4345. ISSN: 0360-3199. DOI: 10.1016/J.IJHYDENE.2021.11.126.

References

- [89] Rittmar von Helmholt e Ulrich Eberle. "Fuel cell vehicles: Status 2007". In: *Journal of Power Sources* 165.2 (mar. 2007), pp. 833–843. ISSN: 0378-7753. DOI: 10.1016/J.JPOWSOUR.2006.12.073.
- [90] Fardin Ghaffari-Tabrizi et al. "Reducing Hydrogen Boil-Off Losses during Fuelling by Pre-Cooling Cryogenic Tank". In: *Hydrogen 2022, Vol. 3, Pages 255-269* 3.2 (giu. 2022), pp. 255–269. ISSN: 2673-4141. DOI: 10.3390/HYDROGEN3020015. URL: <https://www.mdpi.com/2673-4141/3/2/15/htm%20https://www.mdpi.com/2673-4141/3/2/15>.
- [91] Poojan Modi e Kondo Francois Aguey-Zinsou. "Room Temperature Metal Hydrides for Stationary and Heat Storage Applications: A Review". In: *Frontiers in Energy Research* 9 (apr. 2021), p. 616115. ISSN: 2296598X. DOI: 10.3389/FENRG.2021.616115/BIBTEX.
- [92] Gary Sandrock. "A panoramic overview of hydrogen storage alloys from a gas reaction point of view". In: *Journal of Alloys and Compounds* 293-295 (dic. 1999), pp. 877–888. ISSN: 0925-8388. DOI: 10.1016/S0925-8388(99)00384-9.
- [93] M. Latroche. "Structural and thermodynamic properties of metallic hydrides used for energy storage". In: *Journal of Physics and Chemistry of Solids* 65.2-3 (mar. 2004), pp. 517–522. ISSN: 0022-3697. DOI: 10.1016/J.JPCS.2003.08.037.
- [94] Michael Hirscher et al. "Materials for hydrogen-based energy storage – past, recent progress and future outlook". In: *Journal of Alloys and Compounds* 827 (giu. 2020), p. 153548. ISSN: 0925-8388. DOI: 10.1016/J.JALLCOM.2019.153548.
- [95] Andreas Züttel. "Materials for hydrogen storage". In: *Materials Today* 6.9 (set. 2003), pp. 24–33. ISSN: 1369-7021. DOI: 10.1016/S1369-7021(03)00922-2.
- [96] Zollino Giuseppe. "SISTEMI DI ACCUMULO PER L'IDROGENO HYDROGEN STORAGE SYSTEMS". Tesi di dott. 2010. URL: <https://core.ac.uk/download/pdf/11653831.pdf>.
- [97] Arif Hariyadi et al. "Modeling of the hydrogen sorption kinetics in an AB₂ laves type metal hydride alloy". In: *Journal of Alloys and Compounds* 893 (giu. 2022), p. 162135. ISSN: 0925-8388. DOI: 10.1016/J.JALLCOM.2021.162135.
- [98] B A Talagañis, G O Meyer e P A Aguirre. "Modeling and simulation of absorption–desorption cyclic processes for hydrogen storage-compression using metal hydrides". In: *International Journal of Hydrogen Energy* 36.21 (giu. 2011), pp. 13621–13631. ISSN: 0360-3199. DOI: 10.1016/J.IJHYDENE.2011.07.139.
- [99] Martin Dornheim. "Thermodynamics of Metal Hydrides: Tailoring Reaction Enthalpies of Hydrogen Storage Materials". In: (). URL: www.intechopen.com.

- [100] M Gambini. “Metal hydride energy systems performance evaluation. Part A: Dynamic analysis model of heat and mass transfer”. In: *International Journal of Hydrogen Energy* 19.1 (giu. 1994), pp. 67–80. ISSN: 0360-3199. DOI: 10.1016/0360-3199(94)90179-1.
- [101] M Gambini, M Manno e M Vellini. “Numerical analysis and performance assessment of metal hydride-based hydrogen storage systems”. In: *International Journal of Hydrogen Energy* 33.21 (giu. 2008), pp. 6178–6187. ISSN: 0360-3199. DOI: 10.1016/J.IJHYDENE.2008.08.006.
- [102] Xuning Feng et al. “Detecting the internal short circuit in large-format lithium-ion battery using model-based fault-diagnosis algorithm”. In: *Journal of Energy Storage* 18 (ago. 2018), pp. 26–39. ISSN: 2352-152X. DOI: 10.1016/J.EST.2018.04.020.
- [103] Van Mierlo. “Data-driven health estimation and lifetime prediction of lithium-ion batteries: A review”. In: (2019). DOI: 10.1016/j.rser.2019.109254. URL: <http://go.qub.ac.uk/oa-feedback>.
- [104] Huixin Tian et al. *A review of the state of health for lithium-ion batteries: Research status and suggestions*. Lug. 2020. DOI: 10.1016/j.jclepro.2020.120813.
- [105] Jacqueline S. Edge et al. “Lithium ion battery degradation: what you need to know”. In: *Physical Chemistry Chemical Physics* 23.14 (apr. 2021), pp. 8200–8221. ISSN: 1463-9084. DOI: 10.1039/D1CP00359C. URL: <https://pubs.rsc.org/en/content/articlehtml/2021/cp/d1cp00359c> <https://pubs.rsc.org/en/content/articlelanding/2021/cp/d1cp00359c>.
- [106] Sijia Yang et al. *Review on state-of-health of lithium-ion batteries: Characterizations, estimations and applications*. Set. 2021. DOI: 10.1016/j.jclepro.2021.128015.
- [107] Man Fai Ng et al. *Predicting the state of charge and health of batteries using data-driven machine learning*. Mar. 2020. DOI: 10.1038/s42256-020-0156-7.
- [108] Marc Doyle, Thomas F Fuller e John Newman. “Modeling of Galvanostatic Charge and Discharge of the Lithium/Polymer/Insertion Cell”. In: *Journal of The Electrochemical Society* 140.6 (giu. 1993), pp. 1526–1533. ISSN: 0013-4651. DOI: 10.1149/1.2221597/XML. URL: <https://iopscience.iop.org/article/10.1149/1.2221597> <https://iopscience.iop.org/article/10.1149/1.2221597/meta>.
- [109] Thomas F Fuller, Marc Doyle e John Newman. “Simulation and optimization of the dual lithium ion insertion cell”. In: *Journal of the Electrochemical Society* 141.1 (giu. 1994), pp. 1–10. ISSN: 0013-4651. DOI: 10.1149/1.2054684.

References

- [110] Scott G Marquis et al. “An Asymptotic Derivation of a Single Particle Model with Electrolyte”. In: *Journal of The Electrochemical Society* 166.15 (giu. 2019), A3693–A3706. ISSN: 0013-4651. DOI: 10.1149/2.0341915JES/XML. URL: <https://iopscience.iop.org/article/10.1149/2.0341915jes%20https://iopscience.iop.org/article/10.1149/2.0341915jes/meta>.
- [111] Enrico Marchegiani et al. “Li-ion battery aging model robustness: An analysis using univariate and multivariate techniques”. In: *Journal of Energy Storage* 72 (nov. 2023), p. 108591. ISSN: 2352-152X. DOI: 10.1016/J.EST.2023.108591. URL: <https://linkinghub.elsevier.com/retrieve/pii/S2352152X23019886>.
- [112] M Jafari, K Khan e L Gauchia. “Deterministic models of Li-ion battery aging: It is a matter of scale”. In: *Journal of Energy Storage* 20 (2018), pp. 67–77. DOI: <https://doi.org/10.1016/j.est.2018.09.002>. URL: <https://www.sciencedirect.com/science/article/pii/S2352152X18303098?via%3Dihub>.
- [113] Andrzej Łebkowski. “c”. In: *Przegląd Elektrotechniczny* 1.5 (2017), pp. 69–75.
- [114] Yun Bao, Wenbin Dong e Dian Wang. “Online internal resistance measurement application in lithium ion battery capacity and state of charge estimation”. In: *Energies* 11.5 (2018), p. 1073.
- [115] Shuai Ma et al. “Temperature effect and thermal impact in lithium-ion batteries: A review”. In: *Progress in Natural Science: Materials International* 28.6 (2018), pp. 653–666.
- [116] Jia Guo et al. “Lithium-Ion Battery Operation, Degradation, and Aging Mechanism in Electric Vehicles: An Overview”. In: *Energies* 14.17 (2021), p. 5220.
- [117] Noshin Omar et al. “Lithium iron phosphate based battery – Assessment of the aging parameters and development of cycle life model”. In: *Applied Energy* 113 (2014), pp. 1575–1585. ISSN: 0306-2619. DOI: <https://doi.org/10.1016/j.apenergy.2013.09.003>. URL: <https://www.sciencedirect.com/science/article/pii/S0306261913007393>.
- [118] Riccardo Poli, James Kennedy e Tim Blackwell. “Particle swarm optimization”. In: *Swarm intelligence* 1.1 (2007), pp. 33–57.
- [119] John Wang et al. “Cycle-life model for graphite-LiFePO₄ cells”. In: *Journal of Power Sources* 196.8 (2011), pp. 3942–3948. ISSN: 0378-7753. DOI: <https://doi.org/10.1016/j.jpowsour.2010.11.134>. URL: <https://www.sciencedirect.com/science/article/pii/S0378775310021269>.
- [120] Issam Baghdadi et al. “Lithium battery aging model based on Dakin’s degradation approach”. In: *Journal of Power Sources* 325 (2016), pp. 273–285. ISSN: 0378-7753. DOI: <https://doi.org/10.1016/j.jpowsour.2016>.

06.036. URL: <https://www.sciencedirect.com/science/article/pii/S0378775316307388>.

- [121] Nagi Gebraeel. “Sensory-updated residual life distributions for components with exponential degradation patterns”. In: *IEEE Transactions on Automation Science and Engineering* 3.4 (2006), pp. 382–393.
- [122] Christina Papadimitriou et al. *D4.1_Report-on-the-energy-hub-concept-and-the-multi-objective-programming-approach-of-an-energy-hub*. 2022.
- [123] Rahmat Khezri e Amin Mahmoudi. “Review on the state-of-the-art multi-objective optimisation of hybrid standalone/grid-connected energy systems”. In: *IET Generation, Transmission & Distribution* 14.20 (giu. 2020), pp. 4285–4300. ISSN: 1751-8695. DOI: 10.1049/IET-GTD.2020.0453. URL: <https://onlinelibrary.wiley.com/doi/full/10.1049/iet-gtd.2020.0453>.
- [124] Valentin Sulzer et al. “Python Battery Mathematical Modelling (PyBaMM)”. In: *Journal of Open Research Software* 9.1 (2021), pp. 1–8. ISSN: 2049-9647. DOI: 10.5334/JORS.309. URL: <https://openresearchsoftware.metajnl.com/articles/10.5334/jors.309>.
- [125] *Multi-Scale Modelling - The Faraday Institution*. URL: <https://www.faraday.ac.uk/research/lithium-ion/battery-system-modelling/>.
- [126] *pybamm-team/PyBaMM: Fast and flexible physics-based battery models in Python*. URL: <https://github.com/pybamm-team/PyBaMM>.
- [127] Joel A.E. Andersson et al. “CasADi: a software framework for nonlinear optimization and optimal control”. In: *Mathematical Programming Computation* 11.1 (mar. 2019), pp. 1–36. ISSN: 18672957. DOI: 10.1007/S12532-018-0139-4/TABLES/3. URL: <https://link.springer.com/article/10.1007/s12532-018-0139-4>.
- [128] Jun Li et al. “Development of Experimental Techniques for Parameterization of Multi-scale Lithium-ion Battery Models”. In: *Journal of The Electrochemical Society* 167.8 (giu. 2020), p. 80534. ISSN: 1945-7111. DOI: 10.1149/1945-7111/AB9050. URL: <https://iopscience.iop.org/article/10.1149/1945-7111/AB9050>
<https://iopscience.iop.org/article/10.1149/1945-7111/AB9050/meta>.
- [129] Peyman Mohtat et al. “Towards better estimability of electrode-specific state of health: Decoding the cell expansion”. In: *Journal of Power Sources* 427 (giu. 2019), pp. 101–111. ISSN: 0378-7753. DOI: 10.1016/J.JPOWSOUR.2019.03.104.
- [130] Andreas Nyman, Mårten Behm e Göran Lindbergh. “Electrochemical characterisation and modelling of the mass transport phenomena in LiPF₆–EC–EMC electrolyte”. In: *Electrochimica Acta* 53.22 (giu. 2008), pp. 6356–6365. ISSN: 0013-4686. DOI: 10.1016/J.ELECTACTA.2008.04.023.

References

- [131] E Prada et al. “A Simplified Electrochemical and Thermal Aging Model of LiFePO₄-Graphite Li-ion Batteries: Power and Capacity Fade Simulations”. In: *Journal of The Electrochemical Society* 160.4 (giu. 2013), A616–A628. ISSN: 0013-4651. DOI: 10.1149/2.053304JES/XML. URL: <https://iopscience.iop.org/article/10.1149/2.053304jes%20https://iopscience.iop.org/article/10.1149/2.053304jes/meta>.
- [132] Andrew Weng, Jason B Siegel e Anna Stefanopoulou. “Differential voltage analysis for battery manufacturing process control”. In: (giu. 2023). ISSN: 2296598X. DOI: 10.3389/fenrg.2023.1087269. URL: <https://arxiv.org/abs/2303.07088v1>.
- [133] *Parameters Sets — PyBaMM v23.4.1 Manual*. URL: https://pybamm.readthedocs.io/en/latest/source/api/parameters/parameter_sets.html.
- [134] Lingkang Jin et al. “Environmental constrained medium-term energy planning: The case study of an Italian university campus as a multi-carrier local energy community”. In: *Energy Conversion and Management* 278 (feb. 2023), p. 116701. ISSN: 0196-8904. DOI: 10.1016/J.ENCONMAN.2023.116701.
- [135] Andrea Pizzuti et al. “A novel approach for multi-stage investment decisions and dynamic variations in medium-term energy planning for multi-energy carriers community”. In: *Applied Energy* 353 (2024), p. 122177. ISSN: 0306-2619. DOI: <https://doi.org/10.1016/j.apenergy.2023.122177>. URL: <https://www.sciencedirect.com/science/article/pii/S0306261923015416>.
- [136] Gabriela Martinez, Nikolaos Gatsis e Georgios B Giannakis. “Stochastic Programming for Energy Planning in Microgrids with Renewables”. In: ().
- [137] Can Ozay e Melih Soner Celiktaş. “Stochastic optimization energy and reserve scheduling model application for alaçatı, Turkey”. In: *Smart Energy* 3 (ago. 2021), p. 100045. ISSN: 2666-9552. DOI: 10.1016/J.SEGY.2021.100045.
- [138] Chandra Ade Irawan et al. “A stochastic programming model for an energy planning problem: formulation, solution method and application”. In: *Annals of Operations Research* 311.2 (apr. 2022), pp. 695–730. ISSN: 15729338. DOI: 10.1007/S10479-020-03904-1/FIGURES/10. URL: <https://link.springer.com/article/10.1007/s10479-020-03904-1>.
- [139] Stefan Pfenninger e Bryn Pickering. “Calliope: a multi-scale energy systems modelling framework”. In: *Journal of Open Source Software* 3.29 (giu. 2018), p. 825. DOI: 10.21105/JOSS.00825.
- [140] Kai Heussen et al. “Energy storage in power system operation: The power nodes modeling framework”. In: *IEEE PES Innovative Smart Grid Technologies Conference Europe, ISGT Europe (2010)*, pp. 1–8. DOI: 10.1109/ISGTEUROPE.2010.5638865.

- [141] *Calliope*. URL: <https://calliope.readthedocs.io/en/stable/index.html>.
- [142] Kevin Hunter, Sarat Sreepathi e Joseph F DeCarolus. “Modeling for insight using Tools for Energy Model Optimization and Analysis (Temoa)”. In: *Energy Economics* 40 (giu. 2013), pp. 339–349. ISSN: 0140-9883. DOI: 10.1016/J.ENECON.2013.07.014.
- [143] Francesco Lombardi et al. “Policy Decision Support for Renewables Deployment through Spatially Explicit Practically Optimal Alternatives”. In: *Joule* 4.10 (2020), pp. 2185–2207. ISSN: 25424351. DOI: 10.1016/j.joule.2020.08.002. URL: <https://doi.org/10.1016/j.joule.2020.08.002>.
- [144] *GeoPandas 0.12.1 — GeoPandas 0.12.1+0.g195f70b.dirty documentation*. URL: <https://geopandas.org/en/stable/>.
- [145] *Renewables ninja*. URL: <https://www.renewables.ninja/>.
- [146] M J Piao, Y P Li e G H Huang. “Development of a stochastic simulation-optimization model for planning electric power systems - A case study of Shanghai, China”. In: *Energy Conversion and Management* 86 (2014), pp. 111–124. ISSN: 01968904. DOI: 10.1016/j.enconman.2014.05.011.
- [147] George Mavrotas, Kostas Florios e Dimitra Vlachou. “Energy planning of a hospital using Mathematical Programming and Monte Carlo simulation for dealing with uncertainty in the economic parameters”. In: *Energy Conversion and Management* 51.4 (2010), pp. 722–731. ISSN: 01968904. DOI: 10.1016/j.enconman.2009.10.029. URL: <http://dx.doi.org/10.1016/j.enconman.2009.10.029>.
- [148] Andrea Bartolini et al. “A model-based approach for the long term planning of distributed energy systems in the energy transition”. In: *ICAE 2019 – International Conference on Applied Energy*. Västerås, 2019.
- [149] *TERNA 2021 Installed generation capacity*. URL: <https://www.terna.it/it/sistema-elettrico/transparency-report/installed-capacity>.
- [150] Luc Van Nuffel et al. “Sector coupling: how can it be enhanced in the EU to foster grid stability and decarbonise?” In: ().
- [151] SNAM. *Scenari di riferimento per il piano di sviluppo delle reti di trasporto del gas 2022-2031*. 2022.
- [152] IRENA, IEA e REN21. *Renewable Energy Policies in a Time of Transition: Heating and Cooling*. November. 2020, pp. 1–112. ISBN: 9789292600617.
- [153] A. Bartolini et al. “A Matheuristic for the Design and Management of Multi-energy Systems”. In: *Communications in Computer and Information Science* 1162 CCIS (2020), pp. 171–188. ISSN: 18650937. DOI: 10.1007/978-3-030-37584-3_{_}9/COVER. URL: https://link.springer.com/chapter/10.1007/978-3-030-37584-3_9.

References

- [154] Christoph Mazur et al. "Technology is not a Barrier: A Survey of Energy System Technologies Required for Innovative Electricity Business Models Driving the Low Carbon Energy Revolution". In: *Energies 2019, Vol. 12, Page 428* 12.3 (gen. 2019), p. 428. ISSN: 1996-1073. DOI: 10.3390/EN12030428. URL: <https://www.mdpi.com/1996-1073/12/3/428/htm%20https://www.mdpi.com/1996-1073/12/3/428>.
- [155] Us Department of Energy. "AN ASSESSMENT OF ENERGY TECHNOLOGIES AND RESEARCH OPPORTUNITIES". In: (2015).
- [156] *Digitalization and Energy – Analysis - IEA*. URL: <https://www.iea.org/reports/digitalisation-and-energy>.
- [157] Arpit Maheshwari. "Modelling, aging and optimal operation of lithium-ion batteries". Tesi di dott. 2018. URL: www.tue.nl/taverne.
- [158] A Bechmann et al. "The Hydrogen Wind Turbine: Design of a wind turbine optimised for hydrogen production". In: *Journal of Physics: Conference Series* 2507.1 (mag. 2023), p. 012010. ISSN: 1742-6596. DOI: 10.1088/1742-6596/2507/1/012010. URL: <https://iopscience.iop.org/article/10.1088/1742-6596/2507/1/012010%20https://iopscience.iop.org/article/10.1088/1742-6596/2507/1/012010/meta>.
- [159] Lingkang Jin et al. "Integration of battery and hydrogen energy storage systems with small-scale hydropower plants in off-grid local energy communities". In: *Energy Conversion and Management* 286 (giu. 2023), p. 117019. ISSN: 0196-8904. DOI: 10.1016/J.ENCONMAN.2023.117019.
- [160] Mads Nipper. *Need for speed - How offshore wind and renewable power-to-X can help solve Europe's energy crisis*. en. Rapp. tecn. Ørsted, apr. 2022, p. 20. URL: <https://orsted.com/en/about-us/whitepapers/renewables-can-solve-europes-energy-crisis>.
- [161] Juan Gea Bermúdez et al. "Going offshore or not: Where to generate hydrogen in future integrated energy systems?" en. In: *Energy Policy* 174 (gen. 2023), p. 19. DOI: <https://doi.org/10.1016/j.enpol.2022.113382>.
- [162] Michael Moritz, Max Schönfish e Simon Schulte. "Estimating global production and supply costs for green hydrogen and hydrogen-based green energy commodities". en. In: *International Journal of Hydrogen Energy* (dic. 2022), p. 16. ISSN: 03603199. DOI: 10.1016/j.ijhydene.2022.12.046.
- [163] Rik van Rossum et al. *European Hydrogen Backbone*. English. Rapp. tecn. The Netherlands: Guidehouse, apr. 2022, p. 36. URL: <https://www.ehb.eu/>.
- [164] Wei He et al. "Case study on the benefits and risks of green hydrogen production co-location at offshore wind farms". en. In: *Journal of Physics: Conference Series* 2265.4 (mag. 2022), p. 42035. ISSN: 1742-6588, 1742-6596.

DOI: 10.1088/1742-6596/2265/4/042035. URL: <https://iopscience.iop.org/article/10.1088/1742-6596/2265/4/042035>.

- [165] Caine David et al. *Dolphyn Hydrogen - phase 1 final report*. en. Rapp. tecn. Department for Business, Energy & Industrial Strategy, ott. 2019, p. 68.
- [166] Hossein Nami et al. “Techno-economic analysis of current and emerging electrolysis technologies for green hydrogen production”. en. In: *Energy Conversion and Management* 269 (ago. 2022). ISSN: 01968904. DOI: 10.1016/j.enconman.2022.116162. URL: <https://linkinghub.elsevier.com/retrieve/pii/S0196890422009438>.
- [167] Mihir Mehta, Michiel Zaaijer e Dominic von Terzi. “Optimum Turbine Design for Hydrogen Production from Offshore Wind”. en. In: *Journal of Physics: Conference Series* 2265.4 (mag. 2022), p. 42061. ISSN: 1742-6588, 1742-6596. DOI: 10.1088/1742-6596/2265/4/042061. URL: <https://iopscience.iop.org/article/10.1088/1742-6596/2265/4/042061>.
- [168] Jan Willem Langeraar. *Double the energy from wind, with hydrogen as primary energy carrier*. en. Nov. 2021. URL: <https://hy-gro.net/en/newsitem>.
- [169] Pietro Bortolotti et al. *IEA wind task 37 on systems engineering in wind energy – WP2.1 reference wind turbines*. Rapp. tecn. International Energy Agency, 2019, p. 138. URL: <https://www.nrel.gov/docs/fy19osti/73492.pdf>.
- [170] Juan Pablo Murcia et al. “Validation of European-scale simulated wind speed and wind generation time series”. In: *Applied Energy* 305 (gen. 2022), p. 117794. ISSN: 0306-2619. DOI: 10.1016/J.APENERGY.2021.117794.
- [171] Omar S. Ibrahim et al. “Dedicated large-scale floating offshore wind to hydrogen: Assessing design variables in proposed typologies”. In: *Renewable and Sustainable Energy Reviews* 160 (mag. 2022), p. 112310. ISSN: 1364-0321. DOI: 10.1016/J.RSER.2022.112310.
- [172] Juan Pablo Murcia Leon et al. “Power fluctuations in high-installation-density offshore wind fleets”. en. In: *Wind Energy Science* 6.2 (mar. 2021), pp. 461–476. ISSN: 2366-7451. DOI: 10.5194/wes-6-461-2021. URL: <https://wes.copernicus.org/articles/6/461/2021/>.
- [173] Charles R Harris et al. “Array programming with NumPy”. In: *Nature* 585.7825 (set. 2020), pp. 357–362. DOI: 10.1038/s41586-020-2649-2. URL: <https://doi.org/10.1038/s41586-020-2649-2>.
- [174] Pauli Virtanen et al. “SciPy 1.0: Fundamental algorithms for scientific computing in python”. In: *Nature Methods* 17 (2020), pp. 261–272. DOI: 10.1038/s41592-019-0686-2.
- [175] Iain Dunning, Joey Huchette e Miles Lubin. “JuMP: A Modeling Language for Mathematical Optimization”. In: *SIAM Review* 59.2 (2017), pp. 295–320. DOI: 10.1137/15M1020575.

References

- [176] *Gurobi Solver*. URL: <https://www.gurobi.com/>.
- [177] Kenneth Thomsen e Søren Oemann Lind. *DTU offshore cost model*. Apr. 2019. URL: <https://topfarm.pages.windenergy.dtu.dk/TopFarm2>.
- [178] Gunner Chr. Larsen e Pierre-Elouan Réthoré. "TOPFARM – A Tool for Wind Farm Optimization". en. In: *Energy Procedia* 35 (2013), pp. 317–324. ISSN: 18766102. DOI: 10.1016/j.egypro.2013.07.184. URL: <https://linkinghub.elsevier.com/retrieve/pii/S1876610213012708>.
- [179] Motasem Bani Mustafa et al. "Evaluation of a battery energy storage system in hospitals for arbitrage and ancillary services". In: *Journal of Energy Storage* 43 (nov. 2021), p. 103183. ISSN: 2352-152X. DOI: 10.1016/J.EST.2021.103183.
- [180] Herib Blanco e André Faaij. "A review at the role of storage in energy systems with a focus on Power to Gas and long-term storage". In: *Renewable and Sustainable Energy Reviews* 81. August 2017 (2018), pp. 1049–1086. ISSN: 18790690. DOI: 10.1016/j.rser.2017.07.062.
- [181] Tay Son Le et al. "Optimal sizing of renewable energy storage: A techno-economic analysis of hydrogen, battery and hybrid systems considering degradation and seasonal storage". In: *Applied Energy* 336 (apr. 2023), p. 120817. ISSN: 0306-2619. DOI: 10.1016/J.APENERGY.2023.120817.
- [182] Paolo Marocco et al. "The role of hydrogen in the optimal design of off-grid hybrid renewable energy systems". In: *Journal of Energy Storage* 46 (feb. 2022), p. 103893. ISSN: 2352-152X. DOI: 10.1016/J.EST.2021.103893.
- [183] GME. *GME - Gestore dei Mercati Energetici SpA*. 2023. URL: <https://www.mercatoelettrico.org/en/default.aspx>.
- [184] S Maran. "Energy and environmental norms on Minimum Vital Flux". In: *Energia Elettrica* (2008). ISSN: 0013-7308. URL: https://inis.iaea.org/search/search.aspx?orig_q=RN:40103017.
- [185] DOE. *Prototype Building Models | Building Energy Codes Program*. 2023. URL: <https://www.energycodes.gov/prototype-building-models>.
- [186] ARERA. *ARERA data and statistics*. URL: https://www.arera.it/it/dati/elenco_dati.htm.
- [187] Ivalin Petkov e Paolo Gabrielli. "Power-to-hydrogen as seasonal energy storage: an uncertainty analysis for optimal design of low-carbon multi-energy systems". In: *Applied Energy* 274 (2020), p. 115197. ISSN: 0306-2619. DOI: <https://doi.org/10.1016/j.apenergy.2020.115197>. URL: <https://www.sciencedirect.com/science/article/pii/S0306261920307091>.
- [188] A H Zimmerman. "Self-discharge losses in lithium-ion cells". In: *IEEE Aerospace and Electronic Systems Magazine* 19.2 (2004), pp. 19–24. DOI: 10.1109/MAES.2004.1269687.

- [189] I E A International Energy Agency. *The Future of Hydrogen*. 2019. DOI: 10.1787/1e0514c4-en.
- [190] O. Schmidt et al. “Future cost and performance of water electrolysis: An expert elicitation study”. In: *International Journal of Hydrogen Energy* 42.52 (dic. 2017), pp. 30470–30492. ISSN: 0360-3199. DOI: 10.1016/J.IJHYDENE.2017.10.045.
- [191] Saman Rashidi et al. “Progress and challenges on the thermal management of electrochemical energy conversion and storage technologies: Fuel cells, electrolysers, and supercapacitors”. In: *Progress in Energy and Combustion Science* 88 (gen. 2022), p. 100966. ISSN: 0360-1285. DOI: 10.1016/J.PECS.2021.100966.
- [192] Jingjing Liu et al. “Hydrogen storage properties and cycling degradation of single-phase La_{0.60}R_{0.15}Mg_{0.25}Ni_{3.45} alloys with A2B7-type superlattice structure”. In: *Energy* 192 (feb. 2020), p. 116617. ISSN: 0360-5442. DOI: 10.1016/J.ENERGY.2019.116617.
- [193] Li Zhao e Jacob Brouwer. “Dynamic operation and feasibility study of a self-sustainable hydrogen fueling station using renewable energy sources”. In: *International Journal of Hydrogen Energy* 40.10 (mar. 2015), pp. 3822–3837. ISSN: 0360-3199. DOI: 10.1016/J.IJHYDENE.2015.01.044.
- [194] Yi Zheng et al. “Optimal day-ahead dispatch of an alkaline electrolyser system concerning thermal–electric properties and state-transitional dynamics”. In: *Applied Energy* 307 (feb. 2022), p. 118091. ISSN: 0306-2619. DOI: 10.1016/J.APENERGY.2021.118091.
- [195] *liionpack*. URL: <https://liionpack.readthedocs.io/en/latest/>.
- [196] Microsoft. *microsoft/BatteryML*. URL: <https://github.com/microsoft/BatteryML#batteryml-an-open-source-tool-for-machine-learning-on-battery-degradation>.
- [197] Emanuele Michelini et al. “Potential and Most Promising Second-Life Applications for Automotive Lithium-Ion Batteries Considering Technical, Economic and Legal Aspects”. In: *Energies* 2023, Vol. 16, Page 2830 16.6 (mar. 2023), p. 2830. ISSN: 1996-1073. DOI: 10.3390/EN16062830. URL: <https://www.mdpi.com/1996-1073/16/6/2830/htm%20https://www.mdpi.com/1996-1073/16/6/2830>.
- [198] Mojtaba Mirzaeian et al. “Second-Life of Lithium-Ion Batteries from Electric Vehicles: Concept, Aging, Testing, and Applications”. In: *Energies* 2023, Vol. 16, Page 2345 16.5 (feb. 2023), p. 2345. ISSN: 1996-1073. DOI: 10.3390/EN16052345. URL: <https://www.mdpi.com/1996-1073/16/5/2345/htm%20https://www.mdpi.com/1996-1073/16/5/2345>.

References

- [199] Anya Heider et al. “Flexibility options and their representation in open energy modelling tools”. In: *Energy Strategy Reviews* 38 (nov. 2021), p. 100737. ISSN: 2211-467X. DOI: 10.1016/J.ESR.2021.100737.
- [200] N Omar et al. “9 - Aging and degradation of lithium-ion batteries”. In: *Rechargeable Lithium Batteries*. A cura di Alejandro A Franco. Woodhead Publishing Series in Energy. Woodhead Publishing, 2015, pp. 263–279. ISBN: 978-1-78242-090-3. DOI: <https://doi.org/10.1016/B978-1-78242-090-3.00009-2>. URL: <https://www.sciencedirect.com/science/article/pii/B9781782420903000092>.
- [201] Dhruvad Parikh, Tommiejean Christensen e Jianlin Li. “Correlating the influence of porosity, tortuosity, and mass loading on the energy density of LiNi_{0.6}Mn_{0.2}Co_{0.2}O₂ cathodes under extreme fast charging (XFC) conditions”. In: *Journal of Power Sources* 474.C (giu. 2020). ISSN: 0378-7753. DOI: 10.1016/J.JPOWSOUR.2020.228601.
- [202] Simon E.J. O’Kane et al. “Lithium-ion battery degradation: how to model it”. In: *Physical Chemistry Chemical Physics* 24.13 (mar. 2022), pp. 7909–7922. ISSN: 1463-9084. DOI: 10.1039/D2CP00417H. URL: <https://pubs.rsc.org/en/content/articlehtml/2022/cp/d2cp00417h> <https://pubs.rsc.org/en/content/articlelanding/2022/cp/d2cp00417h>.
- [203] Peter Keil, Joern Wilhelm e Simon Schuster. “Calendar Aging of Lithium-Ion Batteries You may also like Insights on Calendar Aging of Lithium-Ion Batteries from Differential Voltage Analysis and Coulometry”. In: (). DOI: 10.1149/2.0411609jes.
- [204] Eduardo Redondo-Iglesias, Pascal Venet e Serge Pelissier. “Calendar and cycling ageing combination of batteries in electric vehicles”. In: *Microelectronics Reliability* 88-90 (giu. 2018), pp. 1212–1215. ISSN: 0026-2714. DOI: 10.1016/J.MICROREL.2018.06.113.
- [205] CEGASA. *LFP Cell datasheet*. URL: https://e2e.ti.com/cfs-file/__key/communityserver-discussions-components-files/196/P3_2D00_Datasheet-Cell%E2%80%93LFP-26650.pdf.
- [206] Stefan Pfenninger. “Dealing with multiple decades of hourly wind and PV time series in energy models: A comparison of methods to reduce time resolution and the planning implications of inter-annual variability”. In: *Applied Energy* 197 (lug. 2017), pp. 1–13. ISSN: 0306-2619. DOI: 10.1016/J.APENERGY.2017.03.051.
- [207] Richard Green, Iain Staffell e Nicholas Vasilakos. “Divide and Conquer? k-means clustering of demand data allows rapid and accurate simulations of the British electricity system”. In: *IEEE Transactions on Engineering Management* 61.2 (2014), pp. 251–260. ISSN: 00189391. DOI: 10.1109/TEM.2013.2284386.

- [208] Nikolay Voutchkov. “Energy use for membrane seawater desalination – current status and trends”. en. In: *Desalination* 431 (apr. 2018), pp. 2–14. ISSN: 00119164. DOI: 10.1016/j.desal.2017.10.033. URL: <https://linkinghub.elsevier.com/retrieve/pii/S0011916417321057>.
- [209] Richard Turton, cur. *Analysis, synthesis, and design of chemical processes*. 4th ed. Upper Saddle River, NJ: Prentice Hall, 2012. ISBN: 978-0-13-261812-0.
- [210] Felipe Ignacio Gallardo et al. “A Techno-Economic Analysis of solar hydrogen production by electrolysis in the north of Chile and the case of exportation from Atacama Desert to Japan”. In: *International Journal of Hydrogen Energy* xxxx (2020). ISSN: 03603199. DOI: 10.1016/j.ijhydene.2020.07.050. URL: <https://doi.org/10.1016/j.ijhydene.2020.07.050>.
- [211] Andrea Bartolini et al. “Energy storage and multi energy systems in local energy communities with high renewable energy penetration”. In: *Renewable Energy* 159 (2020), pp. 595–609. ISSN: 18790682. DOI: 10.1016/j.renene.2020.05.131.

List of journal publications

1. Andrea Pizzuti, Lingkang Jin, Mosè Rossi, Fabrizio Marinelli, Gabriele Comodi, A novel approach for multi-stage investment decisions and dynamic variations in medium-term energy planning for multi-energy carriers community, *Applied Energy*, Volume 353, Part B, 2024, 122177, ISSN 0306-2619, <https://doi.org/10.1016/j.apenergy.2023.122177>
2. Enrico Marchegiani, Francesco Ferracuti, Andrea Monteriù, Lingkang Jin, Mosè Rossi, Gabriele Comodi, Lucio Ciabattoni, Li-ion battery aging model robustness: An analysis using univariate and multivariate techniques, *Journal of Energy Storage*, 2023, <https://doi.org/10.1016/j.est.2023.108591>
3. Lingkang Jin, Mosè Rossi, Andrea Monforti Ferrario, Jacopo Carlo Alberizzi, Massimiliano Renzi, Gabriele Comodi, Integration of battery and hydrogen energy storage systems with small-scale hydropower plants in off-grid local energy communities, *Energy Conversion and Management*, 2023, <https://doi.org/10.1016/j.enconman.2023.117019>
4. Lingkang Jin, Mosè Rossi, Lucio Ciabattoni, Marialaura Di Somma, Giorgio Graditi, Gabriele Comodi, Environmental constrained medium-term energy planning: The case study of an Italian university campus as a multi-carrier local energy community, *Energy Conversion and Management*, 2023, <https://doi.org/10.1016/j.enconman.2023.116701>
5. Lingkang Jin, Andrea Monforti Ferrario, Viviana Cigolotti, Gabriele Comodi, Evaluation of the impact of green hydrogen blending scenarios in the Italian gas network: Optimal design and dynamic simulation of operation strategies, *Renewable and Sustainable Energy Transition*, 2022, <https://doi.org/10.1016/j.rset.2022.100022>
6. Anam Nadeem.; Mosè Rossi, Erica Corradi, Lingkang Jin, Gabriele Comodi, Ahmed Sheikh Nadeem. Energy-Environmental Planning of Electric Vehicles (EVs): A Case Study of the National Energy System of Pakistan. *Energies*, 2022, <https://doi.org/10.3390/en15093054>

Curriculum Vitae

Lingkang Jin was born on 13/09/1995 in Anhui, China. Moved to Italy with the family, in 2005. After achieving two awards for outstanding academic performance in high school, he embarked on his Bachelor's degree in Mechanical Engineering at Università Politecnica delle Marche in Ancona. Thereafter he specialized in the thermo-mechanical curriculum of mechanical engineering master at the same university, and graduated with laude in 2019, presenting work on a preliminary design of an offshore wind farm in the Mediterranean Sea, focusing on the wind resource assessment. While pursuing his Master's degree, he became an integral part of the university's Formula SAE team, contributing as an aerodynamic engineer for two years. Their hard work and dedication paid off when they reached the podium in the 2018 FSAE Italy competition, securing first place in class 3. Following the completion of his Master's studies, he gained valuable industry experience by working as a laboratory test and validation engineer at Whirlpool for one year. Subsequently, he was awarded a Ph.D. grant in 2020, which marked the beginning of his research journey in the field of energy systems. His research activities have covered a broad spectrum within the realm of energy systems. Initially, he delved into energy planning and optimisation. Through the Campusword mobility program grant, which he successfully secured twice, he embarked on two separate international visiting periods to unveil the technology details of energy storage solutions. The first took him to the Technical University of Denmark in 2022, where he honed his expertise in power-to-hydrogen systems. The second visiting period, hosted by Eindhoven Technical University in 2023, provided him with deeper insights into lithium-ion batteries.